Two sides of click chemistry: Synthesis of linkable tomaymycin derivatives as *in situ* activated drugs and a trimethyl lock/ tetrazine-based click-to-release system

Von der Naturwissenschaftlichen Fakultät der

Gottfried Wilhelm Leibniz Universität Hannover

zur Erlangung des Grades

Doktorin der Naturwissenschaften (Dr. rer. nat.)

genehmigte Dissertation

von

Julia Alisa Friederich, M.Sc.

2023

Zusammenfassung

Bei der Entwicklung von Arzneimitteln müssen verschiedene Herausforderungen gemeistert werden, unter anderem die Sicherstellung ausreichender Halbwertszeit, zellulärer Permeabilität oder die Vermeidung rascher Resistenzbildung. Als wichtige Lösungsstrategie werden ‚Prodrug'-Ansätze verfolgt, um den Wirkstoff erst am Zielort zu bilden oder in dort freisetzen. Dabei werden entweder biochemischen Prozesse ausgenutzt oder bioorthogonale Reaktionen, die ein breiteres Spektrum an chemischen Modifikationen ermöglichen. Als bioorthogonale Reaktionen werden alle chemischen Reaktionen bezeichnet, die in lebenden Systemen ablaufen können, ohne die natürlichen biochemischen Prozesse zu stören. Ursprünglich wurden bioorthogonale Reaktionen genutzt, um verschiedene chemische Einheiten miteinander zu verbinden. Neuere Arbeiten beschreiben den sogenannten „Click-to-Release" Ansatz, der die selektive Spaltung zweier chemischer Einheiten durch eine Click-Reaktion ausgelöst.

In dieser Studie wurde die *in situ* Aktivierung von zwei verknüpfbaren Derivaten basierenden auf dem natürlich vorkommenden DNA Binder Tomaymycin untersucht. Es wurden vier verschiedener Heterodimere basierend auf Tomaymycin Derivaten synthetisiert, wobei verschiedene bioorthogonale Reaktionen als Schlüsselschritt zum Einsatz kamen. Mit Hilfe einer Reihe von komplementären biologischen Methoden, wie Plasmid und Oligonucleotid basierten elektrophoretischen Mobilitätsänderungsanalysen, Hochleistungsflüssigchromatographie mit gekoppelter massenspektrometirscher Analyse, Fluoreszenz basierte thermalen DNA-Denaturierungsstudien, sowie DNase basierten DNA-Protektionsexperimenten, konnte innerhalb dieser Studie die DNA-Bindung sowie die DNA-Vernetzung für neuartige Tomaymycin-basierte Heterodimere nachgewiesen werden.

Darüber hinaus wird in dieser Studie über ein neuartiges chemisch aktivierbares, bioorthogonales „Click-to-Release" System berichtet. Dieses kombiniert das Trimethyl-Lock (TML) System mit der bioorthogonalen inversen Elektronenbedarfs-Diels-Alder-Reaktion (IEDDA) an Vinylethern. Es wurden kinetische Studien durchgeführt, die zeigen, dass die Reaktionsgeschwindigkeit je nach Wahl des Diens (hier ausgewählte Tetrazine), reguliert und justiert werden kann, somit konnte eine 42-fache Steigerung der Reaktionsrate erreicht werden.

Schlüsselwörter: Aktivierung von Arzneimitteln, bioorthogonale Reaktionen, DNA-Binder, Click-to-Release, TML

Abstract

In drug development various challenges have to be overcome, including ensuring sufficient half-life, cellular permeability, or avoiding rapid development of resistance. Prodrug approaches, i.e., forming or releasing the active drug at the target site, are being pursued as vital strategies to address these challenges. Such strategies either utilize biochemical processes or bioorthogonal reactions, which provide a wider array of chemical modifications. Bioorthogonal reactions refer to any chemical reaction that can occur in living systems without interfering with native biochemical processes. Initially, bioorthogonal reactions were used to link different chemical entities. Contemporary studies describe the so-called "click-to-release" approach, which allows selective cleavage of two chemical entities triggered by a click reaction.

This study explored the *in situ* activation of two linkable derivatives of the naturally occurring DNA binder tomaymycin. A set of four different tomaymycin-based heterodimers were synthetized utilizing different bioorthogonal reactions as the key step. Using a set of complementary biological evaluation methods, i.e., a plasmid and a oligonucleotide based electrophoretic mobility shift assay, a HPLC-MS assay, a fluorescence based thermal DNA denaturation assay, and a DNase I foot printing assay, this study could prove target binding, i.e., DNA-binding as well as DNA cross-linking for two of the novel tomaymycin based heterodimers.

In addition this study reports a novel chemically triggered, bioorthogonal click-to-release system. Herein the trimethyl lock (TML) system is combined with the bioorthogonal inverse electron demand Diels-Alder (IEDDA) reaction of a vinyl ether and a tetrazine, thus expanding the scope of the TML system. Kinetic studies were carried out showing that the reaction rate can be controlled and adjusted depending on the choice of diene (here selected tetrazines). Thereby a 42-fold increase in reaction rate could be achieved.

Keywords: drug activation, bioorthogonal reactions, DNA binders, click-to-release, TML

List of abbreviations

ACN	Acetonitrile
ADC	Antibody-drug conjugates
ADMET	Absorption, Distribution, Metabolism, Elimination, and Toxicity
AIBN	Azobisisobutyronitrile
BCN	Bicyclo[6.1.0]non-4-yne
COSY	Correlation spectroscopy
CuAAC	Copper-catalyzed azide-alkyne cycloaddition
DBO	Dibenzoyl peroxide
DBU	1,8-Diazabicyclo(5.4.0)undec-7-ene
DCM	Dichloromethane
DIAD	Diisopropyl azodicarboxylate
DIBAL	Diisobutylaluminium hydride
DIPEA	*N*,*N*-Diisopropylethylamine
DNA	Deoxyribonucleic acid
ds	double stranded
EDG	Electron donating group
EDTA	Ethylenediaminetetraacetic acid
ESI	Electrospray ionization
EWG	Electron withdrawing group
GC	Gas chromatography
HATU	1-[Bis(dimethylamino)methylene]-1H-1,2,3-triazolo[4,5-b]pyridinium 3-oxide hexafluorophosphate
HFIP	Hexafluoroisopropanol
HMBC	Heteronuclear multiple bond correlation
HOBt	Hydroxybenzotriazole
HOMO	Highest occupied molecular orbital
HPLC	High performance liquid chromatography
HRMS	High-resolution mass spectrometry
HSAB	Hard-soft acid-base
HSQC	Heteronuclear single quantum coherence
IEDDA	Inverse electron demand Diels–Alder
LC	Liquid chromatography

LRMS	Low-resolution mass spectrometry
LUMO	Lowest occupied molecular orbital
MALDI	Matrix assisted laser desorption ionization
MRM	Multiple reaction monitoring
MS	Mass spectrometry
MTBE	Methyl *tert*-butyl ether
NADH	Nicotinamide adenine dinucleotide
NADPH	Nicotinamide adenine dinucleotide phosphate
NBS	*N*-Bromosuccinimide
NMR	Nuclear magnetic resonance spectroscopy
NOE	Nuclear Overhauser effect
NOESY	Nuclear Overhauser enhancement spectroscopy
NRPS	Nonribosomal peptide synthetases
PAGE	Polyacrylamide gel electrophoresis
PBD	Pyrrolobenzodiazepine
PEG	Polyethylene glycol
PET	Photoinduced electron transfer
QTOF	Quadrupole time-of-flight
RP	Reversed phase
SAM	*S*-Adenosyl methionine
SAR	Structure-activity relationship
SPAAC	Strain-promoted azide-alkyne cycloaddition
ss	single stranded
TBAF	Tetra-*n*-butylammonium fluoride
TCO	*Trans*-cyclooctene
TEAB	Triethylammoniumbicarbonat
TFA	Trifluoroacetic acid
TGS	Target-guided synthesis
TIC	Total-ion count
TLC	Thin layer chromatography
TML	Trimethyl lock
UV	Ultraviolet

List of tables

List of figures

VII

VIII

IX

X

Table of content

1 Introduction

In October 2022, the Royal Swedish Academy of Sciences awarded the Nobel prize in chemistry to Carolyn Bertozzi, Morten Meldal, and K. Barry Sharpless "for the development of click chemistry and bioorthogonal chemistry".[1]

In the early 2000s, Sharpless shaped the idea of click chemistry. Reactions that fall under this concept are characterized by their simplicity, fast reaction kinetics, selectivity, and reliability and are thus called click reactions. The most prominent example is the copper-catalyzed azide-alkyne cycloaddition (CuAAC) developed by Meldal[2] and Sharpless[3] independently in 2002 building on the fundamental studies by Rolf Huisgen.[4] This reaction soon gained popularity in a wide array of fields, reaching from material science[5] to drug development[6] and biochemical studies.[6]

This popularity, especially in the fields of biochemistry, chemical biology, and drug development, is mainly attributed to the fact that CuAAC is a very selective reaction, which leads to little to no interference with biomolecules and can be performed in aqueous media and thus is referred to as bioorthogonal.

However, the CuAAC is limited in its *in vivo* use, due to the toxicity of copper. Yet, in some cases the cycloaddition of an alkyne and an azide can be performed without the need for copper as a catalyst. One example is target-guided synthesis (TGS), also called *in situ* click.[7-8] Herein a target, e.g. a protein, is employed for assembling a drug from reactive building blocks within the confines of the protein binding site. This approach exploits the effect that even though the uncatalyzed cycloaddition reaction is slow at room temperature, it is tremendously accelerated when the reaction partners are brought in close proximity by an outer matrix, i.e. a protein. [7-8]

Nevertheless, copper toxicity remained a challenge for *in vivo* applications. Bertozzi further developed the concept of bioorthogonal reactions and developed click reactions based on the Staudinger ligation that allow *in vivo* applications, as exemplified by studies on glycans.[9]

Several bioorthogonal reactions, including strain-promoted azide-alkyne cycloaddition (SPAAC) and tetrazine ligations, have since been developed and applied (Figure 1).[10]
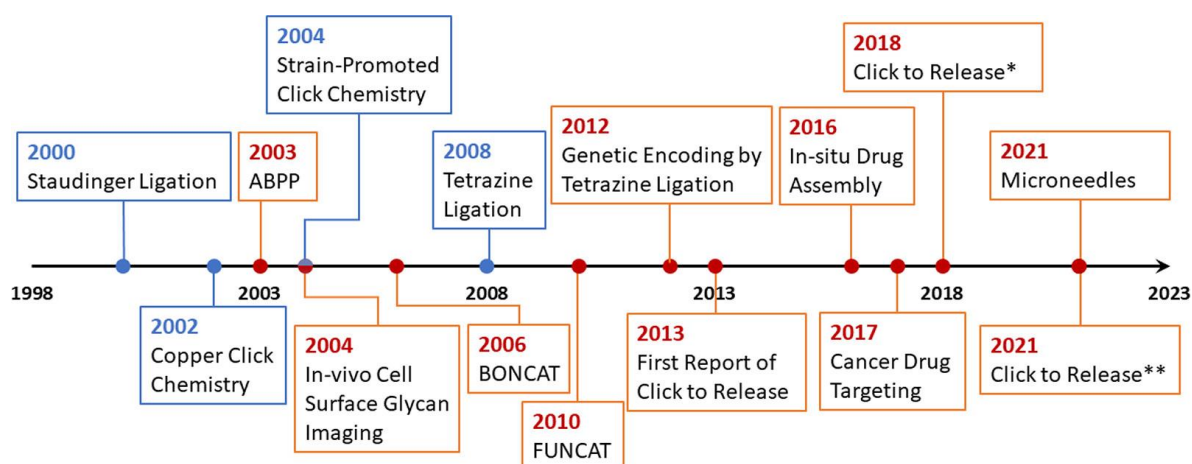
Figure 1: Timeline highlighting major developments of bioorthogonal reactions in blue and selected applications in red. *: from antibody-drug conjugates with systemic tetrazine administration. **: from a systemically administered masked drug with a polymer-bound tetrazine. Reprinted from[10]

Apart from connecting molecular structures under biological conditions, bioorthogonal reactions were further developed to selectively cleave molecular structures. This *click-to-release* concept is, for example, applied in prodrug approaches. This is of particular interest regarding the controlled release of drugs in order to mitigate unwanted side effects or toxicity as well as to influence factors like half-life, metabolic stability, and membrane permeability.[11]

In general, activation strategies forming or releasing the effector molecule at the site of action play an important role in drug development, since many physicochemical, biopharmaceutical, and pharmacokinetic challenges need to be overcome in this process. Additionally, indication-specific challenges arise. In the case of antibiotics, resistance development has to be addressed, whereas, in the field of cancer treatment, the selectivity between different tissues is crucial. These issues can be faced by altering the chemical structure and thus altering the drug's absorption, distribution, metabolism, elimination, and toxicity (ADMET) properties, as well as the selectivity of the parent drug.[12]

Moreover, changes enhancing the efficacy of a drug can lead to lower dosages or less frequent drug administration, thus benefitting the patient.

This thesis focused on the activation of drugs employing the above-described concepts of utilizing bioorthogonal reactions to either connect molecular entities or to trigger a molecular release. Accordingly, this thesis is divided in two chapters. In the first one, the activation of drugs by connecting two molecular entities is explored in the context of the *in situ* dimerization of tomaymycin derivatives. The second one investigates the development of a novel click-to-release system on the basis of a trimethyllock system.

2 Synthesis of linkable tomaymycin derivatives as *in situ* activated antibiotics

2.1 Introduction

2.1.1 DNA binders

Storing the genetic information of living organisms, DNA is one of the most crucial molecules in nature. Its macromolecular structure is composed of two polymeric strands consisting of four building blocks, i.e., the nucleotides, which are connected via phosphodiester bonds. Each nucleotide consists of a ribose carrying a phosphate at its 5' position, which is engaged in the phosphodiester bond with the next nucleotide, and a base (adenine, thymine, guanine, or cytosine) connected via a glycosidic bond to the 2' position. In its native form, DNA strands are joined together via hydrogen bonds forming Watson – Crick base pairs (adenine – thymine and guanine – cytosine). Due to the Watson – Crick base pairs and other factors like the sugar pucker a helical structure, which can adopt diverse conformations, is formed. The major DNA conformations of the helix are the B-form, which is the most abundant form in nature, the A-form and the Z-form (Figure 2).
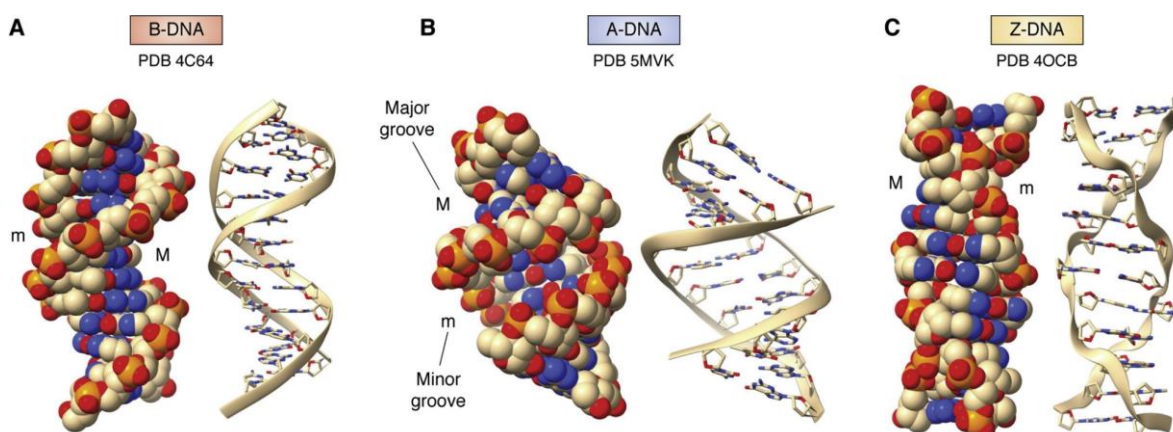
Figure 2: Crystal structures of B, A and Z form double helices depicted as space-filling and cartoon representations. The major (M) and minor (m) grooves are indicated. Reprinted form[13]

The B-form possesses two grooves, i.e., the major and the minor groove (Figure 2), which play an important role in DNA binding. DNA can be bound by a wide variety of molecules,

from large DNA-binding proteins, like DNA topoisomerases or transcription factors, to small molecules such as netropsin or calicheamicin.[14]

Electrostatic interactions as well as shape complementarity are important factors in fostering the sequence specificity of numerous DNA-binding proteins. Additionally, when associating with the target sequence, changes in the three-dimensional shape of the DNA binding protein are induced. The interaction of proteins with DNA often causes significant disruptions in the canonical B-form structure of the DNA double helix. Furthermore, other proteins may be recruited, forming a DNA-binding multi-protein complex that stabilizes the protein-DNA interaction.[15]

In order to gain a better understanding of DNA-protein recognition, a vast array of structural motives has been categorized. However, the complexities in DNA binding, which operate at multiple levels, make it challenging to deduce a simple model or definite recognition codes.[15-21]

Apart from proteins, also small molecules can bind to DNA. The variety of DNA-binding compounds is vast. There are naturally occurring DNA binders; however, since DNA has proven to be one of the prime targets in the field of anticancer drugs, various synthetic small molecules targeting DNA have been developed. Taking these groups together, the differences in their structural features are staggering.[22] Thus, they offer many opportunities for the development of analogues. This wide range of molecules is united by their ability to induce DNA damage. Such damages are mainly caused by either intercalation or binding covalently or non covalently to the grooves, which in case of covalent binding leads to alkylation or cross-linking of DNA.[22] The alternations caused by small molecules are harmful to cells as they can result in transcription errors, the arrest of the replication fork, or errors during the DNA replication, leading to mutations.[23]

2.1.1.1 DNA Intercalators

DNA intercalators are well-known due to their use in many biological assays and diagnostics (e.g., ethidium bromide, Figure 3)[24] and cancer therapy (e.g., doxorubicin or actinomycin D)[25-26] The DNA intercalation process was first described by Lerman in 1961.[27] Lerman could show that intercalators like acridine bind perpendicularly to the helix axis without significantly disturbing the angle of the base pairs to the helix axis. In addition, the hydrogen bonding between the base pairs is not disturbed.[27-28]

It is possible for intercalators to insert reversibly between base pairs of DNA using a combination of π- π stacking and hydrophobic interactions.[29-31] Therefore, intercalators need to be of an appropriate size, shape, and chemical nature to be able to fit between the base pairs, e.g., planar molecules with aromatic structures. In fact, DNA unwinds, opening up a space between its base pairs for the intercalator to fit in. However, this structural change can affect the DNA's function, which makes intercalators potential mutagens.[30] The binding of proteins or enzymes to DNA can be hindered by intercalators; thus, numerous biological process such as transcription, replication, and DNA repair can be impaired.[32-35]

Ethidium bromide   Doxorubicin   Actinomycin D
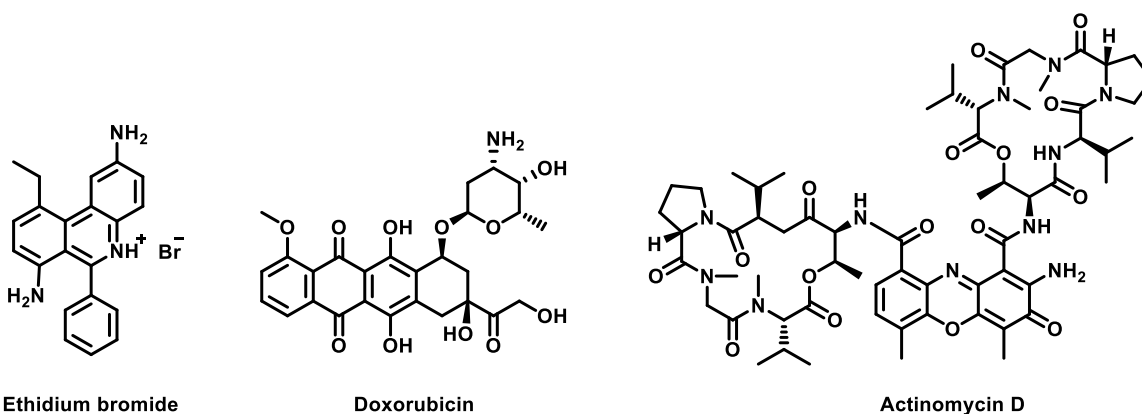
Figure 3: Structures of selected DNA intercalators.

2.1.1.2 DNA alkylation agents

Alkylation agents add methyl or other alkyl groups onto DNA. They react with nucleophilic positions of the different DNA nucleobases. Most of the time, aromatic ring nitrogens and the extracyclic oxygen atoms are impacted by alkylation.[36-38] The different alkylation sites of the four DNA bases are illustrated in Figure 4.

DNA damage is induced in different ways. First, alkylation can lead to mispairing of the base pairs during replication, causing mutations. Second, DNA-processing enzymes (e.g.,

DNA polymerases) can be blocked, and subsequently, DNA synthesis is inhibited. Third, DNA can be cross-linked by an alkylating agent with two binding sites, leading to the formation of *intra-* or *inter-*strand covalent bridges between two base pairs. Such cross-links prevent DNA separation during replication or transcription, thus blocking the DNA synthesis.[39-40]
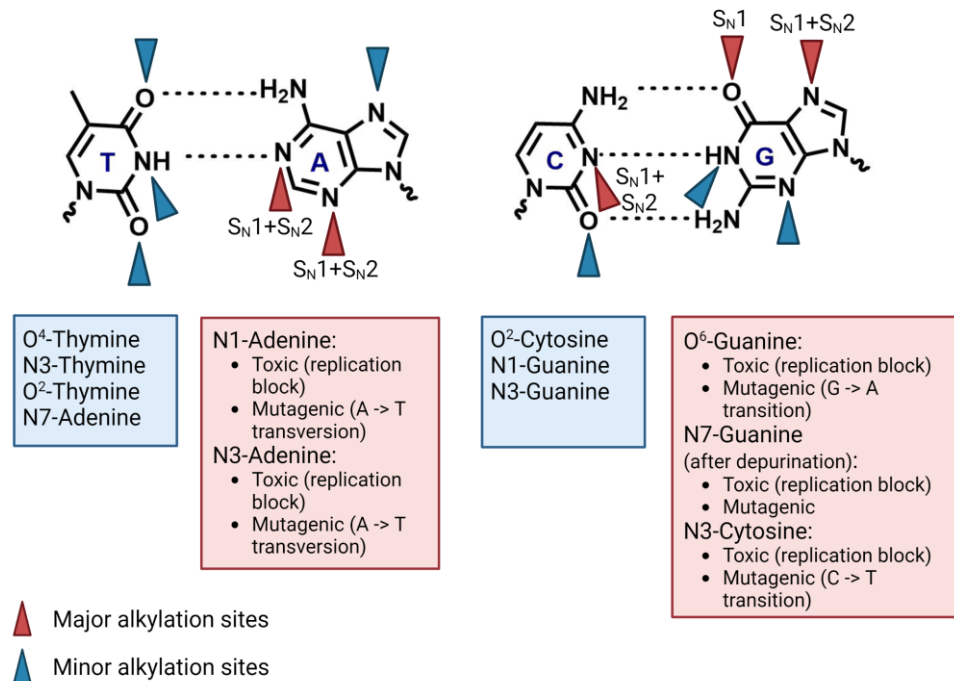
Figure 4: Sites of alkylation on the DNA bases and biological effects of the major alkylation. Major (red) and minor (blue) sites of alkylation indicated by red/blue arrow heads. For the major alkylation sites, the mechanism of alkylation is indicated. Created in analogy to [36], created with BioRender.com.

In general, DNA alkylation can be divided into subcategories based on a set of different factors:[36]

- Number of active sites of the alkylation agent (mono-alkylation vs. cross-linking)
- Chemical mechanism (S_N1 vs. S_N2)
- Type of alkyl group/functional group (methyl vs. chloroethyl, etc.)
- DNA form (single-stranded vs. double-stranded)

Mono-alkylating agents possess one chemical entity that allows the molecule to alkylate DNA. Conversely, cross-linking agents possess two of such chemical entities, allowing them to react with two separate bases of DNA to additionally form cross-links (this topic is discussed in detail in section 2.1.1.3).

Another distinguishing feature is the substitution mechanism. Alkylating agents that follow an S_N2 mechanism mainly target ring nitrogen atoms whereas alkylating agents that follow

an S_N1 mechanism additionally target extracyclic oxygen groups. Interestingly, a large amount of approved chemotherapeutic alkylating drugs belong to the S_N1 category.[36]

The shortest alkylation is methylation. Guanine is particularly affected by methylation and alkylation in general due to the high nucleophilicity of its N7 position. In fact, methylation of the N7 of guanine (7meG) is the predominant methylation adduct, accounting for 60-80% of the total alkylation lesions in DNA.[36],[38] However, larger alkyl groups can also be transferred onto DNA. Such agents can be classified into groups based on their chemical nature. The main groups of alkylating agents are nitrogen mustards, alkyl sulfonates, triazenes, and nitrosoureas (for further details see section 2.1.1.3).[39],[41]

Additionally, the DNA form is also an important factor when it comes to DNA alkylation. In single-stranded DNA, adenine and cytosine can be methylated at the N1 position and N3 position, respectively.[37] Whereas in double-stranded DNA, these functionalities are protected by base pairing. However, exposure during replication, transcription, and recombination likewise poses a danger of alkylation for these groups.[36]

2.1.1.3   DNA cross-linking agents

Cross-linking agents represent a subgroup of DNA-alkylating agents. They are based on the same principle as alkylating molecules and feature two instead of one alkylating moieties. This bifunctionality allows to form *intra-* and *inter*-strand cross-links in addition to mono-alkylation.[32-33]

There are several types of DNA cross-linking agents having different alkylation mechanisms, depending on their chemical structure. Those types include:

- Nitrogen mustards
- Nitrosoureas
- Triazenes
- Alkyl sulfonates
- Epoxide-containing agents
- Platinum compounds
- Photo-activated agents
- Pyrrolobenzodiazepine (PBD) dimers

2.1.1.3.1   Nitrogen mustards

Nitrogen mustards are widely known due to their use in World War II.[42] Aside from being a chemical warfare agent, nitrogen mustards are of great importance in the clinical treatment of cancer. The mode of action of nitrogen mustards exemplified by mustine (Scheme 1).[43] Nitrogen mustards like mustine form an aziridinium intermediate by the attack of the central nitrogen on the ethyl chloride. This highly electrophilic intermediate is subsequently opened by the attack of the N7 of guanine, leading to the first alkylation. The reaction sequence is repeated with the second ethyl chloride group, again leading to an aziridinium intermediate, which is opened by a nucleophilic attack of another guanine. This results in a covalent cross-link between two guanines.[33],[40],[44]
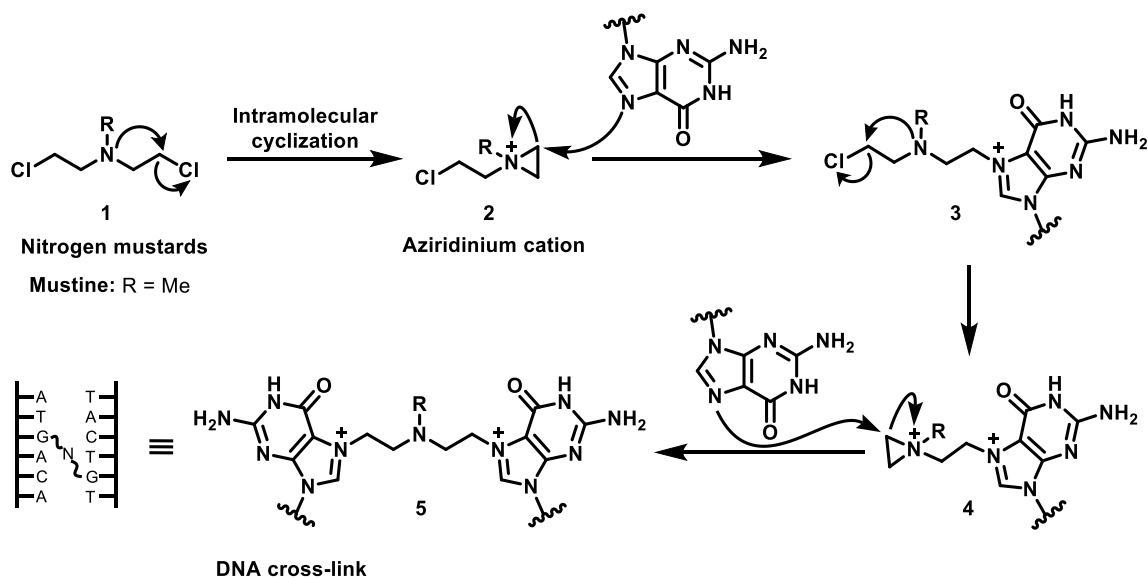
Scheme 1: Structure of nitrogen mustards and their mechanism of action. Created in analogy to[43]

2.1.1.3.2 Nitrosoureas

Nitrosoureas are also cross-linking agents, which first need to be activated by an intramolecular cleavage, yielding a diazohydroxide **8** and an isocyanate **7** (Scheme 2) The diazohydroxide **8** can be easily attacked by the O6 of guanine, releasing molecular nitrogen. Next, the N1 of guanine attacks the chlorinated carbon of the newly introduced alkyl side chain, leading to an oxazolidinium intermediate **10**. This intermediate is opened by the N3 of the pairing cytosine of the complementary DNA strand, finally giving the C-G-cross-link.[45]
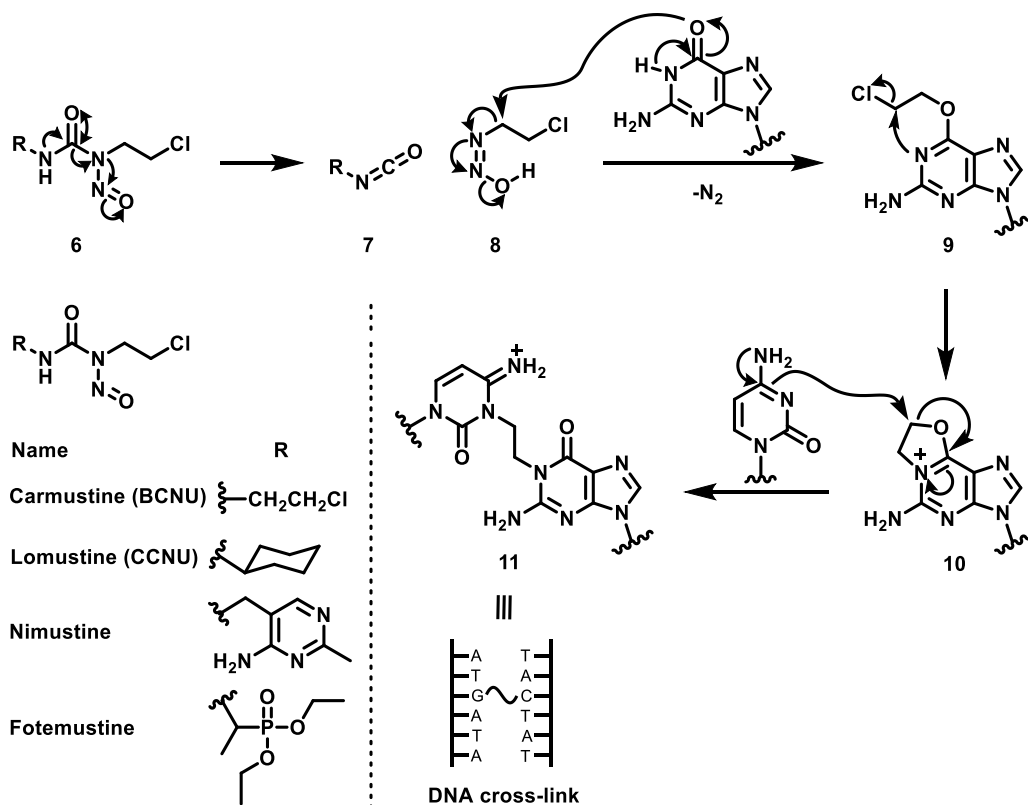
Scheme 2: DNA cross-linking mechanism of nitrosoureas and structures of selected examples. Created in analogy to[45],[46]

2.1.1.3.3 Triazenes

Another class of DNA alkylators are triazenes, which can cause methylation of the N7 and the O6 of guanine. The alkylation mechanism is again driven by the release of molecular nitrogen. The mechanism of action of dacarbazine is shown in Scheme 3.[45]
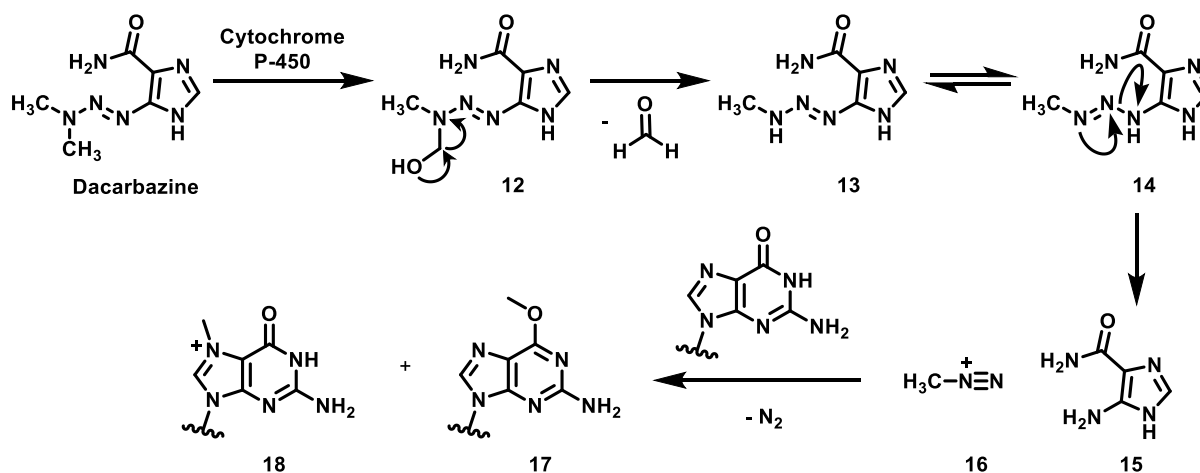
Scheme 3: Mechanism of action of dacarbazine. Created in analogy to[45]

2.1.1.3.4 Alkyl sulfonates

This type of *inter*-strand cross-linking agent is based on the good leaving group characteristics of methanesulfonate, which efficiently delocalizes a negative charge over three oxygen atoms. Busulfan is one of this group's simplest representatives, connecting two methanesulfonates by a butyl linker. Through its two leaving groups, it can cross-link two opposite strands (Scheme 4).[45]
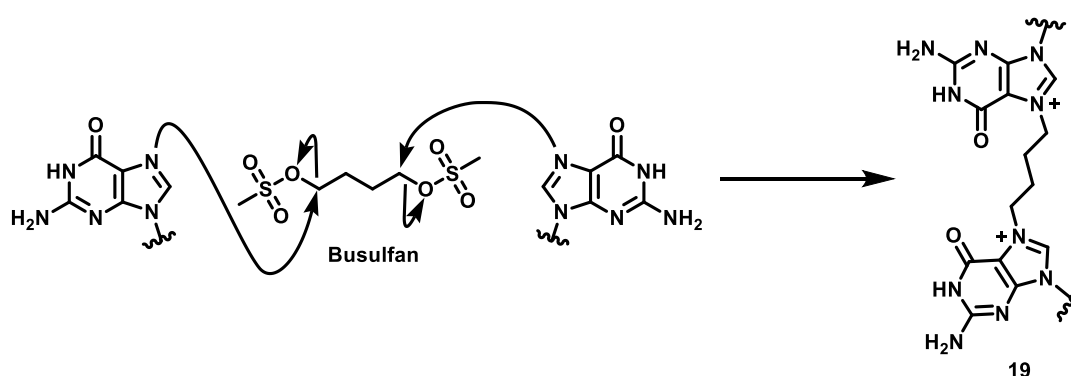
Scheme 4: Mechanism of action of alkyl sulfonates by the example of busulfan. Created in analogy to [45]

2.1.1.3.5 Epoxide-containing agents

Epoxides can be opened by a nucleophilic attack of, e.g., the N7 position of guanine, leading to DNA alkylation. 1,2,3,4-Diepoxybutane is one example of epoxides leading to alkylation and, in this case, even to cross-linking of DNA since it carries two epoxides, which each can be opened by a separate nucleobase, causing the formation of cross-links (Scheme 5).[47]
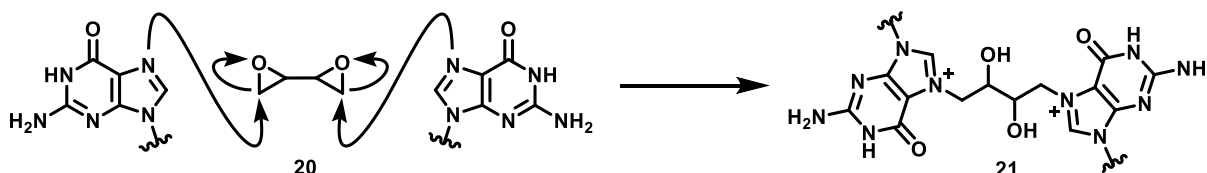
Scheme 5: DNA cross-linking caused by 1,2,3,4-diepoxybutane. Created in analogy to[47]

2.1.1.3.6 Platinum compounds

Different platinum compounds (e.g., oxaliplatin, carboplatin, and cisplatin) are known to cross-link DNA.[48] Their mode of action can be explained using cisplatin as an example. In the first step, a ligand exchange takes place, displacing one of the chloride ligands by water molecules. This newly formed complex, $[PtCl(H_2O)(NH_3)_2]^+$, is in turn reactive towards nucleophiles. As a result, the N7 of guanine can replace the water ligand. Next, the second chloride is replaced by water, which itself is subsequently replaced by a second guanine (Scheme 6). This cross-linking between two guanines, more precisely between the N7-N7 positions, is considered crucial for the cytotoxicity of cisplatin.[48-51]
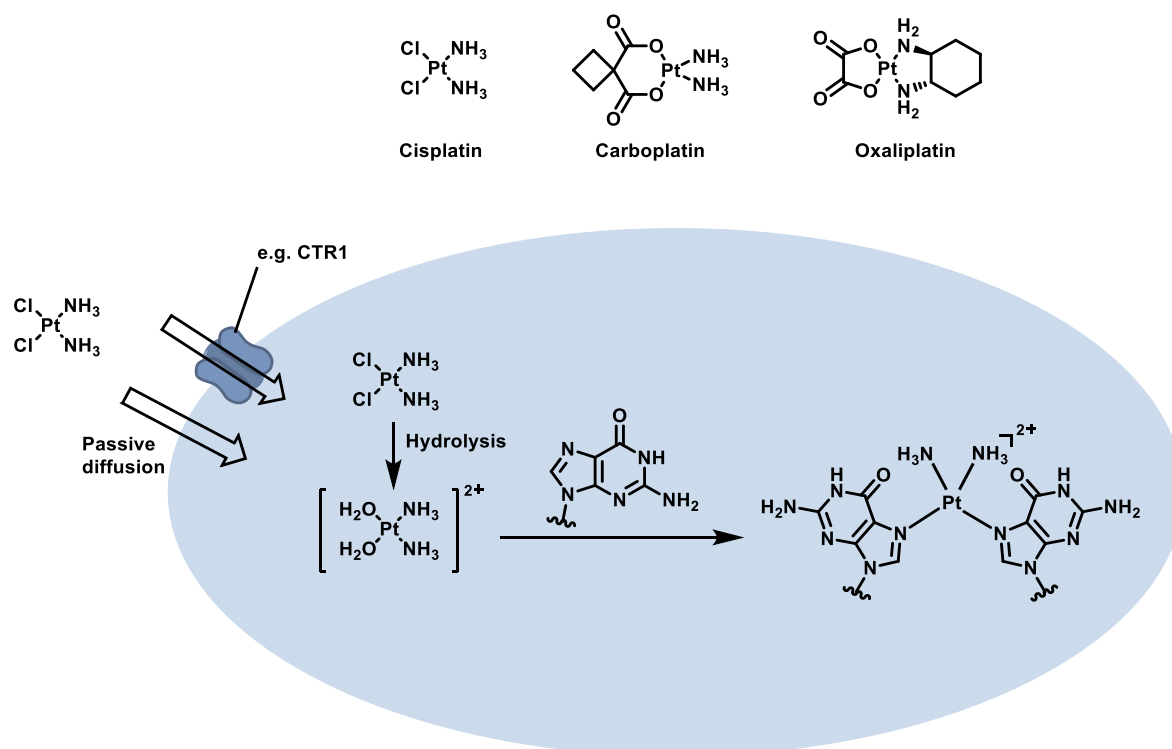
Scheme 6: Structure of cisplatin, carboplatin, oxaliplatin and mechanism of action exemplified using cisplatin. Cisplatin can enter the cell via diffusion or via the copper influx membrane transporter CTR1, followed by hydrolysis/ligand exchange and subsequent cross-linking via another ligand exchange. Created in analogy to[45]

2.1.1.3.7 Photo-activated agents

The advantage of photo-activated agents is that cross-linking can be controlled in a temporal and spatial manner, which makes such compounds especially useful for genomic studies, e.g. for mapping the structure and the dynamics of the genome.[52-53]

Instead of reacting with a nucleophilic moiety of a DNA base, alkylation can also take place by reacting with the double bonds of the bases. To induce such pericyclic reactions, light is often needed.[52],[54-55]

One example of such photo-activated cross-linkers is psoralen (Scheme 7). When exposed to UV light, a [2 + 2] cycloaddition involving the 5,6 double bond of thymine is triggered. Since psoralen can undergo two [2 + 2] cycloadditions it forms, in addition to mono-adducts, also cross-links between two thymine bases.[52],[56-57]
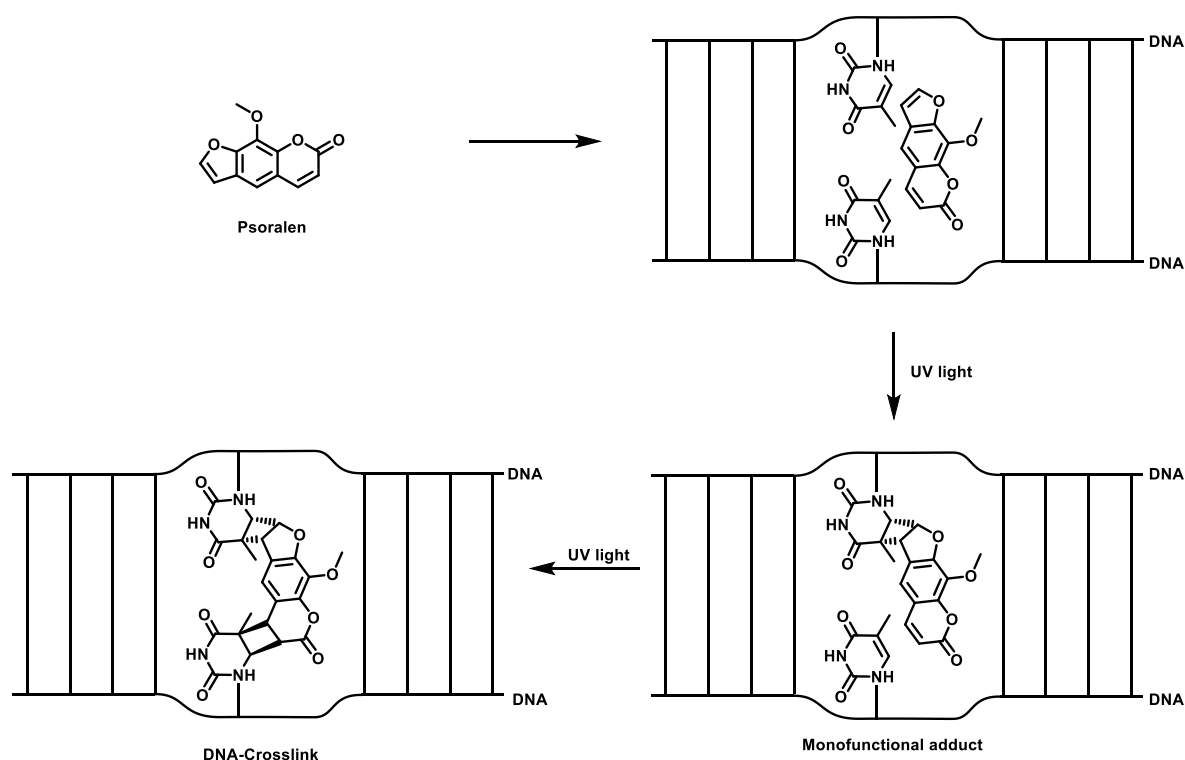
Scheme 7: Mechanism of action of psoralen undergoing two [2 + 2] cycloadditions. Created in analogy to[52]

2.1.1.3.8 Pyrrolobenzodiazepine dimers

Pyrrolobenzodiazepine (PBD) dimers are another representative of the group of DNA-cross-linking agents. They consist of two PBD units connected via a linker. Such dimers often utilize the C8 position as a molecular handle for the linking moiety. Due to their structure, PBDs fit smoothly into the minor groove of the DNA. The imine functionality of each PBD enables the formation of a covalent bond with a guanine base from the DNA. Thus, PBD dimers are able to form cross-links between two guanines.[58] A detailed overview of PBDs and PBD dimers such as SJG-136 is provided in the next section (2.1.2).

2.1.2 Pyrrolobenzodiazepines

PBDs are natural products derived from *Streptomyces achromogenes*, and are of great interest since they display antitumor and antibiotic activity.[58] In 1965, Leimgruber *et al.* reported the first PBD, named anthramycin.[59] Soon thereafter, multiple different analogs were isolated (Figure 5).[60] The eponymous core structure of this natural product family can vary broadly in its substitution patterns.[61]

Several diverse substitutions regarding the aromatic A-ring as well as the dihydropyrrole C-ring can be observed throughout the natural derivatives. Moreover, the C-ring can be either fully saturated or unsaturated at an *endo*cyclic or *exo*cyclic position.[62] A fundamental feature of the PBD core is the imine functionality, since this gives the ability to form a covalent aminal linkage with the *exo*cyclic N2 of guanine. PBDs show a selectivity towards a R-G-R sequence and bind in the minor groove of DNA.[63-65] Renowned representatives of PBDs are the naturally occurring anthramycin,[61] sibiromycin,[66] and neothramycin,[66] which underwent clinical trials. Additionally, SJG-136, a synthetic dimer of two tomaymycin analouges, underwent phase II clinical trials in patients with leukemia and ovarian cancer.[58]

Anthramycin $R^1 = CH_3$; $R^2 = R^3 = R^4 = H$

Mazethramycin $R^1 = CH_3$; $R^2 = H$; $R^3 = CH_3$; $R^4 = H$

Porothramycin $R^1 = H$; $R^2 = R^3 = R^4 = CH_3$

Tomaymycin $R^5 = OH$; $R^6 = OCH_3$

Prothracarcin $R^5 = R^6 = H$

Chicamycin

Abbeymycin

Neothramycin A $R^7 = OH$; $R^8 = H$

Neothramycin B $R^7 = H$; $R^8 = OH$

DC-81

Sibiromycin

Sibanomycin

Limazepine C
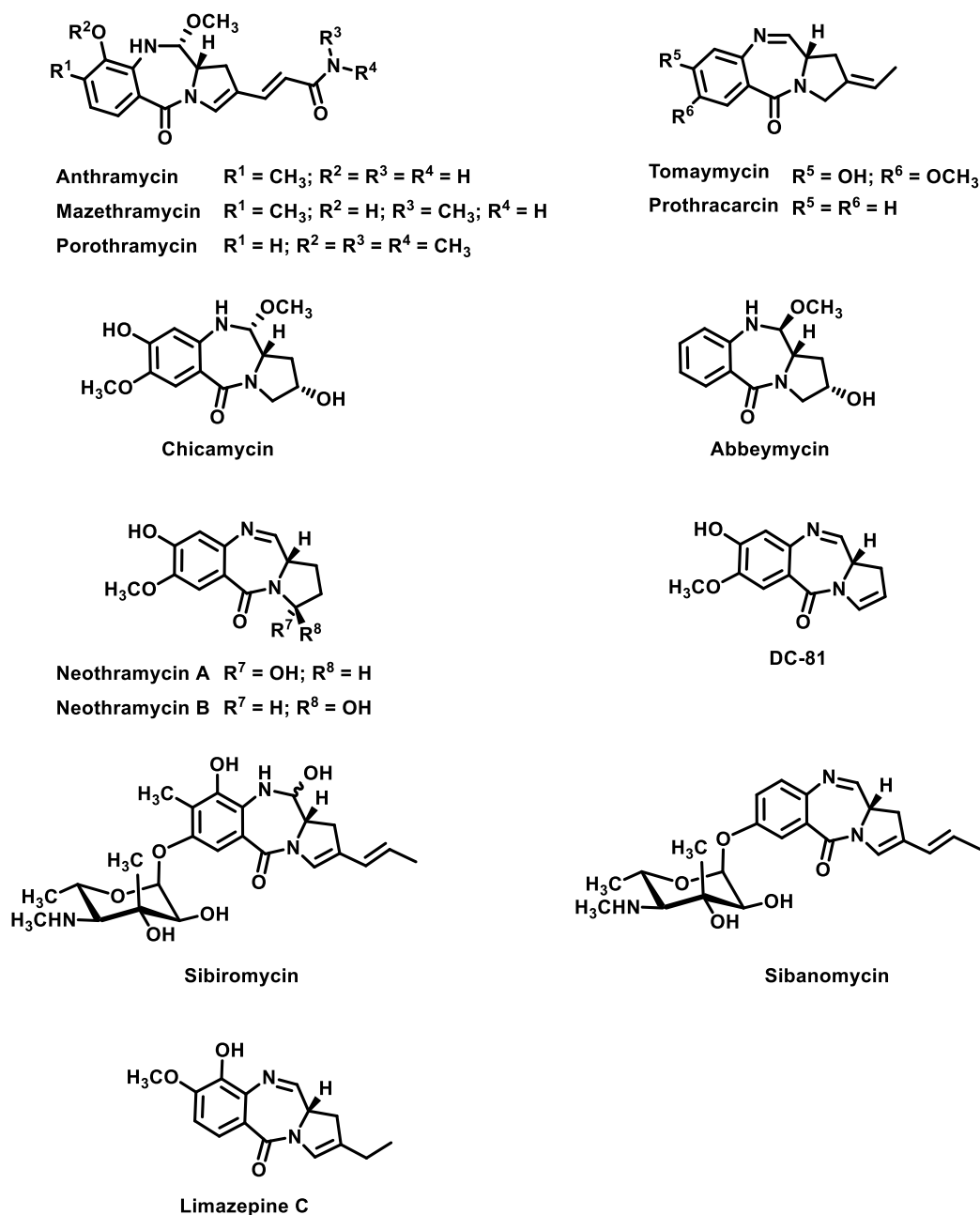
Figure 5: Structures of naturally occurring PBDs.[60]

2.1.2.1   PBD core structure

The tricyclic PBD core structure consists of an aromatic A-ring, a 1-4-diazepin-5-one B-ring, and a pyrrolidine C-ring. Both the A- and the C-ring can be decorated with several different substituents. As mentioned previously, the C-ring can furthermore be either fully saturated or unsaturated at an *endo*cyclic (C2-C3) or an *exo*cyclic (C2) position.

The (*S*)-stereo-configuration at the chiral C11a position provides these molecules with their characteristic right-handed helical shape. This internal twist gives rise to their ability to fit smoothly into the minor groove of DNA.[62]
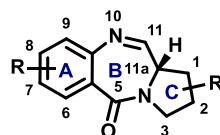
PBD core structure

Figure 6: PBD core structure consisting of the three rings A, B and C.

The imine functionality at the N10-C11 position is in a dynamic equilibrium with two other forms depending on the medium. If the PBD is dissolved in an aprotic, non-nucleophilic solvent, the equilibrium will be on the side of the imine. If the PBD is dissolved in a protic polar solvent like H_2O or MeOH, the imine is reversibly attacked and forms the respective hemiaminal or hemiaminal methyl ether.[60-61]

Under biological conditions, namely in aqueous media, the hemiaminal form is the main species. Yet, because of the above mentioned equilibrium the hemiaminal form is also active. Conversely, it should be noted that the minor groove of DNA creates a different chemical and electrostatic environment than simple solvation in water, which might lead to a shift in equilibrium possibly favoring the imine form.[60-61]
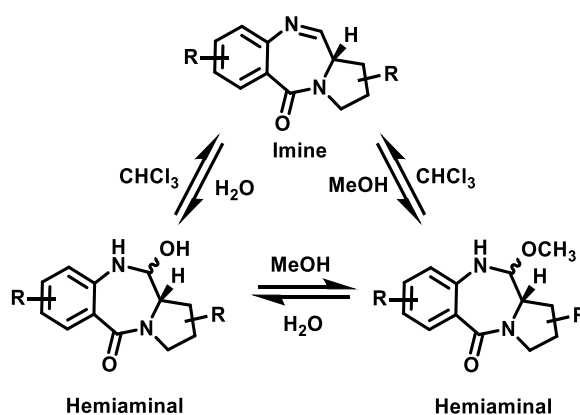
Scheme 8: Equilibrium between imine, hemiaminal and hemiaminal methyl ether forms of PBDs. Created in analogy to[60-61]

2.1.2.2 Mode of action

The mode of action of PBDs is known to be a two-step process (Scheme 8). First, a reversible non-covalent association to the DNA minor groove via H-bonding, van-der-Waals, and electrostatic interactions takes place. This is fostered by the internal twist caused by the (*S*)-configuration of the 11a position giving the PBD core a perfect three-dimensional shape to fit smoothly into the minor groove.[58],[60],[67] However, circular dichromism measurements using anthramycin showed that this non-covalent association into the minor groove is not an intercalation process.[68] In fact, sedimentation data and viscosity measurements of DNA-PBD complexes suggest that the helix is stiffened but not lengthened.[68]

In addition, it has been shown that PBD derivatives featuring a dilactam in ring B and therefore lacking the imine moiety utilize non-covalent interactions to bind to DNA.[69]

In the second step, the *exo*cyclic N2 of guanine attacks the imine bond in a nucleophilic fashion leading to a covalent bond. The newly formed aminal bond thus stabilizes the drug-DNA complex. [69] This is supported by studies of Narayanaswamy *et al*. showing that PBDs like SJG-136 do not react with sequences that do not feature a guanine residue, suggesting a guanine-directed nucleophilic attack.[70] This is supported by NMR studies on the anthramycin-DNA adduct showing a signal shift for the C11 position.[71] Furthermore, there have been several DNA footprinting, X-ray crystallography and molecular modeling studies further supporting this mechanism.[60]

While this is the case, the formation of an aminal bond is reversible, and so is the PBD-DNA bond formation. The relative weakness of the PBD-DNA bond is thought to play a key role in the general sequence selectivity towards R-G-R.[60],[72-73]
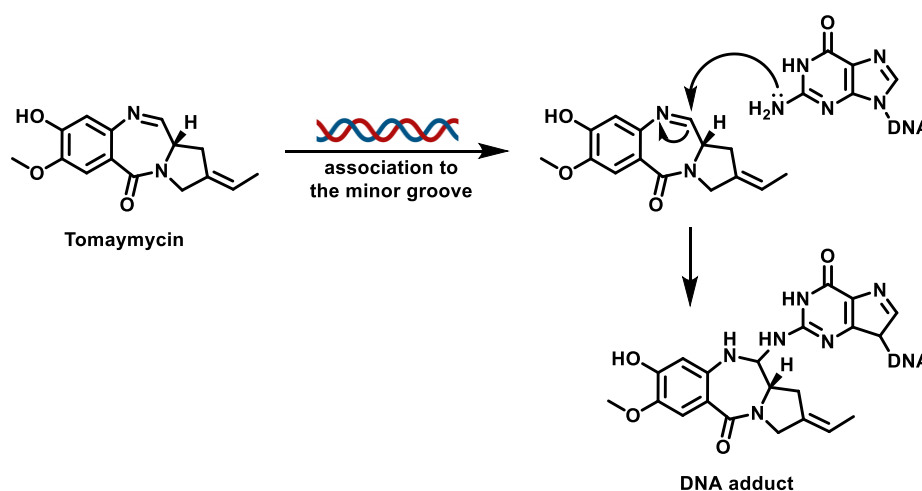
Scheme 9: Mode of action of tomaymycin.[74-76]

As mentioned above, PBDs experience an equilibrium of both the imine and the hemiaminal form in aqueous environments, which both are able to bind DNA as they interconvert continuously. The imine-based mechanism explains the observation of the two conformational forms (*S* vs. *R*) at the C11 position of the tomaymycin-DNA-adduct and the correlation of the proportion between the two. It is viewed as the most likely mode of action.[77]

Due to the alkylation of the DNA, PBDs can block transcription as exemplified by *in vitro* transcription termination assays.[46],[60],[78] Apart from this, it has been shown that DNA modification by PBDs lead to subsequent inhibition of transcription factor binding.[79]

2.1.2.3 PBD Synthesis

Leimgruber *et al*. reported the first total synthesis of anthramycin, laying the grounds for several synthetic routes of PBD scaffolds. The key step of the 16-step synthesis is the reduction of a protected dilactam to the corresponding hemiaminal using $NaBH_4$ (Scheme 10).[80]

The dilactam is obtained via a cascade of steps starting from the amide bond coupling of the amino acid derivative L-hydroxyproline methyl ester and the acid **22** generating the A-C fragment **23**. Reduction using sodium dithionite converted the nitro group to the corresponding aniline, and subsequent cyclization gave the dilactam **24**. The hydroxyl group, which originated from the L-hydroxyproline methyl ester, was oxidized to the corresponding ketone **25** using Jones oxidation. Wadsworth-Emmons olefination gave the ester **26**, which was converted to the aldehyde by DIBAL reduction and further converted to the sodium bisulfite adduct. Formation of the epimeric cyanohydrins and the mesylates was accomplished by reaction with potassium cyanide and methanesulfonyl chloride. Elimination of the mesylates **27** yielded a cis-trans mixture of conjugated nitriles in a 4:1 ratio favoring the trans product. Deprotection of the benzyl group yielded the free phenol, which was again protected by condensation with benzaldehyde dimethyl acetal. The amide **28** was obtained by hydrolysis of the nitrile using polyphosphoric acid. Reduction of the dilactam using $NaBH_4$ in methanol followed by final deprotection using HCl gave the natural product anthramycin methyl ether **29**.[80]
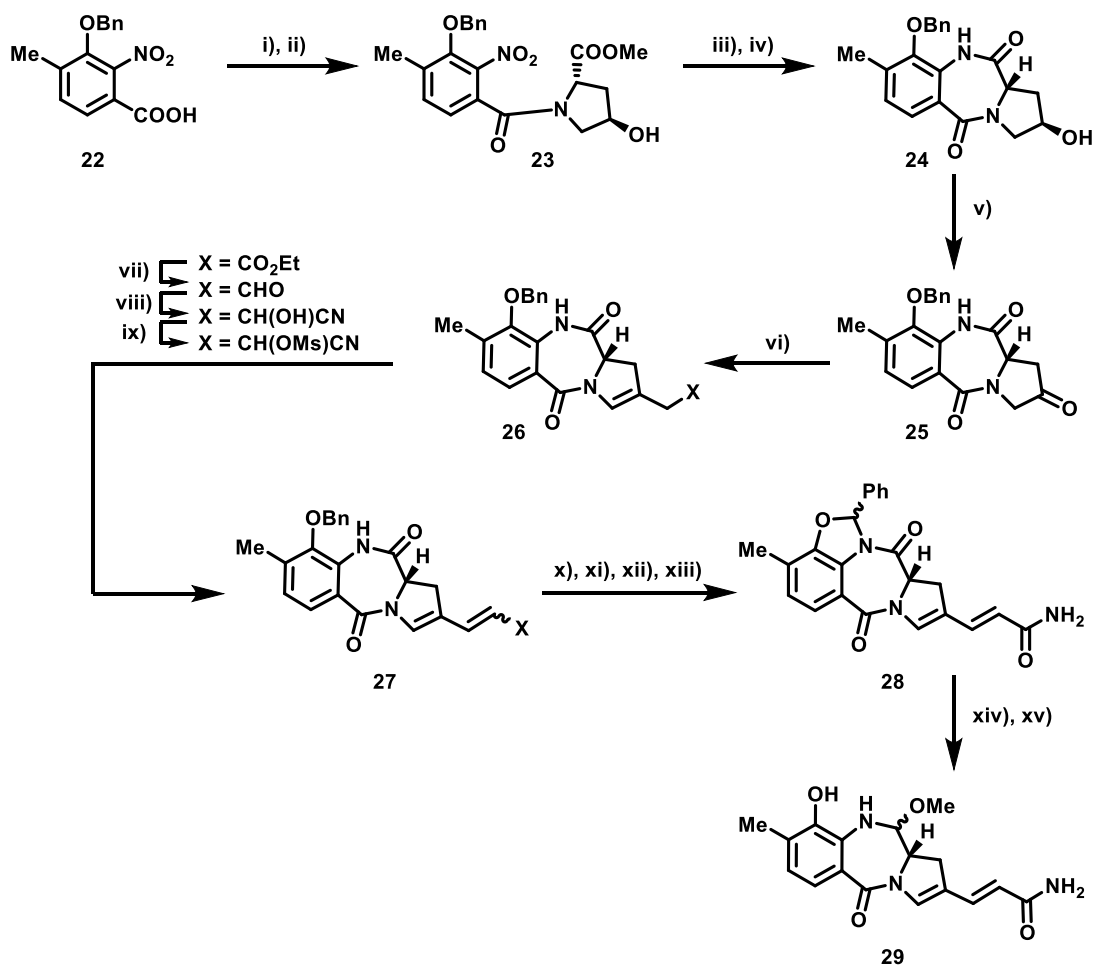
Scheme 10: Leimgruber's total synthesis of anthramycin. i) (COCl)$_2$, CH$_2$Cl$_2$; ii) methyl-L-hydroxyproline hydrochloride, THF, TEA; iii) Na$_2$S$_2$O$_4$, THF, water; iv) H$_2$O/HCl, THF; v) CrO$_3$/H$_2$SO$_4$/Acetone; vi) sodium triethylphosphonoacetate, THF; vii) DIBAL, toluene, -60 °C, viii) 1. NaHSO$_3$ 2. KCN; ix) MsCI, pyridine, 5 °C; x) TEA, benzene, reflux; xi) TFA, BF$_3$ Et$_2$O, r.t., HCl, MeOH; xii) PhCH(OMe)$_2$, H$_2$O/HCl, THF; xiii) PPA (aqueous workup); xiv) NaBH$_4$, MeOH; xv) 0.01 M HCl, MeOH.[80]

Since the first total synthesis of anthramcyin by Leimgruber *et al.* in 1968,[80] several synthetic approaches to various kinds of PBD derivatives have been published and patented. The key step in the synthesis of PBDs is the formation of the imine bond between the N10 and the C11. Different approaches described in the literature can be clustered into two groups. On the one hand, the imine is directly derived from an amine precursor and an electrophilic carbon, i.e., a C11 precursor. On the other hand, the imine is obtained via reduction of an amide bond of a PBD dilactam intermediate, as seen with the Leimgruber synthesis. This dilactam intermediate can be further disconnected opening ring B (Scheme 11).[60]

In both cases, this retrosynthetic analysis leads to a set of different A-C fragments. The electrophilic carbon required for B-ring closure is most often provided as a carboxylic acid

derivative in the case of synthetic routes featuring the dilactam intermediate or as an aldehyde in the case of the direct imine formation. However, aldehydes are frequently protected as acetals or thio acetals or kept as precursors (e.g., methyl ester or alcohol) prior to the final cyclization. The aniline involved in the ring closure is often masked as nitro, azido, or carbamate groups. Further disconnection of the A-C fragment reveals the ring A and ring C precursors. A ring building blocks are based on anthranilic acid derivatives, while the C ring building blocks are based on L-proline derivatives, providing the C11a (*S*) stereochemistry.[60]

This set of different synthetic approaches yielded a wide variety of synthetic PBDs, which gave rise to a better understanding of the structure-activity relationship of this compound class.
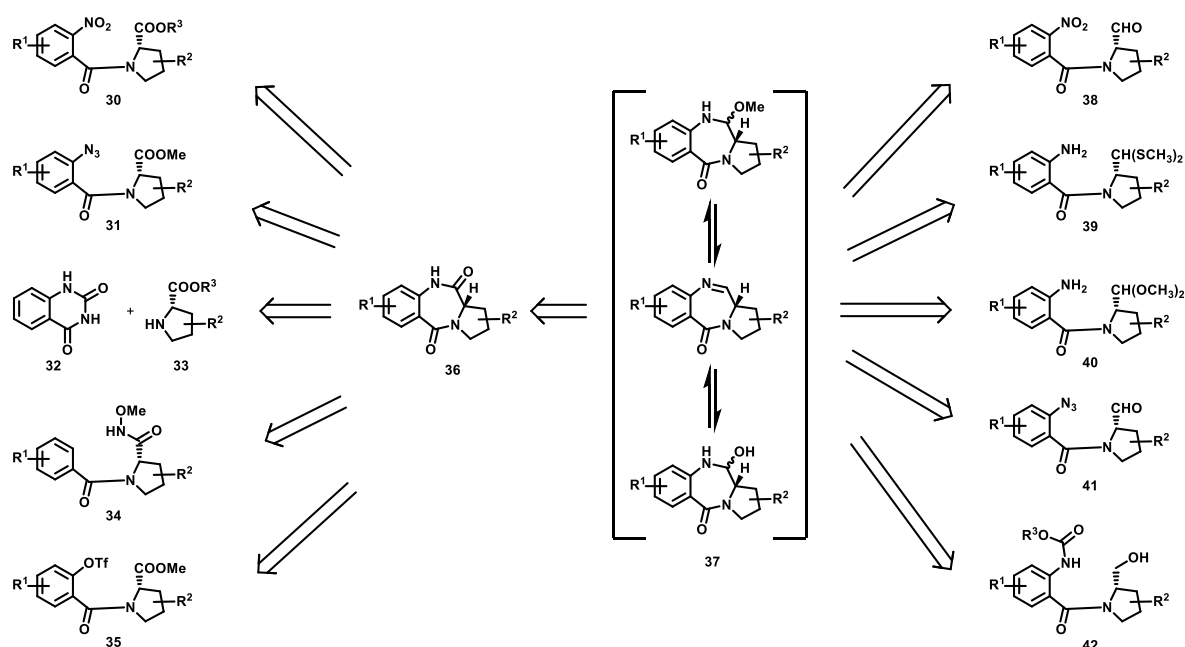
Scheme 11: Most commonly encountered synthons in published synthetic routes. Created in analogy to [60]

2.1.2.4 SAR

2.1.2.4.1 A-Ring

SAR studies on ring A revealed its influence on the cytotoxicity of PBDs. It is assumed that this effect is predominantly based on electronic factors, since electron-donating substituents lead to enhanced biological activity. The increased electron density within the ring enhances the basicity of the vicinal N10-nitrogen. As a results, the imine is more prone to protonation leading to an activated iminium species. This again increases the electrophilicity of the neighboring carbon C11, making it an even better target for the nucleophilic attack of the N2 of guanine. Electron-donating substituents thereby enhance the alkylation potential of PBDs. Consequently, electron-withdrawing groups reduce the alkylation potential.

However, electron-withdrawing groups can also stabilize the hemiaminal form whereas electron donating groups can stabilize the imine form.[72],[81-82]

In the past, a special interest was shown towards the effects of the C8 substitution and its influence on the cytotoxic potential of such derivatives. In order to improve the DNA binding properties by increasing the non-covalent interactions with the DNA many hybrid molecules have been synthesized, including PBD-polyamides, PBD-benzimidazoles, PBD-chrysene conjugates, and PBD-acridines (Figure 7).[78],[83],[83-87] In addition PBD hybrids with a second alkylating agent, including PBD dimers and known anticancer agents have been synthesized.[41],[72],[83],[88-90] Some of these C8 substitutions are well accepted and even lead to a stabilization of the PBD within the minor groove, e.g., PBD-polyamide.[91-93] Various hybrids share common structural features, like the usage of an amide bond to connect the PBD to the second alkylating agent. Furthermore, most hybrids contain a spacer unit based on two or more methylene groups.

43

PBD-polyamide conjugate

44

PBD-benzimidazole conjugate

45

PBD-chrysene conjugate

46

PBD-acridine conjugate

SJG-136
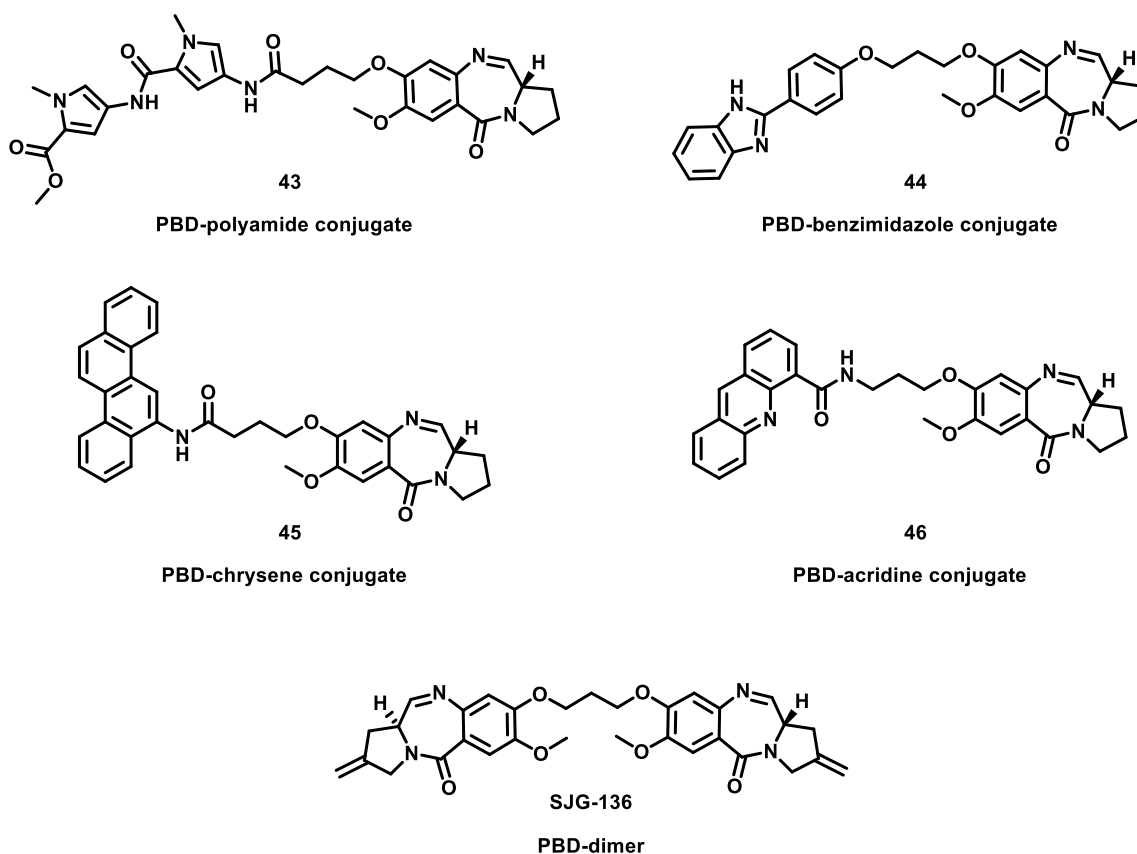
PBD-dimer

Figure 7: Examples for PBD hybrids/conjugates of different classes, i.e. PBD-polyamides, PBD-benzimidazoles, PBD-chrysene, PBD-acridines and PBD-dimers.[78],[83],[83-87]

The number of methylene groups present in the spacer are especially relevant for PBD dimers, which are connected via a simple double ether bridge (Figure 8). Studies showed that the length of C8/C8' ether-linked PBD dimers strongly affected the DNA cross-linking reactivity and the cytotoxic potency of the respective derivatives.[94-95] Changing the linker length from n = 3 (**48a**) to 4, 5 or 6 (**48b-d**) methylene units led to differences in the respective binding affinities. However, DNA binding was still observed. Increasing the linker length from n = 3 to n = 4 resulted in a reduction in cross-linking activity, DNA stabilizing ability and cellular cytotoxicity. Yet, if five methylene units were incorporated the cross-linking activity was similar to the n = 3 derivative (**47a**) and the DNA stabilizing ability was approximately reduced by half, while a significant increase in cellular cytotoxicity could be observed. These findings led to the assumption that linkers with an odd number of CH$_2$ units are advantageous for maximizing the cytotoxicity. This hypothesis was reinforced by molecular modeling studies showing that only linkers with odd numbers of methylene units led to the correct positioning of the PBD imine functionalities to be attacked by the DNA's guanine residue and thus enabling cross-link formation.[94-95]
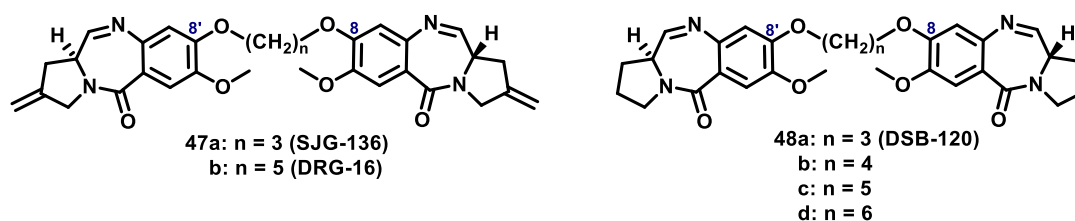
Figure 8: PBD dimers of varying linker length.[94-95]

Apart from C8 substitutions, C7 substitutions have been investigated. However, it is important to note that substituents of the C7 position point out of the minor groove, thus making this position undesirable for DNA-binding agents. Nevertheless, sibiromycin is an example of a natural PBD glycosylated at the C7 position, exhibiting a high DNA affinity and antitumor activity.[66]

Hydroxyl groups at the C9 position, which can be found in sibiromycin, anthramycin and others, on the one hand facilitate DNA interactions through hydrogen bonding, but on the other hand were found to induce dose-dependent cardiotoxicity.[96]

2.1.2.4.2 B-Ring

Ring B features two highly important chemical motives. First, the imine moiety is present in ring B. This functional group is key since it is responsible for the alkylation. The free amine of guanine nucleophilically attacks the imine leading to the formation of a covalent aminal bond and thereby alkylating the DNA. Second, ring B also carries a chiral center at the C11a position. The whole molecule gets slightly twisted, if this chiral center is in (*S*)-configuration, thus it has the right shape to fit smoothly into the minor groove of the DNA.[58] PBDs with an inverted stereochemistry fail to interact with DNA efficiently, since they are not isohelical with the DNA minor groove; this is reflected in the (*R*)-enantiomer's lower cytotoxicity.[72],[97-98]

Notably, PBDs lacking this functionality are still able to interact non-covalently with DNA. This interaction is shown for a PBD-dilactam lacing the imine functionality (Figure 9).[69] Guanine is not able to bind this PBD derivative covalently, due to the lack of the imine functionality, thus the specificity for guanine is lost.
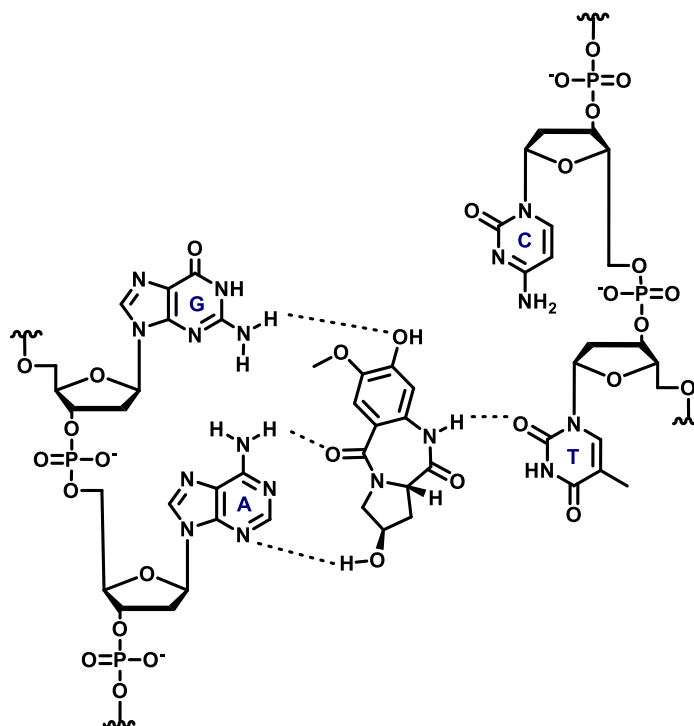
Figure 9: Non-covalent DNA interactions of a dilactam PBD. Created in analogy to[69]

Different types of non-covalent PBDs have been synthesized, replacing the imine functionality with an amide or a secondary amine, and their biological activity has been investigated. In accordance with the weaker nature of non-covalent bonds, the DNA-binding ability and the thermal stability were significantly lower than the ones obtained using PBDs with an imine functionality. [87],[99-100] However, it was reported that a mixed dimer carrying an imine functionality on one PBD and a dilactam on the other PBD led to an increase in DNA melting temperature of 17 °C (Figure 10). In contrast, the corresponding PBD dimer carrying only imines (DSB-120) led only to an increase of 15.4 °C.[101]

Additionally, mixed dimers carrying an imine functionality on one PBD and an amine on the other PBD also enhanced the DNA melting temperature, though only moderately (11 °C).[102] In comparison, studies on PBD dilactams showed an increase in DNA melting temperature by 2-3 °C.[69] PBD amidines led only to an increase of 0.7 °C.[103]

DSB 120
ΔT_m= 15.4 °C

49
ΔT_m= 3.0 °C

50
ΔT_m= 11.0 °C

51
ΔT_m= 0.7 °C

52
ΔT_m= 17.0 °C
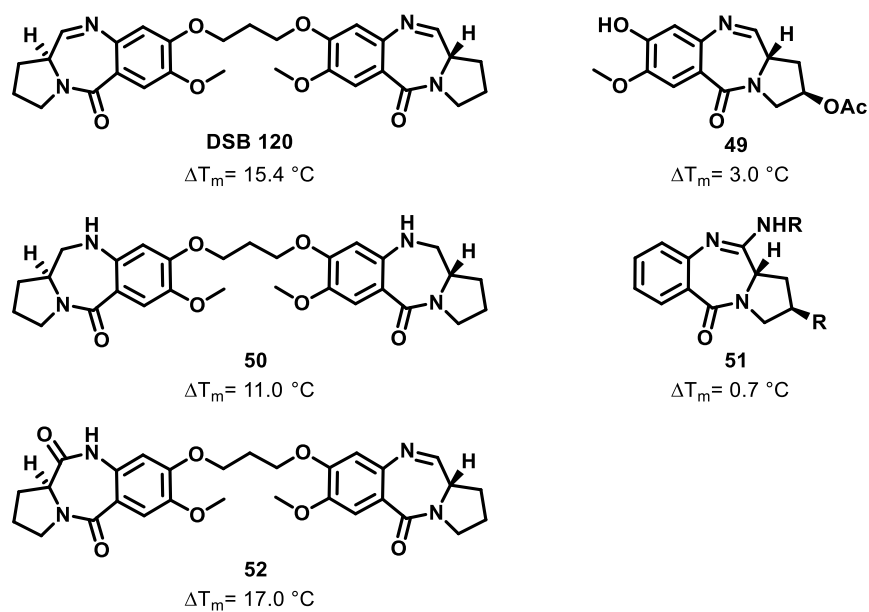
Figure 10: Impact of structural modifications of the N10-C11 bond on the thermal stabilization of DNA. Changes in melting temperature in comparison to the melting temperature of untreated DNA are given as ΔT_m.[69],[101-103]

2.1.2.4.3 C-Ring

In general, PBDs with an unsaturated C2 position show greater DNA binding potency and biological activity compared with unsaturated derivatives. The compounds with an sp^2 hybridization at C2 interact more efficiently and selectively with DNA compared with analogues with a sp^3 hybridization, thus leading to greater bioactivity. This is attributed to several factors such as the reduced reactivity towards cellular nucleophiles, the molecular shape, and the projection of the C2 substituents.[87],[104-107]

Alkylation of proteins or scavenging by cellular thiols could prevent the PBD from reaching its target and thus have a negative influence on PBD activity. These side reactions can be reduced through C2 unsaturation since this can lead to a lower electrophilicity at the N10-C11, thus reducing the likelihood of undesired nucleophilic attacks.[108]

The unsaturation of the C2 position also affects the molecular shape. The sp^2-hybridized C2 leads to a flattening of the C ring, which in turn leads to a change in torsion angles between the C-ring and the B-ring. Equipped with this slightly modified shape, C2 -unsaturated PBDs fit even more smoothly into the minor groove of DNA. It is postulated that this enhanced fit gives the C2-unsaturated PBD the opportunity to remain undetected by DNA repair mechanisms, allowing the PBD-DNA adduct to sustain for a longer period of time.[87]

2.1.2.5 Tomaymycin

First isolated in the 1970s from *Streptomyces achromogenes,* tomaymycin is a natural product belonging to the group of PBDs. It exhibits antitumor as well as antibiotic activity and therefore is the basis for a wide variety of synthetic analogues.[41],[58],[61],[109-110] Investigations on the biosynthesis of tomaymycin, sibiromycin, and anthramycin showed a common set of genes that encode a bimodular nonribosomal peptide synthetase (NRPS).[66],[111-112]

The genes encoding for the NRPS of tomaymycin in particular are denoted *tomA* and *tomB*. Müller and co-workers were able to reconstitute the NRPS system consisting of TomA and TomB *in vitro,* gaining a detailed understanding of the tomaymycin biosynthesis. In the first step, anthranilic acid, which is produced by the Shikimate pathway, is oxidized by TomO, yielding a 5-hydroxy derivative. Next, 5-hydroxyanthranilic acid is loaded onto TomA and subsequently processed by TomE and TomF, incorporating the second hydroxyl group at the C4 position. Still bound to TomA, methylation takes place via TomG employing *S*-adenosylmethionine (SAM) as methyl donor. TomA now transfers the A-ring building block onto TomB, which provides the proline core, forming the amide bond of ring B. A final cyclization catalyzed by TomB using ATP and NADPH yields tomaymycin. Even though this biosynthesis was assessed as the most plausible one, the authors also proposed an alternative second pathway (Scheme 12). This additional possible pathway is characterized by all modifying steps taking place prior to processing by TomA and TomB (i.e., the introduction of the 4-hydroxyl group by TomE and TomF as well as the methylation of the phenol (*para* to the aniline) by TomG). TomA and TomB than, as described above, catalyze the assembly of the A-C fragment and the subsequent cyclisation forming tomaymycin.[113]
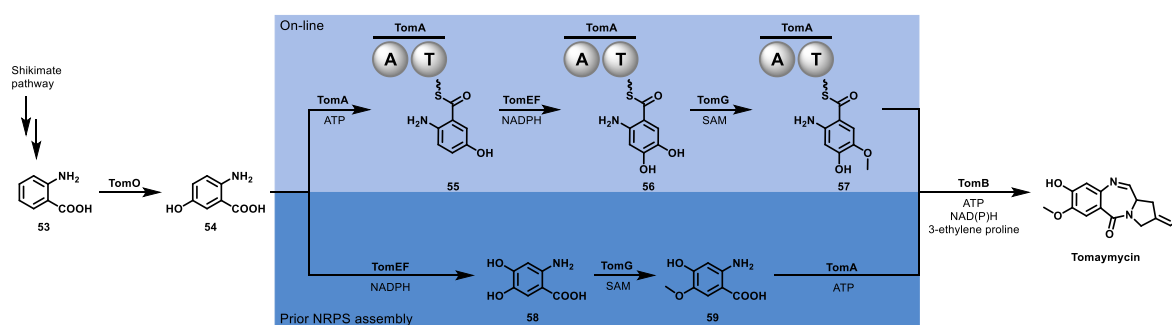
Scheme 12: Two possible pathways for the tomaymycin biosynthesis starting from anthranilic acid. A = adenylation domain, T = thiolation domain. Created in analogy to[113]

2.1.2.6 PBD dimers

PBD dimers possess two PBD cores and therefore two alkylating moieties. Those dimers have the advantage of binding DNA via two imine functionalities and thus broadening their mode of action by adding the ability to form *intra-* and *inter*-strand cross-links.[67] The concept of two linked PBDs was first proposed by Suggs and co-workers by linking two PBDs via their respective C7 position using a set of different linkers including thioethers, ethers, and secondary amines.[114-115] Although initial experiments with C7 linkages resulted in poor DNA binding and low cytotoxicity, the concept was picked up and further developed by Thurston and co-workers. Especially derivatives linked through the C8 position showed enhanced DNA binding and cytotoxicity due to their improved three-dimensional shape, which is more isohelical with the minor groove (Figure 11).[116]
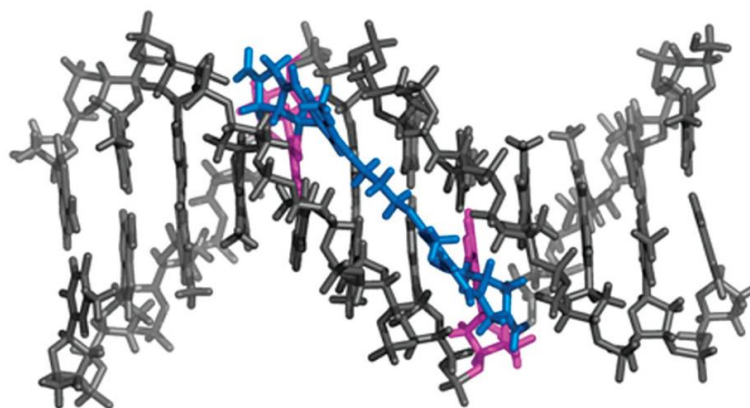
Figure 11: Molecular modeling of the *inter*strand cross-link formed by SJG-136 with R-GATC-Y. SJG-136 highlighted in blue, guanine residues highlighted in pink. Reprinted from [67]

2.1.2.6.1 SJG-136

Reaching phase II clinical trials for treatment of leukemia and ovarian cancer, SJG-136 can be considered one of the most prominent representatives of the group of PBD dimers (Figure 12). A simple 1,3-propanedioxy ether connects two PBD units at their respective C8 positions. The PBD units are deduced from tomaymycin being C2/C2' *exo*methylene derivatives.[58]

Gregson *et al*. investigated the DNA cross-linking ability and could show that SJG-136 is 440-fold more potent DNA cross-linker than melphalan, which belongs to the group of

nitrogen mustards.[87] Furthermore, a comparison with DSB-120, a simpler proline-based analogue, as well as additional modeling studies, suggested that the C2/C2' *exo*methylene moieties of SJG-136 lead to a flattening of the C ring, thus giving the molecule a better fit in the minor groove and thereby giving a lower-energy adduct.[87] A second advantage of the C2/C2' *exo*methylene group is its contribution to the reduced electrophilicity of the PBD, leading to a decrease in collateral interactions with, e.g., proteins carrying thiol groups or other nucleophiles like glutathione.[108],[117] The authors suggested that this might lead to a greater bioavailability of SJG-136.[87] *In vivo* pharmacokinetic data showed differences in blood stability of SJG-136 (loss of ~30% over 6 h) and DSB-120 (loss of 80% within 10 min), even though SJG-136 shows lower levels of plasma protein binding compared to DSB-120.[118]

As mentioned above, the structural features of SJG-136 allow for its enhanced fit into the minor groove. This is also reflected by molecular modeling studies suggesting no or insignificant disruption of the DNA helix after cross-linking by SJG-136.[87] Also, the compound is not exposed to the outside after adduct formation but is completely lodged within the minor groove. Since repair enzymes regularly detect distortion or helical perturbations caused by a variety of alkylating agents,[119] it is hypothesized that the absence of such distortion or perturbation the molecule's perfect fit into the minor groove is the reason for the observed resistance to DNA repair.[58]

Moreover, SJG-136 does not bind randomly to DNA but rather exhibits a certain sequence selectivity as it preferably binds to R-GATC-Y.[67],[70],[87],[107],[120]
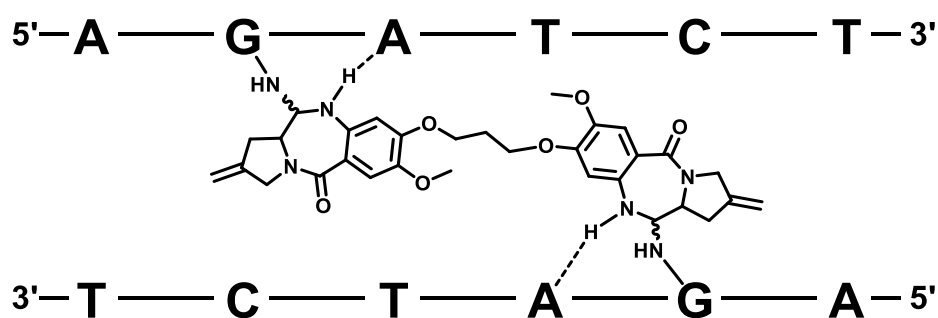
Figure 12: Illustrative depiction of SJG-136 cross-linking DNA via an *inter*-strand linkage. Created in analogy to[58]

However, since SJG-136 exhibits a set of different binding modes (i.e., *intra*-strand linkage, *inter*-strand linkage, and mono-adduct), it also binds to a set of sequences depending on the binding mode. *Intra*-strand cross-links can be observed at R-GATG-Y as well as at the longer sequence of R-GAATG-Y, *inter*-strand cross-links occur at R-GATC-Y

(compare above) as well as R-GAATC-Y and mono-adducts are formed at guanine residues where a second guanine residue is too far away and thus preventing a cross-link. A direct comparison between these sequences showed the following reactivity: R-GAATG-Y > R-GATC-Y > R-GATG-Y > R-GAATC-Y.[67]

According to molecular modeling studies, the imine functionalities of SJG-136 are ideally positioned in order to be attacked by the free amine of the guanines in a R-GATC-Y sequence, leading to an *inter*-strand cross-link. The same holds true for R-GATG-Y leading to an *intra*-strand cross-link. Binding to those two motives leads only to little distortion of the DNA helix. Binding to the R-GAATC-Y and R-GAATG-Y sequences, on the other hand, is accompanied by a distortion of the DNA helix and SJG-136 moving to a slightly lower position in the minor groove to be able to span the increased distance.[67]

2.1.2.6.2 Further relevant dimers

Apart from SJG-136, there are other dimers that are of clinical relevance. About twenty antibody-drug conjugates (ADCs) with PBD dimers as the warhead have entered the clinics so far. Due to the fact that PBD dimers like SJG-136 are highly potent DNA cross-linking agents, this compound class became attractive for the use as warheads in ADCs. This can be explained by two factors. First, using PBD dimers in ADCs reduces the toxic side effects and enhances selectivity. Second, the high potency allows the construction of ADCs with lower drug-antibody ratios.[121-122]

Zylonta is an antibody-drug conjugate that was granted accelerated approval by the FDA in April 2021 for adult patients with relapsed or refractory large B-cell lymphoma after two or more lines of systemic therapy (Scheme 13).[123] Zylonta was given orphan drug designation by the FDA for this indication. The ADC consists of an anti-CD19 humanized IgG1κ antibody, which is conjugated to the PBD dimer SG3199 via a cleavable linker.[123] This specific combination of this linker and SG3199 as the PBD dimer is called tesirine. Thus the ADC is referred to as loncastuximab tesirine.[124]

The linker consists of four different units with specific functions. A maleimide unit is used to connect the linker to one of the cysteine sidechains of the antibody. It is connected via a spacing PEG8 unit to two amino acids (Val-Ala) that provide the proteolytic cleavage site of the linker. Utilizing an amide bond, the two amino acids are connected to a self-immolative *para*-aminobenzyl alcohol (PABA) unit. The PABA unit is, in turn, connected

to the drug, i.e., SG3199, through a carbamate. Upon proteolytic cleavage of the amide bond connecting the alanine and the PABA unit, the latter decomposes via a spontaneous 1,6-elimination, releasing CO_2 and the free drug (Scheme 13).[125]

SG3199 belongs to the family of PBD dimers and represents the active warhead. In contrast to SJG-136, SG3199 consists of two PBD units connected via a pentyldioxyether bridge rather than a propyldioxyether bridge between the two C8/C8' positions of the PBD cores. Another difference can be found in the PBD cores. SJG-136 has a C2 *exo*methylene unit, whereas SG3199 has an *endo* unsaturation at the C2 position. As to be expected with PBD dimers, SG3199 forms cross-links of DNA strands. The cross-linking ability of SG3199 was verified *in vitro* with purified DNA but also *in cellulo* using a comet assay.[126]
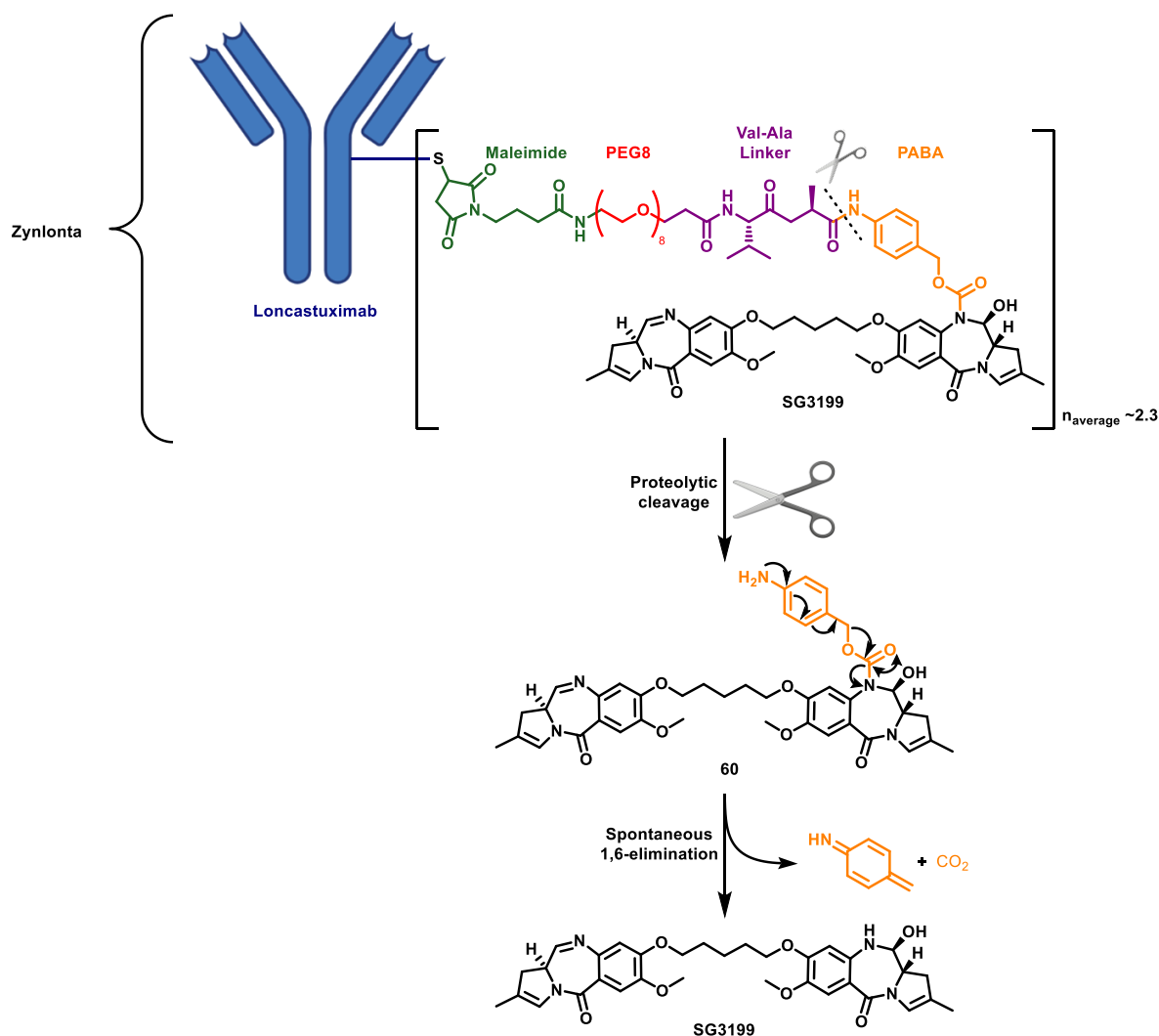
Scheme 13:Architecture and mechanism of release of the marketed antibody-drug conjugate Zynlonta carrying the PBD dimer SG3199 as the active substrate. PEG = polyethylene glycol; Val-Ala = Valine-Alanine; PABA = *para*-aminobenzoic acid. Created in analogy to[125]

Vadastuximab talirine is another antibody-drug conjugate utilizing a PBD dimer as the warhead. More precisely, it consists of the humanized anti-CD33 antibody h2HI2, which is conjugated via a cleavable linker to the drug SGD-1882. The specific combination of this linker and SGD-1882 is referred to as talirine. This linker is simpler than the one used in the Zynlonta ADC. It consists of a maleimide unit in order to provide the linkage to a cysteine of the antibody and the valine-alanine dipeptide. The terminal alanine is connected via an amide bond to SGD-1882. Proteolytic cleavage of the amide bond releases the drug (Scheme 14).[121]

SGD-1882 possesses structural features of both SJG-136 and SG3199. Similarly, to SJG-136, both cores of SGD-1882 are linked via a propyldioxyether bridge. Yet, the cores have an *endo-exo* unsaturation at the C2 position, as is the case for SG3199. The probably most obvious difference to the previously discussed structures is the *para*-methoxyphenyl and the *para*-aminophenyl residues of the respective cores, making SGD-1882 an asymmetrical dimer. This *para*-aminophenyl residue is essential since it enables the conjugation to the linker via a simple amide bond.[121]
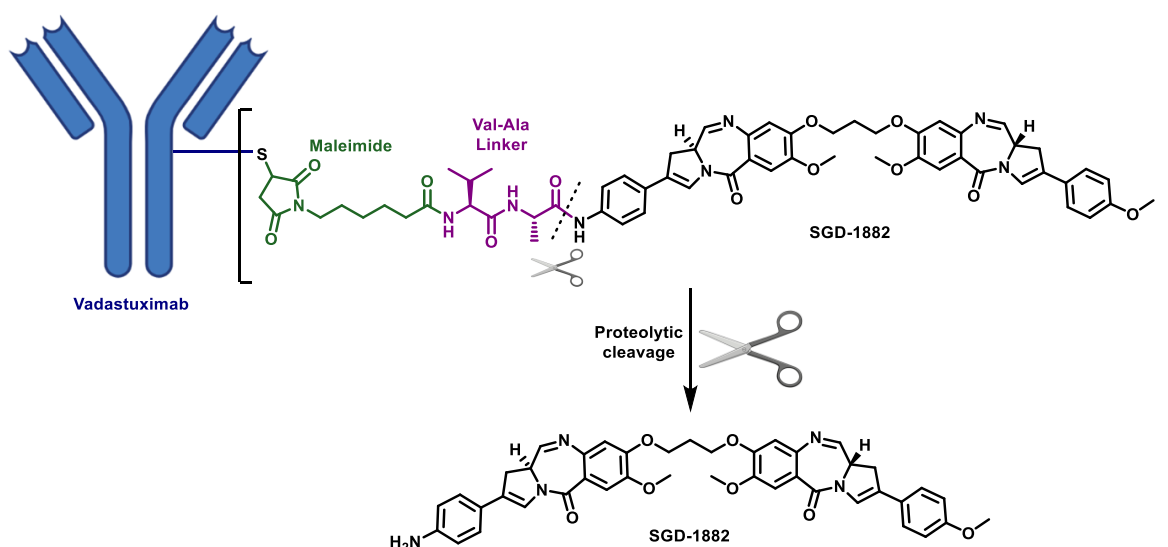
Scheme 14: Architecture and mechanism of release of the antibody-drug conjugate Vadastuximab talirine carrying the PBD dimer SGD-1882 as the active substrate.[121]

However, the phase III clinical trial of vadastuximab talirine was terminated because of an increased rate of deaths, including fatal infections in the vadastuximab talirine-containing arm.[121]

2.1.3 Analytical methods

There are various ways to analyze DNA-drug adducts, including ^{32}P-postlabeling, LC–MS, GC–MS, CE–MS, fluorescence detection, immunoassay, and electrochemical detection.[127-128] This chapter will focus on the use of HPLC-MS to detect DNA-drug adducts.

2.1.3.1 High-performance liquid chromatography

High-performance liquid chromatography (HPLC) is a widespread and popular method. Especially reversed-phase (RP) systems enjoy extensive use, because they enable the separation of polar molecules.[129] In the separation process, the mixture of analytes is exposed to two phases, a stationary and a mobile phase. The stationary phase consists of a porous surface-active material coated onto a solid support. Common stationary phases are based on modified silica. These modifications are based on the hydroxyl groups of silica, which can be modified with different alkyl groups providing a lipophilic surface. Depending on the type of modification, the properties of the solid phase can be adjusted to the application's needs.

The mobile phase, on the other hand, consists of a polar aqueous solution with an organic modifier. The separation of the mixture of analytes is based on the hydrophobic interactions with the stationary phase and the hydrophilic interactions with the liquid phase. Hence, the more hydrophilic an analyte, the less it interacts with the stationary phase and the more it interacts with the mobile phase. Consequently, the more hydrophobic an analyte, the more it interacts with the stationary phase and the less it interacts with the mobile phase, thus achieving separation of the mixture.[130] Usually, this type of separation is carried out mechanically at high pressures, which results in particularly effective separation performance.

In the vast array of applications, HPLC has also been used to separate DNA oligonucleotides. The fact that oligonucleotides are highly polar molecules, which is mainly due to the negatively charged phosphodiester backbone, hamper an efficient separation process since the oligonucleotide undergoes only minimal interactions with the stationary phase and is well dissolved in the mobile phase.[131-132]

However, this problem can be addressed by employing volatile ion-pairing buffers as the mobile phase. The ion-pairing reagents used in these buffers contain amphiphilic ions, i.e.,

ions which carry hydrophobic groups. Therefore, they create a positively charged double layer on the surface of the stationary phase (Figure 13), thus mediating an indirect interaction of the oligonucleotide's negatively charged phosphodiester backbone and the hydrophobic stationary phase. The separation is hence governed by the electrostatic interactions of the phosphodiester backbone with the ion-pairing reagent and the hydrophobic interactions of the ion-pairing reagent with the stationary phase. These interactions are further influenced by the organic modifier in the mobile phase. If the percentage of the organic component is enhanced, the amphiphilic ions are desorbed from the surface of the stationary phase. Thus, the interactions of the oligonucleotides with the stationary phase are weakened, and the samples elute from the column.[132-133]

Frequently used ionpairing agents for RP-HPLC are triethyl ammonium salts, e.g., triethyl ammonium acetate (TEAA).[134] Yet, if the HPLC is coupled to a mass spectrometer for analysis, TEAA often has a negative impact on ionization.[135] Other ion-pair reagents, e.g., 1,1,1,3,3,3-hexafluoroisopropanol (HFIP), triethyl ammonium bicarbonate (TEAB) or butyl dimethylammonium bicarbonate overcome these issues and thus provide a good compromise between LC separation efficiency and ionization in mass spectrometry.[135-136]
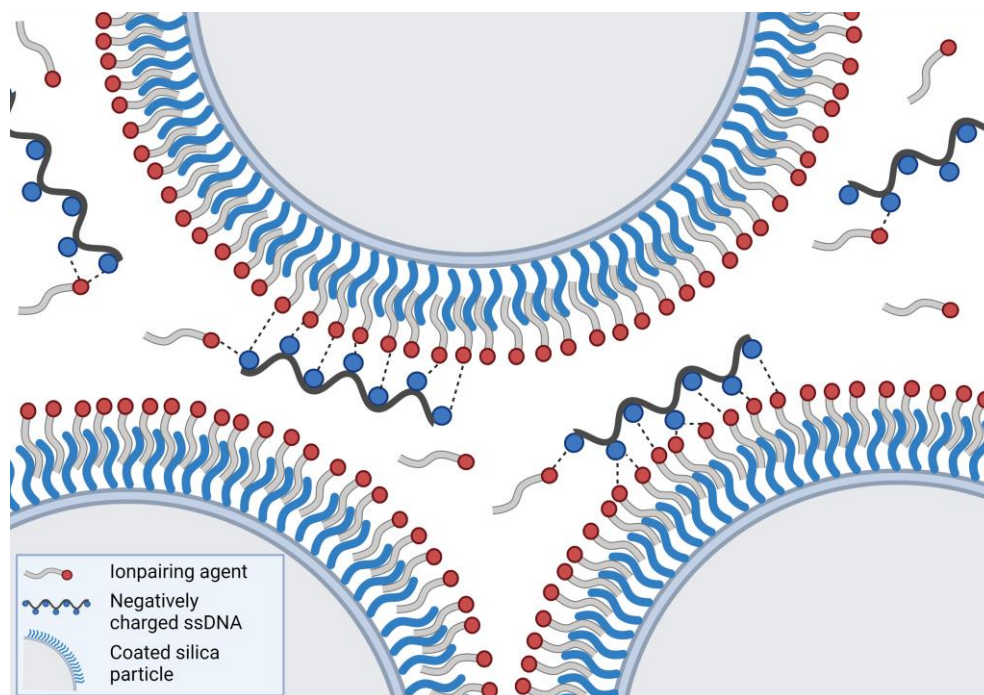
Figure 13: Hydrophobic interactions of the ionpairing agent (e.g triethylamine) with the stationary phase and electrostatic interactions of the same ionpairing agent with the phosphodiester backbone of ssDNA. Created with BioRender.com.

2.1.3.2 Mass spectrometry

Mass spectrometry (MS) is a powerful method, which is reflected by the vast array of fields it is employed in, reaching from proteomics[137] and metabolomics[138] over environmental analysis[139] and forensic analysis[140] to archaeology[141] and space exploration.[142] As mentioned in the previous section, mass spectrometers are often coupled to an HPLC system to analyze the different fractions obtained. High-performance liquid chromatography-mass spectrometry (HPLC-MS) is a widespread method for the characterization and quantification of covalent DNA modifications.[127],[143-144] Gas chromatography-mass spectrometry (GC-MS) is not as commonly used, since many adducts are thermally unstable. Yet, GC-MS is used for DNA adducts resulting from the reaction of reactive oxygen species with DNA and other specific classes of DNA adducts.[145]

In the field of DNA-adduct analysis using mass spectrometry, DNA samples are routinely hydrolyzed or digested in order to obtain nucleobases, nucleosides, or mononucleotides followed by separation via HPLC or capillary electrophoresis before they are analyzed by MS. The analysis often includes collision-induced dissociation (CID). This leads to the fragmentation into daughter ions, which are typically dominated by the neural loss of the deoxyribonucleic acid, leaving the potentially altered nucleobase.[146-147]

Nevertheless, also whole oligonucleotides can be analyzed with mass spectrometry. Due to their mild ionization, electrospray ionization (ESI), as well as matrix-assisted laser desorption/ionization (MALDI) have proven to be particularly beneficial when analyzing full-length oligonucleotides. The spectra obtained by those two methods differ greatly. While MALDI gives spectra with a predominant single charged ion, ESI leads to different charge states of a molecule and thus gives several signals with different mass-to-charge ratios (m/z).[148]

Independent of the ionization method, oligonucleotides are regularly detected in negative ion mode because of their polyanionic nature, which is due to the phosphodiester backbone. Despite that, analysis in positive ion mode has also been reported.[149] Another characteristic resulting from the polyanionic nature is the tendency to form sodium or potassium adducts leading to lower sensitivity and mass accuracy. Meanwhile, the formation of salt adducts is less problematic in HPLC-MS compared to direct MS analysis.[148]

2.1.3.2.1 Multiple reaction monitoring

In addition to the full-length measurement, it is also possible to further fragment the parent ion as indicated above. A method that makes use of this principle is multiple reaction monitoring (MRM). MRM is widely applied in various fields, including proteomics,[150] pharmacokinetic (PK) studies,[151] food forensics,[152] and detection of (oligo-) nucleotides.[153] At its early stage, the technology was mainly used to analyze small molecules.[154]

MRM studies can be performed using triple quadrupole (QQQ) instruments, which consist of three quadrupoles Q1, Q2, and Q3. Q1 and Q3 serve as tandem mass filters, while Q2, which is located between Q1 and Q3, is utilized as a collision cell. A schematic layout is provided in Figure 14.[150] Q1 filters for the often multiply-charged targeted precursor ion. Subsequently, the precursor ion enters the collision cell (Q2), in which fragmentation takes place. One of the daughter ions is then selected by the last quadrupole Q3. Thus, a specific mother/daughter ion pair can be monitored using this method. Such ion pairs are also referred to as transitions. A quantification of the molecule of interest can be provided via the integration of the peaks of each mother/daughter ion pair. Such quantifications can be relative if an internal standard is used but also absolute if an external standard is used.[150]
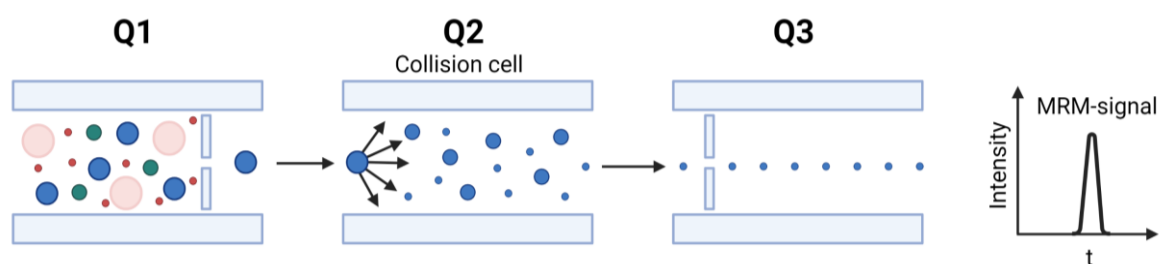
Figure 14: Schematic setup of a triple quad (QQQ) instrument used for multiple reaction monitoring. Filters are only depicted to represent the filtering process of the respective quadrupole and are not physically present in the instrument. Created with BioRender.com.

This method persuades by its ability to detect low quantities of the target in rather complex matrices due to the two filtering steps and thus resulting improved signal-to-noise ratio. It is important to note, though, that the target and its transitions need to be known to select the correct ion pairs.[150]

2.1.4 Self-assembling drugs

Self-assembling drugs exploit the synergistic interaction of two components that form a new chemical bond and, thus, a new drug with higher biological activity. The two components act as prodrugs or precursors, which assemble the product drug *in situ*.

The advantages of this approach include an enhancement in the therapeutic index if one of the precursors accumulates at the target site resulting in higher concentrations compared to normal tissue or off-targets. The resulting higher rates of active compound formation at the target site lead to a target-selective synergism. At the same time, the toxic effects on healthy tissue are reduced as the drug formation rate is decreased compared to the target site due to the lower concentration of the respective precursors.[155]

Furthermore, a self-assembling of drugs in situ leads to a steeper dose response curve compared to the pre-assembled drug, which could translate into an enlarged therapeutic window.[156] This could be successfully shown for the combination of decanal (**61**) and *N*-amino-*N*-1-octylguanidine (**62**), mediating erythrocyte lysis (Scheme 15).[156]

Another advantage inherent to the self-assembling approach is the fact that if the biophysical properties of the preassembled drug are poor, they can be refined by administering a combination of precursors with improved biophysical properties. As the two precursors have lower molecular weights than the preassembled drug, they should exhibit higher solubility, better membrane permeability, and less serum protein binding than the preassembled drug, thus enhancing the overall potency by tuning the bioavailability of the active compound at the target site.[157]
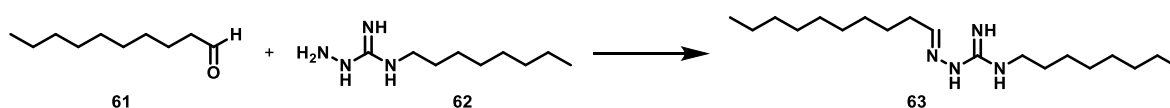
Scheme 15: In situ formation of the cytotoxic *N*-decylidenimino-*N*'-1-octylguani-dine (**63**) from precursors decanal (**61**) and *N*-amino-*N*-1-octylguanidine (**62**).[156]

Such strategies have been employed in antimicrobial as well as anticancer drug development. One example is the combination of aldehydes with acrylhydrazines for the *in situ* formation of antimicrobial hydrazones to address the intracellular pathogen *Salmonella typhimurium*. This pathogen can evade the immune system of mice as they survive in the acidic macrophage phagolysosome. The combinations of 2-hydrazinopyridine (**64**) and pyridine-2-carboxaldehyde (**65**), as well as 5-nitro-2-furaldehyde (**67**) and semicarbazide (**68**), exhibit

a higher selectivity towards bacteria at pH5 as the hydrazone formation is acid-catalyzed and thus is accelerated in acidic media (Scheme 16).[155, 157-158]

In addition to the selectivity, the precursors 5-nitro-2-furaldehyde (**67**) and semicarbazide (**68**) show enhanced water solubility (~100×) compared to the active drug **69**. Underlining the physiochemical advantages of this approach in regard to administering drugs.[157-158]
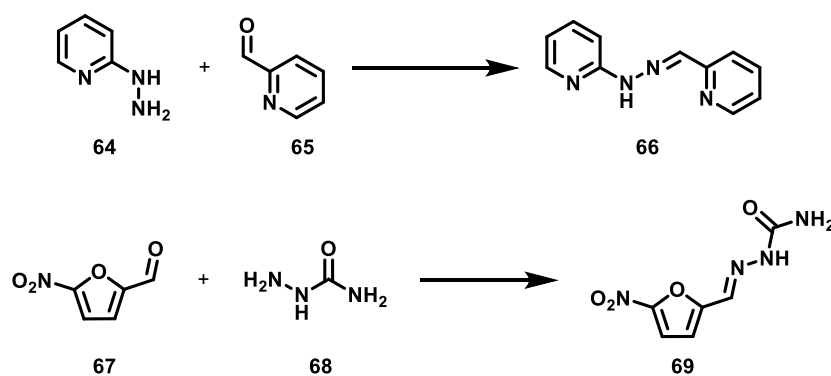
Scheme 16: Synergistic antibacterial combinations.[155, 157-158]

Another example of self-assembling drugs is the combination of **70** and **71** as protein kinase C (PKC) inhibitors (Scheme 17). PKC is involved in tumor progression and tumor cell proliferation as it phosphorylates proteins, which are associated with the regulation of gene expression and, thus, a target for antitumor drugs. The two single components **70** and **71** do not inhibit PKC (IC$_{50}$ > 200 µm); the newly formed hydrazone **72**, on the other hand, is capable of inhibiting PKC (IC$_{50}$ = 20.4 µm). The synergistic effect is also reflected by the cytotoxicity of hydrazone **72** being more than twice as toxic as the individual components. Studies further showed that combinations of the unreactive compounds **73** and **74** do not show synergistic effects against tumor cells.[157],[159-160]

A

B

C
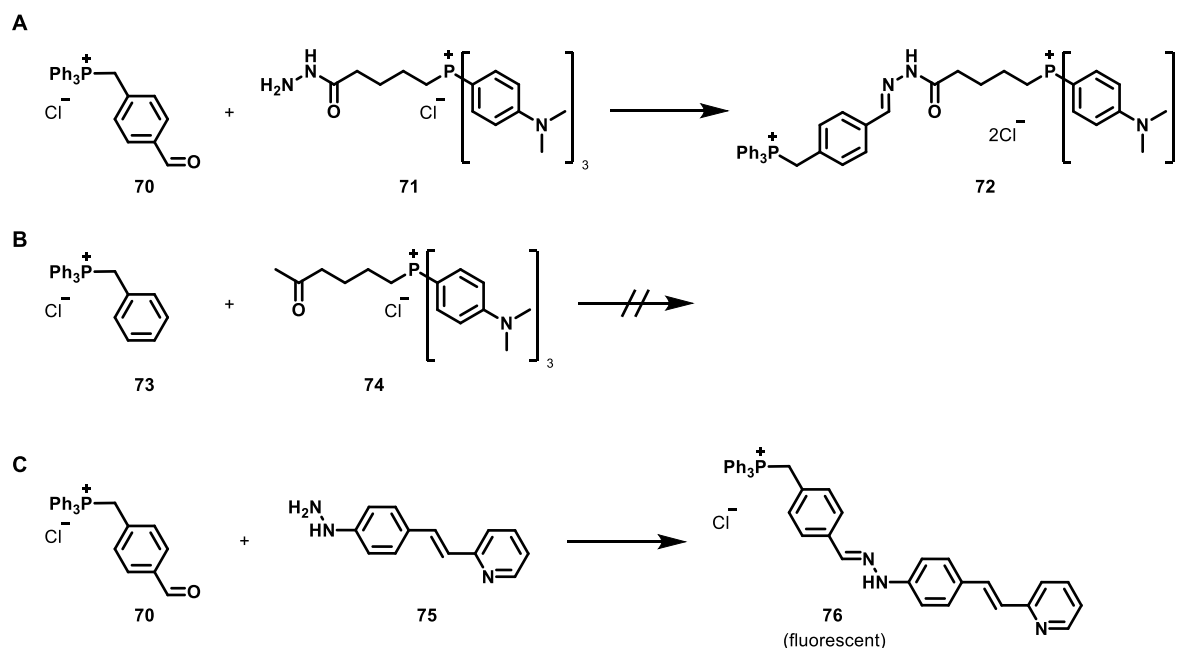
Scheme 17: A) Self-assembling of cytotoxin **72** from precursors **70** and **71**; B) Unreactive negative controls **73** and **74**; C) Self-assembling of the fluorescent cytotoxin **76** from precursors **70** and **75**.[157-160]

Further efforts building on this system gave rise to the combination of **70** and **75**, forming the active drug **76**, which exhibits an 11-fold increase in cytotoxicity compared to **72**, but is also more fluorescent than both prodrugs. Especially the increase in fluorescence is of great importance as it allowed for direct observation of the self-assembly in vivo.[157-158]
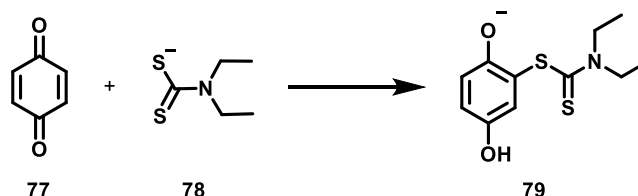
Scheme 18: Self-assembly of **79** from precursors **77** and **78** by carbon sulfur bond formation.[157]

Apart from hydrazone formation, other reactions can also be used for the self-assembling approach. Rideout *et al*. reported the formation of a carbon-sulfur bond leading to a synergistic cytotoxic effect.[157] Herein, benzoquinone (**77**) and diethyldithiocarbonate (**78**) are combined, yielding hydroquinone **79** (Scheme 18). In this case, the mechanism of action is altered; while the cytotoxicity of benzoquinone is caused by its alkylating properties, adduct **79** induces oxidative stress by catalyzing the formation of hydrogen peroxide from oxygen and NADH.[157]
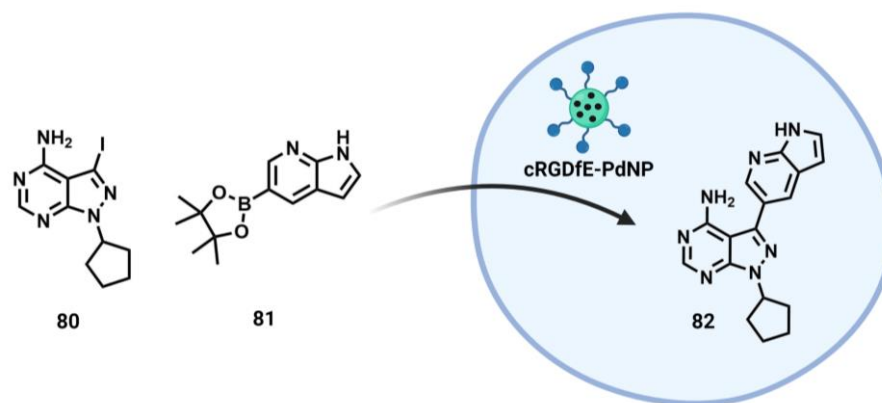
Scheme 19: Pd-catalyzed Suzuki–Miyaura cross-coupling synthesis of anticancer agent **82**. **cRGDfE-PdNP** = cRGD functionalized Pd-loaded particles. Created in analogy to [161]. Created with BioRender.com.

More recently, transition metal-catalyzed reactions have also been employed for the *in situ* synthesis of drugs. Bradley and co-workers reported the use of a targeted Pd catalyst consisting of Pd nanoparticles entrapped within polystyrene microspheres conjugated to the cyclic peptide cRGD.[161] cRGD is frequently used as a targeting ligand, representing a potent antagonist of the $\alpha_v\beta_3$ receptor, which is involved in angiogenesis and overexpressed in many tumors. The Pd nanoparticle is used to mediate a Suzuki-Miyaura cross-coupling for the intra-cellular formation of the cytotoxic agent PP-121 (**82**) (Scheme 19). Notably, both precursors **80** and **81** are noncytotoxic, and only the *in situ* formed PP-121 exhibits cytotoxicity.[161]

The principle of self-assembly has also been applied to other fields. In 2016 Logan *et al*. developed a two-component system based on an *in situ* strain-promoted azide-alkyne cycloaddition to measure the mitochondrial membrane potential.[162] Each component consists of a triphenylphosphonium lipophilic cation, which causes probe accumulation in the mitochondria in response to the mitochondrial membrane potential. Additionally, one probe carries an azide, while the other one carries a cyclooctyne moiety, allowing for a SPAAC within the mitochondria (Scheme 20). LC-MS/MS can then be used to quantify the formation of the product **84** and thus information about the membrane potential can be obtained.[162]
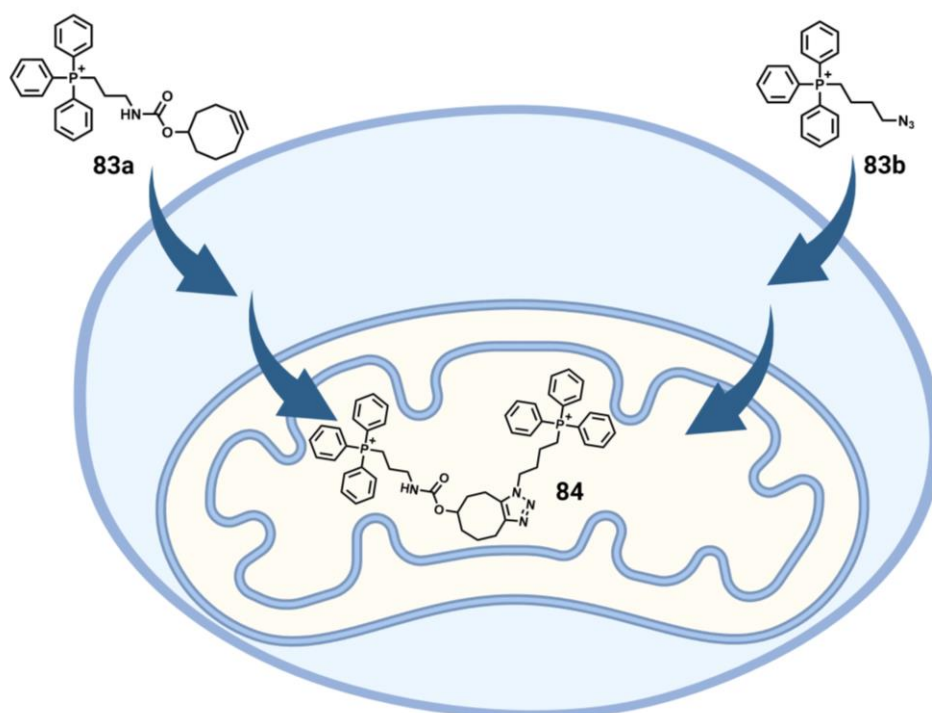
Scheme 20: Uptake of **83a** and **83b** into the cell and the mitochondria followed by a click reaction forming **84**. Created in analogy to [162]. Created with BioRender.com

2.2 Objective

For many natural products, the therapeutic window is too small or non-existing due to unwanted side effects or poor pharmaceutical properties. Tomaymycin is a DNA-binding antitumor and antibiotic natural product belonging to the class of pyrrolo[4,2]benzodiazepines (PBDs). The structure-activity relationship is well-studied and gave rise to various PBDs. Dimeric derivatives, e.g., SJG-136, reached phase II clinical trials for the treatment of ovarian cancer and leukemia.[58] Furthermore, the use of PBDs as payloads for antibody-drug conjugates has been reported.[163] However, a dimerization based on self-assembly at the target site has not been reported yet.

In general, such an assembling approach is based on the synergistic interaction of two components. By forming a new chemical bond between the two components, a new agent is generated, which exhibits a higher biological activity. This approach has various advantages; The two components have a lower molecular weight compared to the coupled molecule, which should generally lead to a higher solubility of each component. Moreover, due to the low molecular weight, the membrane permeability should be enhanced, and less avid binding to serum proteins should be observed.[157]

As the activity and toxicity of PBD dimers is generally higher compared to their respective monomers, an assembling approach based on two monomers should also lead to reduced toxicity. Similarly, such an approach may reduce the occurrence of resistance, since the less active monomers may be applied at concentrations not inducing resistance, while the dimer, that is assembled *in situ* at the target site leads to cell death even at low concentrations.

Hence, the main objective of this thesis was the design a two-component system based on tomaymycin derivatives that allows for *in situ* dimerization, transferring the concept of on-target synthesized drugs to the tomaymycin dimer scaffold. This approach is aimed to make use of the higher efficacy of dimeric PBD scaffolds, while less toxic monomeric building blocks, which stay unassembled prior to target engagement, should enhance tolerance.

The dimerization should be based on a bioorthogonal reaction to minimize side reactions in biological systems. The Huisgen cycloaddition, for example, was already successfully used for other structurally guided *in situ* reactions.[7],[164-165] However, also other bioorthogonal reactions should be explored.

First of all, the PBD core structure should be synthesized. The synthesis should be designed to provide an easily modifiable core to serve as a basic building block for further derivatization. Next, a set of different monomer pairs based on bioorthogonal reactions should be designed and synthesized. Consequently, different linkers should be designed, synthesized, and subsequently attached to the PBD core structure. After the assembly of the single monomers, the respective dimers should be synthesized to serve as a reference in the biological evaluation of the novel compounds.

Afterwards, the dimers and the monomer combinations should be studied with regard to their DNA binding properties. Herein, the focus should be set on gaining information about the cross-linking abilities since, by design, cross-links can only be formed by the dimers. This way, the possibility of *in situ* dimerization should be investigated.

On account of this, a set of complementary assays utilizing independent methods to study DNA cross-links should be developed and established. Furthermore, the binding properties of the dimers as well as the monomer combinations should be investigated and analyzed based on these established assays.
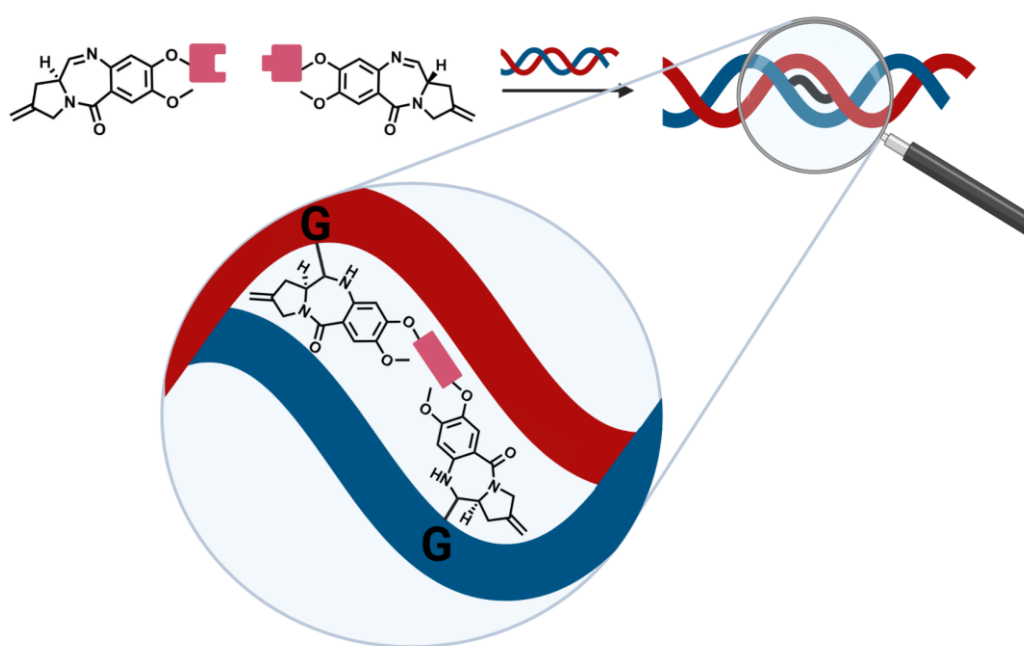
Figure 15: *In situ* dimerization based on self-assembly at the target site. Created with BioRender.com.

2.3 Results and discussion

2.3.1 Synthesis of tomaymycin derivatives

2.3.1.1 Synthesis of the tomaymycin based core structure

In conformity with SJG-136, the most successful representative from the group of PBDs, a tomaymycin derivative missing an *exo*cyclic methyl residue was chosen as the core structure. This particular tomaymycin derivative is from now on referred to as nortomaymycin, indicating the absence of the methyl group.

The nortomaymycin core structure can be divided in the three rings A, B, and C. On the basis of the previously published synthetic routes of several PBDs (see section 2.1.2.3), a retrosynthetic approach was drawn (Scheme 21). Ring B can be retrosynthetically obtained by hydrolysis of the imine functionality. Further cleavage of the amide bond leads to the complete fragmentation of ring B, thereby revealing the synthons of ring A and C. 2-Amino-4-hydroxy-5-methoxybenzoic acid (**87**) can be derived from vanillic acid by introducing an aniline function. Ring C, on the other hand, can be synthesized starting from the naturally occurring amino acid hydroxyproline. Hydroxyproline features the correct stereochemistry and is readily available, as it is widely used in the food and dietary supplement industries.[166]
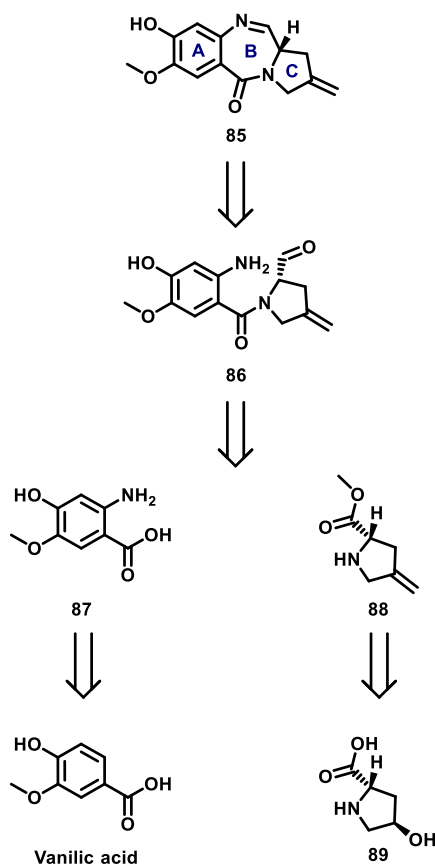
Scheme 21: Retrosynthetic planning of the nortomaymycin core structure.

However, considering that the *N*-Boc protected methyl (*S*)-4-methylenepyrrolidine-2-carboxylate (**90**) is commercially available, the synthesis starting from hydroxyproline (**89**) was omitted. Instead, **90** was deprotected to give the cyclic amine as the hydrochloride salt **88**, as shown in Scheme 22A.
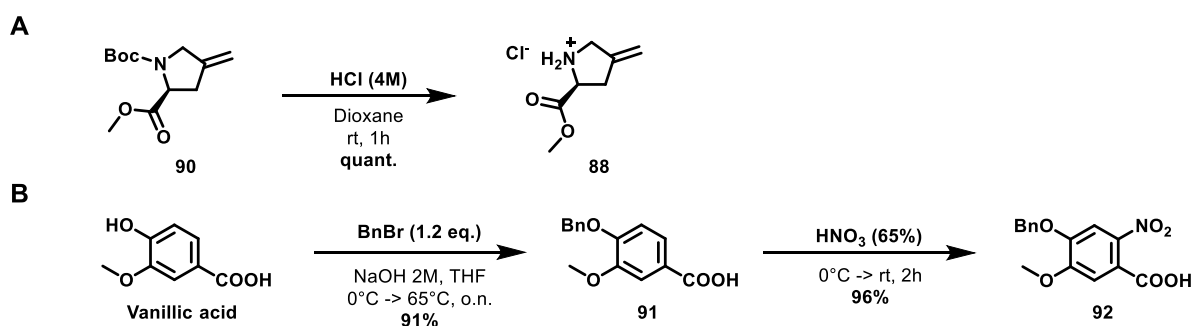
Scheme 22: A) Preparation of **88** via deprotection of the commercially available starting material **90**; B) Synthesis of the ring A fragment **92** through benzylation followed by nitration.

The ring A fragment was synthesized starting from vanillic acid as an inexpensive starting material. Benzylation using a slight excess of benzyl bromide gave **91** in 91% yield. Next, **92** was obtained in 96% yield via nitration of **91** using concentrated HNO_3 (Scheme 22B).

The introduced nitro group served as a precursor for an aniline, which can be obtained in one step via reduction.

For the formation of ring B, the ring A and C fragments were connected. The amide bond formation between benzylic acid derivative **92** and proline derivative **88** was realized by a HATU coupling, which gave product **93** in 90% yield (Scheme 23). An ester reduction to the corresponding aldehyde **96** followed by the reduction of the nitro group to an aniline **97** would lay the ground for the ring B closure via carbonyl-amine condensation to the cyclic imine as previously reported in literature.[167] However, reducing the ester **93** to the aldehyde **96** proved challenging under various conditions. Nevertheless, those challenges could be overcome mainly by changing the supplier of the DIBAL solution as well as optimizing the speed of reagent addition. DIBAL is traditionally used to selectively reduce esters to aldehydes via a tetrahedral intermediate, which allows the elimination of an aluminum alkoxide, leading to the formation of the aldehyde. The aldehyde is the more reactive species compared to the ester, thus over-reduction can be problematic. However, the right choice of reaction conditions stabilizing the intermediate and slowing down the subsequent elimination of the aluminum alkoxide, thus preventing the formation of the more reactive aldehyde in the presence of unreacted DIBAL, enables the selective reduction to the aldehyde. For this reason, the speed of DIBAL addition needs to be carefully balanced between two factors. First, its influence on the internal temperature, which should be kept as low as possible (i.e. slow addition); and the fact that a too slow addition leads to the formation of alcohol as the aldehyde species is already formed while the addition is still ongoing. Furthermore the right choice of solvent, the quality of the reagent, quenching at -78 °C and a constant monitoring of the reaction to detect alcohol formation is key in order to minimize formation of the alcohol side product. It was possible to separate the different components by column chromatography and thereby re-isolate the remaining starting material.

Considering the 24% yield of the aldehyde **96**, the synthetic strategy was adapted by completely reducing the ester **93** to the corresponding alcohol **94** in 87% yield. However, subsequent oxidation to the aldehyde **96** using Dess-Martin periodinane or Parikh-Doering conditions was unsuccessful. Hence the strategy was adapted, aiming for the final imine formation via first reducing the nitro group of **94** to the aniline **95**, followed by oxidation to the aldehyde **97**. Several oxidation methods including Dess-Martin periodinane, MnO_2, Parikh-Doering, Swern as well as Corey-Suggs oxidation did not yield the desired product.

Taking this into account, the 24% yield of the DIBAL reduction was tolerated, and this route was pursued with the reduction of **96** to the corresponding aniline with successive ring closure. Consequently, different reduction methods were examined. It was found that selective reduction of the nitro group in presence of the aldehyde was not possible, because the desired imine, formed by condensation, was immediately further reduced to the secondary amine **98** according to LC-MS experiments.
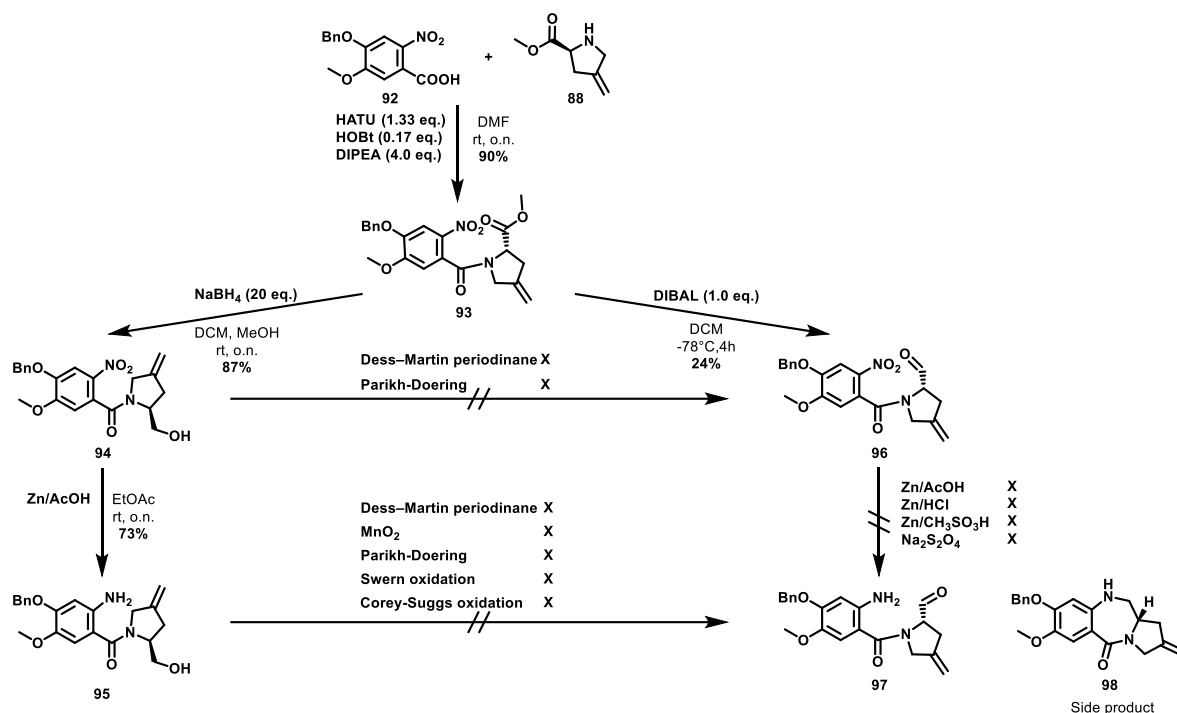
Scheme 23: Overview on multiple unsuccessful synthetic strategies for the formation of ring B starting from **92**.

To overcome the above-described challenges, the synthetic route was slightly altered, rejecting the thought of using the nitro group as a masked aniline, which aimed for avoiding protection and subsequent deprotection. Instead, the nitro group of **92** was reduced to the corresponding aniline **99** in 48% yield, which was subsequently Boc protected applying a strategy previously used by von Tesmar *et al*. for similar PBD derivatives (Scheme 24).[113] The yield of the reduction (48%) could be easily improved to >90% when using Zn/HCl as the reducing agent while also drastically reducing the reaction time (10 min vs. o.n.). Yet, these conditions affected the Boc protection in the next step, as the product was not formed. Picha *et al*. and Wiejak *et al*. reported that bivalent ions can be used as protecting groups for the amine of α-amino acids, claiming a bidental coordination by two α-amino acids.[168-169] These findings, in combination with the observation of complete suppression of the Boc

protection, suggest a similar role of the Zn^{2+} ion formed during the reduction. For these reasons, a direct Boc protection after nitro reduction with sodium dithionite was performed.
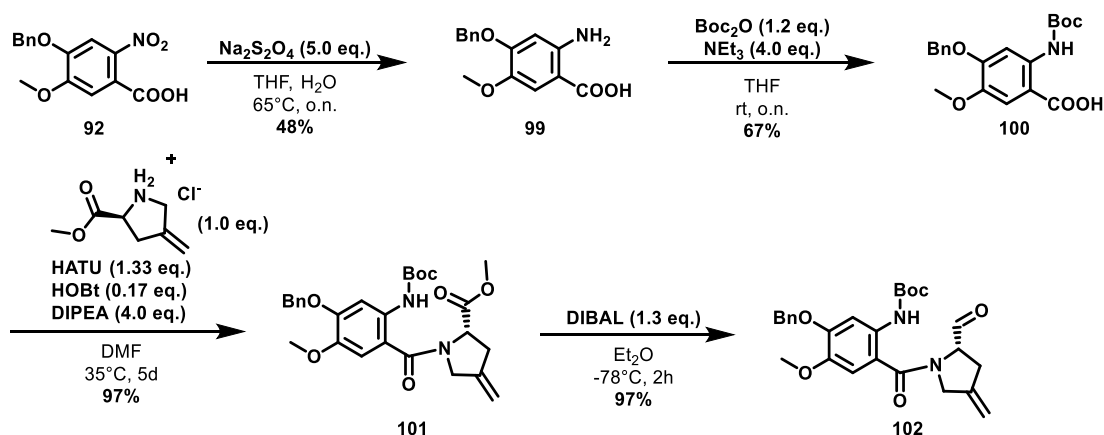
Scheme 24: Synthesis of the Boc protected ring A/C-derivative **102**.

Next, carboxylic acid **100** was coupled to amine **88** via a HATU coupling, giving A/C-derivative **101** in 97% yield. In the following step, the DIBAL reduction furnished aldehyde **102**.

As previously discussed, DIBAL reductions can be delicate as over reduction to the alcohol may occour. Thus reaction conditions including internal temperature, speed of addition, quality of the DIBAL reagent, quenching conditions as well as the work up procedure of this reaction were optimized such that the yield for **102** was increased from 16% in initial attempts to 97%.
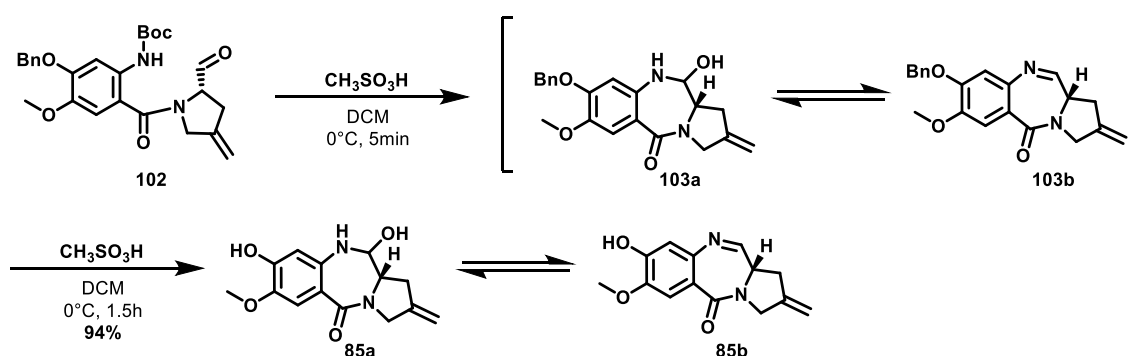
Scheme 25: Formation of the nortomaymycin core by global deprotection and ring closure.

The final step of the nortomaymycin core synthesis was the formation of ring B and the global deprotection. LC-MS analysis after treatment of **102** with methanesulfonic acid in DCM at 0 °C showed that within 5 minutes deprotection of the Boc group and subsequent ring closure to the hemiaminal takes place, which is in an equilibrium with the imine due to

water elimination. If the reaction is continued to stir for 1.5 h, the benzyl protection group is cleaved, releasing the free phenol (Scheme 25). Even though LC-MS monitoring showed a clean and complete turnover of the starting material to the desired product, initial yields after purification were poor. This phenomenon was attributed to the fast degradation of the crude product, especially when concentrated under reduced pressure. Yet, by optimizing the workflow of the workup and the column purification, the yield could be increased from 8% to 94%.

The nortomaymycin core was thus obtained in 25% yield over 7 steps. Herein the key step was the double deprotection and subsequent cyclization performed as a one-pot reaction. In contrast the literature synthesis[167] used the reduction of a nitro group with subsequent cyclization as their key step. With this strategy, the authors were able to obtain the target molecule in 26% yield over 6 steps. Nevertheless, initial attempts to form ring B using the published strategy proved challenging with respect to the DIBAL reduction and the nitro group reduction. These challenges could be circumvented by altering the synthetic strategy while not compromising on the overall yield.

2.3.1.2 Synthesis of distinctive sets of linking moieties

To enable and explore linkage of two nortomaymycin-based entities at the DNA employing target-guided synthesis, numerous nortomaymycin monomers with reactive linkers based on different reactions were prepared. The reactions for the so-called *in situ* click needed to be bioorthogonal to avoid unwanted side reactions with the cellular environment. Additionally, the reactions were chosen with regard to a broad spectrum of reaction kinetics,[170] as on the one hand dimerization in absence of the DNA should be avoided and on the other hand the reaction needs to be fast enough to form the active drug on a biologically reasonable timescale. In this framework, nortomaymycin monomers with reactive linkers for the azid-alkyne cycloaddition, strain-promoted azide-alkyne cycloaddition (SPAAC) and the Diels-Alder reaction were prepared. The syntheses of these sets of monomers are discussed below.

Implementation of the azide-alkyne cycloaddition as a dimerization reaction requires two monomers carrying an azide or alkyne. The azide was obtained in two steps. First, treating the nortomaymycin core **85** with a tenfold excess of 1,2-dibromoethane under basic conditions gave the bromide **104** in 94% yield (Scheme 26). The excess of 1,2-dibromoethane is crucial to prevent the formation of a symmetric tomaymycin-dimer in a double nucleophilic substitution. Afterwards, the bromide **104** underwent a second substitution with sodium azide giving the desired azide monomer **MbA** (**M**onomer-**b**asic **A**zide) in 80% yield.
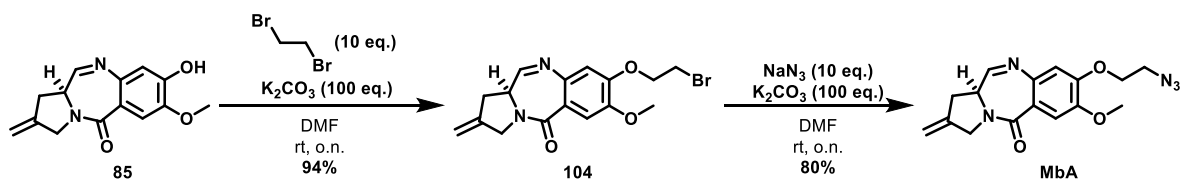
Scheme 26: Functionalization of the phenolic position of the nortomaymycin core structure by introduction of a $C_2H_4N_3$-spacer.

Two alkynes of different lengths were synthesized to serve as the second reaction partner in the CuAAC reaction. The first one (**M1**) was designed to have a methylene unit between the phenol and the alkyne moiety, while the second one (**M2**) carries an ethylene unit. Both compounds were obtained via a substitution reaction of the respective alkyl bromide under basic conditions (Scheme 27). A difference in yield between using propargyl bromide and homopropargyl bromide could be observed. Apart from being less reactive since the bromide is not in the allylic position, homopropargyl bromide readily underwent an elimination reaction. To compensate for this effect a vast excess of 60 eq. was used.
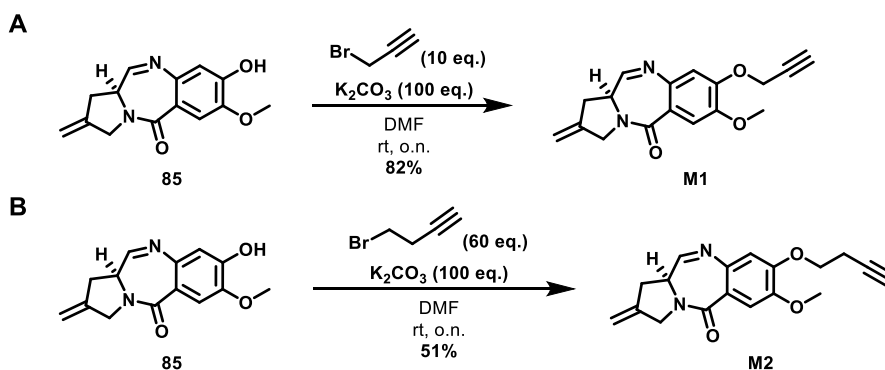
Scheme 27: A) Incorporation of an alkyne linker with a one-carbon spacer between the alkyne and the phenol; B) Incorporation of an alkyne linker with an ethylene spacer.

The second group of monomers was designed to be linked by strain-promoted azide-alkyne cycloaddition. Two types of strained alkyne linkers were added to the core, whose syntheses will be discussed in the following. The first target molecule **M3** carries a cyclooctyne ring, which is connected via an ethylene glycol bridge to the nortomaymycin core.
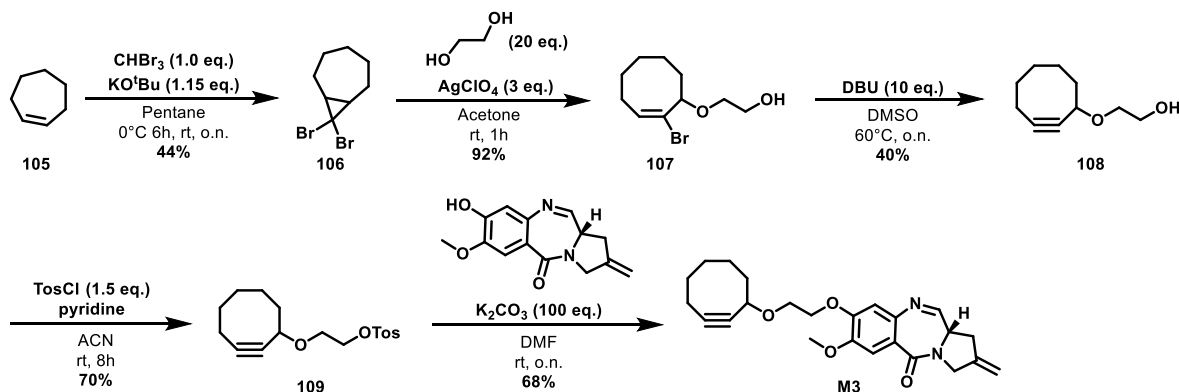
Scheme 28: Synthesis of monomer **M3**.

The synthetic sequence started with the addition of bromoform to the double bond of cycloheptene under basic conditions yielding the bicyclic intermediate **106**. Subsequently, **106** underwent an electrocyclic ring-opening mediated by silver perchlorate, to the eight-membered monocycle, incorporating the ethylene glycol-based handle in the same step. Next, a base-promoted elimination was performed to form the strained cyclooctyne **108**. The alcohol of **108** was converted into the tosylate in 70% yield by treatment with tosyl chloride under basic conditions. **109** was connected to nortomaymycin by a nucleophilic substitution using potassium carbonate as a base and DMF as the solvent.

Despite the simplicity of this strained cyclooctyne, it potentially suffers from two disadvantages.

First, during the synthesis, the C1 position of the handle is obtained as an enantiomeric mixture. Hence the reaction with the azide not only lead to two regioisomers, but also to two

diastereomers, overall, four potential products could be formed (Scheme 29). Some of those products may not bind in the sterically restricted minor groove, which makes the product variety a potential problem. The second disadvantage of SPAAC, albeit less decisive, is the relatively low reaction rate constant.[171]

Consequently, a second strained cyclooctyne (**M4**) was included in the set of monomers to overcome the aforementioned disadvantages. Bicyclo[6.1.0]non-4-yne (BCN) was chosen as the cyclooctyne moiety based on its symmetry, defined stereocenters, and enhanced reactivity in the SPAAC, translating to shorter reaction times and only two potential products upon heterodimerization (Scheme 29).
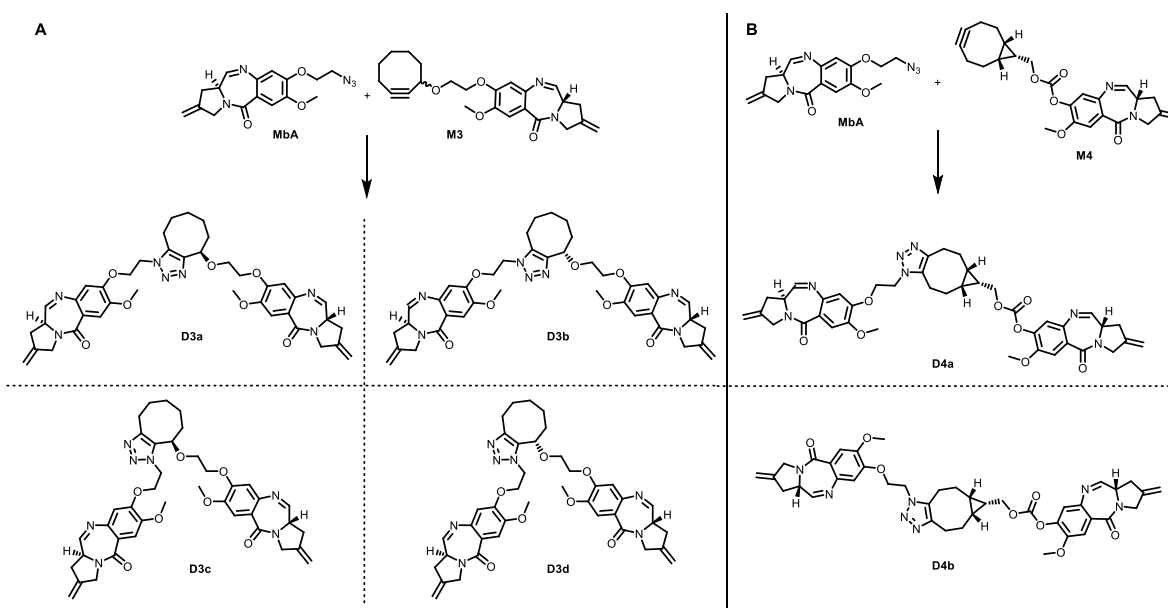
Scheme 29: Potential product isomers of the SPAAC of azide **MbA** reacting with either **M3** (A) or **M4** (B).

To link the BCN residue with the central core, several approaches were pursued. The first attempts focused on forming an ether bond via Williamson ether synthesis as the most straightforward and shortest connection between the handle and the core. Different efforts were undertaken to convert the aliphatic hydroxyl group into a bromide leaving group (Scheme 30). Under harsh conditions with phosphorus tribromide, no product formation could be observed. Even when using the milder bromination reagent triphenylphosphine dibromide in the presence of imidazole, no desired product could be obtained. Thus, for the next attempt, the Mukaiyama redox condensation[172] was chosen, but neither the use of tetrafluorobenzoquinone, nor 2,6-ditertbutylbenzoquinone resulted in product formation.
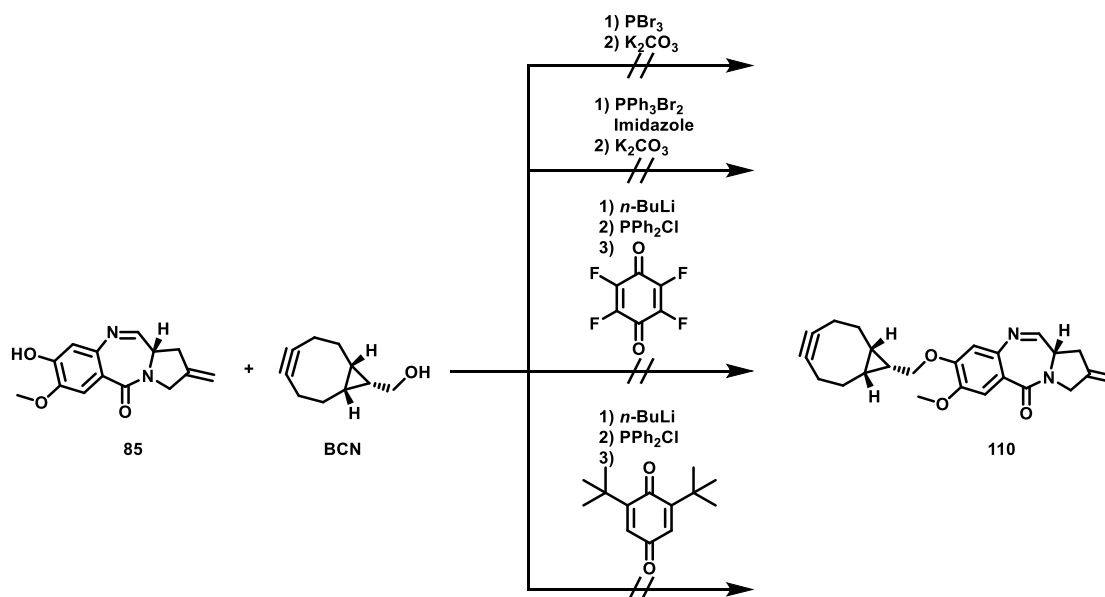
Scheme 30: Synthetic attempts towards **110**.

Therefore, a different synthetic strategy was pursued, using the already discussed ethylene linker with a bromide leaving group attached to the nortomaymycin core that can be substituted by the BCN hydroxyl group (Scheme 31A). After deprotonation of the BCN hydroxyl group using n-BuLi, the bromide **104** was added at -78 °C in order to trap the alcoholate. However, the desired product could not be obtained. Hence, the system was reversed by introducing an electrophile via a linker on the BCN core and subsequently using the phenol of the nortomaymycin as the nucleophile. However, under previously established substitution conditions (K$_2$CO$_3$ in DMF), no product could be isolated (Scheme 31).
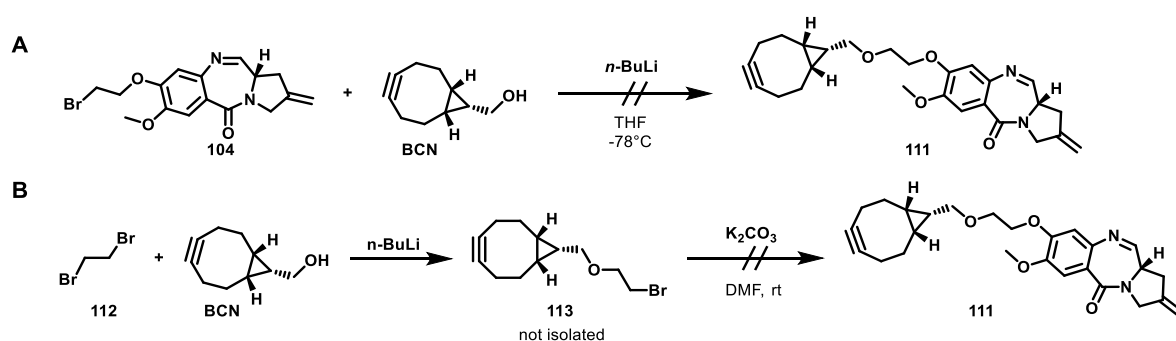
Scheme 31: Synthetic attempts towards **M4**.

The synthetic strategy was further adjusted by introducing a sterically more demanding carbonate linker between the core and the BCN moiety (Scheme 32). Using 4-nitrophenyl chloroformate (**114**) and pyridine in DCM gave the mixed carbonate **115** in 88% yield. The final compound **M4** was obtained by treating nortomaymycin with **115** under basic

conditions in DMF. Although the stability of a carbonate linker can be a concern for further biological testing, no instabilities could be observed under neutral or acidic aqueous conditions.
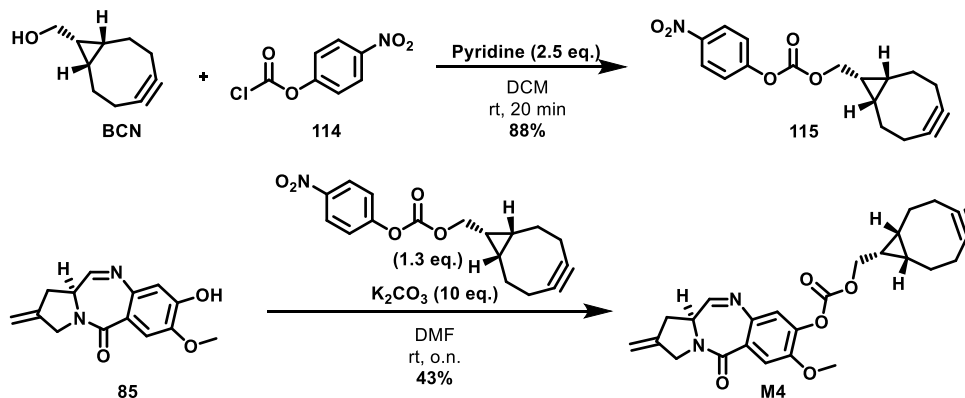
Scheme 32: Synthesis of monomer **M4**.

The third group of monomers was designed to be linked via a Diels-Alder reaction, a further bioorthogonal variant applied in this project. A furane and an alkyne were chosen as the diene and the dienophile, respectively. Low-cost furfuryl alcohol (**116**) was converted with PBr$_3$ into furfuryl bromide (**117)** (Scheme 33). Due to the high reactivity and instability of **73**, the product was not isolated but kept as a DMF stock solution, which was directly used in the next step to avoid decomposition. The high reactivity of **117** was also reflected in the 92% yield of the substitution reaction with nortomaymycin under basic conditions.
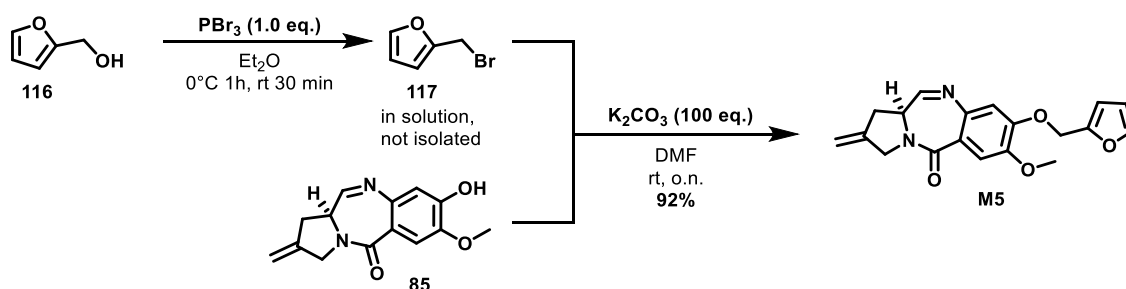
Scheme 33: Synthesis of monomer **M5**.

The synthesis of the counterparts, i.e., alkynes **M1** and **M2**, was discussed earlier in this chapter.

In addition to the unsubstituted alkyne, alkynes carrying an electron-withdrawing group (EWG) were assessed due to their elevated reactivity towards dienes. A methyl ester and a nitrile substituent were chosen based on synthetic feasibility and electron-withdrawing properties.

118 is the key intermediate for a modular synthesis building on nortomaymycin (Figure 16). As shown, the respective EWG must be introduced and a leaving group for the attachment of nortomaymycin has to be provided.
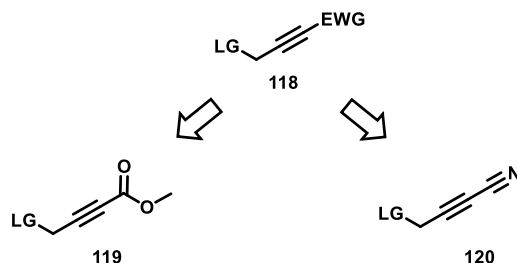
Figure 16: Key intermediates for EWG-substituted alkynes.

As illustrated in Scheme 34, different methods to obtain the key methyl ester intermediate **119** were evaluated. The most promising synthetic route started with propargyl alcohol, which was protected in 97% yield using TIPS-Cl in *N*-methylimidazole. Next, **129** was treated with methyl chloroformate under basic conditions resulting in the methyl ester **130** in 70% yield. **130** was reacted with triphenylphosphine dibromide in the presence of imidazole and the crude was immediately used as a solution in the next step due to instability issues. Nevertheless, a test reaction between phenol, serving as a test system for nortomaymycin, and bromide **133** did not yield the desired substitution product **134**, although the reaction conditions were well established for previous functionalization reactions of nortomaymycin. Therefore, this idea was discarded and the focus was set on introducing the nitrile as an EWG.

A

B
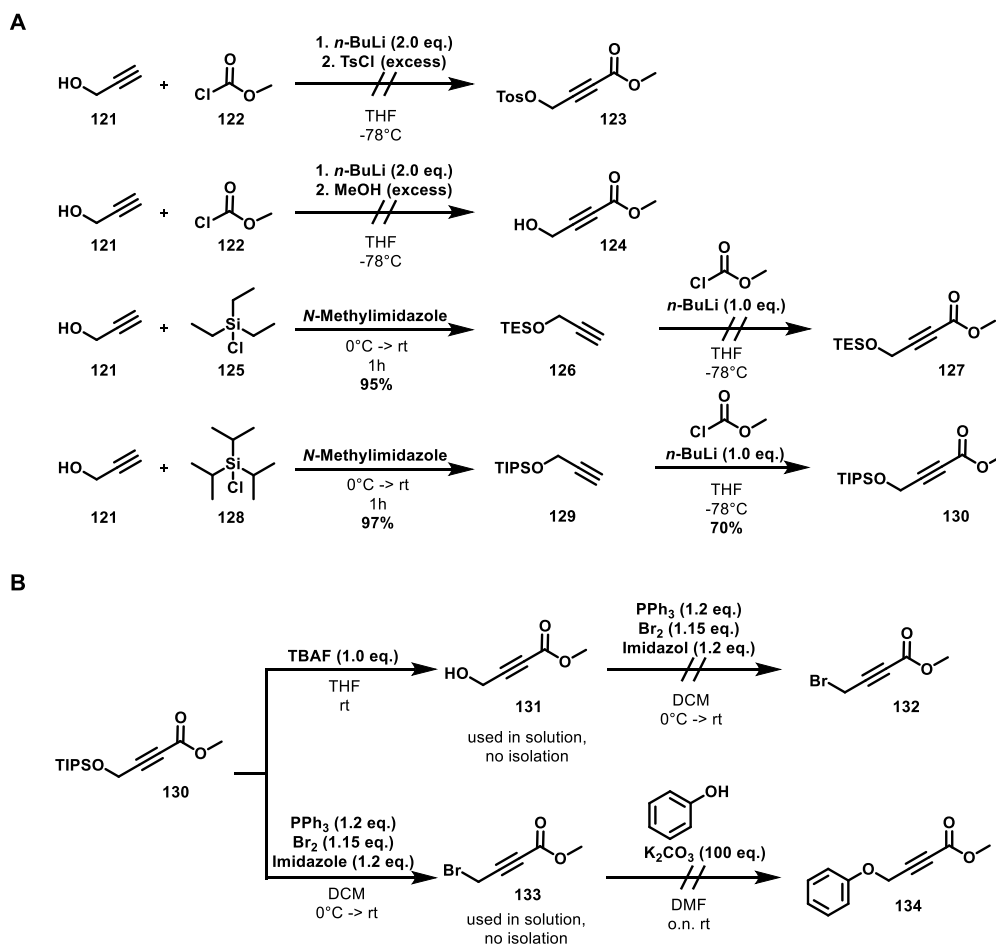
Scheme 34: A) Different strategies to introduce the methyl ester as an EWG; B) Synthetic strategies to introduce a bromide as a leaving group.

Key intermediate 4-bromobut-2-ynenitrile (**137**) was be obtained in three steps from propargyl alcohol (**121**) (Scheme 35). First, the bromide **135** was obtained via treatment with an *in situ* prepared sodium hypobromite solution in 41% yield. In the next step, the bromide was converted to the corresponding nitrile using copper (I) cyanide at slightly elevated temperatures. To leverage the same strategy to connect the handle to the core structure, the hydroxy group of **136** first needed to be transformed into a leaving group. Several approaches to introduce different leaving groups had been tested (not shown). In spite of 48% yield, the bromide **137** could be obtained using *in situ* formed triphenylphosphine dibromide. Since compound **137** turned out to be unstable over time, immediately after preparation the substitution with phenol **85** was conducted. However, the desired product **138** could not be obtained. Consequently, the electron-deficient analogs were deemed unfeasible, and further evaluations were carried out using the successfully synthesized alkyne–furane pairs.
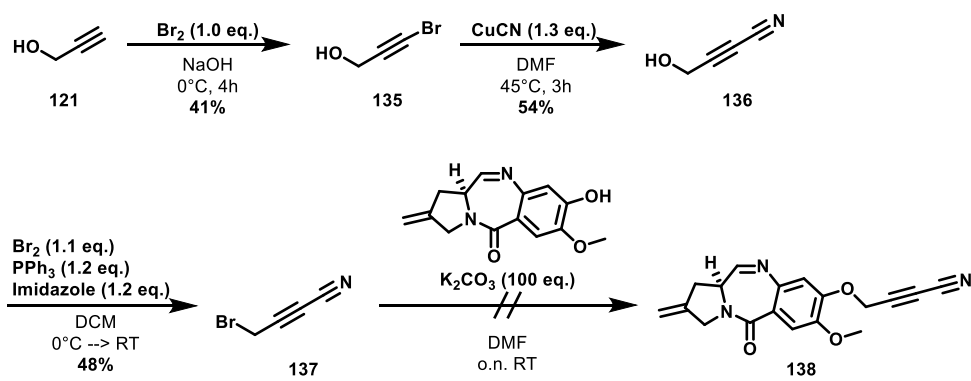
Scheme 35: Synthetic attempt towards **138**.

2.3.1.3 Synthesis of PBD heterodimers

The heterodimers were synthesized from the previously mentioned monomers, although their on target synthesis was the ultimate goal the dimerized substances were needed as positive controls in the biological evaluation. For the heterodimerization, a set of different bioorthogonal reactions were deployed, namely the azide-alkyne cycloaddition, strain-promoted azide-alkyne cycloaddition (SPAAC) and the Diels-Alder reaction.

The first dimer was prepared by a cycloaddition between the azide **MbA** and the alkyne **M1**. In biological systems, click reactions were preferably enabled by proximity and orientation provided by an external matrix (e.g. DNA). So-called *in situ* click chemistry allowed the formation of both the 1,4- and the 1,5- regioisomer.[165],[173] However, the three-dimensional structures indicate that the 1,5-regioisomer forms a loop and thus is less likely to fit into the minor groove of the DNA (Figure 17). Therefore, only the 1,4-regioisomer was chosen to be synthesized using the CuAAC instead of both regioisomers with a thermal azide-alkyne cycloaddition (Scheme 36).
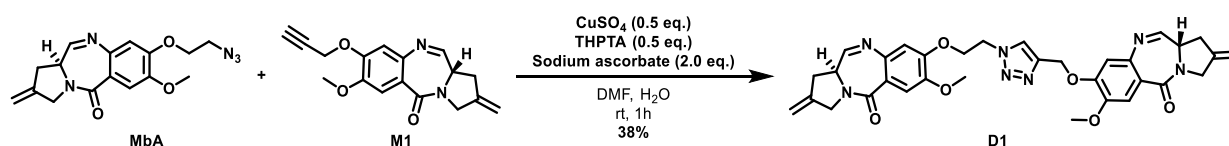
Scheme 36: Synthesis of the heterodimer **D1** via a CuAAC between monomers **MbA** and **M1**.

CuSO$_4$ was selected as a copper source, with sodium ascorbate as a reducing agent and THPTA as the ligand. Under those conditions, the heterodimer **D1** was obtained in 38% yield. This low yield can be attributed mainly to the purification process involving five consecutive preparative TLCs to fully remove traces of remaining **MbA**. Purification being the source of the low yield observed was further confirmed by the LC-MS measurements of the reaction mixture, which showed 100% conversion (based on the alkyne) after 1h.
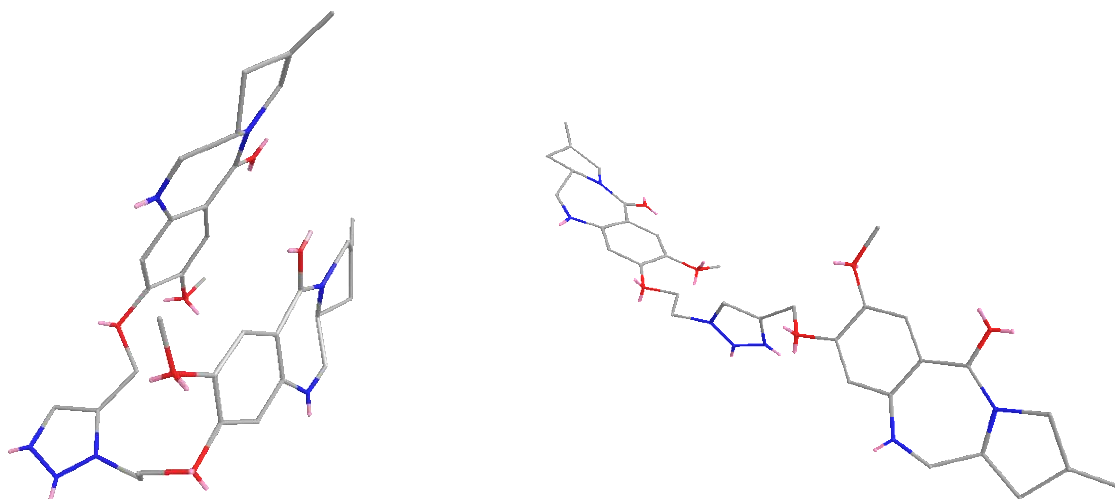
Figure 17: Three-dimensional structures of the 1,5 regioisomer (left) and the 1,4 regioisomer (right) obtained using Chem3D's MM2 energy minimization.

Apart from **D1** a second heterodimer **D2** was synthesized based on the CuAAC reaction possessing an ethylene spacer on both residues of the triazole (Scheme 37).
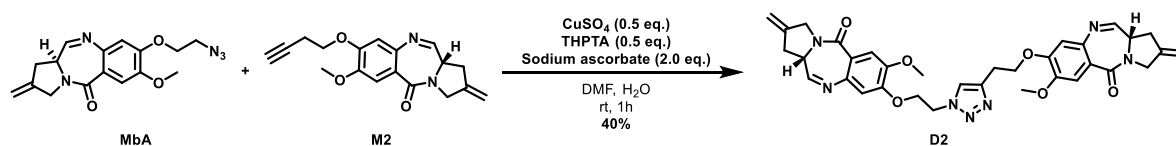
Scheme 37: Synthesis of the heterodimer **D2** via a CuAAC between the monomers **MbA** and **M2**.

Again, the three-dimensional structures of the 1,4-regioisomer (right) and the 1,5-regioisomer (left), shown in Figure 18, made it evident that the 1,5-regioisomer is unlikely to fit into the minor groove since the two cores form almost a right angle.
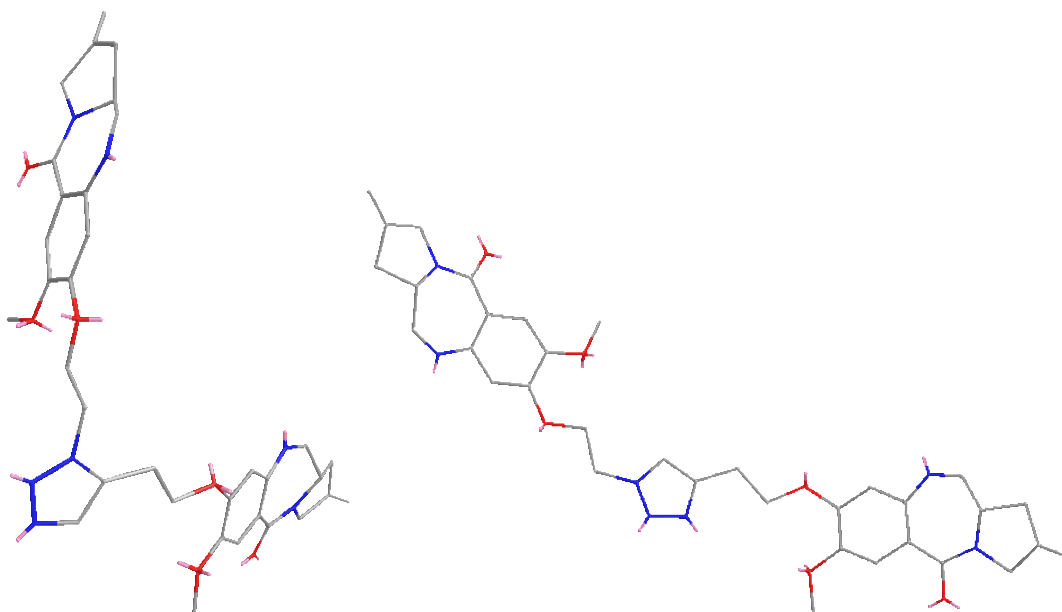
Figure 18: Three-dimensional structures of the 1,5 regioisomer (left) and the 1,4 regioisomer (right) obtained using Chem3D's MM2 energy minimization.

The next pair of heterodimers was synthetized using the SPAAC. For this purpose, the previously mentioned terminal alkynes of **M1** and **M2** were exchanged for cyclooctyne derivatives, representing highly strained ring systems.
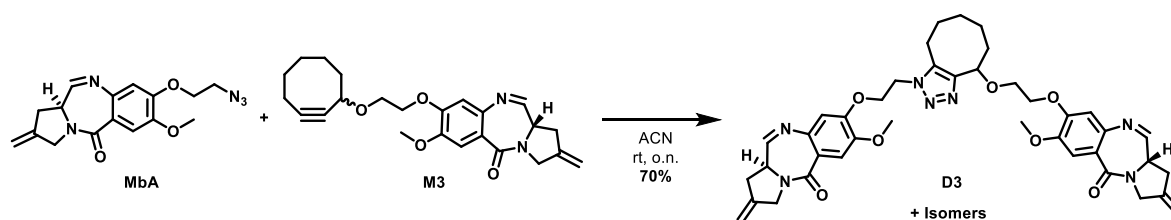
Scheme 38: Synthesis of heterodimer **D3** via SPAAC. Only one isomer depicted.

The heterodimer **D3** was obtained in 70% yield by stirring the azide **MbA** with cyclooctyne **M3** in acetonitrile at room temperature overnight (Scheme 38). This reaction yields a mixture of up to four isomers (Scheme 29, page 53). The product was used as a mixture of isomers for all further experiments since it is not known whether an isomer is preferentially formed in the presence of DNA.
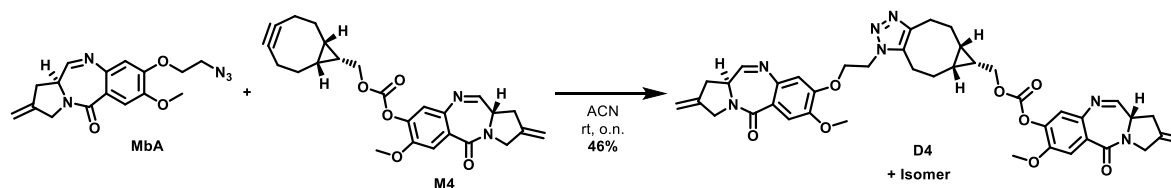
Scheme 39: Synthesis of heterodimer **D4** via SPAAC. Only one isomer depicted.

Nonetheless, the number of potential products was decreased by substituting the asymmetric cyclooctyne **M3** with a symmetric alternative. By reacting the BCN-based monomer **M4** with the azide **MbA**, only the heterodimer **D4** and its triazole-regioisomer was formed (Scheme 39). Although the yield of the isolated products was 46%, LC-MS analysis of the reaction showed full conversion. As in the case of heterodimer **D3**, the yield is attributed to the workup and purification process.

The next pair of heterodimers was synthesized based on the Diels-Alder reaction between a furan analog and a terminal alkyne. An overview is provided in Scheme 40. At both reaction temperatures, 50 °C and 100 °C, no heterodimer was obtained and only the starting materials could be detected by LC-MS. However, heating the reaction to 200 °C using a microwave reactor led to decomposition of the starting materials. Due to the fact that even after 12 h at 100 °C no conversion was detected, the dimerization via the Diels-Alder reaction was not further pursued, since a conversion in biological systems cannot be expected.
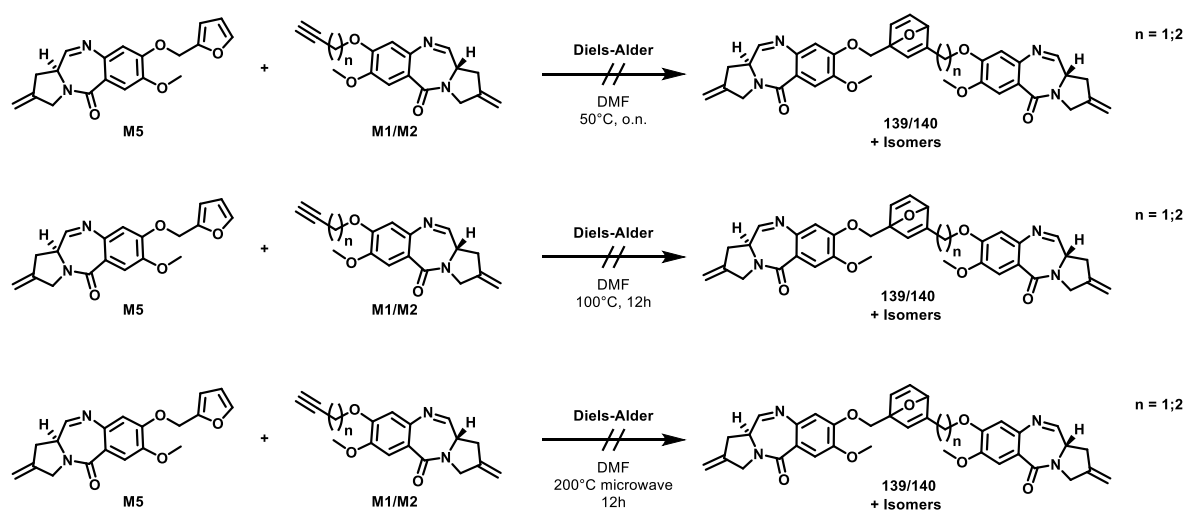
Scheme 40: Attempts to react monomers **M1** and **M2** with **M5** in a Diels-Alder reaction to form the heterodimers **139** and **140**.

2.3.2 Evaluation of DNA binding abilities of tomaymycin derivatives

Various methods were employed to assess whether the monomer combinations as well as the synthetic hetero dimers bind to the target and link two DNA strands. The methods were selected with regard to their orthogonal measurement techniques.

2.3.2.1 Mobility shift assays

2.3.2.1.1 Plasmid-based mobility shift assay

To investigate the capability of monomer combinations as well as the synthetic dimers to link two DNA strands, a mobility shift assay using a plasmid was developed building on previous studies by Thurston and Hartley.[87],[174] A schematic overview is presented in Figure 19.
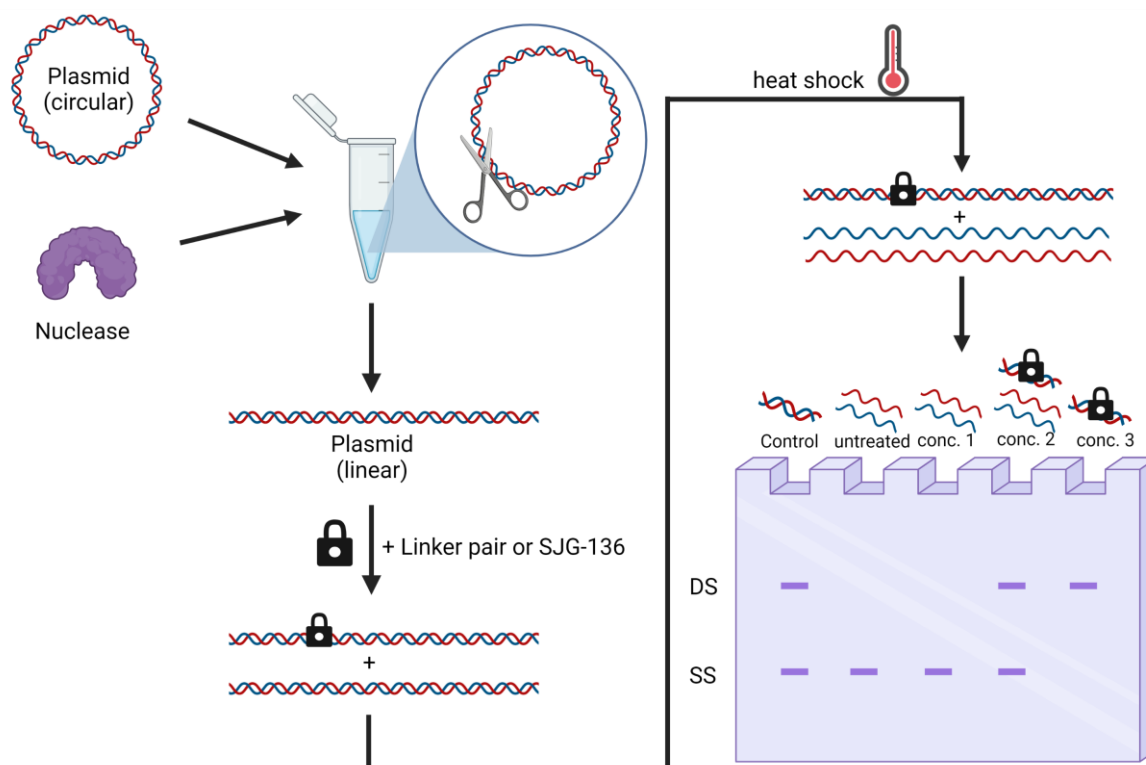
Figure 19: Schematic overview of the plasmid-based mobility shift assay. DS: double strand, SS: single strand, conc. 1 < conc. 2 < conc. 3. Created with BioRender.com.

As a model plasmid, pUC19 was used. pUC19 was replicated in *Escherichia coli* DH5α and subsequently isolated using standard procedures. The isolated plasmid was then sequenced to confirm identity. pUC19 was digested using the restriction enzymes *Bam*HI and/or *Sca*I-

HF, followed by gel extraction using standard protocols. The linearized DNA was incubated with the respective compounds and the samples were subsequently analyzed by gel electrophoresis (Figure 20).

Denaturation conditions led to strand separation for non-treated samples, as shown for the control. This is reflected in the difference in shift observed in a neutral agarose gel. While the dsDNA control is observed at about 3000 bp, ssDNA is observed at about 900 bp. At the same time, *inter*-strand cross-links caused by the compound prevent denaturation and should lead to renaturation of the two DNA strands. Accordingly, the cross-linked samples were expected at about 3000 bp.

By increasing the molar compound:DNA ratio, an increase in the fraction of linked double stranded DNA could be observed. Since the molar ratio between the compound (SJG-136) and the DNA is essential, both the concentrations and the corresponding molar equivalents of the respective compound are specified in the respective Figures. Figure 20 shows the DNA cross-linking of SJG-136 at different molar ratios and concentrations, respectively.

	SJG-136 concentration [µM]	Fold compound excess
1	0.3	10
2	1	33
3	3	100
4	10	333
5	30	1.000
6	100	3.333
7	200	6.666
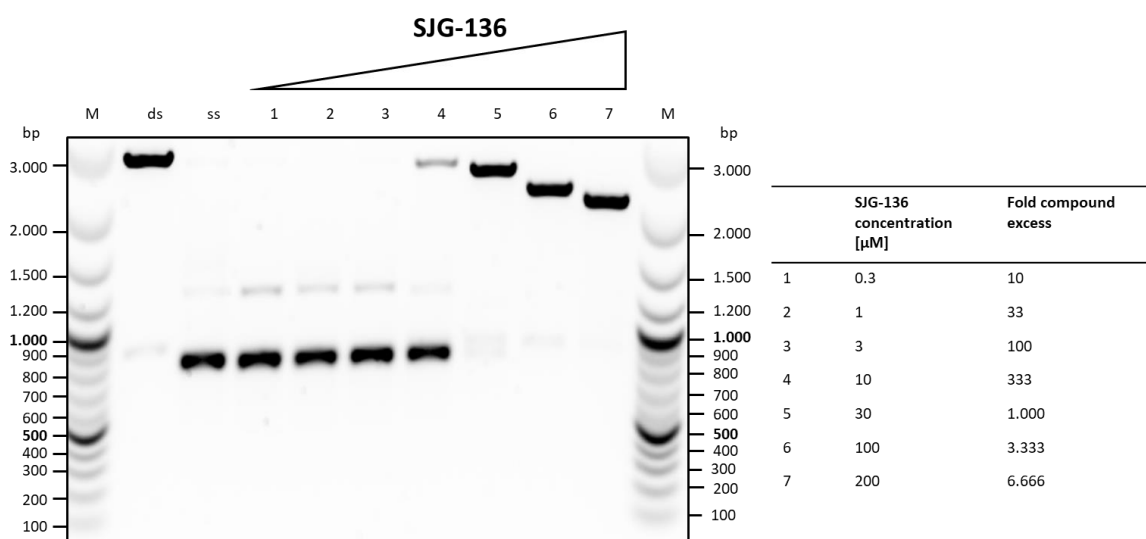
Figure 20: Plasmid-based mobility shift assay showing DNA cross-linking by SJG-136 at different molar ratios/concentrations. ds: untreated DNA, heat shock not applied; ss: untreated DNA, heat shock applied; M: Thermo Scientific™ GeneRuler™ 100 bp Plus DNA Ladder. All samples were prepared starting from equal amounts of dsDNA (0.03 µM), the respective compound concentrations listed on the right.

Incubation time, incubation temperature, strand separation buffer, and heat shock conditions have been optimized using SJG-136 as a positive control. Linking experiments were conducted with both the plasmid fragments, obtained from digestion with *Bam*HI and *Sca*I-HF, and with the linearized plasmid, obtained using only one of the respective restriction enzymes. However, no significant differences using DNA fragments of different lengths could be observed. During the optimization, the assay was conducted with various DNA concentrations (5 to 100 nM) as well as SJG-136 concentrations (0.1 nM to 200 µM). As

mentioned above, the concentrations are not decisive, but the molar ratios between DNA and compound are critical.

The optimized plasmid-based mobility shift assay was used in order to study the cross-linking ability of obtained monomer combinations as well as the synthetic heterodimers (Figure 21).

The assay was conducted with three different controls. The first control shows DNA with no compound added, and no heat shock applied. The second control shows DNA with no compound added, but with the denaturing heat shock applied, and the third control shows SJG-136 treated DNA at a molar ratio of 1:20.000.

This ratio was chosen since the previous results (Figure 20) showed cross-linking for SJG-136 starting from a molar ratio of 1:1.000, which is consistent with the findings of Thurston and co-workers and Hartley and co-workers.[87],[174] A ratio of 1:20.000 should therefore ensure complete cross-linking. In addition, all compounds were tested in this ratio to achieve good comparability.

However, the results showed that none of the four heterodimers cause cross-links under these conditions, as can be seen by the respective bands at about 900 bp, which corresponds to the ssDNA control. Equally, the monomer combinations, which were incubated at a molar ratio of 1:20.000:20.000 showed no cross-links using this method. Nevertheless, it should be kept in mind that PBD dimers have a set of different binding modes, including, apart from cross-links, also *intra*-strand binding and mono-adducts. Consequently, additional methods, which will be discussed in the following chapters, were used to further investigate the binding of the hetero dimers and the monomer combinations.
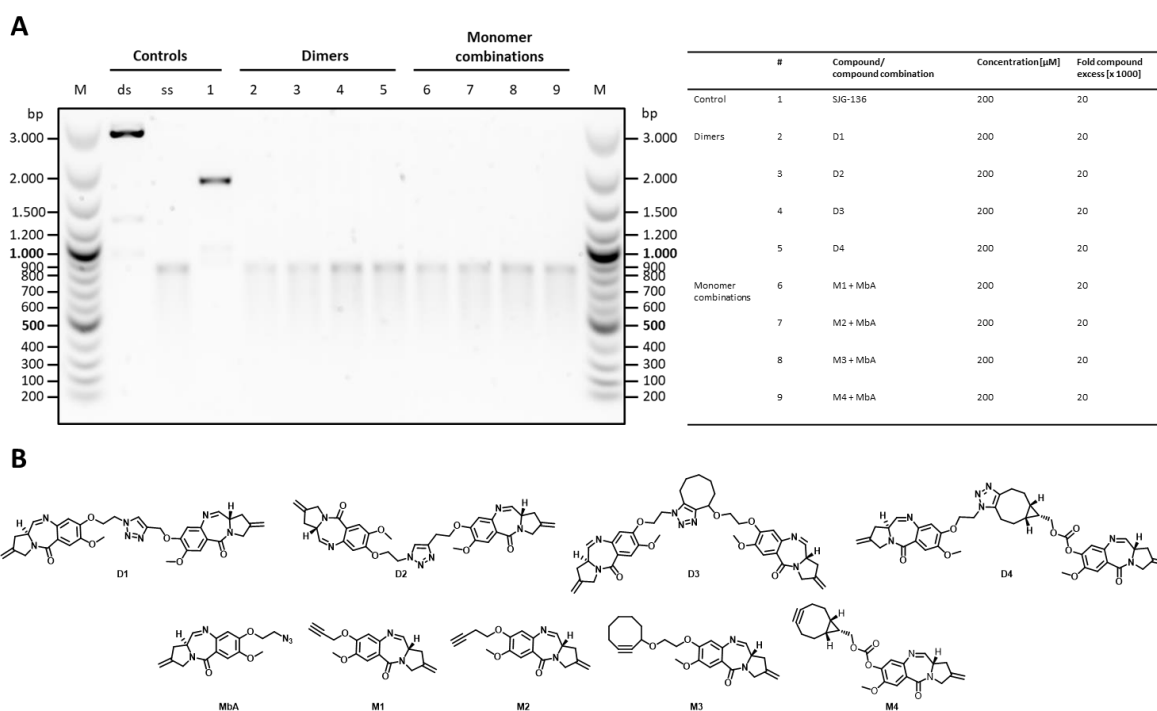
Figure 21: A) Plasmid-based mobility shift assay showing DNA cross-linking ability of SJG-136, heterodimers (**D1**, **D2**, **D3**, and **D4**), and monomer combinations (**MbA**+**M1**, **MbA**+**M2**, **MbA**+**M3**, and **MbA**+**M4**) at a compound concentration of 200 μM, corresponding to a 20.000 fold compound excess. ds: untreated DNA, heat shock not applied; ss: untreated DNA, heat shock applied; M: Thermo Scientific™ GeneRuler™ 100 bp Plus DNA Ladder. The investigated dimers and monomer combinations are listed on the right; B) Chemical structures of the investigated dimers and monomers

2.3.2.1.2 Oligonucleotide-based mobility shift assay

The binding of the heterodimers as well as the monomer combinations was further investigated using a newly developed oligonucleotide-based mobility shift assay. Previous studies by Thurston[87] laid the ground for the development of this assay. The use of an oligonucleotide allows a higher degree of control since only a short distinctive nucleotide sequence is provided, which e.g. only possesses two guanines for binding. Furthermore, the possibility of two monomers binding on distant sites, not reaching one another, is avoided. Similarly to the plasmid-based mobility shift assay described above, the oligonucleotides were incubated with the respective compound and analyzed via gel electrophoresis. However, herein only a short oligonucleotide was used instead of a whole plasmid. Hence, two single-stranded complementary oligonucleotides consisting of 12 nucleotides were annealed using standard procedures. Next, the obtained double-stranded DNA was incubated for 24 h with the respective compounds or compound combinations at different concentrations (Figure 22). The samples were analyzed using a native 20% polyacrylamide

gel in order to separate single-stranded and the linked oligonucleotides. As with the previously described assay, an increase in compound concentration or molar ratio, respectively, is expected to result in a shift from single-stranded to double-stranded species (i.e., linked).
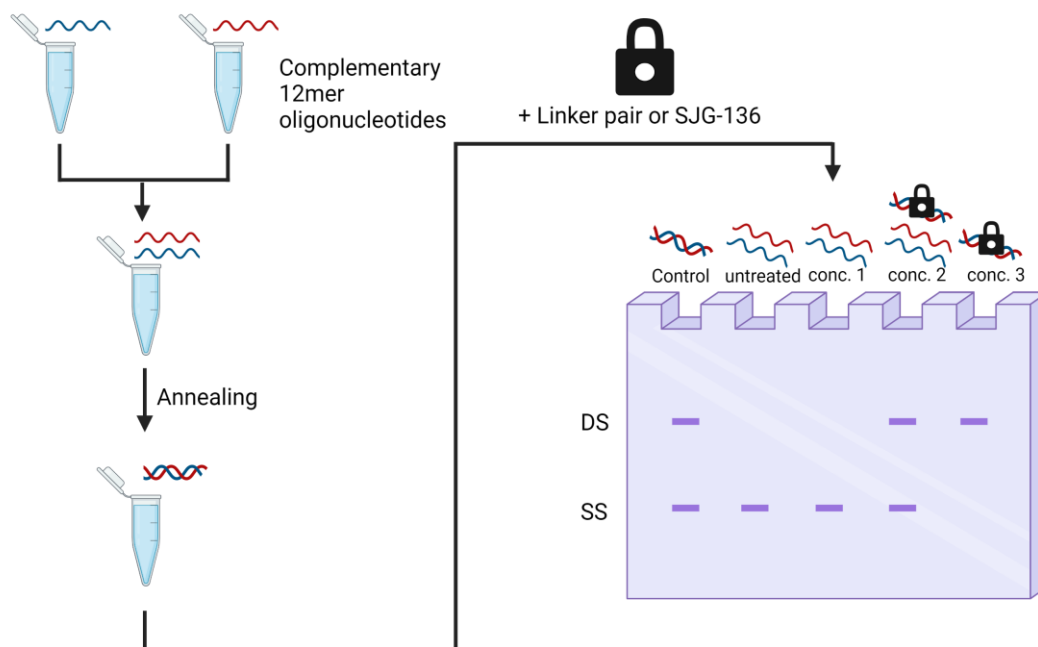
Figure 22: Schematic overview of the oligonucleotide-based mobility shift assay. DS: double strand, SS: single strand. Created with BioRender.com.

The assay was established and optimized using SJG-136 as a model compound. While SJG-136 is capable of binding to different binding motives that consist of the general pattern CXXG, it has been shown that the GATC motif is preferred.[70] As a result, an oligonucleotide containing this sequence and two additional AT units on each side (i.e., TATAGATCTATA) was used. This sequence has the advantage of being palindromic, thus slightly simplifying the workflow. The DNA cross-linking of SJG-136 was investigated at different molar ratios or concentrations, respectively (Figure 23). With increasing molar ratios, a shift from single-stranded to double-stranded (i.e., linked) can be observed. The molar ratio needed to form a linkage between the two strands of the oligonucleotide is 1:2.56 (DNA:SJG-136) for complete linkage.

Moreover, a first band appears at a SJG-136 concentration of 4 µM, corresponding to a molar ratio of 1:0.16 (DNA:SJG-136), indicating the high potency of SJG-136. Comparing these results with the plasmid-based assay, it can be observed that using oligonucleotides instead of a plasmid decreases the needed molar ratio from 1:1.000 to 1:2.56 (DNA:SJG-136). This

effect underlines the advantage of the assay providing a higher degree of control of the binding site, thereby avoiding binding to guanine bases that do not possess another guanine in sufficient proximity.
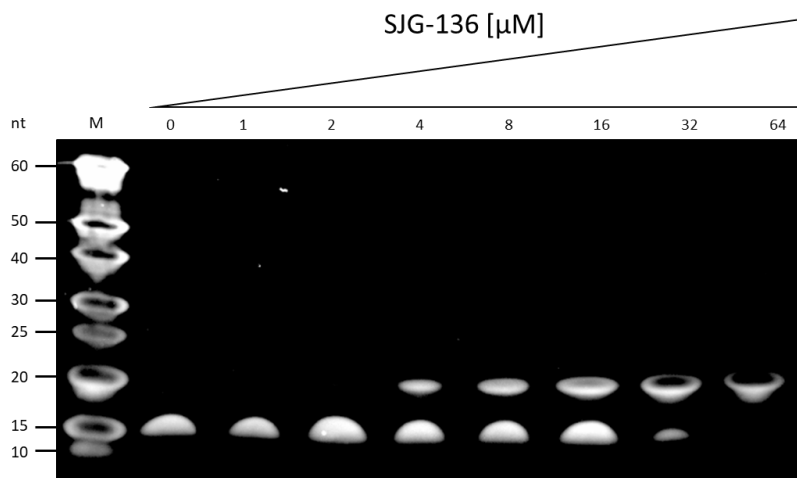
Figure 23: Oligonucleotide-based mobility shift assay showing DNA cross-linking of SJG-136 at different concentrations ranging form 0 to 64 µM. All samples were prepared starting from equal amounts of dsDNA (25 µM) M: 10/60 ladder by Integrated DNA Technologies™.

The oligonucleotide-based mobility shift assay was used to investigate the binding of the different dimers (Figure 24). All compounds tested showed only one band in the polyacrylamide gel at about 15 nt corresponding to the single-stranded oligonucleotide. These findings are consistent with the results of the plasmid-based mobility shift assay.

Nevertheless, also the respective monomer combinations were analyzed using the oligonucleotide-based mobility shift assay (Figure 25). Similarly to the hetero dimers, the tested combinations (**MbA**+**M1**, **MbA**+**M2**, **MbA**+**M3**, and **MbA**+**M4**) showed no cross-links as only single-stranded oligonucleotide (band at 15 nt) could be observed upon compound treatment.

As only compound concentrations similar to SJG-136-treated samples were evaluated, probing higher compound:oligonucleotide ratios could be beneficial to account for lower target affinities. However, since a reduction of oligonucleotide concentration is limited by the stain sensitivity needed for the assay readout, this would imply a much higher compound consumption. Nevertheless, this assay is well-suited to investigate binding site preferences of highly active DNA binders like SJG-136 and derivatives (e.g DSB-120) in a fast and inexpensive manner.
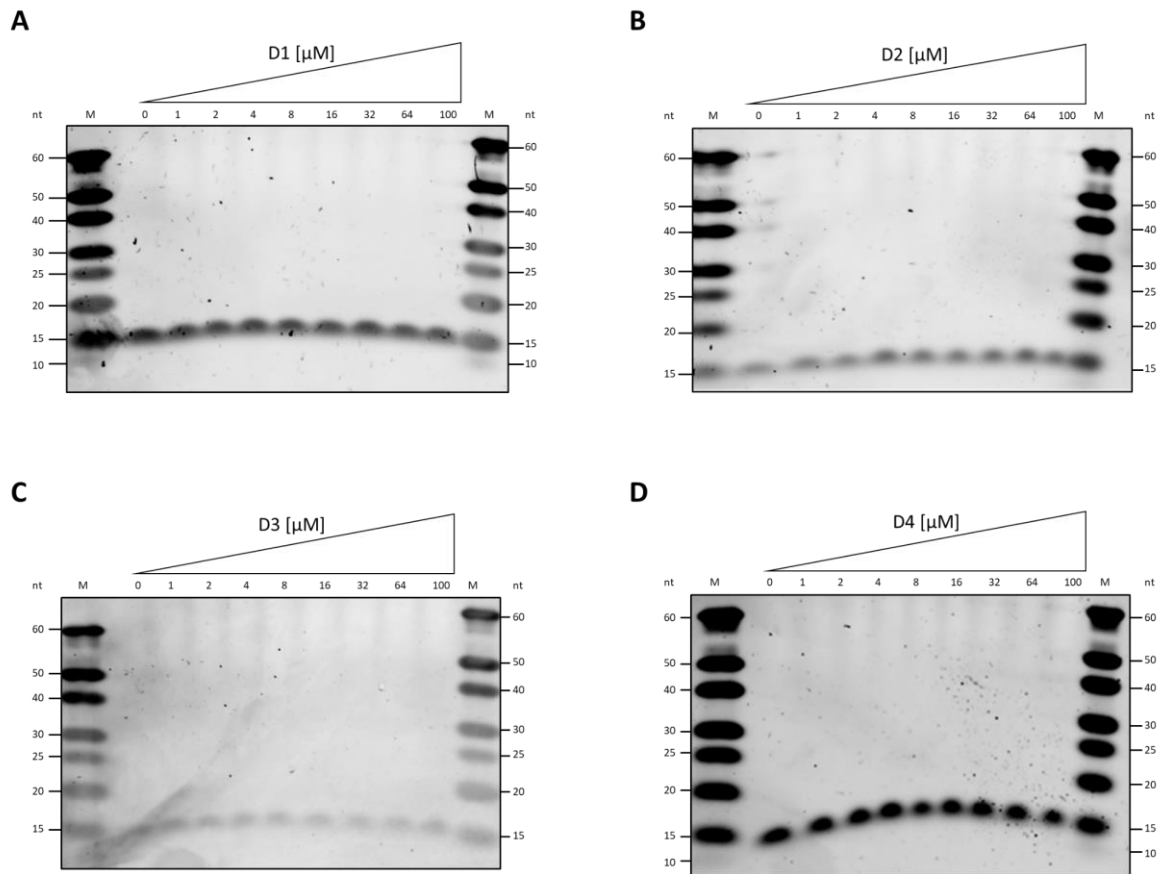
Figure 24: Oligonucleotide-based mobility shift assay showing DNA cross-linking ability of heterodimers A) **D1**; B) **D2**; C) **D3**; D) **D4** at different compound concentration ranging from 0 µM to 100 µM (final concentration). M: 10/60 ladder by Integrated DNA Technologies™.
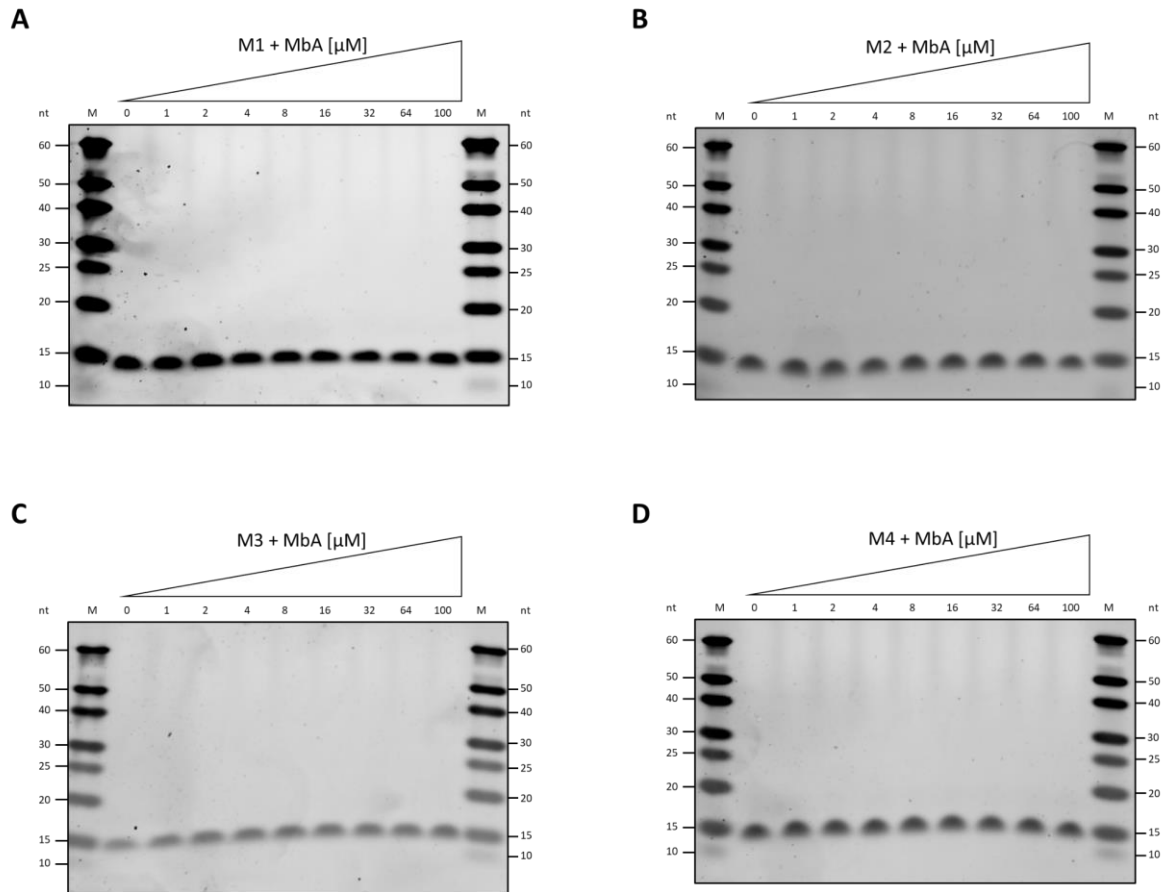
Figure 25: Oligonucleotide-based mobility shift assay showing DNA cross-linking ability of monomer combinations A) **MbA**+**M1**; B) **MbA**+**M2**; C) **MbA**+**M3**; D) **MbA**+**M4** at different compound concentration ranging from 0 µM to 100 µM (final concentration). M: 10/60 ladder by Integrated DNA Technologies™.

2.3.2.2 LC-MS-Assay

Further investigations of the binding properties of the heterodimers as well as the monomer towards DNA were carried out using a newly developed LC-MS assay. The assay development was based on previous publications by Thurston and co-workers.[65] In fact, mass spectrometry represents a direct measurement technique that allows the detection of DNA cross-links instead of measuring downstream implications on the biophysical properties of the DNA-drug adduct. Another advantage of employing mass spectrometry is its enhanced sensitivity and low detection limits compared to gel-based readouts.

This LC-MS assay is again based on oligonucleotides; hence in the first step, two single-stranded complementary oligonucleotides consisting of 12 nucleotides were annealed using standard procedures. Next, the obtained double-stranded DNA was incubated with the respective compounds or compound combinations for 24 h and subsequently subjected to HPLC (Figure 26). The denaturing conditions of the HPLC (due to the organic solvent content) cause unlinked dsDNA oligonucleotides to dissociate into ssDNA oligonucleotides. In contrast, in the case of cross-linked dsDNA oligonucleotides, the strands stay connected due to the covalent bond formation by the *inter*-strand cross-linking agent.

ssDNA and cross-linked DNA can be separated by HPLC due to the change in physiochemical properties upon cross-linkage, which influence the interactions with the solid phase. The HPLC was directly connected to a triple quad mass spectrometer allowing analysis using MRM. This MS/MS technique is particularly suitable due to its superb signal-to-noise ratios, leading to low limits of detection. Additionally, MS/MS causes the fragmentation of a mother ion into its daughter ions, providing further information of the analyte. In the case of the cross-linked DNA, the mother ion (mass corresponding to the dsDNA cross-linked by the compound) was observed to fragment into daughter ions with masses corresponding to free ssDNA, e.g. mother ion: 1119.0 (= $[\text{dsDNA+SJG-136}]^{7-}$) $\rightarrow$ daughter ion: 909.6 (= $[\text{ssDNA}]^{4-}$). Such pairs were observed for all compounds that lead to cross-links and thus formed the basis for the MRM analysis (Table 1).

Table 1: List of most prominent MRM transitions showing compound binding and cross-link formation for **SJG-136**, **D1** and **D2**. Complete list of MRMs used for detection provided in the materials and methods section.

	Mother ion	Description	Daughter ion	Description
SJG-136	1119.0	[dsDNA+SJG-136]$^{7-}$	909.6	[ssDNA]$^{4-}$
	1568.0	[dsDNA+SJG-136]$^{5-}$	1213.2	[ssDNA]$^{3-}$
	1959.5	[dsDNA+SJG-136]$^{4-}$	1820.6	[ssDNA]$^{2-}$
D1	1128.9	[dsDNA+D1]$^{7-}$	909.6	[ssDNA]$^{4-}$
	1421.0	[ssDNA+D1]$^{3-}$	1213.1	[ssDNA]$^{3-}$
	1580.0	[dsDNA+D1]$^{5-}$	1213.2	[ssDNA]$^{3-}$
	1976.0	[dsDNA+D1]$^{4-}$	1212.9	[ssDNA]$^{3-}$
D2	1425.6	[ssDNA+D2]$^{3-}$	1213.1	[ssDNA]$^{3-}$
	1583.9	[dsDNA+D2]$^{5-}$	1213.2	[ssDNA]$^{3-}$
	1979.2	[dsDNA+D2]$^{4-}$	1820.2	[ssDNA]$^{2-}$
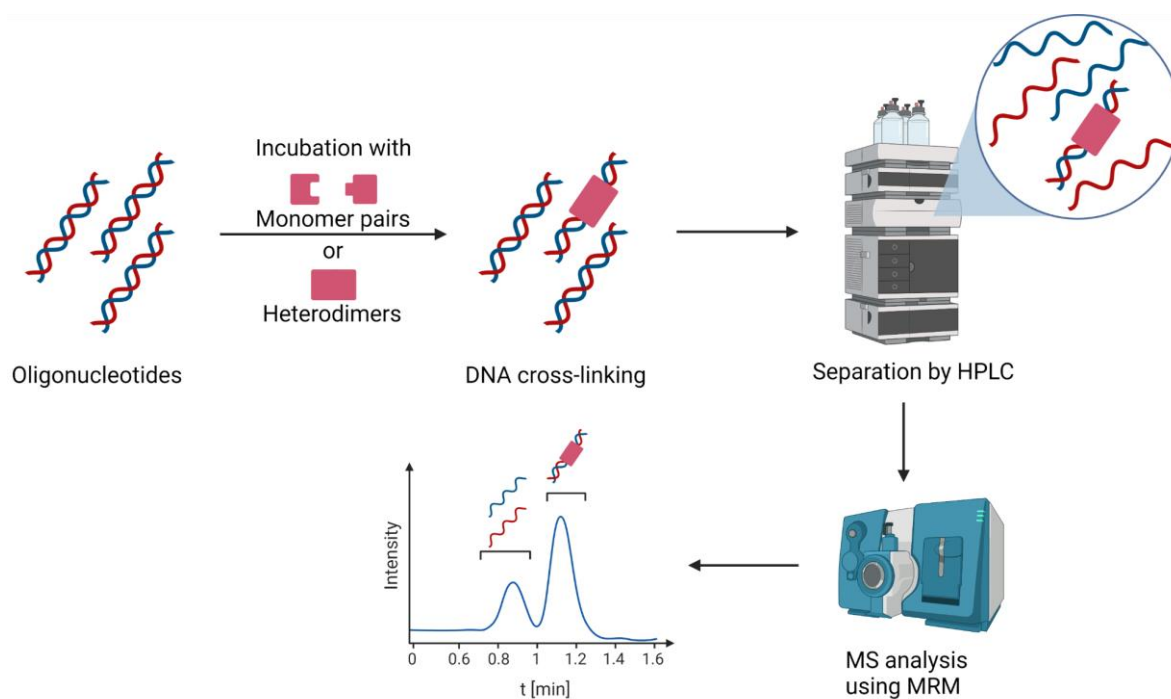
Figure 26: Schematic overview of the LC-MS assay. Created with BioRender.com.

For the development and optimization of the assay, the reference compound SJG-136 and the sequence utilized previously in the oligonucleotide-based mobility shift assay were used. The signal-to-noise ratio, the peak shape, and the peak separation could be improved significantly through intensive method optimization. Best results were obtained using a Zorbax eclipse plus C18 RRHD 1.8 µm 2.1 × 50 mm column, at a flow rate of 0.7 mL/min, a water-acetonitrile solvent system (solvent A: 100% water + 15 mm TEAB + 100 mm HFIP; solvent B: 90% ACN 10% water + 15 mm TEAB + 100 mm HFIP) applying a linear gradient from 1% to 60% B over 8 min, while the source temperature was set to 400 °C and the spray voltage was set to 3500 V.

This optimized method allowed for oligonucleotide detection at concentrations of as low as 10 nM, which corresponds to a load on column of 100 fmol (Figure 27).
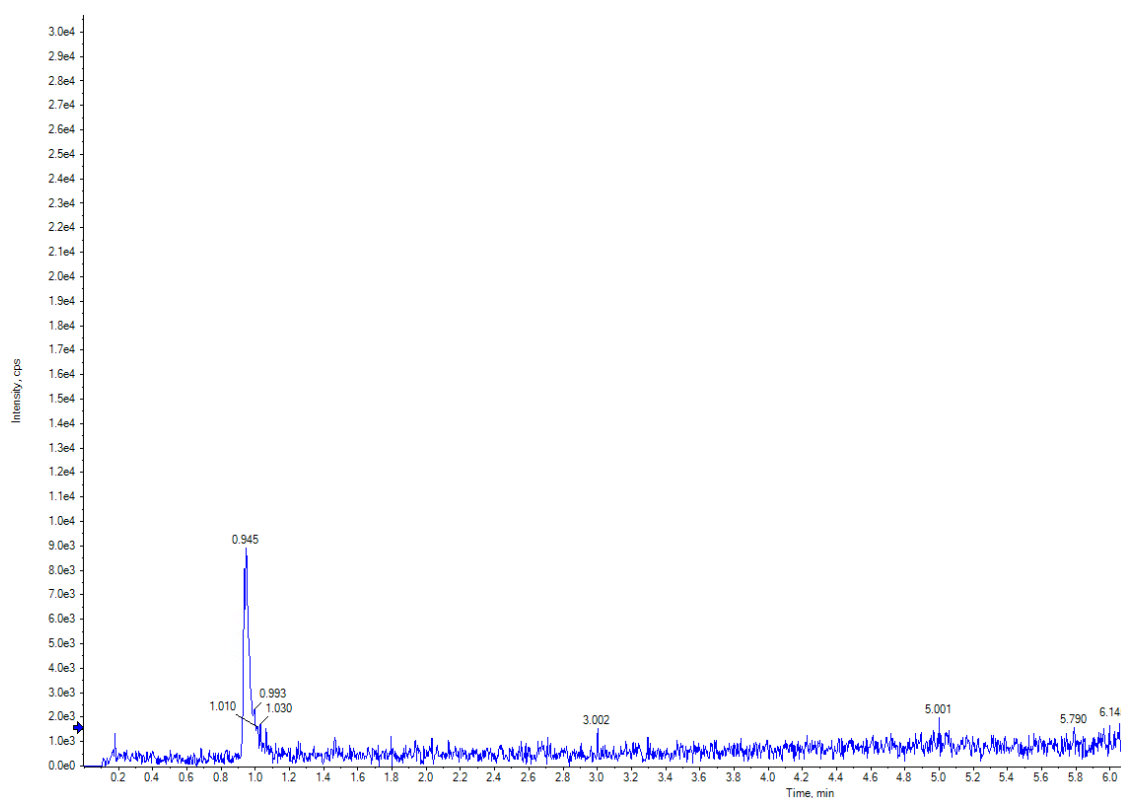
Figure 27: Oligonucleotide detection at concentrations of 10 nM using MRM.

Treating the ds oligonucleotides with SJG-136 (molar ratio 1:4), two fractions are expected to be obtained. One corresponds to the cross-linked oligonucleotide, and the other corresponds to the free double-stranded oligonucleotide. As mentioned above, the free double-stranded oligonucleotide is denatured under HPLC conditions. It is, therefore, present in its single-stranded form, while the cross-linked oligonucleotides are covalently attached to each other via the cross-linking agent, i.e., SJG-136. For the detection several

MRMs were measured, because ionization in Q1 led to a set of differently charged ions that correspond to cross-linked DNA, which can be further fragmented to their daughter ions. (Figure 28A). If MRM transitions of the free/ss oligonucleotide are measured in parallel, a second peak corresponding to the free/ss oligonucleotide appears (Figure 28B). In the case of SJG-136, this shows clearly, that the cross-linked form is the predominant form, underlying the highly effective cross-linking ability of SJG-136.
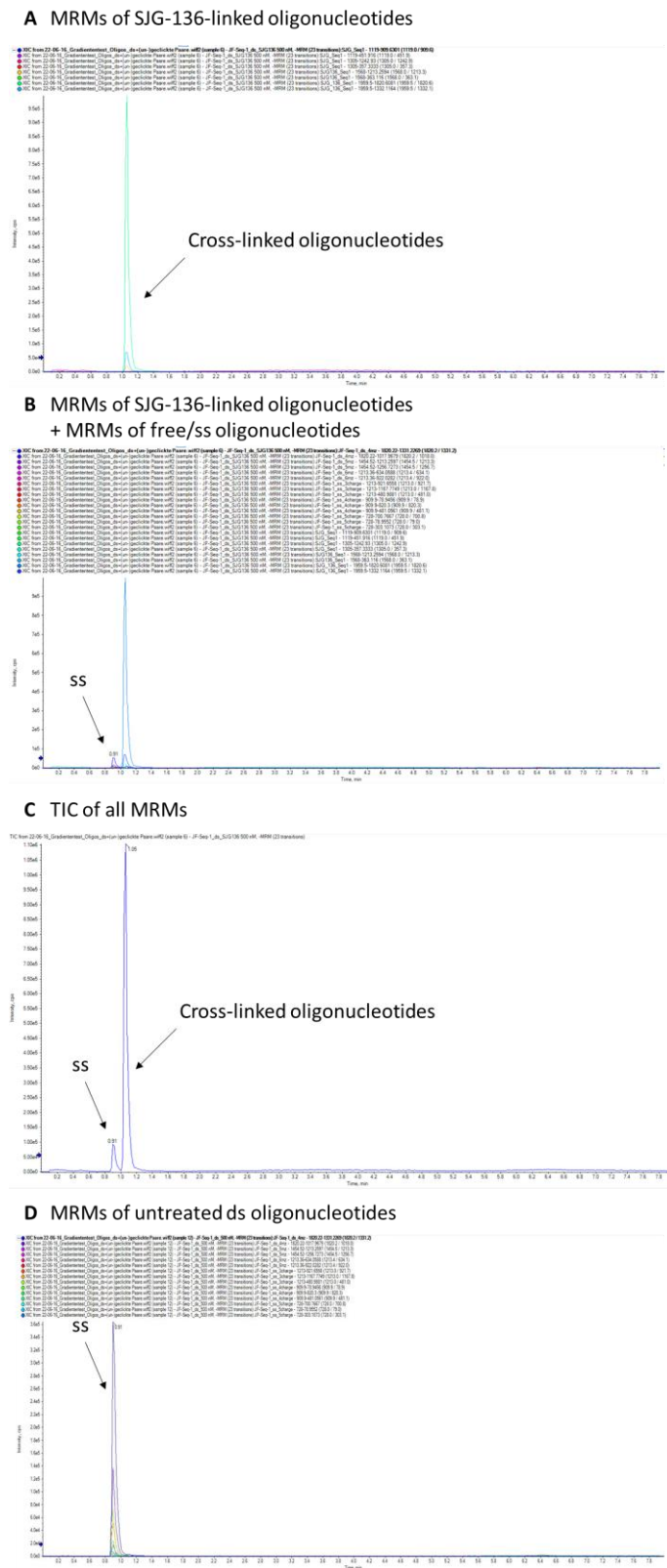
Figure 28: LC-MS assay showing DNA cross-linking of SJG-136. Different MRMs are depicted in different colors. All MRMs shown in the respective chromatogram are listed in the top left corner of that chromatogram. A: MRMs of SJG-136 linked oligonucleotides; B: MRMs of SJG-136 linked and free oligonucleotides; C: Total ion count (TIC) of all MRMs; D: MRMs of only dsDNA, appearing as ssDNA due to denaturing conditions during HPLC, serving as control.

The LC-MS assay was used to investigate the binding of the different dimers as well as the monomer combinations (Figure 29). In the case of the dimers, a clear trend was observed. SJG-136 shows the highest levels of cross-linking followed by **D1** and **D2**. The two heterodimers based on SPAAC, **D4** and **D3**, do not show any DNA cross-linkage. This can be rationalized by their sterically demanding structure involving an eight-membered ring, which may not fit into the narrow minor groove.

Next, combinations of PDB monomers were tested. Throughout all four combinations, no cross-link formation could be observed. This is in line with the previous results obtained from the conducted mobility shift assays. The monomers for the SPAAC-based dimerization may not be ideal due to their sterically demanding structure, as the preformed dimers also do not cross-link the DNA. In the case of the azide-alkyne cycloaddition-based monomers, the absence of the cross-linked product may be attributed to insufficient steric guidance provided by the DNA matrix, thus not allowing target-guided activation. Steric demand of the individual compounds should not be of great concern as the dimers are capable of forming cross-links and the molecular handles themselves are not sterically demanding.

This assay represents a direct method proving for the first time that **D1** and **D2** can form cross-links with DNA.
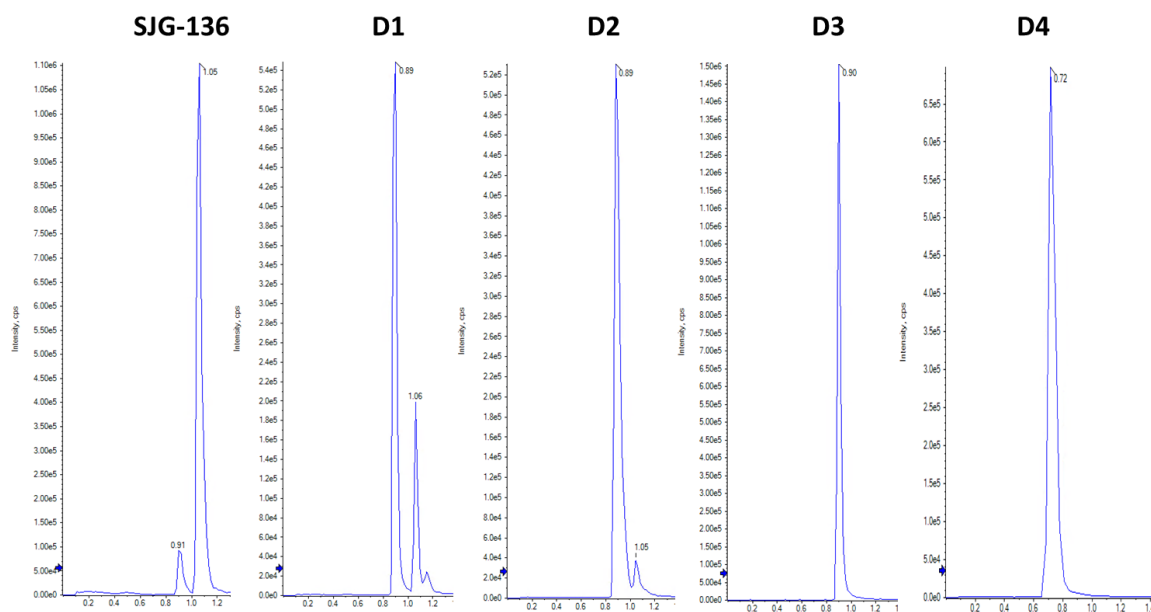
Figure 29: LC-MS assay examining DNA cross-linking ability of SJG-136 and heterodimeric PBDs obtained in this work displayed as total ion count (TIC) of all MRMs.

The particular setup of this assay provided several advantages compared to the methods described previously in the literature.[65],[70] First and foremost, the workflow is simplified by connecting the HPLC directly to the mass spectrometer. This allows for shorter assay

times by eliminating the fraction collection of the HPLC run, followed by lyophilization of each fraction and analyzing it separately by MALDI–mass spectrometry. The hyphenated workflow is thus more time-efficient. Due to the utilization of an MRM method for the oligonucleotide detection, concentrations limits and load on column limits can be improved, thus allowing a more economical usage of compound and oligonucleotide compared to the previously published procedure.[65],[70]

2.3.2.3 Fluorescence DNA thermal denaturation studies

The dimer's and monomer's DNA binding properties were further investigated by exploring their effects on the melting temperature of a series of oligonucleotides. These duplexes consist of a binding motif embedded within an $A_n \cdot T_n$ tract in which the A-strand was labeled with 5′-fluorescein and the T-strand with 3′-dabcyl. Fluorescein acts as a fluorophore, which is quenched upon duplex formation due to the close proximity to the dabcyl moiety. Through an increase in temperature, the duplex is melted. As a result, the distance between the fluorophore and the quencher is expanded. Thus, the fluorescein signal is not further quenched, and an increase in fluorescence can be measured (Figure 30).[92]

If treated with a DNA-cross-linking compound, more energy, reflected in higher temperatures, is needed to separate the two strands. As a result, a shift in melting temperature $(T_m^1 \rightarrow T_m^2)$ is observed (Figure 30, second row).

Insufficient compound binding may lead to a mixture of bound and unbound DNA. Upon temperature increase the unbound DNA is melted first, creating a first transition in the fluorescence plot. If the temperature is raised further the bound DNA is also melted, leading to a second transition in the fluorescence plot. Apart from indicating the different melting temperatures of the different species, the relative distribution of those species can also be evaluated by the relative positioning of those two transitions on the y-axis (Figure 30, third row).
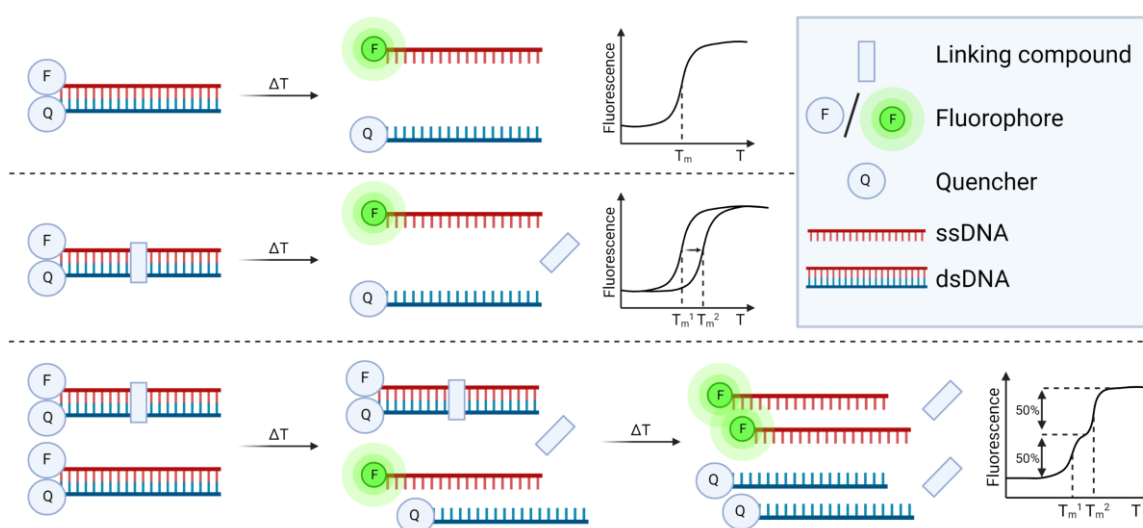
Figure 30: Schematic overview of the fluorescence DNA thermal denaturation assay. Created with BioRender.com.

A set of different binding motives was chosen representing different C-G distances as well as *inter-* and *intra*-molecular cross-links (Table 2). Additionally, a sequence designed to only allow mono-adducts was investigated.

Table 2: Overview of fluorescently labelled oligonucleotides for fluorescence DNA thermal denaturation studies. F = Fluorophore (fluorescein), Q = Quencher (dabcyl).

Name	Binding Motif	Sequence
Sequence 1	AGA	F-AAAAAAA**G**AAAAAAAA 3'
		Q-TTTTTTT**C**TTTTTTTT 5'
Sequence 2	GAAG	F-AAAAA**GAAG**AAAAAAAA-3'
		Q-TTTTT**CTTC**TTTTTTTT-5'
Sequence 3	GAAC	F-AAAAA**GAAC**AAAAAAAA-3'
		Q-TTTTT**CTTG**TTTTTTTT-5'
Sequence 4	GAAAG	F-AAAAA**GAAAG**AAAAAAA-3'
		Q-TTTTT**CTTTC**TTTTTTT-5'
Sequence 5	GAAAC	F-AAAAA**GAAAC**AAAAAAA-3'
		Q-TTTTT**CTTTG**TTTTTTT-5'
Sequence 6	GAAAAG	F-AAAAA**GAAAAG**AAAAAA-3'
		Q-TTTTT**CTTTTC**TTTTTT-5'
Sequence 7	GAAAAC	F-AAAAA**GAAAAC**AAAAAA-3'
		Q-TTTTT**CTTTTG**TTTTTT-5'

The influence of each compound on the melting curve of each of the oligonucleotides was investigated (Figure 31 to Figure 34; the melting temperatures are presented in Table 3). Each data set contains a control, which corresponds to the melting curve of the respective untreated oligonucleotide. In addition, the melting curve of the sequence incubated with SJG-136 was measured.

The control showed only one sigmoidal transition with its inflection point indicating the respective sequence's melting temperature (T_m). Several compounds affect the melting profiles causing multiple transitions, which will be discussed in greater detail down below.

Sequence 1, with the binding motif of AGA, provides only one guanine for binding. It therefore has no possibility of either cross-linking or multiple drug binding, thus providing information about the formation of mono-adducts and the associated shift in melting temperature produced with only one PBD bound per duplex. PBD dimers are generally

capable of engaging with DNA in form of a mono-adduct (Figure 31A). Besides, it can be observed that **D1** and **D2** lead to a significant shift in T_m.

Furthermore, **D1** and SJG-136 both lead to an increase in the melting temperature reaching a final T_m of 66.7 °C and 67.4 °C, respectively. **D2** also stabilizes the double helix, as represented by the increase in T_m. However, the stabilization is less pronounced (62.0 °C). Moreover, the melting profile of **D2**-incubated sequence 1 showed two transitions. The first one represents the melting of the free oligonucleotide, as a comparison with the T_m of the control (sequence 1, no compound added) showed. The second one represents the melting of the duplex stabilized through **D2**, which leads to an increase in T_m. Looking at the relative positioning of those two transitions on the y-axis provides additional insights regarding the ratio of the free duplex and the duplex that has been modified within the incubation period (Figure 30, third row). Herein it was observed that **D1** binds to sequence 1 to a higher proportion and leads to a higher stabilization of the double strand compared to **D2**. **D4** and **D3** both led to little to no change in the T_m of sequence 1 upon incubation. This indicates that even with only one guanine present in the test oligonucleotide, **D4** and **D3** are not capable of engaging said nucleobase, which hints towards steric clashes between the demanding cyclooctyne ring present in those structures and the minor groove of the DNA, which may affect the binding properties of **D4** and **D3**.

The same experiment was conducted using the single monomers to investigate their binding abilities independently. Figure 31B shows that all monomers affect the melting profile of sequence 1, although **D4** and **D3** showed only little changes. Meanwhile, **MbA**, **M1**, and **M2** have partially overlapping profiles. Interestingly, this group of three not only has very similar effects on the melting temperature, but also showed similarities in the ratio of free sequence and compound-bound sequence.
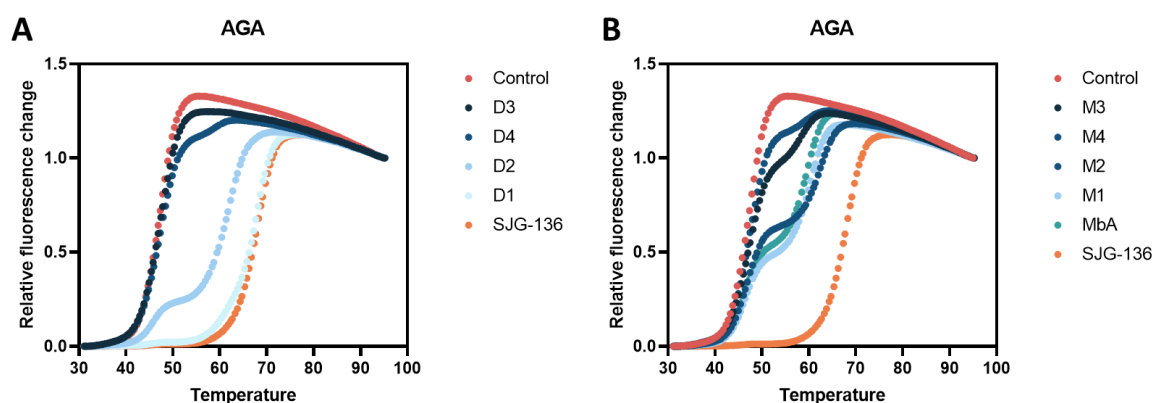
Figure 31: Fluorescence melting profiles of sequence 1 (binding motif AGA) in presence of A) heterodimers **D1**, **D2**, **D3**, and **D4** and B) monomers **M1**, **M2**, **M3**, **M4** and **MbA**. The control (red) represents the DNA duplex without any compound added. SJG-136 (orange) serves as a positive control. The identity of the central three bases is indicated above each panel. Experimental work was performed by Prof. Keith Fox.

Next, the binding properties of the compounds were tested in the presence of two guanine residues (Figure 32 to Figure 34). Depending on the positioning of the two guanine residues, different G-G distances as well as *intra*-strand and *inter*-strand cross-links can be distinguished. In addition, as indicated above, mono-adducts can also be formed. The set of different possibilities is reflected in the design of the different sequences (Table 2).

In sequence 2 the two guanines are separated by two adenines and are positioned on the same strand, enabling *intra*-strand cross-links. Figure 32A and Figure 32B show the melting profiles of sequence 2 after incubation with dimeric and monomeric compounds. SJG-136 lad to the highest increase in melting temperature. Yet, **D1** also causes a significant shift in melting temperature. Herein three transitions can be observed. The first corresponds to the free duplex, as can be seen from a comparison of the melting temperature of the free control. The second transition can be assigned to the mono-adduct based on the results obtained using sequence 1, which is by design only capable of forming mono-adducts. The third transition corresponds to the highest melting temperature indicating the most effective stabilization, indicating a cross-link. In addition, it is important to note that the different proportions of the above-discussed binding forms vary depending on the compound used. SJG-136, for example, showed no transition in the range of 40 °C to 50 °C, indicating that no free duplex was present when incubated with SJG-136. On the other hand, the first transition of **D1**-incubated sequence 2 accounts for about 13% of the different species present. The two other transitions, which correspond to the mono-adduct and the cross-linked species, account for ca. 36% and 51%, respectively, in the case of incubation with **D1**.

Besides, **D1** is the best binder out of all dimers, excluding the SJG-136 control (Figure 32A). **D2** caused some shift in the melting profile, **D4** and **D3** however, did not cause any

significant change in melting temperature, which is in line with the previously observed lack of binding to AGA-containing sequence 1.

The melting profiles of the single monomers show a second melting point (T_m) of about 61.1 °C, 61.3 °C, 63.5 °C, and 59.9 °C respectively (Figure 32B). This is in the same range (~60 °C) as the T_m measured for sequence 1, which corresponds to the respective mono-adducts. Yet, the relative positioning of the transitions on the y-axis reveals that ca. 72% to 84% of the sample in the case of **M1**, **M2**, and **MbA** corresponded to the free duplex and only approx. 16% to 28% were bound by one of the monomers (Figure 32 and Table 3). When using sequence 1, around 46% to 60% of the oligonucleotide were bound by the monomers. For **M4** and **M3** the fraction of free duplex in the case of sequence 2 was even higher (100% and 90%, respectively), while sequence 1 led to 77% and 90% of free oligonucleotides. At this point, it should be emphasized that not only for the dimers but even for the monomers, a change in the sequence had a non-negligible effect on the percentage of compound bound to the duplex.

Next, the binding properties towards sequence 3 were examined. The binding motif was chosen to be GAAC so that two adenines still separate the two guanines, but here the second guanine is on the opposite strand, allowing for inter-strand cross-links. Introducing this change compared to sequence 2 positively impacted the melting profiles. While **D3** did not show any effect, all other compounds caused a change in T_m. **D4** changed from not-binding (sequence 2) to 34% binding (sequence 3) while causing T_m to shift to 62.1 °C.

Similarly, **D2** showed an improved bound and unbound duplex ratio, as reflected by the relative change in the proportion of the different transitions. Yet, **D1** treatment gave the best results, leading to an almost complete overlap with the SJG-136 treated control (Figure 32C). Treatment of sequence 3 with **D1** led to close to 0% of free duplex, 18% mono-adduct, and 82% cross-links. The change in the ratio of free to bound or cross-linked DNA implies that **D1** preferentially forms *inter*-strand cross-links rather than *intra*-strand cross-links.

The change in sequence also had a positive effect on most of the melting profiles of the individual monomers (Figure 32D). An interesting effect that was observed when using this sequence, and was even more pronounced in the sequences 4 - 7 (discussed below), is that e.g., **M1** showed a triphasic progression, though cross-links are not possible since only one monomer was provided. This effect could be explained by two single monomers binding independently to each of the guanines. This assumption is supported by the fact that the

effect is amplified with increasing distance between the guanines, which makes binding a second monomer easier due to reduced steric hindrance caused by the first monomer (Figure 32 to Figure 34).
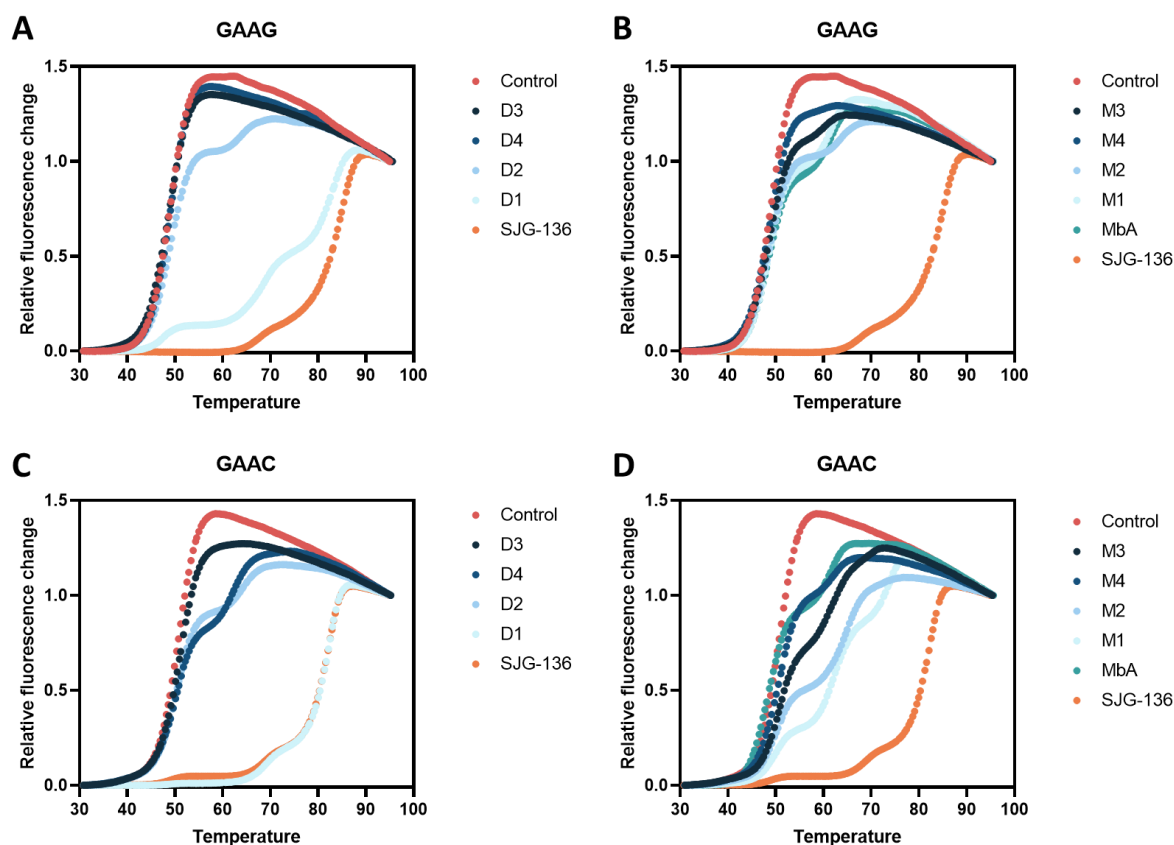
Figure 32: Fluorescence melting profiles of sequence 2 (binding motif GAAG) and 3 (binding motive GAAC) in presence of heterodimers and monomers. The control (red) represents the DNA duplex without any compound added. SJG-136 (orange) serves as a positive control. The identity of the central three bases is indicated above each panel. Left (A and C): heterodimers **D1**, **D2**, **D3**, and **D4**. Right (B and D): monomers **M1**, **M2**, **M3**, **M4** and **MbA**. Experimental work was performed by Prof. Keith Fox.

To further investigate the impact of the G-G distance, sequences 4 to 7 were tested (Figure 33 and Figure 34; Table 3). The G-G distance was increased, placing three as well as four adenines in between the two guanines. Additionally, the guanines were placed to either allow *intra*-strand cross-links or *inter*-strand cross-links. A similar pattern within the group of compounds can be observed in all four cases. **D1** was also for those sequences the best-performing dimer, followed by **D2**. **D4** and **D3** only showed minor to no effects on the respective melting profiles. For the monomers, the above-described effect of two single monomers binding to the same duplex can be observed, especially for **M1**, **M2**, and **MbA**. The effect was smaller for **M4** and **M3**, which may be due to their higher steric demand, causing a potential steric clash if a second monomer was bound.
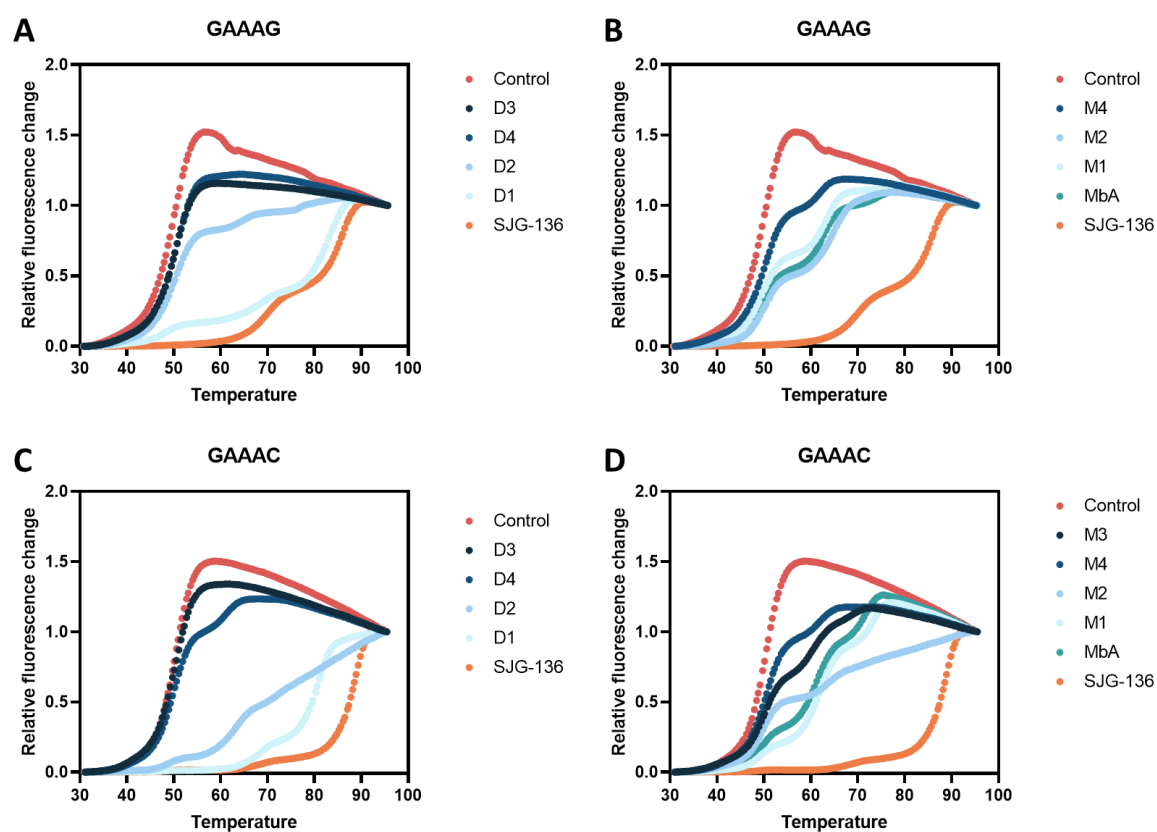
Figure 33: Fluorescence melting profiles of sequence 4 (binding motif GAAAG) and 5 (binding motif GAAAC) in presence of heterodimers and monomers. The control (red) represents the DNA duplex without any compound added. SJG-136 (orange) serves as a positive control. The identity of the central three bases is indicated above each panel. Left (A and C): heterodimers **D1**, **D2**, **D3**, and **D4**. Right (B and D): monomers **M1**, **M2**, **M3**, **M4** and **MbA**. Experimental work was performed by Prof. Keith Fox.
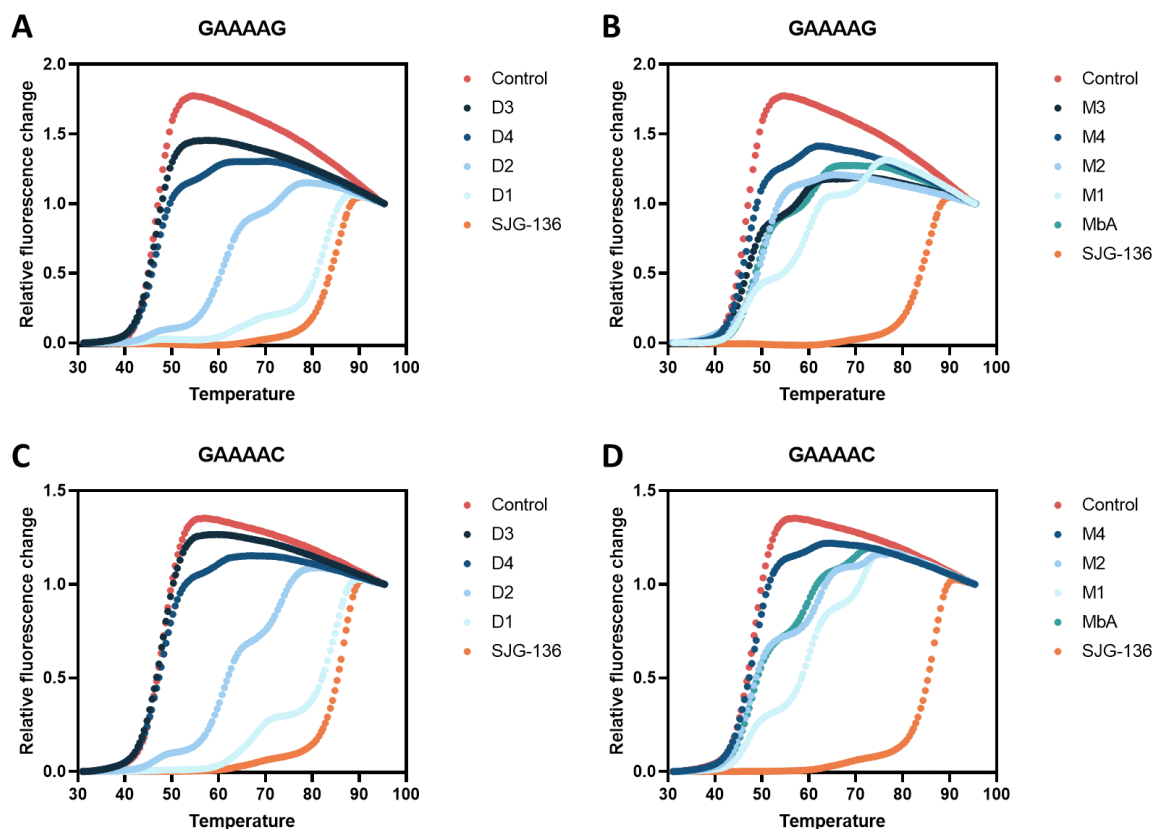
Figure 34: Fluorescence melting profiles of sequence 6 (binding motif GAAAAG) and 7 (binding motif GAAAAC) in presence of hetero dimers and monomers. The control (red) represents the DNA duplex without any compound added. SJG-136 (orange) serves as a positive control. The identity of the central three bases is indicated above each panel. Left (A and C): heterodimers **D1**, **D2**, **D3**, and **D4**. Right (B and D): monomers **M1**, **M2**, **M3**, **M4** and **MbA**. Experimental work was performed by Prof. Keith Fox.

In general, the experiments with the different sequences showed a clear trend of duplex stabilization by the different dimers. The duplexes treated with the asymmetrical SPAAC based dimer **D3** showed only one transition, which is in the range of the untreated duplex. Therefore, **D3** appears to be the poorest binder out of the compounds tested. **D3** is closely followed by **D4**, which is also based on the strain-promoted azide-alkyne cycloaddition but utilizes a symmetric cyclooctyne. **D4** did show some stabilization; however, the melting profiles indicate that only ca. 10% of the duplex is stabilized by **D4**. A significantly larger effect on duplex stabilization as well as on the relative proportion of stabilized duplex is obtained by incubation with **D2**. This dimer connects two nortomaymycin cores via a triazole unit, which is obtained by a CuAAC. The linking unit between the two cores is significantly smaller than for the SPAAC-based dimers **D4** and **D3**. Nonetheless, **D1**, which has a linker that is one carbon shorter than the one in **D2**, gives by far the best results, both in terms of T_m and also in terms of the relative proportion of the stabilized duplex.

A similar trend can be seen for the monomers. Herein, the two monomers carrying a cyclooctyne moiety tended to perform poorer than the alkynes and the azide, most likely due to the steric bulk of the cyclooctyne rings. Although the trend was similar for the monomers, the differences in the melting profiles were not as pronounced as with the dimers.

Another observation is that for all tested compounds, the ability to stabilize the duplex and the relative percentage of the stabilized duplex varies depending on the sequence. SJG-136, despite its preference for the binding motif R-GATC-Y,[70] was also able to bind to motives that were, in some cases, significantly different. In this context, SJG-136 showed to be more robust towards sequence changes than all tested compounds. In addition, SJG-136 induced the highest T_m shift and, thus, the best stabilization of the double strand in all experiments. However, for sequence 3, the measured T_m for **D1** (81.6 °C) was almost identical to the one of SJG-136 (81.5 °C), indicating equally good stabilization of this particular duplex.

Table 3: Melting temperatures of the fluorescently labelled oligonucleotides incubated with compounds **D1**, **D2**, **D3**, **D4**, **MbA**, **M1**, **M2**, **M3**, **M4** and SJG-136. T_m^1, T_m^2 and T_m^3 correspond to the melting temperatures of the first, second and third transition. Values in parentheses correspond to the proportion (in %) of the transition by the free DNA and the first and second melting transition respectively. Percentages are rounded to the next full percentage. * indicates that the transition is broad and could therefore not be precisely resolved.

		SJG-136	D1	D2	D4	D3	MbA	M1	M2	M3	M4
AGA											
$T_m = 47.0$ °C	T_m^1	67.4	66.7	45.8	47.1	47.1	46.4	46.4	46.7	47.1	47.3
		(100)	(100)	(20)	(93)	(100)	(43)	(40)	(54)	(77)	(90)
	T_m^2			61.4	58.7		59.2	59.9	62.0	58.0	58.8
				(80)	(7)		(57)	(60)	(46)	(23)	(10)
	T_m^3										
GAAG	T_m^1	68.0	47.4	48.9	48.9	48.5	48.4	48.5	48.5	48.5	48.6
$T_m = 48.8$ °C		(15)	(13)	(85)	(100)	(100)	(73)	(72)	(84)	(90)	(100)
	T_m^2	84.1	68.2	63.9			61.1	61.3	63.5	59.9	
		(85)	(36)	(15)			(27)	(28)	(16)	(10)	
	T_m^3		82.4								
			(51)								
GAAAG	T_m^1	70.2	47.7	49.8	49.8	49.7	49.3	49.3	49.9	49.7	49.8
$T_m = 49.7$ °C		(39)	(16)	(78)	(100)	(100)	(50)	(56)	(95)	(100)	(81)
	T_m^2	85.3	68.4	64.4			62.5	63.0	61.5		61.6
		(61)	(24)	(12)			(40)	(41)	(5)		(19)
	T_m^3		82.7	78.1			73.5	74.6			
			(60)	(10)			(10)	(3)			
GAAAAG	T_m^1	85.5	44.4	45.2	46.4	46.4	46.2	46.2	45.9	46.5	46.6
$T_m = 46.6$ °C		(100)	(2)	(8)	(88)	(100)	(44)	(33)	(32)	(77)	(89)
	T_m^2		65.0	60.7	57.7		58.9	59.3	61.0	58.2	57.7
			(18)*	(72)	(12)		(41)	(48)	(63)	(23)	(11)
	T_m^3		82.4	73.1			71.0	72.1	73.2		
			(80)	(20)			(15)	(19)	(5)		
GAAC	T_m^1	48.7	69.9	50.2	50.0	50.7	49.6	49.8	50.0	50.8	50.5
$T_m = 50.6$ °C		(5)	(18)	(77)	(66)	(100)	(15)	(25)	(46)	(56)	(83)
	T_m^2	68.9	81.6	64.0	62.1		62.0	62.4	64.5	61.8	61.6
		(13)	(82)	(23)	(34)		(37)	(47)	(54)	(44)	(17)
	T_m^3	81.5					71.8	73.3			
		(82)					(48)	(28)			
GAAAC	T_m^1	48.3	47.4	48.9	49.9	49.8	49.7	49.7	49.4	50.3	50.3
$T_m = 50.0$ °C		(1)	(1)	(22)	(79)	(100)	(24)	(17)	(69)*	(59)	(80)
	T_m^2	68.8	68.4	63.0	60.7		61.2	61.8	63.8	60.5	61.4
		(9)	(21)	(78)	(21)		(48)	(57)	(31)	(32)	(20)
	T_m^3	88.2	80.5				71.1	72.9		68.4	
		(90)	(78)				(28)	(26)		(9)	
GAAAAC	T_m^1	67.8	66.5	46.3	47.6	47.7	47.6	46.9	47.3	47.7	48.0
$T_m = 48.1$ °C		(8)	(29)	(10)	(90)	(100)	(59)	(26)	(62)	(100)	(93)
	T_m^2	86.1	84.2	60.8	59.0		59.6	59.8	61.9		59.6
		(92)	(71)	(55)	(10)		(31)	(49)	(32)		(7)
	T_m^3			73.1			69.3	71.4	72.5		
				(35)			(10)	(25)	(6)		

Since **D1** and **D2** showed the most promising results in the previous experiments, the combination of the corresponding monomers, i.e., **MbA** + **M1** and **MbA** + **M2** were tested in order to gain information about the potential *in situ* dimerization at the DNA. The results are shown in Figure 35 for the combination of **MbA** + **M1** and in Figure 36 for the combination of **MbA** + **M2**. Additionally, the results are summarized in Table 4. All plots comprise the control, which corresponds to the neat duplex as well as the respective oligo duplex incubated with the two monomers alone, the combination of both monomers, and the respective synthesized dimer serving as the positive control. Four different sequences (sequences 2, 3, 4, and 5, see Table 2) were used for the study.

 M1 (light blue) and **MbA** (green) induced only minor changes within the melting profile of the different sequences (Figure 35). On the other hand, incubation of the respective sequence with **D1** (orange) led to a significantly greater change in the melting profile indicating stabilization of the oligonucleotide duplex. However, the combination of the monomers (dark blue), which in principle are able to dimerize via a structurally guided *in situ* click reaction,[7],[164],[165] showed melting profiles that cluster with the melting profiles of the single monomers. If the dimerization had been successful, a profile analogous to the **D1** incubated samples would have been expected. Instead, T_m values in the range of the monomers are observed (Table 4). These findings suggest that an *in situ* dimerization did not occur.
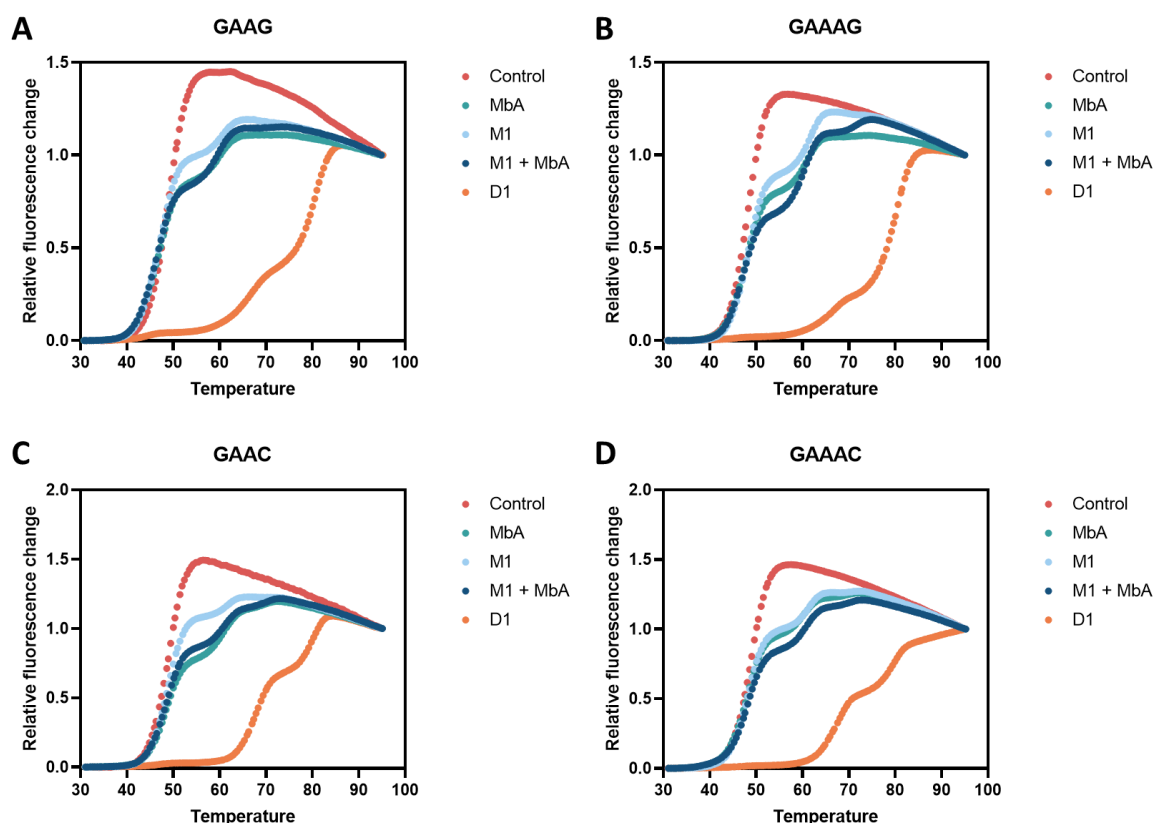
Figure 35: Fluorescence melting profiles of sequence 2, 3, 4, and 5 in presence of a heterodimer **D1**, the corresponding monomer combinations **MbA** + **M1** and the corresponding single monomers **MbA** and **M1**. The control (red) represents the DNA duplex without any compound added. The identity of the central three bases is indicated above each panel. A) sequence 2; B) sequence 4; C) sequence 3; D) sequence 5. Experimental work was performed by Prof. Keith Fox.

The same experiment was also conducted with the monomers **MbA** and **M2**, which are, in principle, able to form **D2** upon dimerization via a click reaction (Figure 36). For the sequences incubated with **D2** the differences in melting profiles were not as pronounced as with **D1**. Hence, the different melting profiles partly overlap. Nevertheless, the combination of the monomers (dark blue) led to melting profiles that showed higher shares of the unbound DNA and the mono-adducts compared to the melting profiles of the **D2** treated sequences (orange).

In the case of sequences 2, 3 and 5 the melting profiles showed higher shares of the unbound DNA and the mono-adducts even when compared to the azide, negating the expected synergistic effect of the two monomers. Thus, the results imply that an *in situ* dimerization did not occur.
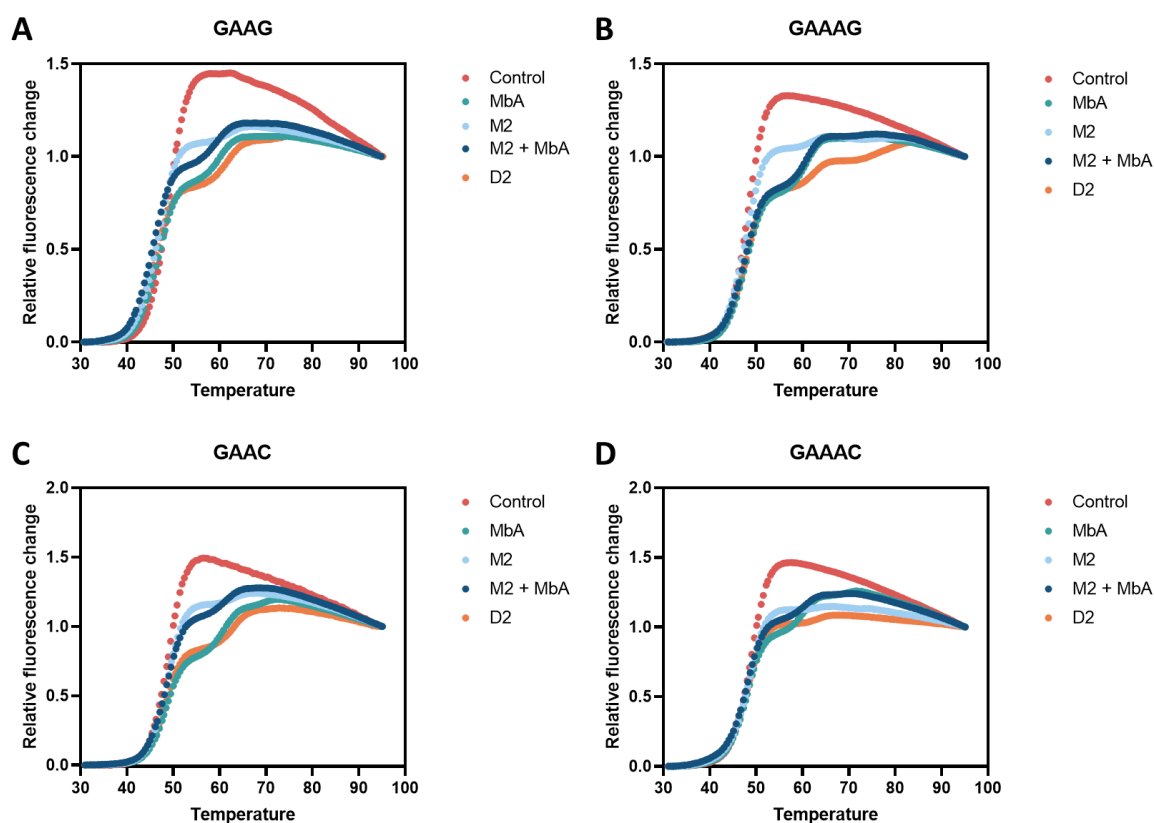
Figure 36: Fluorescence melting profiles of sequence 2, 3, 4, and 5 in presence of a heterodimer **D2**, the corresponding monomer combinations **MbA** + **M2** and the corresponding single monomers **MbA** and **M2**. The control (red) represents the DNA duplex without any compound added. The identity of the central three bases is indicated above each panel. A) sequence 2; B) sequence 4; C) sequence 3; D) sequence 5. Experimental work was performed by Prof. Keith Fox.

Although the synergistic effect expected as a result of potential *in situ* dimerization was absent for both monomer combinations using this method, a number of important pieces of information can be gleaned from the obtained data sets. First, it should be noted that **D1** and **D2** bound to a set of sequences and possess the ability to form cross-links and mono-adducts. Likewise, the single monomers were able to bind to the different sequences in the form of mono-adducts as well and thereby cause an increase in T_m.

Table 4: Melting temperatures of the fluorescently labelled oligonucleotides incubated with compounds **D1**, **D2**, **M1**, **M2**, **MbA** as well as the two combinations **MbA** + **M1** and **MbA** + **M2**. T_m^1, T_m^2 and T_m^3 correspond to the melting temperatures of the first, second and third transition. Values in parentheses correspond to the proportion (in percent) of the transition that is represented by the free DNA, first and second melting transition respectively. Percentages are rounded to the next full percentage. * indicates that the transition is broad and could therefore not be precisely resolved.

		D1	MbA	M1	MbA + M1	D2	MbA	M2	MbA + M2
GAAG	T_m^1	47.4	48.4	48.5	46.2	48.9	48.4	48.5	45.4
		(13)	(73)	(72)	(72)	(85)	(73)	(84)	(80)
T_m = 48.8 °C	T_m^2	68.2	61.1	61.3	59.3	63.9	61.1	63.5	58.9
		(36)	(27)	(28)	(18)	(15)	(27)	(16)	(20)
	T_m^3	82.4			47.1				
		(51)			(56)				
GAAAG	T_m^1	47.7	49.3	49.3	60.4	49.8	49.3	49.9	47.4
T_m =49.7 °C		(16)	(50)	(56)	(36)	(78)	(50)	(95)	(74)
	T_m^2	68.4	62.5	63.0	71.3	64.4	62.5	61.5	60.5
		(24)	(40)	(41)	(8)	(12)	(40)	(5)	(26)
	T_m^3	82.7	73.5	74.6		78.1	73.5		
		(60)	(10)	(3)		(10)	(10)		
GAAC	T_m^1	69.9	49.6	49.8	48.3	50.2	49.6	50.0	48.4
T_m = 50.6 °C		(18)	(15)	(25)	(71)	(77)	(15)	(46)	(83)
	T_m^2	81.6	62.0	62.4	60.8	64.0	62.0	64.5	60.9
		(82)	(37)	(47)	(22)	(23)	(37)	(54)	(17)
	T_m^3		71.8	73.3	68.9		71.8		
			(48)	(28)	(7)		(48)		
GAAAC	T_m^1	47.4	49.7	49.7	48.0	48.9	49.7	49.4	47.8
T_m = 50.0 °C		(1)	(24)	(17)	(70)	(22)	(24)	(69)*	(85)
	T_m^2	68.4	61.2	61.8	60.7	63.0	61.2	63.8	60.0
		(21)	(48)	(57)	(23)	(78)	(48)	(31)	(15)
	T_m^3	80.5	71.1	72.9	68.4		71.1		
		(78)	(28)	(26)	(7)		(28)		

2.3.2.4 DNase I footprinting

In order to further explore the binding sites of the compounds, DNase I footprinting was deployed.[92],[175] The DNA fragments MS1 and MS2, which were designed to contain all 134 tetranucleotide sequences, were used.[92],[175] MS1 and MS2 have the same sequence, which is cloned in opposite orientations; thus MS1 is one strand, while MS2 is the complementary strand.[92],[175]. Therefore, sites at the top of the gel for MS1 are at the bottom for MS2 and vice versa. The DNA strands were ^{32}P-labeled at the 3'-end to allow for radioactive readout. The DNA was incubated with the respective compound and afterwards digested by DNase I, resulting in smaller DNA fragments. If a compound was bound to the DNA, this resulted in local protection of DNA processing by DNase I. Therefore, when analyzing the digested samples via gel electrophoresis, the position of the bound compound showed up as a gap within the DNA fragment pattern (a schematic overview of this assay is presented in Figure 37).
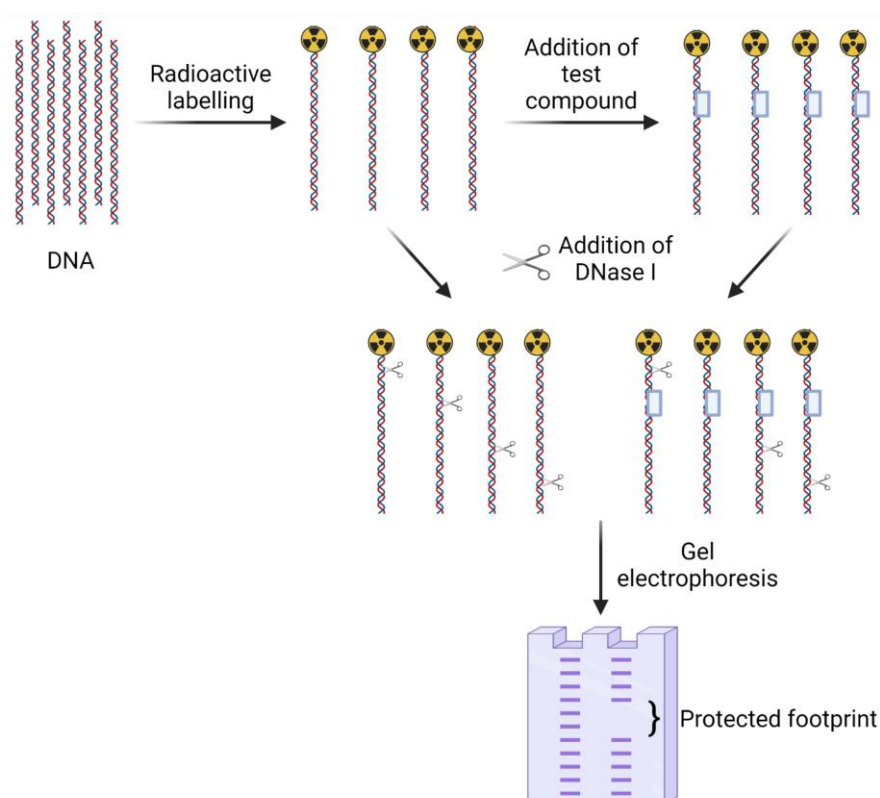
Figure 37: Schematic overview of DNase I footprinting assay. Created with BioRender.com.

DNase I has been found to overestimate the size of ligand binding sites and generates footprints that are offset toward the 3′-end of the actual binding site.[92]

The footprints of the dimers (**D1**, **D2**, **D3**, **D4**) as well as for the monomers (**M1**, **M2**, **M3**, **M4**, and **MbA**) are presented in Figure 38. The dimers were tested at two different concentrations (1 µM and 10 µM), whereas the monomers were only tested at 10 µM. For all tested dimers, no difference between the two concentrations was observed (Figure 38).
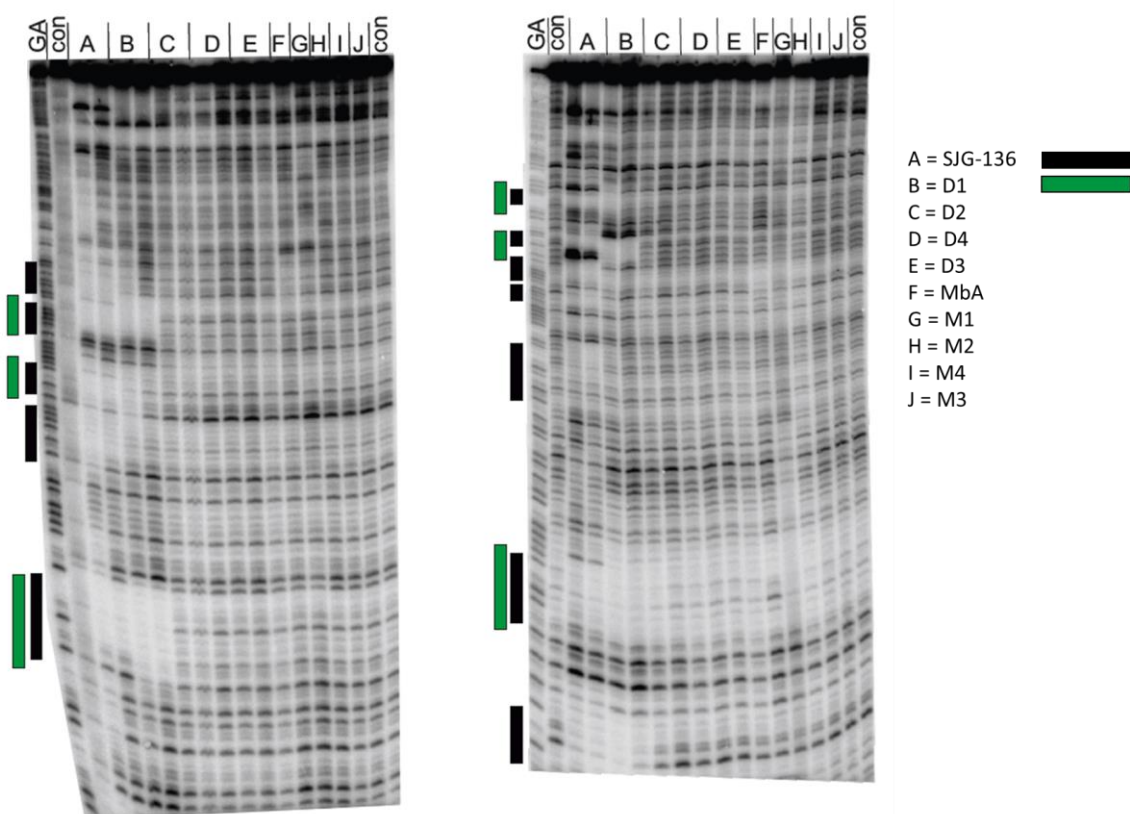
Figure 38: DNase I footprinting of compounds **SJG-136** (= A) **D1** (= B), **D2** (= C), **D3** (= E), **D4** (= D)**, M1** (= G), **M2** (= H), **M3** (= J), **M4** (= I), and **MbA** (= F). MS1 and MS2 were used as DNA fragments. Sites at the top of the gel for MS1 (left) are at the bottom for MS2 (right) and *vice versa*. Lanes labeled with "con" refer to the control. Controls show DNase cleavage without any added compound. Lanes labeled with "GA" are Maxam-Gilbert markers specific for purines. The regions protected from DNase I cleavage are highlighted by the boxes on the left-hand side of the gels. Protected regions were identified by visual inspection of the gels. Experimental work was performed by Prof. Keith Fox.
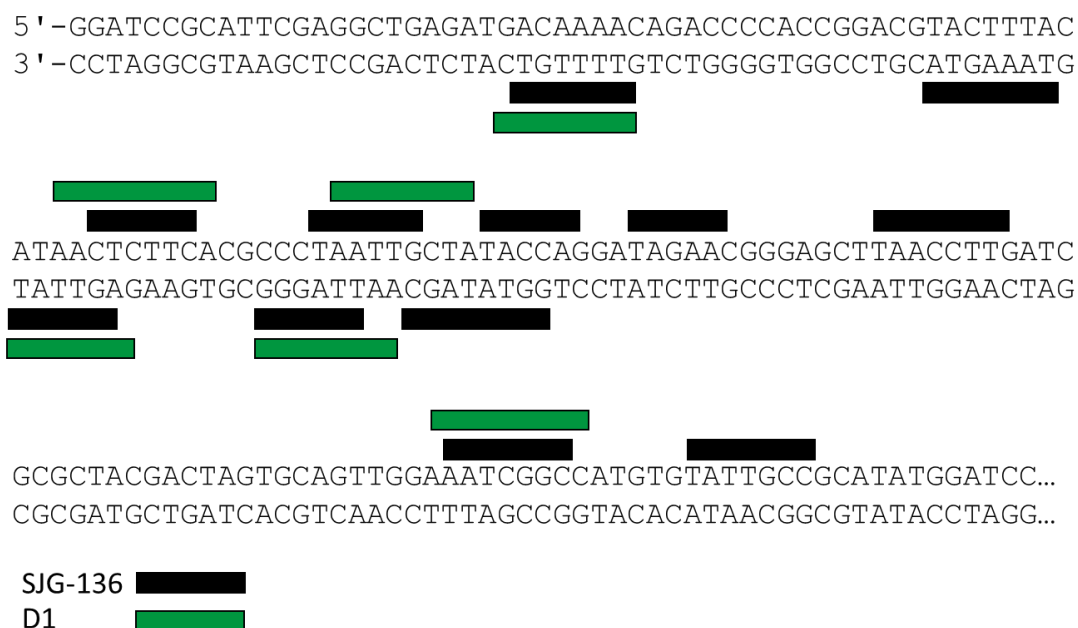
Figure 39: Sequence of MS2 (top) and MS1 (bottom) with boxes indicating the positions of the footprints produced by **SJG-136** (labeled in black) and **D1** (labeled in green). Experimental work was performed by Prof. Keith Fox.

D1 (labeled as B in Figure 38) showed several footprints, as indicated by the green bars in Figure 39. In addition, SJG-136 was deployed as a control. It is to be expected that the footprinting patterns of SJG-136 are different from those produced by the compounds, since the change of the linker between the two nortomaymycin cores affects the binding motives and patterns, as previously shown in the literature.[176] However, when comparing the footprints of **D1** with the cleavage pattern in the presence of SJG-136, a partial overlap can be observed. Even though **D1** produced fewer footprints than SJG-136, all identified footprints overlap with regions protected by SJG-136, thus showing a similar preference in the binding pattern. For the monomers, only the azide (**MbA**) and the alkyne (**M1**) showed slight differences compared to the control. One explanation for this outcome can be that footprints are much easier to recognize when the ligand binds a larger section of the DNA and thus blocks the DNase I over a larger segment. With correspondingly larger or longer molecules, such an increased binding area is much easier to achieve. Small or short molecules, such as the monomers with only short handles attached, therefore, often show little to no observable footprints.

On top of that, compounds like SJG-136 or **D1** are capable of forming cross-links (see section 2.3.2.2 and 2.3.2.3). Hence, these compounds benefit from a tighter binding, which may also contribute to a stronger footprinting pattern, whereas compounds only forming mono-adducts may not benefit from such effects.

Besides, the thermal denaturation studies (see section 2.3.2.3) showed that in many cases, especially for the monomers, a significant proportion of the compound was not bound to the DNA. If this also holds true in the footprinting assay, a lack of pattern can also be explained by a lower proportion of compound-DNA adducts.

2.4 Summary and outlook

The main objective of this study was the design a two-component system based on tomaymycin derivatives that allows for *in situ* dimerization, transferring the concept of on-target synthesized antibiotics to the tomaymycin dimer scaffold. Thus, a nortomaymycin derivative was synthesized to serve as an easily modifiable core structure. Different synthetic routes to this essential intermediate were explored. Key steps were optimized with regard to the reaction conditions and the workup procedures.

In order to enable an *in situ* dimerization, reactive handles were added to the nortomaymycin core structure. Governed by the design of SJG-136 and other PBD dimers, the C8 position of the core structure was utilized to introduce the different reactive handles. Each of these derivatives represents one monomer. The corresponding monomer pairs were designed based on different bioorthogonal reactions enabling dimerization. The CuAAC, the SPAAC, and the Diels-Alder reaction were chosen, as the underlying reactions offered a set of different kinetics and varying steric demand of the functional groups. Additionally, derivatives with different linker lengths were synthesized, since the DNA cross-linking reactivity and the cytotoxic potency of PBD dimers is known to be dependent on the linker length.[81],[95] In the case of the strain-promoted dimerization, two derivatives were synthesized, representing a symmetric and an asymmetric variant of the SPAAC.

Next, the dimers were synthesized based on the respective monomers. The dimerization was successful in the case of the CuAAC-based dimers as well as the SPAAC-based dimers. The Diels-Alder-based dimers could not be obtained under reasonable conditions. The synthesis of monomer derivatives with more favorable electronic properties in order to enable the underlying Diels-Alder reaction was explored.

Subsequently, the dimers and the monomer combinations were studied with regard to their DNA binding properties. The focus was set on the cross-linking ability, as DNA cross-linking is only possible after a successful *in situ* dimerization. Hence, numerous tailored, complementary assays were developed, established, and optimized. These include plasmid-based as well as oligonucleotide-based mobility shift assays, an LC-MS assay, a fluorescent DNA thermal denaturation assay, and a DNase I footprinting assay.

Both mobility shift assays carried out in this work could not show any DNA cross-linking activity for the obtained dimers as well as the monomer combinations, while for SJG-136, DNA cross-links could be observed under the same conditions. However, SJG-136 is an

exceptionally potent DNA cross-linking agent. Cross-linking of less active reagents may not be observed using this assay due to concentration limits as well as detection limits.

In case of the plasmid-based mobility shift assay, this observation may also be attributed to the fact that the incubated samples were treated with a heat shock of 98 °C for DNA-denaturation. This temperature might affect compound stability or lead to a breakage of the reversible halfaminal bond between the PBD (-Dimer) and the guanine residue. Lower temperatures on the other hand were not sufficient in fully denaturing dsDNA to ssDNA.

In the case of the oligonucleotide-based mobility shift assay, it should be taken into account that a 12mer oligonucleotide was used, which was found to be ideal for SJG-136 binding, as reported in the literature,[70] and may not be ideal for the binding of the dimers as well as the monomer combinations studied in this thesis. Furthermore, the helix of DNA has 10 base pairs per winding in case of the B form, thus a 12mer oligonucleotide may not be sufficient in providing enough structural guidance for the binding of the herein studied compounds.

Thus, the binding properties were further assessed by an LC-MS assay established in this work. Herein, the formation of an *inter*-strand cross-link was shown for **D1** and **D2**. It should be pointed out that since mass spectrometry represents a direct method for the detection of cross-links, the data provided direct evidence for the formation of DNA cross-links by **D1** and **D2**. This revealed that **D1** and **D2** share the same mode of action as SJG-136. Furthermore, it was shown that the PBD dimers exhibited different levels of cross-linking ability. **D1** showed the highest levels of cross-linking, followed by **D2**. For **D4** and **D3**, as well as for the monomer combinations, no cross-links were detected using this method. On the one hand, these results suggest a superior molecular design of **D1** and **D2** over **D4** and **D3**, hinting towards potential steric clashes in case of the more sterically demanding structures of **D4** and **D3** during target engagement. On the other hand, an *in situ* dimerization of the monomer combinations could not be detected, suggesting that the steric guidance provided by the DNA matrix may not be sufficient for the target-guided activation aimed for in this approach.

Using this assay it was for the first time proven, that **D1** and **D2** are capable of cross-linking the DNA. To investigate the alkylation abilities of the dimers and the monomers further, additional studies were carried out utilizing a fluorescent DNA thermal denaturation assay. These studies showed that all monomers (**M1**, **M2**, **M3**, **M4**, and **MbA**) as well as three out of four dimers, namely **D1**, **D2**, and **D4**, were able to form mono-adducts with DNA. The dimeric compounds did not only rely on cross-linking, but were also capable of efficiently forming mono-adducts, hence broadening their mode of action. The studies further showed

that **D1** and **D2** exhibited the highest shifts in melting temperature upon incubation, indicating superior duplex stabilization compared to the other compounds and thus suggesting preferable target binding properties. Also, the relative proportion of bound versus unbound PBD dimers was highest for **D1**, followed by **D2**. In fact, the data showed that the treatment with dimers led to a mixture of binding events, including unbound DNA, mono-adducts, and cross-links, with the relative proportions between these stages depending on the compound investigated. Additionally, it could be shown that not only *inter*-strand cross-links but also *intra*-strand cross-links were formed, further diversifying their mode of action. As indicated above, **D1** showed the highest T_m shifts and the highest shares of bound DNA and thus the most promising binding and cross-linking properties. Using a set of sequences featuring varying binding motives, a preference of **D1** for the binding motif GAAC could be identified.

In the case of **D1** and **D2**, their respective monomer combinations were also evaluated. A synergistic effect of the monomer combinations compared to the stand-alone monomers was not observed, and the T_m shifts lagged behind those of the synthetic dimer.

The DNA footprinting data of the PBD dimers and monomers showed that **D1** was the most effective compound out of the series, leading to several defined DNA footprints by binding to the DNA. These footprints all overlap with SJG136, which was used as a control. This suggests a similar preference in binding patterns. The footprints also indicate that **D1** bound strong enough to DNA to block a DNA-processing enzyme, i.e., DNaseI, even though the aminal formation between the guanine bases of DNA and **D1** is, in principle, reversible.

The sum of the findings and particularly the outcomes of the LC-MS studies suggest that **D1** and **D2** were in fact able to cross-link two DNA strands. Moreover, they exhibited a wider range of binding modes, forming mono-adducts, *inter*-strand as well was *intra*-strand cross-links. In the case of **D1**, it could also be shown that binding to DNA might block DNA processing, as exemplified by DNase I. Thus, these findings paved the way for further studies on the toxicity of these structures to evaluate their use in anti-cancer treatment. Such studies are currently carried out in collaboration with Prof. Rahman and Prof. Thurston, who are also investigating the compounds **D1** and **D2** in modeling studies evaluating the structural features of the target engagement. The potential insights generated by those studies will help to unravel the binding mode of the compounds within the minor groove, with a particular focus on the interactions of the triazole with the surface of the minor groove. If the triazole is well accepted, this would encourage the use of the herein-described structures as platforms

for synthesizing mixed dimers utilizing other DNA alkylating agents. Performing simple CuAAC click reactions with either the azide **MbA** or the alkyne **M1** on the one hand, and another alkylating agent of choice on the other hand, would readily give rise to a larger array of potential cross-linkers. Additionally, less selective DNA binders could benefit from a combination of the nortomaymycin derivatives, as they showed enhanced selectivity for certain binding motives, as shown by the DNA thermal denaturation studies. The sequence selectivity of mixed dimers may be carefully tailored to allow even more sequence-selective binding, which may result in a selective change in gene expression of modified open reading frames.

2.5 Materials and methods

2.5.1 Chemical synthesis

2.5.1.1 General remarks

Unless stated otherwise, all reagents were purchased from commercial suppliers and used without further purification. All solvents used for workup and purification were of HPLC grade. Anhydrous solvents were used for all reactions in which water was not also used as a solvent and in which the total amount of organic solvent did not exceed 100 mL. All anhydrous solvents were purchased from commercial suppliers. Moisture-sensitive reactions were performed under argon atmosphere in dried glassware. Reactions were monitored by TLC, LC-MS or NMR. The removal of organic solvents took place using rotary evaporators at 30 °C, the removal of water at 40 °C. For lyophilization of substances, the solutions in question were frozen with liquid nitrogen and freeze-dried on an Alpha 2-4 LSCbasic (CHRIST) instrument. Centrifugations were performed using a Universal 32 R centrifuge (HETTICH). If yields are given for unpurified intermediates, this is only done for the purpose of calculating the amount of reagents needed for the next synthesis step.

2.5.1.2 Purification methods

2.5.1.2.1 Column chromatography

Column chromatographic purifications were carried out on silica gel (Si 60, 40 - 63 µm particle size) from the producer MERCK under elevated pressure (flash chromatography). The eluents used are listed after the indicated retention factors.

2.5.1.2.2 Automated column chromatography

Automatic preparative column chromatography was carried out on a Grace Reveleris® X2 instrument (Büchi).

Automatic preparative column chromatography with C18 Silica was performed on a Pure C-850 instrument (Büchi).

2.5.1.2.3 HPLC

Purifications by HPLC were performed on a Dionex Ultimate instrument (Thermo Fisher Scientific). Unless stated otherwise, the following C18 separation columns (Phenomenex) were used:

- Luna 5 μm, 100 Å, 00G-4252-PO-AX.
- Gemini 10 μm, 110 Å, 00G-4436-PO.
- Gemini 10 μm, 110 Å, 00G-4436-NO.

Product containing fractions were combined, diluted with milliQ H_2O (min. 1:1/solvent:H_2O), frozen and lyophilized.

2.5.1.2.4 Preparative thin layer chromatography

Preparative thin layer chromatography was performed on pre-coated glass plates (Merck TLC Silicagel 60 F254, 1.05715.0001, 20×20 cm, max. 10-15 mg/plate and Analtech Uniplate Silica gel GF Z51305-9, 20×20 cm × 2 mm, max 100-150 mg/plate). Eluent or eluent-mixtures used are reported in parentheses. Compounds were visualized by observation under UV light (λ = 254 or 366 nm). Compound containing silica gel fractions were scratched from the plate with a scalpel, crushed to small pieces and compounds were dissolved by appropriate solvent mixtures.

2.5.1.3   Analytical methods

2.5.1.3.1   Thin layer chromatography

For thin layer chromatography TLC plates (silica gel 60 F_{254}, on aluminum) from the manufacturer MERCK were used. TLC plates were visualized by UV light (λ = 254 nm/ λ = 365 nm), or using staining reagents. A potassium permanganate solution (2 g $KMnO_4$, 6.5 g K_2CO_3, 200 mL water) or Iodine served as staining reagents.

2.5.1.3.2   NMR

Nuclear Magnetic Resonance (NMR) spectra were recorded on a BRUKER Avance III 500 with the probe head PABBO BB/^{19}F-^{1}H/D Z-GRD (500 MHz für ^{1}H, 125 MHz für ^{13}C) or a BRUKER Avance III HD 700 with the probe head CPTCI ^{1}H-^{13}C/^{15}N/D Z-GRD (700 MHz for ^{1}H, 176 MHz for ^{13}C) at room temperature. Samples were measured as solutions in deuterated solvents. Chemical shifts are reported in ppm relative to solvent signal. Multiplicity is indicated as follows: s (singlet); bs (broad singlet); d (doublet); t (triplet); q (quartet); quin (quintet), m (multiplet); as well as combination of those e.g. dd (doublet of doublets), etc.

2.5.1.3.3   Mass spectrometry

Low resolution mass spectrometry (LRMS) data were recorded using an AGILENT 1100 HPLC system equipped with DAD detector and an API 150 EX quadrupole mass detector with electrospray ionization (ESI) (ACN-H_2O + 0.05 % TFA)

High resolution mass spectrometry (HRMS) data were recorded using a DIONEX Dionex Ultimate 3000 HPLC system equipped with a DAD detector and a BRUKER maXis HD QTOF mass detector with electrospray ionization (ESI). Samples were directly injected via an Ultimate 3000RS autosampler (THERMO FISHER SCIENTIFIC). The mass-to-charge ratio *m/z* is being reported.

2.5.1.4 Synthesis procedures

(*S*)-2-(methoxycarbonyl)-4-methylenepyrrolidiniumchloride (88)
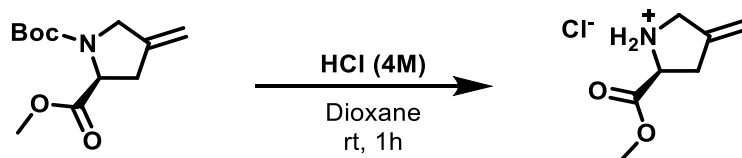
To 1-(*tert*-butyl) 2-methyl (*S*)-4-methylenepyrrolidine-1,2-dicarboxylate (169 mg, 0.70 mmol, 1.0 eq.) was added 0.79 mL of HCl (4 M in dioxane). The solution was stirred at RT for 1 h. Et$_2$O was added and the precipitate was separated by centrifugation of the mixture. The resulting pellet was washed twice with Et$_2$O. The remaining solvent residues were removed under reduced pressure to obtain the analytically pure product as a colorless solid (124 mg, 0.70 mmol, 99.7%).

^{1}H NMR (500 MHz, DMSO): δ [ppm] = 5.16 (sx, *J* = 2.1 Hz, 2H), 4.60 (t, *J* = 8.4 Hz, 1H), 3.86 (td, *J* = 30.9, 1.5 Hz, 2H), 3.77 (s, 3H), 3.57 (s, 1H), 2.99 – 2.69 (m, 2H).

^{13}C NMR (126 MHz, DMSO): δ [ppm] = 168.5, 139.8, 109.8, 66.3, 58.3, 53.0, 48.6, 33.2.

4-(benzyloxy)-3-methoxybenzoic acid (91)
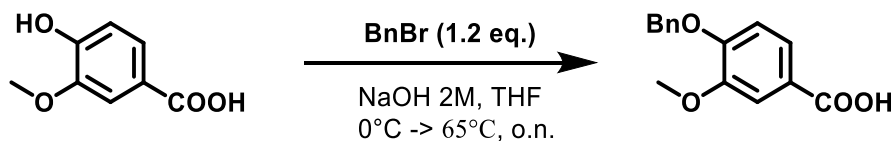
Vanillic acid (25.0 g, 148 mmol, 1.0 eq.) was dissolved in THF (75 mL), NaOH (188 mL, 2 M) was added and the stirred mixture was cooled down to 0 °C. A solution of benzyl bromide in THF (75 mL) was added dropwise at 0 °C over 1 h. The mixture was allowed to warm up to RT and was subsequently stirred under reflux overnight. The reaction was monitored by LC-MS. When no starting material remained, the mixture was allowed to cool to RT and was washed with hexane (2×50 mL). Remaining THF was removed under reduced pressure. The remaining aqueous phase was acidified to pH = 1 with HCl (6 M). The white participate was collected by centrifugation. The pellet was washed with water. After removing remaining water by lyophilization of the pellet, the product was obtained as an analytically pure colorless solid (35.1 g, 135.8 mmol, 91%).

TLC: R_f = 0.59 (PE:EtOAc 5:1, HOAc) [UV]

^{1}H NMR (500 MHz, DMSO): δ [ppm] = 12.68 (s, 1H), 7.54 (dd, J = 8.3, 2.0 Hz, 1H), 7.46 – 7.45 (m, 3H), 7.40 (t, J = 7.5 Hz, 2H), 7.35 (t, J = 7.3 Hz, 1H), 7.14 (d, J = 8.5 Hz, 1H), 5.16 (s, 2H), 3.81 (s, 3H).

^{13}C NMR (126 MHz, DMSO): δ [ppm] = 167.0, 151.6, 148.6, 136.5, 128.4, 128.0, 127.9, 123.2, 123.0, 112.4, 112.1, 69.8, 55.5.

HRMS (ESI) *m/z*: ($C_{15}H_{13}O_4^-$ [M-H]$^-$)   calc.: 257.0819

found: 257.0813

4-(benzyloxy)-5-methoxy-2-nitrobenzoic acid (92)
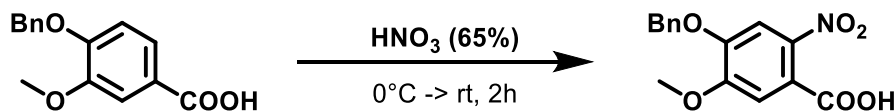
4-(benzyloxy)-3-methoxybenzoic acid (7.64 g, 29.6 mmol, 1.0 eq.) was dissolved in HNO_3 (65%, 100 mL) at 0 °C. The mixture was allowed to warm to room temperature and stirred for 2 h. The reaction mixture was poured on ice followed by extraction with DCM. The combined organic layers were dried over Na_2SO_4 and concentrated under reduced pressure. 4-(benzyloxy)-5-methoxy-2-nitrobenzoic acid was obtained as an analytically pure orange solid (7.35 g, 28.5 mmol, 96%).

TLC: R_f = 0.33 (20% MeOH/DCM, HOAc) [UV]

^{1}H NMR (500 MHz, DMSO): δ [ppm] = 13.59 (s, 1H), 7.69 (s, 1H), 7.47 – 7.45 (m, 2H), 7.43 – 7.40 (m, 2H), 7.38 – 7.35 (m, 2H), 7.31 (s, 1H), 5.24 (s, 2H), 3.91 (s, 3H).

^{13}C NMR (126 MHz, DMSO): δ [ppm] = 166.0, 152.0, 149.0, 141.1, 135.8, 128.5, 128.2, 128.1, 121.4, 111.4, 108.5, 70.5, 56.4.

HRMS (ESI) *m/z*: ($C_{15}H_{14}NO_6^+$ [M-H]$^+$)　　calc.:　304.0816
　　　　　　　　　　　　　　　　　　　　　　　　　found: 304.0815

2-amino-4-(benzyloxy)-5-methoxybenzoic acid (99)
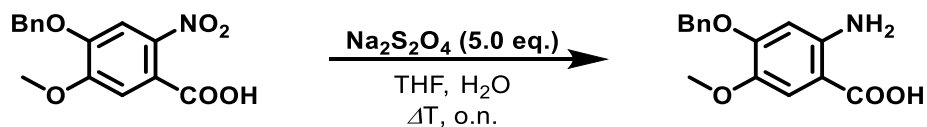
4-(benzyloxy)-5-methoxy-2-nitrobenzoic acid (5.68 g, 18.8 mmol, 1.0 eq.) was dissolved in 60 mL THF and 50 mL H_2O. $Na_2S_2O_4$ (16.3 g, 93.8 mmol, 5.0 eq.) was added. The reaction mixture was stirred under reflux overnight. The phases formed were separated and the aqueous phase was extracted with EtOAc. The combined organic layers were concentrated under reduced pressure. The crude product was loaded onto C18 silica and purified by reversed-phase flash chromatography. The title compound was obtained as golden needles (2.47 g, 9.01 mmol, 48%).

TLC: R_f = 0.22 (5% MeOH/DCM) [UV]

^{1}H NMR (500 MHz, DMSO): δ [ppm] = 7.46 – 7.42 (m, 1H), 7.42 – 7.39 (m, 1H), 7.36 – 7.33 (m, 1H), 7.17 (s, 1H), 6.44 (s, 1H), 5.05 (s, 2H), 3.65 (s, 3H).

^{13}C NMR (126 MHz, DMSO): δ [ppm] = 169.0, 153.6, 148.1, 139.3, 136.5, 128.4, 128.0, 127.9, 113.7, 100.9, 100.4, 69.4, 56.1.

HRMS (ESI) *m/z*: ($C_{15}H_{16}NO_4^+$ [M+H]$^+$)   calc.: 274.1074

                                             found: 274.1072

4-(benzyloxy)-2-((*tert*-butoxycarbonyl)amino)-5-methoxybenzoic acid (100)
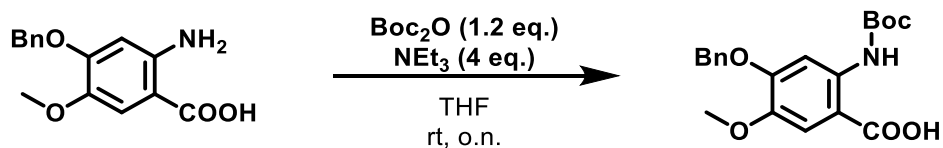
2-amino-4-(benzyloxy)-5-methoxybenzoic acid (2.96 g, 10.8 mmol, 1.0 eq.) was dissolved in THF (60 mL). NEt$_3$ (6 mL) was added. Boc$_2$O (2.79 mL, 2.83 g, 1.2 eq.) was added. The mixture was stirred overnight at room temperature. The solvent was removed under reduced pressure. The residue was dissolved in EtOAc and washed successively with HCl (0.1 M, 10 × 10 mL) and brine (2 × 10 mL). The organic phase was dried over Na$_2$SO$_4$ and the solvent was removed under reduced pressure. The oily residue was filtered through a cake of sand using PE as a solvent. The solid was further washed with DCM. The mother solution was concentrated under reduced pressure. The procedure was repeated three times, yielding the title compound as a beige solid (2.69 g, 7.21 mmol, 67%).

TLC: R_f = 0.79 (PE:EtOAc, HOAc 5:1) [UV]

^{1}H NMR (500 MHz, DMSO): δ [ppm] = 13.34 (s, 1H), 10.57 (s, 1H), 8.14 (s, 1H), 7.72 – 7.28 (m, 5H), 5.12 (d, J = 8.6 Hz, 2H), 3.74 (s, 3H), 1.48 (s, 9H).

^{13}C NMR (126 MHz, DMSO): δ [ppm] = 169.3, 152.6, 152.1, 142.9, 137.3, 136.1, 128.4, 128.3, 128.2, 113.2, 106.4, 102.5, 80.1, 69.9, 55.6, 28.0.

HRMS (ESI) *m/z*: (C$_{20}$H$_{24}$NO$_6^+$ [M+H]$^+$)   calc.:   374.1598

found: 374.1596

methyl(*S*)-1-(4-(benzyloxy)-2-((*tert*-butoxycarbonyl)amino)-5-methoxybenzoyl)-4-methylenepyrrolidine-2-carboxylate (101)
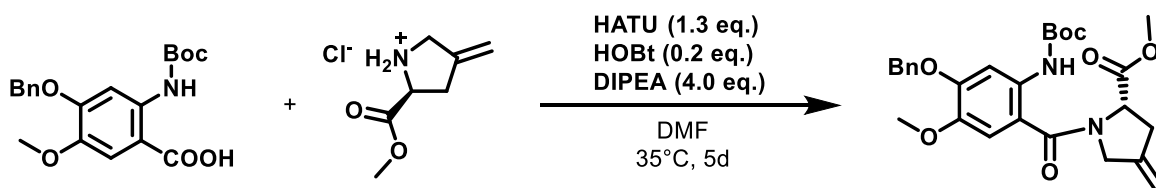
To a solution of 4-(benzyloxy)-2-((*tert*-butoxycarbonyl)amino)-5-methoxybenzoic acid (2.20 g, 5.88 mmol, 1.3 eq.) in dry DMF (28 mL) and dry ACN (28 mL) HATU (2.23 g, 5.88 mmol, 1.3 eq.), HOBt (101 mg, 0.75 mmol, 0.2 eq.) and DIPEA (1.50 mL, 1.14 g, 8.85 mmol, 2.0 eq.) were added. After stirring for 30 min a solution of (*S*)-2-(methoxycarbonyl)-4-methylenepyrrolidiniumchloride (783 mg, 4.42 mmol, 1.0 eq.) in DMF (28 mL), Acetonitrile (28 mL) and DIPEA (1.50 mL, 1.14 g, 8.85 mmol, 2.0 eq.) was added. The mixture was stirred for 5 days at 35 °C. The amber-colored solution was diluted with EtOAc, washed with 0.1 M HCl and sat. NaCl aq.. The organic phase was dried over Na_2SO_4, and concentrated under reduced pressure. The crude product was purified by column chromatography (silica, PE:EtOAc, 10% → 100% EtOAc) to obtain the product as a light yellow foam (2.12 g, 4.27 mmol, 96%).

TLC: R_f = 0.55 (PE:EE 1:1) [UV]

¹H NMR (700 MHz, DMSO)[*]: δ [ppm] = 8.69/8.57 (s, 1H, CH$_{arom}$), 7.50 – 7.47 (m, 2H, CH$_{arom}$ (OBn)), 7.42 – 7.40 (m, 2H, CH$_{arom}$ (OBn)) , 7.36 – 7.34 (m, 1H, CH$_{arom}$ (OBn)), 6.91/6.71 (s, 1H, CH$_{arom}$), 5.08 – 4.98 (m, 4H, CH$_2$ (OBn), CH$_{2exo}$), 4.71 – 4.59 (m, 1H, C*H*COOMe), 4.33 – 3.97 (m, 2H, C*H$_2$*N), 3.78/3.68 (s, 3H, CH$_3$), 3.68/3.59 (s, 3H, CH$_3$), 3.05 – 2.60 (m, 1H, CC*H$_2$*CHN), 2.64 – 2.50 (m, 1H, CC*H$_2$*CHN), 1.43 (s, 9H).

¹³C NMR (176 MHz, DMSO)[*]: δ [ppm] = 172.5, 171.9, 170.3, 168.1, 168.0, 153.3, 152.8, 149.0, 148.6, 145.0, 144.5, 143.1, 142.6, 136.6, 130.0, 129.1, 128.4, 128.0, 121.0, 118.3, 110.6, 110.0, 109.2, 108.0, 107.4, 79.3, 79.2, 70.0, 61.2, 58.3, 56.0, 55.6, 52.9, 52.3, 52.1, 49.9, 36.9, 34.7, 28.0.

[*]Splitting of signals due to a 2:3 mixture of rotamers.

HRMS (ESI) *m/z*: ($C_{27}H_{33}N_2O_7^+$ [M+H]$^+$)   calc.:   497.2282

found: 497.2283

tert-butyl(*S*)-(5-(benzyloxy)-2-(2-formyl-4-methylenepyrrolidine-1-carbonyl)-4-methoxyphenyl)carbamate (102)
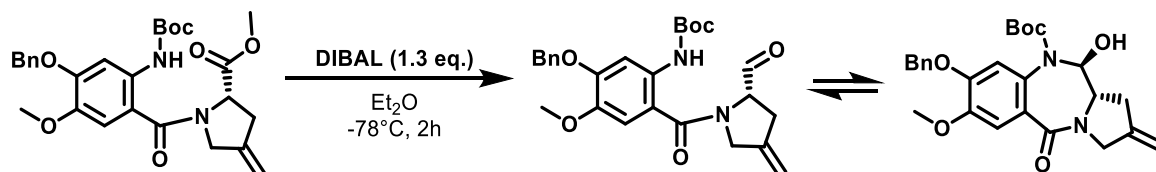
1.60 mL DIBAL (1 M in toluene, 1.60 mmol, 1.3 eq.) were added dropwise over a period of 10 min to a solution of methyl(S)-1-(4-(benzyloxy)-2-((*tert*-butoxycarbonyl)amino)-5-methoxybenzoyl)-4-methylenepyrrolidine-2-carboxylate (610 mg, 1.23 mmol, 1.0 eq.) in Et_2O at -78 °C. After stirring for 2 h at the same temperature, MeOH (6 mL) and H_2O (6 mL) were added dropwise. The mixture was allowed to warm up to room temperatureovernight. The formed layers were separated. Citric acid was added to the aqueous layer followed by extraction with EtOAc. The combined organic layers were dried over Na_2SO_4 and the solvent was removed under reduced pressure. The aldehyde was precipitated by dissolving in a small amount of EtOAc followed by the addition of PE. Alternatively, the product can be purified by column chromatography (silica, PE:EtOAc 2:1 → 0:1). The desired compound was obtained as a colorless solid (555 g, 1.19 mmol, 97%).

TLC: R_f = 0.35 (PE:EtOAc 1:1) [UV]

^{1}H NMR (500 MHz, DMSO): δ [ppm] = 7.46 (d, *J* = 7.4 Hz, 2H, CH$_{arom}$ (OBn)), 7.41 (t, *J* = 7.4 Hz, 2H, CH$_{arom}$ (OBn)), 7.35 (t, *J* = 7.2 Hz, 1H, CH$_{arom}$ (OBn)), 7.07 (s, 1H, CH$_{arom}$), 6.77 (s, 1H, CH$_{arom}$), 6.53 (s, 1H, OH), 5.33 (dd, *J* = 9.3, 5.9 Hz, 1H, CHC*H*OHN), 5.18 (d, *J* = 11.9 Hz, 1H, CH$_2$ (OBn)), 5.13 (d, *J* = 11.9 Hz, 1H, CH$_{2exo}$), 5.06 (d, *J* = 11.9 Hz, 1H, CH$_2$ (OBn)), 4.09 (d, *J* = 15.8 Hz, 1H, CH$_2$N), 3.97 (d, *J* = 15.8 Hz, 1H, CH$_2$N), 3.82 (s, 3H, OCH$_3$), 3.41 (t, *J* = 9.1 Hz, 1H, CH$_2$C*H*N), 2.87 (dd, *J* = 15.6, 9.2 Hz, 1H, CC*H*$_2$CHN), 2.52 (s, 1H, CC*H*$_2$CHN), 1.20 (s, 9H, Boc).

^{13}C NMR (126 MHz, DMSO): δ [ppm] = 165.9, 153.7, 149.2, 147.9, 142.9, 136.6, 129.3, 128.5, 128.0, 127.5, 125.6, 114.8, 110.1, 109.0, 84.6, 80.1, 70.1, 60.2, 55.6, 50.2, 40.0, 39.9, 39.8, 39.7, 39.6, 39.6, 39.5, 39.3, 39.1, 38.0, 34.7, 27.8.

HRMS (ESI) *m/z*: ($C_{26}H_{31}N_2O_6^+$ [M+H]$^+$)   calc.:   467.2177

found: 467.2177

(S)-8-hydroxy-7-methoxy-2-methylene-1,2,3,11a-tetrahydro-5H-benzo[e]pyrrolo[1,2-a][1,4]diazepin-5-one (85)
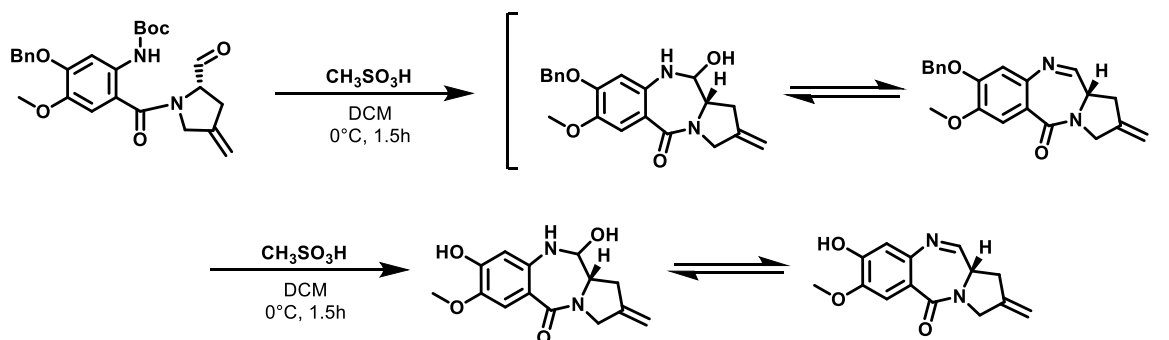
tert-butyl(S)-(5-(benzyloxy)-2-(2-formyl-4-methylenepyrrolidine-1-carbonyl)-4-methoxyphenyl)carbamate (100 mg, 0.21 mmol, 1.0 eq.) was dissolved in DCM and cooled to 0 °C. Methanesulfonic acid (0.7 mL) was added dropwise. After stirring the mixture for 1.5 h at 0 °C, sat. NaHCO$_3$ and AcOH were added and the pH was adjusted to pH = 4. The resulting phases were separated and the aqueous phase was thoroughly extracted with DCM. The combined organic layers were dried over Na$_2$SO$_4$ and directly purified, without a concentration step, by column chromatography (silica, DCM → 5% ^{t}BuOH/DCM → 7% ^{t}BuOH/DCM → 10% ^{i}PrOH/DCM → 22% ^{i}PrOH/DCM →100% ^{i}PrOH). The product could be obtained as a colorless to light yellow solid (44.0 mg, 0.17 mmol, 81%).

TLC: R_f = 0.48(MeOH/DCM 10%) [UV]

^{1}H NMR (500 MHz, DMSO)*: δ [ppm] = 7.72 (d, *J* = 4.4 Hz, 1H, CHN), 7.31 (s, 1H, CH$_{arom}$), 7.17 (s, 1H, CH$_{arom}$), 7.02 (s, 1H, CH$_{arom}$), 6.68 (s, 1H, CH$_{arom}$), 6.37 (s, 1H, CH$_{arom}$), 6.17 (s, 1H, CH$_{arom}$), 5.13 (d, *J* = 6.6 Hz, 2H, CH$_{2exo}$), 5.08 (d, *J* = 17.6 Hz, 2H, CH$_{2exo}$), 4.94 (d, *J* = 14.9 Hz, 2H, CH$_{2exo}$), 4.83 (t, *J* = 6.1 Hz, 1H, C*H*OHN), 4.48 (dd, *J* = 8.7, 4.9 Hz, 1H, C*H*OHN), 4.26 – 3.94 (m, 6H, CH$_2$N), 3.85 (quin, *J* = 4.2 Hz, 1H, CH$_2$C*H*N), 3.82 (s, 3H, CH$_3$), 3.81 – 3.77 (m, 1H, CH$_2$C*H*N), 3.70 (s, 3H, CH$_3$), 3.66 (s, 3H, CH$_3$), 3.51 (td, *J* = 9.1, 2.1 Hz, 1H, CH$_2$C*H*N), 3.08 – 2.52 (m, 6H, CC*H*$_2$CHN).

^{13}C NMR (126 MHz, DMSO)*: δ [ppm] = 166.9, 165.9, 164.1, 163.8, 150.5, 149.9, 149.5, 146.2, 144.4, 143.4, 142.8, 142.0, 140.8, 140.1, 140.1, 139.0, 118.2, 116.2, 114.7, 112.9, 112.8, 111.6, 109.6, 108.5, 108.4, 108.2, 105.7, 104.1, 85.9, 81.5, 59.6, 59.1, 56.0, 55.9, 55.7, 53.5, 53.1, 51.1, 51.0, 35.6, 35.1, 34.7.

HRMS (ESI) *m/z*: ($C_{14}H_{15}N_2O_3^+$ [M+H]$^+$)   calc.:   259.1077

found: 259.1078

* Due to residual water in the DMSO-*d$_6$* the NMR corresponds to a mixture of the imine form and the two hemiaminal forms (diastereomers).

(S)-8-(2-bromoethoxy)-7-methoxy-2-methylene-1,2,3,11a-tetrahydro-5H-benzo[e]pyrrolo[1,2-a][1,4]diazepin-5-one (104)
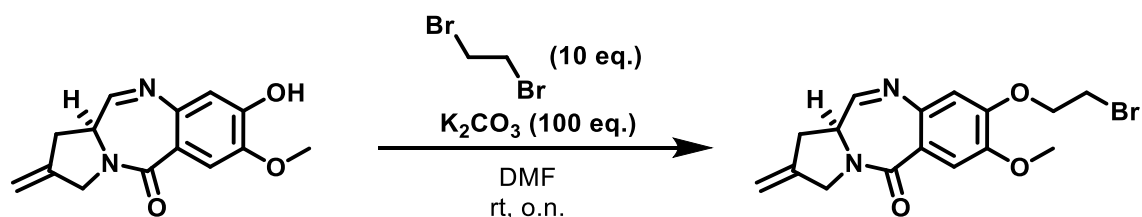
(S)-8-hydroxy-7-methoxy-2-methylene-1,2,3,11a-tetrahydro-5H-benzo[e]pyrrolo[1,2-a][1,4]diazepin-5-one (30.0 mg, 116 µmol, 1.0 eq.) and K_2CO_3 (1.60 g, 11.6 mmol, 100 eq.) were dissolved in 2 mL dry DMF. 0.10 mL 1,2-dibromoethane (217 mg, 1.16 mmol, 10 eq.) were added. The mixture was stirred at RT overnight. After the addition of H_2O and DCM, the aqueous phase was thoroughly extracted with DCM. The organic layers were dried over Na_2SO_4, filtered and evaporated under reduced pressure. The crude product was purified by column chromatography (silica, 100% EtOAc) yielding the title compound as a yellow film (32.8 mg, 89.8 µmol, 80%).

TLC: R_f = 0.30 (100% EtOAc) [UV]

^{1}H NMR (500 MHz, CDCl$_3$): δ [ppm] = 7.68 (d, J = 4.4 Hz, 1H), 7.51 (s, 1H), 6.81 (s, 1H), 5.17 (d, J = 14.1 Hz, 2H), 4.37 (ddt, J = 32.0, 10.7, 6.7 Hz, 2H), 4.27 (s, 2H), 3.94 (s, 3H), 3.89 – 3.84 (m, 1H), 3.68 (t, J = 6.7 Hz, 2H), 3.16 – 2.90 (m, 3H).

^{13}C NMR (126 MHz, CDCl$_3$): δ [ppm] = 164.7, 162.9, 162.7, 150.0, 148.1, 141.6, 140.6, 120.9, 112.1, 111.4, 109.6, 77.4, 77.2, 76.9, 68.8, 56.4, 53.9, 51.5, 35.6, 28.3.

HRMS (ESI) *m/z*: ($C_{16}H_{18}BrN_2O_3^+$ [M+H]$^+$)   calc.: 365.0495

found: 365.0497

(*S*)-8-(2-azidoethoxy)-7-methoxy-2-methylene-1,2,3,11a-tetrahydro-5H-benzo[e]pyrrolo[1,2-a][1,4]diazepin-5-one (MbA)
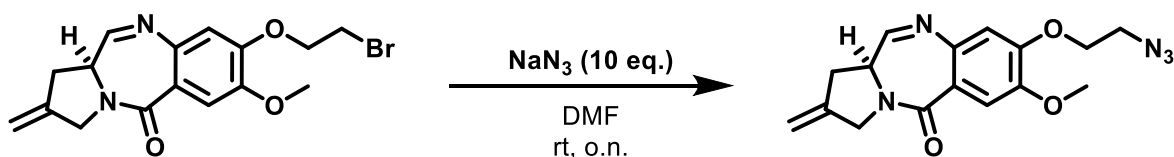
(*S*)-8-(2-bromoethoxy)-7-methoxy-2-methylene-1,2,3,11a-tetrahydro-5H-benzo[e]pyrrolo[1,2-a][1,4]diazepin-5-one (36.0 mg, 98.6 µmol, 1.0 eq.) was dissolved in DMF (0.66 mL). NaN_3 (64.1 mg, 986 µmol, 10.0 eq.) was added and the mixture was stirred over night at 50 °C. After DCM and water were added, the aqueous phase was thoroughly extracted with DCM. The organic phase was dried over Na_2SO_4, filtered and evaporated under reduced pressure. The crude product was purified by column chromatography (silica, MeOH/DCM, 1% → 5%). The pure product was obtained as a colorless solid (25.7 mg, 78.6 µmol, 80%).

TLC: R_f = 0.31(EtOAc 100%) [UV]

¹H NMR (700 MHz, DMSO)*: δ [ppm] = 7.78 (d, *J* = 4.4 Hz, 1H, CHN), 7.22 (s, 1H, CH$_{arom}$), 7.07 (s, 1H, CH$_{arom}$), 6.88 (s, 1H, CH$_{arom}$), 6.84 (d, *J* = 6.1 Hz, 1H, OH), 6.58 (s, 1H, CH$_{arom}$), 6.36 (s, 1H, CH$_{arom}$), 5.99 (d, *J* = 6.9 Hz, 1H, OH), 5.50 (d, *J* = 5.7 Hz, 2H, NH), 5.14 (d, *J* = 9.1 Hz, 2H, CH$_{2exo}$) 5.09 (d, *J* = 25.0 Hz, 2H, CH$_{2exo}$), 4.95 (d, *J* = 21.5 Hz, 2H, CH$_{2exo}$), 4.87 (t, *J* = 6.2 Hz, 1H, C*H*OHN), 4.53 (t, *J* = 7.9 Hz, 1H, C*H*OHN), 4.25 – 4.14 (m, 4H, CH$_2$N and OC*H*$_2$CH$_2$), 4.13 – 4.08 (m, 2H, OC*H*$_2$CH$_2$), 4.06 (t, *J* = 4.9 Hz, 2H, OC*H*$_2$CH$_2$), 3.97 (d, *J* = 15.7 Hz, 1H, CH$_2$N), 3.87 (quin, *J* = 6.1 Hz, 1H, CH$_2$C*H*N), 3.83 – 3.80 (m, 1H, CH$_2$C*H*N), 3.82 – 3.81 (m, 2H, CH$_2$C*H*$_2$N$_3$), 3.70 (s, 3H, CH$_3$), 3.68 (m, 2H, CH$_2$C*H*$_2$N$_3$), 3.68 (s, 3H, CH$_3$), 3.66 (s, 3H, CH$_3$), 3.54 (td, *J* = 9.0, 1.9 Hz, 1H, CH$_2$C*H*N), 3.06 – 3.04 (m, 2H, CC*H*$_2$CHN), 2.94 – 2.86 (m, 2H, CC*H*$_2$CHN), 2.66 (d, *J* = 16.3 Hz, 1H CC*H*$_2$CHN), 2.55 (d, *J* = 15.8 Hz, 1H, CC*H*$_2$CHN).

¹³C NMR (176 MHz, DMSO)*: δ [ppm] = 166.6, 165.7, 164.5, 163.5, 151.1, 150.4, 149.9, 147.1, 144.2, 143.2, 142.9, 142.7, 140.8, 140.5, 139.9, 138.9, 119.8, 117.2, 114.8, 112.9, 111.4, 110.5, 108.5, 108.4, 106.3, 105.9, 102.2, 85.8, 81.4, 67.5, 67.3, 67.0, 59.5, 59.1, 56.0, 56.0, 55.8, 53.5, 53.2, 51.2, 51.0, 49.6, 35.6, 35.1, 34.7.

HRMS (ESI) *m/z*: ($C_{16}H_{18}N_5O_3^+$ [M+H]$^+$)   calc.:   328.1404

found: 328.1405

* Due to residual water in the DMSO-*d$_6$* the NMR corresponds to a mixture of the imine form and the two hemiaminal forms (diastereomers). The two hemiaminals are the predominant forms in the mixture, the imine is only found in minor quantities (ca. 7-10%).

(S)-7-methoxy-2-methylene-8-(prop-2-yn-1-yloxy)-1,2,3,11a-tetrahydro-5H-benzo[e]pyrrolo[1,2-a][1,4]diazepin-5-one (M1)
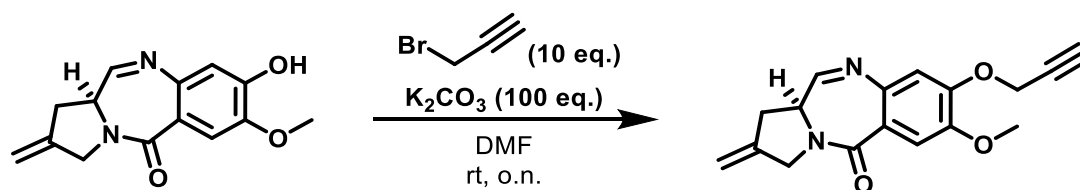
(S)-8-hydroxy-7-methoxy-2-methylene-1,2,3,11a-tetrahydro-5H-benzo[e]pyrrolo[1,2-a][1,4]diazepin-5-one (20.0 mg, 78.0 µmol, 1.0 eq.) and K_2CO_3 (1.08 g, 7.80 mmol, 100 eq.) were dissolved in dry DMF (1.00 mL). 100 µL Propargyl bromide (80w% in toluene, 107 mg, 0.78 mmol, 10 eq.) was added. The reaction was stirred at RT overnight. H_2O was added to the reaction and the mixture was extracted thoroughly with DCM. The combined organic phase was washed with water and brine. The solvent was removed under reduced pressure. The crude product was purified by column chromatography (silica, PE:EtOAc 1:1 → 1:3) yielding the title compound as a light yellow highly viscous oil (15.0 mg, 50.6 µmol, 65%).

**TLC**: R_f = 0.35 (PE:EtOAc 1:4) [UV]

¹H NMR (700 MHz, DMSO)*: δ [ppm] = 7.78 (d, J = 4.5 Hz, 1H, CHN), 7.35 (s, 1H, CH_{arom}), 7.22 (s, 1H, CH_{arom}), 7.07 (s, 1H, CH_{arom}), 6.93 (s, 1H, CH_{arom}), 6.91 (d, J = 6.2 Hz, 1H, OH), 6.61 (s, 1H, CH_{arom}), 6.39 (s, 1H, CH_{arom}), 5.53 (s, 1H, NH), 5.50 (d, J = 4.8 Hz, 1H, NH), 5.14 (d, J = 9.2 Hz, 2H, CH_{2exo}), 5.08 (d, J = 24.8 Hz, 2H, CH_{2exo}), 4.94 (dt, J = 21.9, 1.7 Hz, 2H, CH_{2exo}), 4.90 (d, J = 2.3 Hz, 2H, OCH_2CCH), 4.75 – 4.73 (m, 2H, OCH_2CCH), 4.72 (d, J = 2.4 Hz, 2H, OCH_2CCH), 4.24 – 4.11 (m, 5H, CH_2N), 3.97 (dd, J = 15.7, 1.2 Hz, 1H, CH_2N), 3.88 (quin, J = 4.3 Hz, 1H, CH₂CHN), 3.83 (s, 3H, CH_3), 3.81 (dd, J = 9.2, 4.6 Hz, 1H, CH₂CHN), 3.70 (s, 3H, CH_3), 3.66 (s, 3H, CH_3), 3.63 (t, J = 2.4 Hz, 1H, CH), 3.61 (t, J = 2.4 Hz, 1H, CH), 3.60 (t, J = 2.4 Hz, 1H, CH), 3.55 (td, J = 9.1, 2.2 Hz, 1H, CH₂CHN), 3.10 – 3.00 (m, 2H, CCH_2CHN), 2.93 – 2.87 (m, 2H, CCH_2CHN), 2.66 (dd, J = 16.4, 2.2 Hz, 1H, CCH_2CHN), 2.55 (d, J = 15.2 Hz, 1H, CCH_2CHN).

¹³C NMR (176 MHz, DMSO)*: δ [ppm] = 166.5, 165.6, 164.6, 163.5, 149.9, 149.5, 148.8, 147.1, 144.2, 143.2, 142.9, 142.7, 140.8, 140.3, 139.6, 138.6, 120.1, 117.4, 114.5, 112.6, 111.3, 110.9, 110.6, 108.5, 108.3, 106.6, 105.9, 102.6, 85.7, 81.1, 78.9, 78.9, 78.8, 78.7, 78.5, 78.5, 59.4, 59.1, 56.0, 55.9, 55.8, 55.7, 55.6, 53.5, 53.2, 51.1, 51.0, 35.7, 35.1, 34.7.

HRMS (ESI) *m/z*: ($C_{17}H_{17}N_2O_3^+$ [M+H]$^+$)   calc.:   297.1234

found: 297.1235

* Due to residual water in the DMSO-d_6 the NMR corresponds to a mixture of the imine form and the two hemiaminal forms (diastereomers).

(*S*)-8-(but-3-yn-1-yloxy)-7-methoxy-2-methylene-1,2,3,11a-tetrahydro-5H-benzo[e]pyrrolo[1,2-a][1,4]diazepin-5-one (M2)
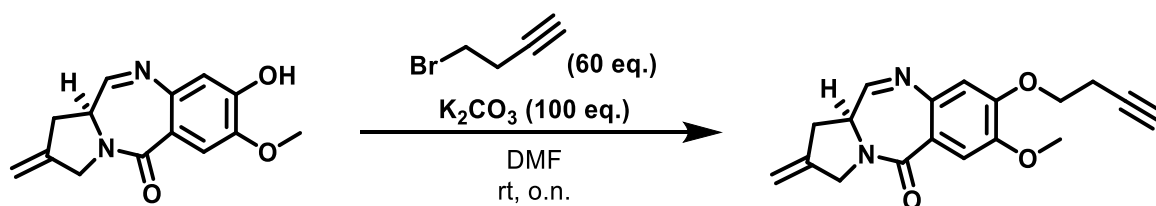
(*S*)-8-hydroxy-7-methoxy-2-methylene-1,2,3,11a-tetrahydro-5H-benzo[e]pyrrolo[1,2-a][1,4]diazepin-5-one (20.0 mg, 78.0 µmol, 1.0 eq.) and K_2CO_3 (1.08 g, 7.80 mmol, 100 eq.) were dissolved in dry DMF (1.00 mL). 4-bromobut-1-yne (439 µL, 4.68 mmol, 60 eq.) was added in portions throughout the reaction. The mixture was stirred at room temperature over the weekend. H_2O was added to the reaction and the mixture was extracted thoroughly with DCM. The combined organic phases were washed with water and brine. The solvent was removed under reduced pressure. The crude product was purified by column chromatography (silica, PE:EtOAc 1:4) yielding the title compound as a light yellow highly viscous oil (12.5 mg, 40.0 µmol, 51%)

TLC: R_f = 0.39 (PE:EtOAc 1:4) [UV]

¹H NMR (700 MHz, DMSO)*: δ [ppm] = 7.77 (d, *J* = 4.4 Hz, 1H, CHN), 7.34 (s, 1H, CH_arom), 7.20 (s, 1H, CH_arom), 7.05 (s, 1H, CH_arom), 6.84 (s, 1H, CH_arom), 6.82 (d, *J* = 6.2 Hz, 1H, OH), 6.58 (s, 1H, CH_arom), 6.35 (s, 1H, CH_arom), 6.07 – 5.94 (m, 1H, OH), 5.52 – 5.50 (m, 2H, NH), 5.14 (d, *J* = 9.5 Hz, 2H, CH_2exo), 5.08 (d, *J* = 24.7 Hz, 2H, CH_2exo), 4.95 (d, *J* = 21.1 Hz, 2H, CH_2exo), 4.87 (t, *J* = 5.2 Hz, 1H, C*H*OHN), 4.53 – 4.52 (m, 1H, C*H*OHN) 4.27 – 3.95 (m, 12H, CH_2N (3x), OC*H*_2CH_2 (3x)), 3.86 (quin, *J* = 4.2 Hz, 1H, CH_2C*H*N), 3.83 (s, 3H, OCH_3), 3.82 – 3.80 (m, 1H, CH_2C*H*N), 3.70 (s, 3H, OCH_3), 3.66 (s, 3H, OCH_3), 3.53 (dt, *J* = 9.1, 1.9 Hz, 1H, CH_2C*H*N), 3.08 – 3.00 (m, 1H, CC*H*_2CHN), 2.95 – 2.86 (m, 4H, CC*H*_2CHN), 2.69 – 2.63 (m, 6H, CC*H*_2CHN), 2.54 (d, *J* = 15.8 Hz, 1H, CC*H*_2CHN).

¹³C NMR (176 MHz, DMSO)*: δ [ppm] = 166.6, 165.7, 164.5, 151.1, 150.5, 144.2, 143.2, 142.7, 140.6, 139.9, 138.9, 116.8, 114.6, 112.7, 111.4, 110.2, 108.5, 108.4, 105.9, 101.9, 85.8, 81.3, 81.2, 72.6, 66.3, 66.1, 59.5, 59.1, 55.9, 55.8, 55.7, 53.5, 53.2, 51.1, 51.0, 39.5, 35.6, 35.1, 18.8.

HRMS (ESI) *m/z*: ($C_{18}H_{19}O_3^+$ [M+H]$^+$)   calc.: 311.1390

                                                    found: 311.1392

* Due to residual water in the DMSO-*d_6* the NMR corresponds to a mixture of the imine form and the two hemiaminal forms (diastereomers). The imine form is only percent in minor quantities (1:1:0.22).

8,8-dibromobicyclo[5.1.0]octane (106)
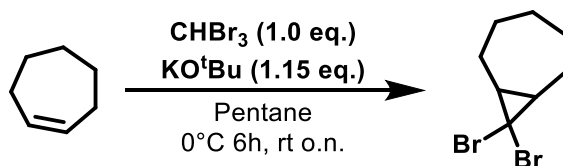
A stirred suspension of *cis*-cycloheptene (3.00 g, 31.3 mmol, 1.0 eq.) and potassium *tert*-butoxide (4.02 g, 35.9 mmol, 1.15 eq) in anhydrous pentane (100 ml) was cooled to 0 °C. A solution of bromoform (2.72 mL, 7.87 g, 31.3 mmol, 1.0 eq.) in anhydrous pentane (120 mL) was added dropwise over a period of 6 h at 0 °C. After complete addition, the resulting brown mixture was warmed to room temperature and stirred overnight. After addition of water (200 mL), the mixture was acidified with HCl (6 M) and the aqueous layer was extracted with Et_2O. The combined organic layers were dried over Na_2SO_4. The product (4.50 g, 16.8 mmol, 53%) was obtained as a brown oil and used without further purification.

TLC: R_f = 0.65(PE) [UV]

^{1}H NMR (500 MHz, $CDCl_3$): δ [ppm] = 2.27 – 2.23 (m, 2H), 1.93 – 1.86 (m, 1H), 1.85 – 1.80 (m, 2H), 1.74 – 1.67 (m, 2H), 1.32 – 1.28 (m, 2H), 1.22 – 1.15 (m, 3H).

^{13}C NMR (126 MHz, $CDCl_3$): δ [ppm] = 40.8, 34.8, 32.4, 29.0, 28.1.

(*E*)-2-((2-bromocyclooct-2-en-1-yl)oxy)ethan-1-ol (107)
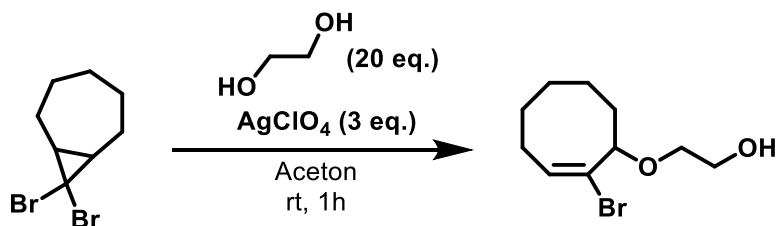
8,8-dibromobicyclo[5.1.0]octane (4.50 g, 16.8 mmol, 1.0 eq.) and ethane-1,2-diol (18.7 mL, 20.8 g, 63.1 mmol, 20.0 eq.) were dissolved in acetone (30 mL). Anhydrous AgClO$_4$ (10.4 g, 50.4 mmol, 3.0 eq.) was added in small portions under the exclusion of light and stirred at room temperaturefor 4 h. After the addition of EtOAc (100 mL) and filtration, 1 M HCl (100 mL) was added and the aqueous layer was extracted with EtOAc. The combined organic layers were washed with 1 M HCl, H$_2$O, sat. NaCl solution and dried over Na$_2$SO$_4$. The solvent was evaporated under reduced pressure and the (crude) product (3.84 g, 15.4 mmol, 92%) was obtained as a brown oil and used without further purification, due to light sensitivity.

TLC: R_f = 0.36(PE:EtOAc 2:1) [UV, KMnO$_4$]

2-(cyclooct-2-yn-1-yloxy)ethan-1-ol (108)
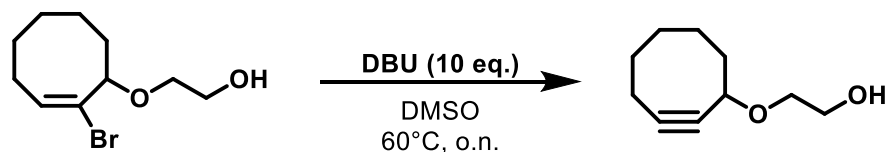
DBU (23 mL, 23.4 g, 154 mmol, 10.0 eq.) was added in portions to a solution of (*E*)-2-((2-bromocyclooct-2-en-1-yl)oxy)ethan-1-ol (3.84 g, 15.4 mmol, 1.0 eq.) in DMSO (30 mL) at 60 °C. After stirring overnight, the solution was allowed to cool to room temperatureand EtOAc and H_2O were added. After acidification to pH = 1 with conc. HCl, the aqueous phase was extracted with EtOAc. The combined organic layers were washed with 1 M HCl, sat. NaCl, dried over Na_2SO_4 and concentrated under reduced pressure. The crude product was purified by flash column chromatography (silica, PE:EtOAc 1:0 → 2:3) yielding 2-(cyclooct-2-yn-1-yloxy)ethan-1-ol as a light yellow oil (1.03 g, 6.12 mmol, 40%).

TLC: R_f = 0.39(PE:EtOAc 2:1) [UV, Iodine]

^{1}H NMR (500 MHz, CDCl$_3$): δ [ppm] = 4.23 – 4.20 (m, 1H), 3.78 – 3.72 (m, 2H), 3.70 – 3.65 (m, 1H), 3.48 – 3.44 (m, 1H), 2.28 – 2.10 (m, 3H), 2.01 – 1.90 (m, 2H), 1.86 – 1.78 (m, 2H), 1.71 – 1.60 (m, 2H), 1.48 – 1.42 (m, 1H).

^{13}C NMR (126 MHz, CDCl$_3$): δ [ppm] = 100.6, 92.7, 62.0, 42.4, 34.4, 29.9, 26.5, 20.8.

HRMS (ESI) *m/z*: ($C_{10}H_{17}O_2^+$ [M+H]$^+$)   calc.: 169.1223

found: 169.1223

2-(clooct-2-yn-1-yloxy)ethyl 4-methylbenzenesulfonate (109)
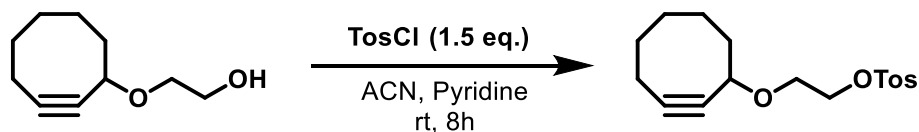
2-(clooct-2-yn-1-yloxy)ethan-1-ol was dissolved in 16 mL ACN. Pyridine (2.58 mL, 2.53 g, 32.0 mmol, 11.1 eq.) and TosCl (809 mg, 4.26 mmol, 1.5 eq.) were added in portions. The mixture was stirred for 8 h at room temperature. The reaction was monitored by TLC. The solution was filtered. PE was added to the solution and the mixture was washed with NaCl aq. and NH$_4$Cl aq.. The organic phase was separated and the solvent was removed under reduced pressure. The crude product was purified by column chromatography (silica, PE:EtOAc 2:3). The product was obtained as a colorless oil (648 mg, 2.01 mmol, 70%).

TLC: R_f = 0.73 (PE:EtOAc 2:1) [Iodine]

R_f = 0.28 (PE:EtOAc 4:1) [K$_2$MnO$_4$]

^{1}H NMR (500 MHz, CD$_2$Cl$_2$): δ [ppm] = 7.37 (d, J = 8.05 Hz, 1H), 7.78 (d, J = 8.30 Hz, 1H), 4.13 –4.11 (m, 1H), 3.71 –3.67 (m, 1H), 3.50 –3.46 (m, 1H), 2.45 (s, 3H), 2.25 –2.19 (m, 1H), 2.17 –2.10 (m, 1H), 2.06 –2.00 (m, 1H), 1.93 – 1.71 (m, 5H), 1.67 – 1.55 (m, 2H).

^{13}C NMR (126 MHz, CD$_2$Cl$_2$): δ [ppm] = 145.1, 133.0, 129.9, 127.9, 100.6, 92.0, 72.7, 69.5, 66.4, 42.2, 34.3, 29.7, 26.3, 21.4, 20.6.

HRMS (ESI) m/z: (C$_{17}$H$_{26}$NO$_4$S$^+$ [M+H]$^+$) calc.: 340.1577

found: 340.1578

(11aS)-8-(2-(cyclooct-2-yn-1-yloxy)ethoxy)-7-methoxy-2-methylene-1,2,3,11a-tetrahydro-5H-benzo[e]pyrrolo[1,2-a][1,4]diazepin-5-one (M3)
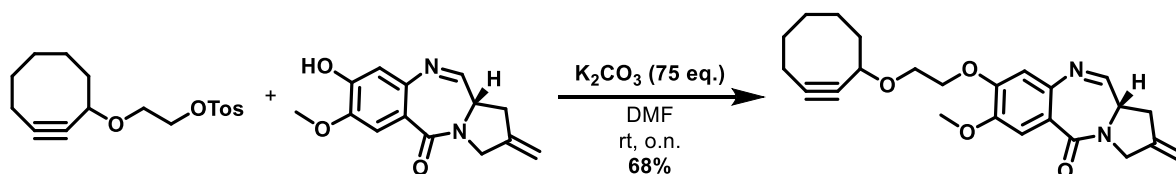
A flask equipped with K_2CO_3 (1.00 g, 7.24 mmol, 75 eq.) was dried under vacuum using a heat gun. After cooling to room temperature, (*S*)-8-hydroxy-7-methoxy-2-methylene-1,2,3,11a-tetrahydro-5H-benzo[e]pyrrolo[1,2-a][1,4]diazepin-5-one (25.0 mg, 96.9 µmol, 1.0 eq.) and 2-(cyclooct-2-yn-1-yloxy)ethyl 4-methylbenzenesulfonate (94.0 mg, 291 µmol, 3.0 eq.) were added. Upon addition of DMF (9.7 mL) the reaction mixture was stirred at RT overnight. The reaction was monitored by LC–MS. H_2O and DMF were added. The aqueous phase was thoroughly extracted with DCM. The combined organic layers were dried over Na_2SO_4 and concentrated under vacuum. The crude product was purified by column chromatography (1. column: DCM:MeOH 5%, 2. column: DCM:MeOH 0.5%) to yield the title compound (26.7 mg, 65.4 µmol, 68%).

TLC: R_f = 0.40 (EtOAc 100%) [UV]

^{1}H NMR (700 MHz, DMSO)*: δ [ppm] = 7.77 (d, *J* = 4.4 Hz, 1H, CHN), 7.33 (s, 1H, CH$_{arom}$), 7.19 (s, 1H, CH$_{arom}$), 7.05 (s, 1H, CH$_{arom}$), 6.85 (s, 1H, CH$_{arom}$), 6.83 (d, *J* = 5.8 Hz, 1H, OH), 6.55 (s, 1H, CH$_{arom}$), 6.33 (s, 1H, CH$_{arom}$), 5.58 (d, *J* = 4.4 Hz, 1H, NH), 5.14 (d, *J* = 8.8 Hz, 2H, CH$_{2exo}$), 5.08 (d, *J* = 24.3 Hz, 2H, CH$_{2exo}$), 4.95 (d, *J* = 21.2 Hz, 2H, CH$_{2exo}$), 4.87 (d, *J* = 6.2 Hz, 1H, CHC*H*OHNH), 4.53 (d, *J* = 9.0 Hz, 1H, CHC*H*OHNH), 4.30 (brs, 3H, CH$_{propargyl}$), 4.24 – 3.94 (m, 12H, CH$_{2ethyl}$, CH$_2$N), 3.85 (quin, *J* = 4.2 Hz, 1H, CH$_2$C*H*N), 3.82 (s, 3H, OCH$_3$), 3.82 – 3.74 (m, 4H, CH$_{2ethyl}$, CH$_2$C*H*N), 3.70 (s, 3H, OCH$_3$), 3.66 (s, 3H, OCH$_3$), 3.64 – 3.60 (m, 3H, CH$_{2ethyl}$), 3.52 (td, *J* = 9.0, 2.0 Hz, 1H, CH$_2$C*H*N), 3.09 – 3.00 (m, 2H, CC*H*$_2$CHN), 2.95 – 2.85 (m, 2H, CC*H*$_2$CHN), 2.66 (dd, *J* = 16.3, 2.0 Hz, 1H, CC*H*$_2$CHN), 2.54 (d, *J* = 15.6 Hz, 1H, CC*H*$_2$CHN), 2.26 – 2.20 (m, 3H, CH$_{2octyne}$), 2.14 (dtd, *J* = 16.7, 5.8, 2.2 Hz, 3H, CH$_{2octyne}$), 2.09 – 2.03 (m, 3H, CH$_{2octyne}$), 1.86 (dt, *J* = 13.4, 6.8 Hz, 6H, CH$_{2octyne}$), 1.80 – 1.70 (m, 6H, CH$_{2octyne}$), 1.66 – 1.59 (m, 3H, CH$_{2octyne}$), 1.52 (dt, *J* = 27.2, 10.0 Hz, 3H, CH$_{2octyne}$), 1.41 – 1.34 (m, 3H, CH$_{2octyne}$).

¹³C NMR (176 MHz, DMSO)*: δ [ppm] = 166.6, 165.7, 165.3, 164.3, 163.6, 151.4, 150.8, 150.3, 147.0, 144.2, 143.3, 142.7, 140.7, 140.6, 139.9, 139.0, 119.4, 116.6, 114.6, 112.7, 111.3, 110.3, 110.0, 108.5, 108.3, 105.8, 101.9, 100.0, 93.0, 85.8, 81.3, 71.9, 67.9, 67.9, 67.6, 67.3, 66.9, 59.5, 59.1, 55.8, 55.6, 53.5, 53.2, 51.1, 51.0, 41.9, 35.6, 35.1, 34.7, 33.9, 29.3, 25.9, 20.0.

HRMS (ESI) *m/z*: ($C_{24}H_{29}N_2O_4^+$ [M+H]⁺)   calc.:   409.2122

found: 409.2121

* Due to residual water in the DMSO-*d₆* the NMR corresponds to a mixture of the imine form and the two hemiaminal forms (diastereomers).

bicyclo[6.1.0]non-4-yn-9-ylmethyl (4-nitrophenyl) carbonate (115)
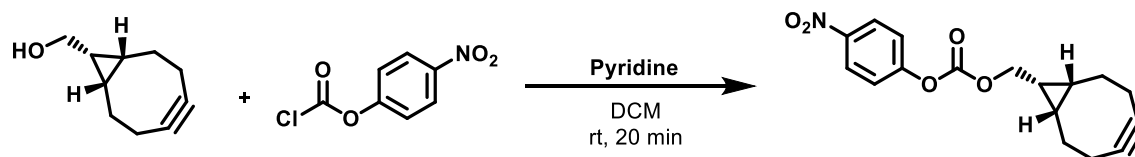
To a solution of 10 mg (0.07 mmol, 1.0 eq.) of ((1R,8S,9S)- bicyclo[6.1.0]non-4-yn-9-yl)methanol in 1.66 mL dry DCM was added 13.4 µL (0.17 mmol, 2.5 eq.) pyridine and 16.8 mg (0.08 mmol, 1.25 eq.) 4-nitrophenyl chloroformate and the mixture was stirred for 20 min at room temperature, before it was quenched by addition of 20 mL saturated ammonium chloride solution. The mixture was extracted with DCM, the combined organic layers were dried over Na_2SO_4 and concentrated under reduced pressure. The crude product was purified by column chromatography (silica, PE:EtOAc 95:5 → 9:1). The product was obtained as a colorless solid (18.4 mg, 58.5 µmol, 88%).

TLC: R_f = 0.50 (PE:EtOAc 9:1) [Iodine]

^{1}H NMR (500 MHz, CD_2Cl_2): δ [ppm] = 8.27 (d, J = 9.2 Hz, 2H), 7.40 (d, J = 9.2 Hz, 2H), 4.40 (d, J = 8.3 Hz, 2H), 2.33 – 2.28 (m, 4H), 2.24 – 2.20 (m, 2H), 1.65 – 1.57 (m, 2H), 1.54 – 1.48 (m, 1H), 1.07 – 1.03 (m, 1H).

^{13}C NMR (126 MHz, CD_2Cl_2): δ [ppm] = 155.8, 152.6, 145.4, 125.3, 122.0, 98.6, 68.1, 29.1, 21.3, 20.5, 17.3.

HRMS (ESI) m/z: ($C_{17}H_{18}NO_5^+$ [M+H]$^+$)   calc.:   316.1179

found: 316.1173

bicyclo[6.1.0]non-4-yn-9-ylmethyl((S)-7-methoxy-2-methylene-5-oxo-2,3,5,11a-tetrahydro-1H-benzo[e]pyrrolo[1,2-a][1,4]diazepin-8-yl) carbonate (M4)
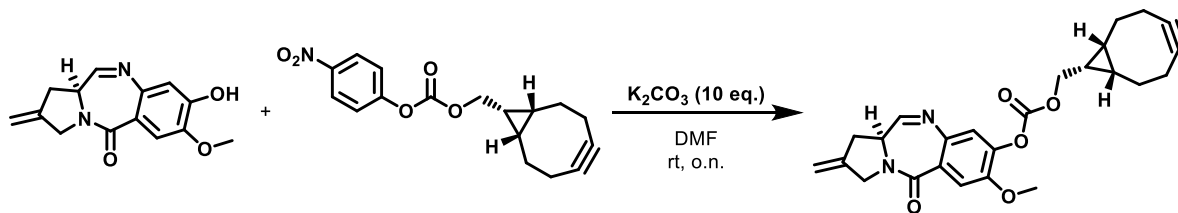
A flask equipped with K_2CO_3 (1.00 g, 7.24 mmol, 75 eq.) was dried under vacuum using a heat gun. After cooling to rt, (S)-8-hydroxy-7-methoxy-2-methylene-1,2,3,11a-tetrahydro-5H-benzo[e]pyrrolo[1,2-a][1,4]diazepin-5-one (25 mg, 96.9 µmol, 1.0 eq.) and bicyclo[6.1.0]non-4-yn-9-ylmethyl (4-nitrophenyl) carbonate (40 mg, 125 µmol, 1.3 eq.) were added. Upon addition of DMF (9.70 mL) the reaction mixture, which immediately turned bright yellow, was stirred at RT over night. DCM was added and the mixture was filtered (pore 5 filter). The filtrate was concentrated under reduced pressure and purified by column chromatography (silica, PE:EtOAc 1:0 →1:3; alternatively 10% MeOH/DCM). The product was obtained as a yellow film (18.1 mg, 41.8 µmol, 43%).

**TLC**: R_f = 0.34 (PE:EtOAc 1:2)

¹H NMR (700 MHz, DMSO)*: δ [ppm] = 7.82 (d, J = 4.5 Hz, 1H, CHN), 7.51 (s, 1H, CH$_{arom}$), 7.20 (s, 1H, CH$_{arom}$), 5.15 (d, J = 8.8 Hz, 2H, CH$_{2exo}$), 4.36 (d, J = 8.3 Hz, 2H, OCH$_2$CH), 4.15 (dd, J = 41.7, 15.8 Hz, 2H, CH$_2$N), 3.95 (quin, J = 4.22 Hz, 1H, CH$_2$CHN), 3.87 (s, 3H, CH$_3$), 3.09 – 3.01 (m, 2H, CCH$_2$CHN), 2.27 – 2.24 (m, J = 13.5 Hz, 2H, CH$_2$CH$_2$CC$_{octyne}$), 2.17 – 2.14 (m, 4H, CH$_2$CH$_2$CC$_{octyne}$, CH$_2$CH$_2$CC$_{octyne}$), 1.63 – 1.52 (m, 2H, , CH$_2$CH$_2$CC$_{octyne}$), 1.40 (q, J = 8.6 Hz, 1H, OCH$_2$CH$_{cyclopropane}$), 1.00 – 0.92 (m, 2H, CHCH$_2$CH$_{2cyclopropane}$).

¹³C NMR (176 MHz, DMSO)*: δ [ppm] = 165.7, 163.0, 152.1, 148.9, 142.5, 141.6, 139.7, 125.7, 120.8, 112.6, 108.7, 98.9, 67.3, 56.2, 54.9, 53.5, 51.2, 49.8, 34.7, 28.5, 20.8, 19.9, 17.1.

* Due to residual water in the DMSO-d_6 the NMR corresponds to a mixture of the imine form and the two hemiaminal forms (diastereomers).

HRMS (ESI) *m/z*: ($C_{25}H_{27}N_2O_5^+$ [M+H]$^+$)   calc.:   435.1914

found: 435.1914

(*S*)-8-(furan-2-ylmethoxy)-7-methoxy-2-methylene-1,2,3,11a-tetrahydro-5H-benzo[e]pyrrolo[1,2-a][1,4]diazepin-5-one (M5)
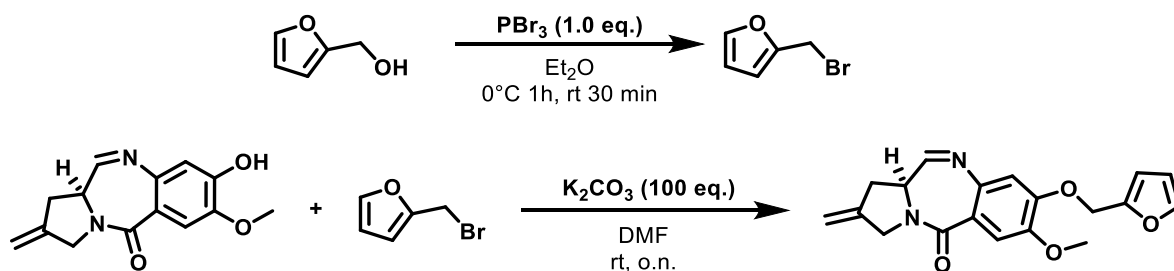
Furfuryl alcohol (0.33 mL, 372 mg, 3.80 mmol, 100 eq.) was dissolved in dry Et_2O (13 mL). The solution was cooled to 0 °C before PBr_3 (0.36 ml, 1.03 g, 3.80 mmol, 100 eq.) was added dropwise over a period of 5 min). The mixture was stirred at 0 °C for 1 h. Afterwards, the reaction was stirred for 30 min at room temperature. Water (3 mL) was added and the phases were separated. The aqueous phase was extracted with MTBE (4 × 10 mL). The combined organic layers were washed with brine (2 × 10 mL), and dried over Na_2SO_4. 50% of the solvent was removed under reduced pressure before 5 mL DMF were added. The remaining ether war removed by a rotary evaporator. Assuming a 100% yield this gave a 0.76 M solution of 2-furfuryl bromide.

(*S*)-8-hydroxy-7-methoxy-2-methylene-1,2,3,11a-tetrahydro-5H-benzo[e]pyrrolo[1,2-a][1,4]diazepin-5-one (10.0 mg, 38.0 µmol, 1.0 eq.) and K_2CO_3 (500 mg, 3.80 mmol, 100 eq.) were dissolved in dry DMF (0.50 mL). 1 mL (0.5 mmol, 10 eq.) of the earlier prepared solution was added. The mixture was stirred at RT overnight. H_2O was added to the reaction and the mixture was purified by HPLC (H_2O/ACN, no additives). The title compound was obtained as a yellow solid (12.0 mg, 35.0µmol, 92%).

TLC: R_f = 0.27 (PE:EtOAc 1:4) [UV]

¹H NMR (500 MHz, DMSO): δ [ppm] = 7.78 (d, *J* = 4.4 Hz, 1H, CHN), 7.72 (dd, *J* = 1.8, 0.8 Hz, 1H, CHO_{Furan}), 7.34 (s, 1H, CH_{arom}), 7.02 (s, 1H, CH_{arom}), 6.61 (d, *J* = 3.1 Hz, 1H, CH_{Furan}), 6.49 (dd, *J* = 3.2, 1.9 Hz, 1H, CH_{Furan}), 5.18 – 5.08 (m, 4H, OCH_2C, CH_{2exo}), 4.20 – 4.09 (m, 2H, CH_2N), 3.91 – 3.84 (qin., *J* = 4.2 Hz, 1H, CH_2C*H*N), 3.09 – 2.01 (m, 2H, CC*H*_2CHN).

^{13}C NMR (126 MHz, DMSO): δ [ppm] = 165.0, 164.4, 163.5, 149.6, 149.6, 147.1, 143.8, 142.7, 140.4, 119.7, 111.2, 111.1, 110.7, 110.6, 108.5, 62.2, 55.6, 53.5, 51.1, 34.7.

HRMS (ESI) *m/z*: ($C_{19}H_{19}N_2O_4^+$ [M+H]$^+$)   calc.:   339.1339
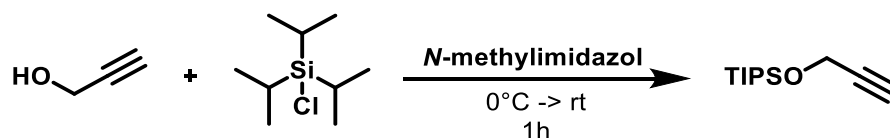
found: 339.1340

triethyl(prop-2-yn-1-yloxy)silane (126)
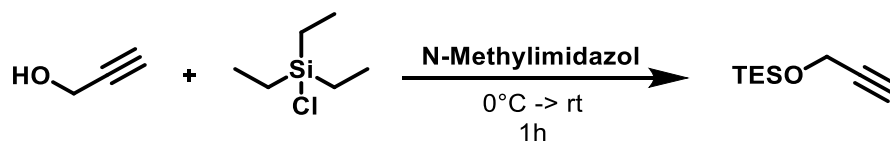
TESCl (2.62 g, 17.4 mmol, 1.03 eq.) was dissolved in *N*-methylimidazol (2.69 mL, 2.78 g, 33.8 mmol, 2.0 eq.) and was intensively stirred. Propargyl alcohol (948 mg, 16.9 mmol, 1.0 eq.) was added dropwise to the solution, which was cooled by an ice bath. After 30 min 300 mL water were added to the reaction. The mixture was extracted with PE. The combined organic phases were dried over Na_2SO_4, filtered, and carefully evaporated. Triethyl(prop-2-yn-1-yloxy)silane was obtained as a colorless liquid (2.66 g, 15.7 mmol, 95%).

¹H NMR (500 MHz, CDCl₃): δ [ppm] = 4.30 (1H, d, *J* = 2.40 Hz, 2H), 2.39 (1H, t, *J* = 2.40 Hz, 1H), 0.97 (1H, t, *J* = 7.93 Hz, 9H), 0.65 (1H, q, *J* = 7.94 Hz, 6H).

¹³C NMR (126 MHz, DMSO): δ [ppm] = 82.4, 73.0, 51.2, 6.8, 4.5.

triisopropyl(prop-2-yn-1-yloxy)silane (129)

TIPSCl (3.71 mL, 3.34 mg, 17.4 mmol, 1.03 eq.) was dissolved in *N*-methylimidazol (2.69 mL, 2.78 g, 33.8 mmol, 2.0 eq.) and was intensively stirred. Propargyl alcohol (948 mg, 16.9 mmol, 1.0 eq.) was added dropwise to the solution, which was cooled by an ice bath. After 1 h water (300 mL) was added to the reaction. The mixture was extracted with PE. The combined organic phases were dried over Na_2SO_4, filtered, and carefully evaporated. Triisopropyl(prop-2-yn-1-yloxy)silane was obtained as a colorless liquid (3.50 g, 16.4 mmol, 97%).

^{1}H NMR (500 MHz, CDCl$_3$): δ [ppm] = 4.39 (d, *J* = 2.4 Hz, 2H), 2.40 (t, *J* = 2.4 Hz, 1H), 1.11-1.06 (m, 21H).

^{13}C NMR (126 MHz, CDCl$_3$): δ [ppm] = 82.6, 72.8, 51.9, 18.0, 12.1.

methyl 4-((triisopropylsilyl)oxy)but-2-ynoate (130)
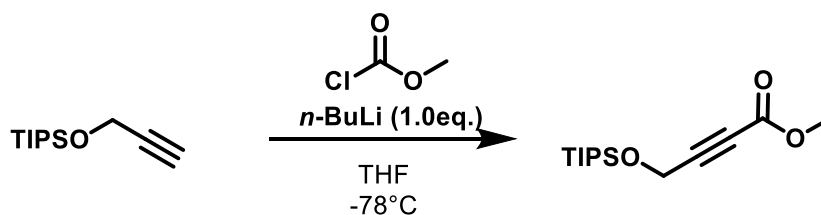
Triisopropyl(prop-2-yn-1-yloxy)silane (3.48 g, 16.4 mmol, 1.0 eq.) was dissolved in dry THF. The solution was cooled to -78 °C. *n*-BuLi (2.5 M in hexane, 6.56 mL, 16.4 mmol, 1.0 eq.) was added dropwise over a period of 10 min. The mixture was stirred at -78 °C for 1 h. Mehtyl chloroformate (1.27 mL, 1.55 g, 16.4 mmol, 1.0 eq.) was added rapidly and the mixture was stirred at -78 °C for 1 h. The reaction was allowed to warm to room temperature over night. MeOH and H_2O were added to the solution. The mixture was extracted with EtOAc. The combined organic layers were washed with brine, dried over Na_2SO_4, filtered and concentrated under reduced pressure. Methyl 4-((triisopropylsilyl)oxy)but-2-ynoate was obtained as a colorless oil (3.10 g, 11.5 mmol, 70%).

^{1}H NMR (500 MHz, CDCl$_3$): δ [ppm] = 4.50 (s, 2H), 3.78 (s, 3H), 1.15 – 1.04 (m, 21H).

^{13}C NMR (126 MHz, CDCl$_3$): δ [ppm] = 154.0, 86.4, 76.2, 52.9, 51.8, 18.0, 12.0.

1-bromopropyn-3-ol (135)
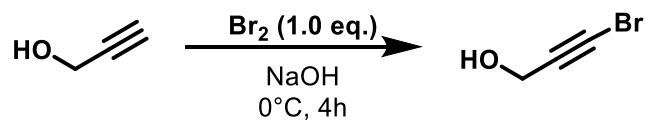
An ice-cold solution of sodium hypobromite obtained from addition of 4.6 mL Br_2 (14.2 g, 89.2 mmol, 1.0 eq.) to a solution of 10.7 g NaOH (268 mmol, 3.0 eq.) in water (50 mL) and ice (20 g) was added to propargyl alcohol (5.27 mL, 5.0 g, 89.2 mmol, 1.0 eq.). The mixture was stirred for 4 h at 0 °C, allowed to reach room temperature, and extracted with chloroform, and the organic layer was separated, dried over Na_2SO_4, and concentrated to give 1-bromopropyn3-ol (4.89 g, 35.6 mmol, 41 %) as a yellow oil.

**^{1}H NMR** (700 MHz, DMSO): δ [ppm] = 5.26 (s, 1H), 4.09 (s, 2H).

^{13}C NMR (176 MHz, DMSO): δ [ppm] = 80.3, 49.9, 45.4.

4-hydroxybut-2-ynenitrile (136)
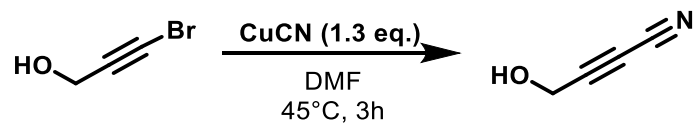
To a vigorously stirred suspension of anhydrous copper(I) cyanide (11.0 g, 120 mmol, 3.5 eq.) in DMF (80 mL) was added dropwise 1-bromopropyn-3-ol (4.89 g, 35.6 mmol, 1.0 eq.) in DMF (10 mL) under Ar, the temperature not being allowed to exceed 50 °C. The mixture was stirred at 45 – 50 °C for 3 h and then cooled, and a mixture of DMF (25 mL) and water (50 mL) was added to the vigorously stirred reaction mixture, with stirring continued until the precipitated solid becomes granular. The precipitate was filtered and washed with CH_2Cl_2, and the filtrate was extracted with CH_2Cl_2. The combined organic layer was dried (Na_2SO_4) and concentrated, and the residue was subjected to column chromatography (CH_2Cl_2:MeOH, 10:1) to give 4-hydroxy-2-butynenitrile (1.58 g, 19.5 mmol, 55%) as colorless crystals.

^{1}H NMR (700 MHz, DMSO): δ [ppm] = 5.39 (t, J = 6.1 Hz, 1H), 4.17 (d, J = 6.1 Hz, 2H).

**^{13}C NMR** (176 MHz, DMSO): δ [ppm] = 79.6, 67.9, 49.3.

4-bromobut-2-ynenitrile (137)
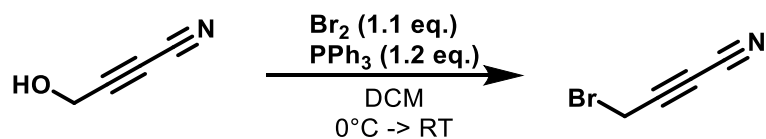
PPh$_3$ (386 mg, 1.48 mmol, 1.2 eq.) was dissolved in 1 mL DCM and cooled to 0 °C. Br$_2$ (216 mg, 1.35 mmol, 1.1 eq.) was added to the solution. The solution loses instantly its color and a white solid is formed after ca. 10 − 15 min. A premixed solution of 4-hydroxy-2-butynenitrile (100 mg, 1.23 mmol, 1.0 eq.) with imidazole (100 mg, 1.48 mmol, 1.2 eq.) in DCM was added at 0 °C. The mixture was stirred at room temperature. After 5 min EtOAc and H$_2$O were added and the phases were separated. The aqueous phase was extracted with EtOAc. The combined organic layers were dried over Na$_2$SO$_4$, filtered and concentrated under vacuum. 4-bromobut-2-ynenitrile (84.2 mg, 0.59 mmol, 48%) was obtained as a colorless oil.

^{1}H NMR (500 MHz, DMSO): δ [ppm] = 4.43 (s, 2H).

^{13}C NMR (126 MHz, DMSO): δ [ppm] = 77.0, 69.2, 15.5.

(S)-7-methoxy-8-((1-(2-(((S)-7-methoxy-2-methylene-5-oxo-2,3,5,11a-tetrahydro-1H-benzo[e]pyrrolo[1,2-a][1,4]diazepin-8-yl)oxy)ethyl)-1H-1,2,3-triazol-4-yl)methoxy)-2-methylene-1,2,3,11a-tetrahydro-5H-benzo[e]pyrrolo[1,2-a][1,4]diazepin-5-one (D1)
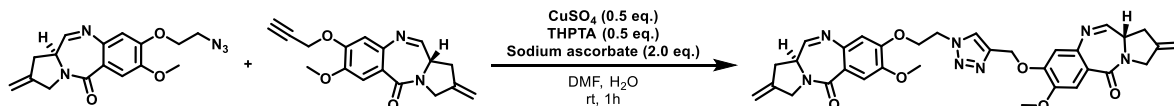
(*S*)-8-(2-azidoethoxy)-7-methoxy-2-methylene-1,2,3,11a-tetrahydro-5H-benzo[e]pyrrolo [1,2-a][1,4]diazepin-5-one (8.0 mg, 24.0 µmol, 1.0 eq.) and (*S*)-8-(but-3-yn-1-yloxy)-7-methoxy-2-methylene-1,2,3,11a-tetrahydro-5H-benzo[e]pyrrolo[1,2-a][1,4]diazepin-5-one (7.0 mg, 24.0 µmol, 1.0 eq.) were dissolved in DMF (0.4 mL) and stirred at room temperature.

480 µL of a sodium ascorbate solution (100 mM, 48.0 µmol, 2.0 eq.) and 120 µL of a $CuSO_4$ solution (100 mM, 12.0 µmol, 0.5 eq.) were mixed, 120 µL of a THPTA solution (100 mM, 12.0 µmol, 0.5 eq.) was added to the solution. The mixture was added to the previously prepared solution. After 1 h EtOAc and H_2O were added to the mixture. The phases were separated and the aqueous phase was extracted with DCM and EtOAc. The combined organic layers were dried over Na_2SO_4, filtered, and concentrated under reduced pressure. Purification by preparative TLC (4% MeOH/DCM) gave the title compound as a colorless solid (5.7 mg, 9.0 µmol, 38%).

TLC: R_f = 0.36(MeOH/DCM, 1%) [UV]

¹H NMR (700 MHz, DMSO)*: δ [ppm] = 8.31 – 8.29 (m, 1H), 8.06 (s, 0.2H), 7.78 – 7.77 (m, 0.3H), 7.33 – 7.32 (m, 0.3 H), 7.29 – 7.25 (m, 1H), 7.22 – 7.20 (m, 1H), 7.08 (s, 0.2H), 7.05 (d, J = 1.7 Hz, 2H), 6.90 (t, J = 2.6 Hz, 0.2H), 6.80 (s, 0.5H), 6.63 (s, 0.5H), 6.54 (s, 0.3H), 6.40 (s, 0.3H), 6.13 (d, J = 9.3 Hz, 1H), 5.32 (t, J = 4.7 Hz, 0.2H), 5.27 (d, J = 12.1 Hz, 0.2H), 5.20 – 5.07 (m, 6H), 4.96 (dd, J = 17.7, 2.0 Hz, 2H), 4.82 (brs, 2H), 4.66 (s, 0.3H), 4.53 (t, 6.0 Hz, 1H), 4.48 – 4.43 (m, 1H), 4.40 – 4.24 (m, 2H), 4.26 (td, J = 9.2, 1.3 Hz, 1H), 4.19 – 4.11 (m, 4H), 3.97 (dd, J = 15.6, 2.9 Hz, 1H), 3.87 – 3.85 (m, 1H), 3.79 – 3.76 (m, 2H), 3.69 – 3.59 (m, 7H), 3.51 (s, 0.3H), 3.36 (d, J = 4.0 Hz, 3H), 3.21 (d, J = 4.8 Hz, 2H), 3.00 – 2.91 (m, 2H), 2.68 (d, J = 16.3 Hz, 1H), 2.46 (d, J = 15.9 Hz), 2.02 – 1.97 (m, 1H), 1.23 (brs, 6H).

¹³C NMR (176 MHz, DMSO)*: δ [ppm] = 174.2, 166.8, 166.7, 165.1, 165.0, 164.7, 164.5, 164.4, 163.5, 163.4, 151.0, 151.0, 150.2, 150.1, 149.8, 149.6, 147.1, 147.0, 143.8, 143.7, 143.7, 143.2, 143.1, 142.7, 142.6, 142.4, 142.3, 140.8, 140.8, 140.5, 140.5, 139.3, 139.2, 138.1, 138.0, 133.5, 129.6, 129.6, 125.4, 125.3, 125.3, 120.3, 120.0, 119.8, 119.6, 115.4, 114.6, 112.9, 112.2, 111.6, 111.1, 110.9, 110.6, 110.2, 109.7, 108.5, 108.4, 107.8, 107.5, 106.0, 102.3, 102.0, 94.5, 88.4, 88.3, 69.8, 67.1, 67.0, 66.6, 62.8, 61.7, 61.6, 61.4, 58.3, 58.2, 56.1, 56.0, 55.8, 55.7, 55.6, 55.6, 54.9, 54.2, 54.1, 53.9, 53.9, 53.5, 53.5, 53.4, 51.1, 50.8, 49.0, 49.0, 36.2, 35.3, 35.3, 35.1, 34.7, 31.3, 29.1, 29.0, 28.8, 28.7, 28.7, 28.6, 28.5, 26.6, 26.5, 25.1, 22.1, 15.0, 13.9.

HRMS (ESI) *m/z*: ($C_{33}H_{34}N_7O_6^+$ [M+H]$^+$)   calc.:   624.2565

found: 624.2564

* Due to residual water in the DMSO-d_6 the NMR corresponds to a complex mixture of the imine form, the hemiaminal forms (diastereomers) and the mixed forms.

(11aS,11a'S)-8,8'-(((1H-1,2,3-triazole-1,4-diyl)bis(ethane-2,1-diyl))bis(oxy))bis(7-methoxy-2-methylene-1,2,3,11a-tetrahydro-5H-benzo[e]pyrrolo[1,2-a][1,4]diazepin-5-one) (D2)
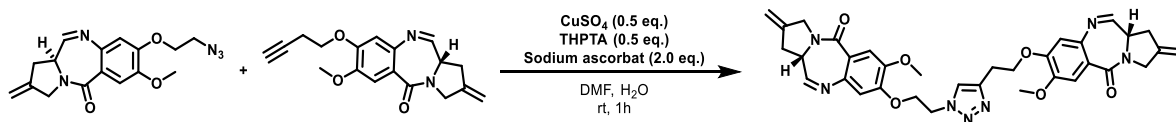
(*S*)-8-(2-azidoethoxy)-7-methoxy-2-methylene-1,2,3,11a-tetrahydro-5H-benzo[e]pyrrolo [1,2-a][1,4]diazepin-5-one (7.0 mg, 24.0 µmol, 1.0 eq.) and (*S*)-7-methoxy-2-methylene-8-(prop-2-yn-1-yloxy)-1,2,3,11a-tetrahydro-5H-benzo[e]pyrrolo[1,2-a][1,4]diazepin-5-one (8.0 mg, 24.0 µmol, 1.0 eq.) were dissolved in DMF (0.4 mL) and stirred at room temperature.

480 µL of a sodium ascorbate solution (100 mM, 48.0 µmol, 2.0 eq.) and 120 µL of a CuSO4 solution (100 mM, 12.0 µmol, 0.5 eq.) were mixed, 120 µL of a THPTA solution (100 mM, 12.0 µmol, 0.5 eq.) was added to the solution. The mixture was added to the previously prepared solution. After 1 h EtOAc and H2O were added to the mixture. The phases were separated and the aqueous phase was extracted with DCM and EtOAc. The combined organic layers were dried over Na2SO4, filtered, and concentrated under reduced pressure. Purification by preparative TLC (4% MeOH/DCM) gave the title compound as a colorless solid (3.2 mg, 5.0 µmol, 21%).


TLC: R_f = 0.40 (MeOH/DCM, 1%) [UV]

¹H NMR (700 MHz, DMSO)*: δ [ppm] = 8.04 – 8.02 (m, 1H), 7.95 (s, 1H), 7.77 – 7.76 (m, 1H), 7.31 – 7.29 (m, 1H), 7.25 – 7.22 (m, 1H), 7.20 – 7.17 (m, 1H), 7.04 – 7.00 (m, 1H), 6.87 – 6.84 (m, 1H), 6.83 – 6.81 (m, 0.4H), 6.62 – 6.56 (m, 1H), 6.40 – 6.34 (m, 2H), 6.11 (s, 0.2H), 5.98 – 5.96 (m, 0.4H), 5.75 (s, 0.2H), 5.50 – 5.47 (m, 0.8H), 5.14 (d, *J* = 9.1 Hz, 2H), 5.10 (d, *J* = 8.3 Hz, 1H), 5.07 (d, *J* = 12.1 Hz, 1H), 4.97 – 4.93 (m, 3H), 4.86 (t, *J* = 6.1 Hz, 0.6H), 4.76 (brs, 4H), 4.54 – 4.50 (m, 2H), 4.44 – 4.29 (m, 5H), 4.25 – 4.08 (m, 11H), 3.96 (d, *J* = 15.6 Hz, 1H), 3.88 – 3.82 (m, 2H), 3.80 – 3.73 (m, 4H), 3.67 – 3.55 (m, 9H), 3.35 (s, 0.6H), 3.29 (s, 1H), 3.20 (s, 3H), 3.14 – 3.12 (m, 3H), 3.06 – 2.97 (m, 3H), 2.69 – 2.64 (m, 2H), 2.55 – 2.51 (m, 0.6H), 2.47 – 2.40 (m, 0.8H), 1.71 (d, *J* = 39.7 Hz, 0.6H), 1.23 (brs, 1H).

¹³C NMR (176 MHz, DMSO)*: δ [ppm] = 164.5, 164.4, 163.5, 163.5, 162.3, 151.5, 151.0, 150.1, 147.0, 1.43.8, 143.3, 142.7, 142.6, 140.7, 140.6, 140.5, 139.3, 123.3, 120.7, 120.0, 119.4, 111.6, 111.3, 110.4, 110.1, 109.5, 108.5, 106.0, 102.2, 101.6, 88.4, 88.3, 67.4, 67.1, 66.9, 66.7, 59.1, 58.3, 56.1, 55.9, 55.7, 55.6, 54.9, 54.2, 53.9, 53.5, 53.4, 53.1, 51.1, 48.8, 36.2, 34.7, 30.7, 25.4.

HRMS (ESI) *m/z*: ($C_{34}H_{36}N_7O_6^+$ [M+H]⁺)   calc.:   638.2722

found: 638.2723

* Due to residual water in the DMSO-*d₆* the NMR corresponds to a complex mixture of the imine form, the hemiaminal forms (diastereomers) and the mixed forms.

(11aS)-7-methoxy-8-(2-(4-(2-(((S)-7-methoxy-2-methylene-5-oxo-2,3,5,11a-tetrahydro-1H-benzo[e]pyrrolo[1,2-a][1,4]diazepin-8-yl)oxy)ethoxy)-4,5,6,7,8,9-hexahydro-1H-cycloocta[d][1,2,3]triazol-1-yl)ethoxy)-2-methylene-1,2,3,11a-tetrahydro-5H-benzo[e]pyrrolo[1,2-a][1,4]diazepin-5-one (D3)
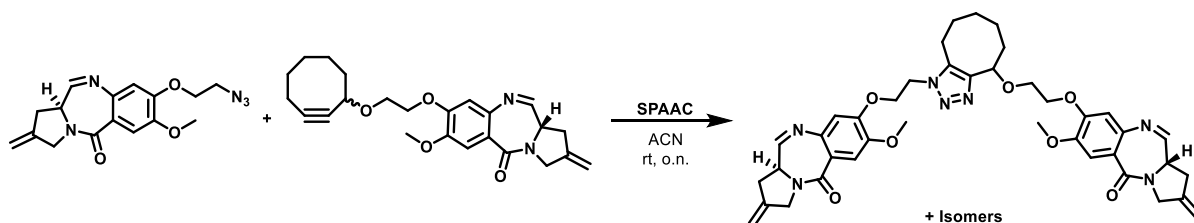
(*S*)-8-(2-azidoethoxy)-7-methoxy-2-methylene-1,2,3,11a-tetrahydro-5H-benzo[e]pyrrolo[1,2-a][1,4]diazepin-5-one (5.0 mg, 15.0 µmol, 1.0 eq.) and (11a*S*)-8-(2-(cyclooct-2-yn-1-yloxy)ethoxy)-7-methoxy-2-methylene-1,2,3,11a-tetrahydro-5H-benzo[e]pyrrolo[1,2-a][1,4]diazepin-5-one (6.1 mg, 15.0 µmol, 1.0 eq.) were dissolved in 0.5 mL ACN. The mixture was stirred at room temperature over night. The solvent was removed under reduced pressure. Purification by column chromatography (silica, MeOH/DCM 0% → 5%) yielded the title compound as a colorless solid (7.74 mg, 10.5 µmol, 70%).

TLC: R_f = 0.47 (MeOH/DCM, 1%) [UV]

^{1}H NMR (700 MHz, DMSO)*: δ [ppm] = 7.76 – 7.68 (m, 1H), 7.32 – 7.22 (m, 1H), 7.11 – 7.04 (m, 1H), 6.82 – 6.76 (m, 1H), 6.56 – 6.45 (m, 1H), 6.18 – 6.00 (m, 1H), 5.48 – 5.40 (m, 1H), 5.14 – 4.99 (m, 6H), 4.86 – 4.62 (m, 3H), 4.54 – 4.22 (m, 5H), 4.14 – 4.09 (m, 5H), 3.84 – 3.56 (m, 14H), 3.10 – 2.78 (m, 8H), 2.28 – 1.99 (m, 3H), 1.81 – 1.67 (m, 3H), 1.56 – 1.48 (m, 7H), 1.22 – 1.03 (m, 4H).

^{13}C NMR (176 MHz, DMSO)*,**: δ [ppm] = 1.74.4, 165.2, 164.3, 161.8, 1.61.3, 151.8, 151.5, 151.2, 150.6, 147.0, 145.9, 145.3, 143.4, 142.9, 142.2, 141.9, 140.4, 137.5, 135.2, 130.7, 127.9, 121.05, 120.7, 120.6, 118.2, 113.2, 112.7, 102.4, 73.9, 66.9, 66.1, 62.4, 55.8, 55.6, 54.9, 54.7, 51.9, 48.1, 46.2, 39.4, 35.1, 34.9, 34.5, 34.2, 31.0, 30.3, 29.7, 28.9, 28.7, 27.0, 25.5, 24.4, 22.0, 20.7, 18.2, 7.0.

HRMS (ESI) *m/z*: ($C_{40}H_{46}N_7O_7^+$ [M+H]$^+$)   calc.:   736.3453

                                                                        found: 736.3454

* Due to residual water in the DMSO-*d_6* the NMR corresponds to a complex mixture of the imine form, the hemiaminal forms (diastereomers) and the mixed forms.

**Determined by HMBC.

**(S)-7-methoxy-2-methylene-5-oxo-2,3,5,11a-tetrahydro-1H-benzo[e]pyrrolo[1,2-a]
[1,4]diazepin-8-yl (((5aS,6R,6aR)-1-(2-(((S)-7-methoxy-2-methylene-5-oxo-2,3,5,11a-
tetrahydro-1H-benzo[e]pyrrolo[1,2-a][1,4]diazepin-8-yl)oxy)ethyl)-1,4,5,5a,6,6a,7,8-
octahydrocyclopropa[5,6]cycloocta[1,2-d][1,2,3]triazol-6-yl)methyl) carbonate (D4)**
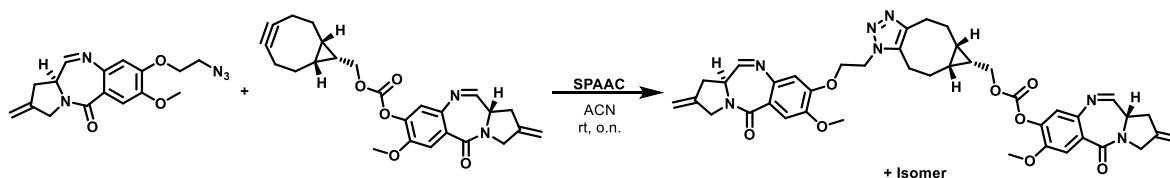
(*S*)-8-(2-azidoethoxy)-7-methoxy-2-methylene-1,2,3,11a-tetrahydro-5H-
benzo[e]pyrrolo[1,2-a][1,4]diazepin-5-one   (5.0 mg,   15.0 µmol,   1.0 eq.)   and
bicyclo[6.1.0]non-4-yn-9-ylmethyl((*S*)-7-methoxy-2-methylene-5-oxo-2,3,5,11a-
tetrahydro-1H-benzo[e]pyrrolo[1,2-a][1,4]diazepin-8-yl)   carbonate   (6.5 mg,   15.0 µmol,
1.0 eq.) were dissolved in 0.5 mL MeOH. The mixture was stirred at room temperature over
night. The solvent was removed under reduced pressure. Purification by column
chromatography (silica, MeOH/DCM 0% → 10%) yielded the title compound as a colorless
solid (5.3 mg, 6.97 µmol, 46%).

TLC: R_f = 0.31 (MeOH/DCM, 1%) [UV]

¹H NMR (700 MHz, DMSO)*: δ [ppm] = 7.83 (d, *J* = 4.4 Hz, 1H), 7.76 (d, *J* = 2.9 Hz, 1H),
7.51 (s, 1H), 7.31 (d, *J* = 2.60, 1H), 7.21 (s, 1H), 6.82 (d, *J* = 11.0 Hz, 1H), 5.16 – 5.12 (m,
4H), 5.06 – 4.89 (m, 2H), 4.68 (brs, 3H), 4.47 – 4.45 (m, 1H), 4.38 – 4.34 (m, 4H), 4.23 (t,
J = 5.2 Hz, 1H), 4.20 – 4.17 (m, 2H), 4.12 – 4.08 (m, 4H), 3.96 – 3.94 (m, 1H), 3.87 (s, 3H),
3.84 – 3.83 (m, 1H), 3.79 (s, 3H), 3.69 (brs, 1H), 3.63 – 3.60 (m, 1H), 3.13 – 2.98 (m, 8H),
2.90 – 2.76 (m, 4H), 2.19 – 2.06 (m, 3H), 1.67 – 1.58 (m, 3H), 1.28 – 1.22 (m, 3H), 1.09 –
0.98 (m, 3H).

¹³C NMR (176 MHz, DMSO)*: δ [ppm] = 165.7, 165.3, 152.6, 151.8, 146.5, 145.9, 144.7,
143.5, 142.5, 140.9, 140.5, 134.6, 128.5, 126.0, 121.7, 121.2, 120.4, 116.7, 115.9, 115.2,
113.6, 112.6, 107.8, 107.6, 102.9, 67.8, 56.5, 56.2, 55.4, 53.5, 53.4, 49.1, 47.0, 35.7, 35.6,
33.6, 32.5, 31.0, 27.4, 25.9, 22.7, 22.1, 21.4, 19.9, 19.4, 17.1.

HRMS (ESI) *m/z*: ($C_{41}H_{44}N_7O_8^+$ [M+H]$^+$)   calc.:   762.3246

found: 762.3245

* Due to residual water in the DMSO-*d$_6$* the NMR corresponds to a complex mixture of the imine form, the hemiaminal forms (diastereomers) and the mixed forms.

2.5.2 Biological methods

2.5.2.1 Media, buffers, electrophoresis

Media

Media	Content	
LB Agar (Luria/Miller)	Tryptone	10 g/l
	Yeast extract	5 g/l
	Sodium chloride (NaCl)	10 g/l
	Agar-Agar	15 g/l
	pH value	7,0 ±0,2
LB-Medium (Luria/Miller)	Tryptone	10 g/l
	Yeast extract	5 g/l
	Sodium chloride (NaCl)	10 g/l
	pH value	7,0 ±0,2

Buffers

Buffer	Content
Annealing buffer	10 mM Tris-HCl 50 mM NaCl 1 mM $Na_2EDTA * 2\,H_2O$
Ammonium acetate Buffer	100 mM Ammonium acetate
10× TBE Buffer	27 g Tris-HCl 13.75 g boric acid 1.86 g $Na_2EDTA * 2\,H_2O$ 250 mL H_2O
Strand Separation Buffer	30% DMSO 1 mM $Na_2EDTA * 2\,H_2O$ 0.04% Xylene cylanol

Non-denaturing PAGE – 20% acrylamide

Buffer	Content
Separating Gel (15 mL)	1.5 mL 10 × TBE
	1.5 mL glycerol/water (1:1 v/v)
	7.5 mL 40% acrylamide/bis (29:1)
	4.365 mL ddH$_2$O
	1 µL 20.000× RotiRed GelStain
	22.5 µL TEMED
	112.5 µL 10% APS
Stacking Gel (5 mL)	2.9 mL H$_2$O
	0.85 mL 30% acrylamide/bis
	1.25 mL 0.5 м Tris-HCl
	4 µL Bromophenol blue
	7.5 µL TEMED
	37.5 µL 10% APS
Running Buffer	1× TBE
Loading Buffer	5.8 mL of 86% glycerol
	37 mg Na$_2$EDTA * 2H$_2$O
	4.2 mL ddH$_2$O
Staining solution	2 µL 20.000× RotiRed GelStain
	100 mL TBE (1×)

Agarose gel (0.7%)

Buffer	Content
Separating Gel (80 mL)	0.56 g agarose 80 mL TAE (1×) buffer 8 µL SYBR® Gold Nucleic Acid Gel Stain (Thermo Scientific™)
Running Buffer	1× TBE
Loading Buffer	30% DMSO 1 mM Na$_2$EDTA * 2H$_2$O 0.04% Xylene cylanol

2.5.2.2 Plasmid-based mobility shift assay

DNA Isolation

Glycerol stock of *E. coli* DH5α was used to grow single colonies (LB-Agar, 100 uL/mL ampicilin). The plate was incubated at 37 °C overnight. A single colony was picked and used to inoculate a 200 mL culture (LB-Medium, 100 µL/mL ampicilin). The culture was incubated shaking at 37°C until an OD$_{600}$ of ~1.2. The DNA was isolated with NucleoBond® Xtra Midi (MACHEREY-NAGEL) according to manufacturer's instructions. Elution was performed with 2×100 µL nuclease-free water (VWR International GmbH). DNA concentration was determined using NanoDrop™ One^C (Thermo Scientific™). Identity of the isolated plasmid was confirmed by Sanger sequencing (Eurofins Genomics).

Restriction digestion

Restriction enzymes (BamHI, ScaI-HF) were purchased from New England Biolabs GmbH. Digestion was performed according to manufacturer's recommendations using either BamHI or ScaI HF and purified with E.Z.N.A. Gel Extraction Kit (Omega Bio-tek) after agarose gel electrophoresis The choice of restriction enzyme did not influence the assay results.

Sample incubation

Digested DNA fragments were diluted with nuclease-free water to a final concentration of 0.01 µM. Equal volumes (each 2 µL) of DNA stock solution (c = 0.01 µM) and compound stock solution (c = 200 µM) were mixed. After incubating (37 °C, 30 min), 4 µL strand separation buffer was added, the sample was boiled (95 °C, 2 min) and kept on until gel electrophoresis.

For controls resembling double-stranded DNA, 2 µL digested DNA (c = 0.01 µM) and 2 µL nuclease-free water were incubated (37 °C, 30 min) and subsequently kept on ice until gel electrophoresis.

For controls resembling single-stranded DNA, 2 µL digested DNA (c = 0.01 µM) and 2 µL nuclease-free water were incubated (37 °C, 30 min) and 4 µL strand separation buffer were added. Samples were boiled (95 °C, 2 min) and kept on until gel electrophoresis

Different DNA and compound concentrations were tested. All leading to the same result as long as the relative fold excess is retained. Different incubation times reaching from 0.5 h to 16 h were tested but no difference was observed.

Agarose gel electrophoresis

8 µL of each sample were loaded onto a 0.7% agarose gel containing SYBR® Gold Nucleic Acid Gel Stain (Thermo Scientific™) alongside a marker (Thermo Scientific™ GeneRuler™ 100 bp Plus DNA Ladder) and subjected to agarose gel electrophoresis (150 V, 2 h). Images were obtained with a ChemiDoc™ (BioRad) equipped with a cooled CCD 6 megapixel detector using the Blot/UV/stain-free sample tray (BioRad). Image processing was performed with Image Lab Version 5.2.1 (BioRad).

2.5.2.3 Oligonucleotide-based mobility shift assay

Annealing of DNA oligonucleotides

Single-stranded oligonucleotides were obtained in lyophilized form from Eurofins Genomics Germany GmbH and dissolved in 100 mM ammonium acetate to stock concentration of 2 mM. Oligonucleotides were then diluted to 1 mM with annealing buffer and boiled (95 °C, 10 min). To avoid secondary structures, samples were subsequently slowly cooled down over four hours by turning off the heating block and frozen at -20 °C until analysis. Working solutions of dsDNA of 50 µM were prepared by diluting stored stock solutions (500 µM) with 20 mM ammonium acetate.

Sample incubation and sample analysis

Equal volumes of dsDNA working stock (50 µM) and the investigated compound (varying final concentration) were mixed and incubated at 37 °C for 16 h.

Samples were prepared by diluting 1 µL of the previously incubated mixture with 4 µL loading buffer and 15 µL ddH$_2$O. 8 µL of the obtained samples were loaded onto a 20% non-denaturing polyacrylamide gel electrophoresis (PAGE) gel. 10/60 ladder by Integrated DNA Technologies™ (#51-05-15-01) was used as a marker. Gels were subjected to gel electrophoresis (150 V, 2 h) and stained with staining solution for 1 h at room temperatureunder gentle shaking. Images were obtained with a ChemiDoc™ (BioRad) equipped with a cooled CCD 6 megapixel detector using the Blot/UV/stain-free sample tray (BioRad). Image processing was performed with Image Lab Version 5.2.1 (BioRad).

2.5.2.4   LC-MS-Assay

Sample incubation

Equal volumes of dsDNA working stock (50 µM) and the investigated compound (200 µM) were mixed and incubated at 37 °C for 16 h. For subsequent LC-MS measurements, the samples were diluted to a final dsDNA concentration of 500 nM.

Mass Spectrometry

General:

Mass spectrometer:	Triple Quad 7500 HighMass
Software:	SCIEX OS 2.1.6.59781
Method duration (minutes):	8
Total scan time (s):	1.079
Estimated cycles:	445
Actual method duration (minutes):	8.87

Ion source:

Source name:	E-ANLYT 200+ µL
Curtain gas (psi):	55
Ion source gas 1 (psi):	80
Ion source gas 2 (psi):	70
Temperature (°C):	400

Experiment:

Scan type:	MRM
Polarity:	Negative
Ionspray voltage (V):	3500
Q1 resolution:	Unit
CAD gas:	N_2
Q3 resolution:	Unit
Pause time (ms):	2
Settling time (ms):	5
High mass cooling time (ms):	0
Q0 dissociation:	False

Table 5: List of all MRM transitions used for detection.

Group ID	Q1 mass	Q3 mass	Dwell time	EP	CE	CXP
JF-Seq-1	1820.22	1331.227	47.556	-10	-72	-24
	1820.22	1017.968	47.556	-10	-71	-34
	1454.52	1213.26	47.556	-10	-35	-22
	1454.52	1256.727	47.556	-10	-11	-7
	1213.36	634.059	47.556	-10	-55	-18
	1213.36	922.028	47.556	-10	-46	-16
	1213.36	921.656	47.556	-10	-42	-16
	1213.36	1167.775	47.556	-10	-32	-12
	1213.36	480.988	47.556	-10	-61	-13
	909.9	78.946	47.556	-10	-179	-11
	909.9	820.3	47.556	-10	-35	-26
	909.9	481.056	47.556	-10	-44	-19
	728.0	700.767	47.556	-10	-20	-8
	728.0	78.955	47.556	-10	-175	-6
	728.0	303.107	47.556	-10	-41	-6
SJG-136	1119.0	909.63	40	-10	-21	-13
	1119.0	451.916	40	-10	-36	-23
	1305.0	1242.93	40	-10	-11	-15
	1305.0	357.333	40	-10	-55	-6
	1568.0	1213.259	40	-10	-36	-22
	1568.0	363.116	40	-10	-65	-16
	1959.5	1820.608	40	-10	-38	-32
	1959.5	1332.116	40	-10	-82	-21
D1	1128.9	909.567	40	-10	-23	-21
	1128.9	880.2	40	-10	-44	-22
	1421.0	1213.074	40	-10	-34	-24
	1421.0	1212.472	40	-10	-31	-28
	1580.0	1213.193	40	-10	-37	-20
	1580.0	1212.407	40	-10	-39	-28
	1976.0	1212.973	40	-10	-58	-47
	1976.0	1819.869	40	-10	-43	-28
D2	1068.5	992.265	40	-10	-13	-53
	1068.5	97.052	40	-10	-148	-9
	1425.6	1213.113	40	-10	-33	-26
	1425.6	679.276	40	-10	-43	-20
	1583.9	1214.174	40	-10	-36	-17
	1583.9	1213.293	40	-10	-32	-19
	1979.2	1820.179	40	-10	-41	-28
	1979.2	1196.307	40	-10	-82	-23
D4	733.4	566.256	20	-10	-17	-10
	733.4	56.952	20	-10	-109	-4
	733.4	86.844	20	-10	-94	-7
	733.4	58.924	20	-10	-100	-6
	733.4	68.889	20	-10	-112	-10
	1467.4	1213.147	20	-10	-28	-20
	1467.4	1214.694	20	-10	-28	-53
	1467.4	1338.3	20	-10	-13	-10
	1467.4	923.314	20	-10	-56	-15

	1467.4	489.46	20	-10	-73	-14
D3	1884.3	1819.997	40	-10	-32	-18
	1884.3	1213.337	40	-10	-57	-22
	1949.5	1820.418	40	-10	-34	-25
	1949.5	1331.135	40	-10	-78	-20
	1957.3	1820.319	40	-10	-38	-26
	1957.3	1893.065	40	-10	-12	-12
	1892.6	1820.103	40	-10	-34	-25
	1892.6	1251.054	40	-10	-84	-23
MbA + M1	1312.9	1213.701	40	-10	-24	-21
	1312.9	207.119	40	-10	-127	-10
	1322.1	1213.174	40	-10	-25	-20
	1322.1	1259.635	40	-10	-15	-16
	1831.5	1213.07	40	-10	-51	-40
	1831.5	506.088	40	-10	-128	-19
	1893.1	1820.454	40	-10	-34	-27
	1893.1	1331.136	40	-10	-74	-48
	1903.7	1831.272	40	-10	-40	-25
	1903.7	1213.163	40	-10	-54	-18
	1968.5	1831.375	40	-10	-38	-28
	1968.5	1331.151	40	-10	-83	-30
	1983.9	1820.344	40	-10	-38	-12
	1983.9	1212.929	40	-10	-52	-38
MbA + M2	1884.6	1820.193	40	-10	-35	-25
	1884.6	1331.13	40	-10	-75	-22
	1892.5	1820.01	40	-10	-31	-27
	1892.5	793.465	40	-10	-100	-12
	1949.6	1820.463	40	-10	-36	-23
	1949.6	1331.154	40	-10	-84	-23
	1957.5	1892.967	40	-10	-11	-22
	1957.5	1820.294	40	-10	-34	-26
MbA + M4	1983.7	1212.842	100	-10	-55	-20
	1983.7	1213.55	100	-10	-58	-41
	1983.7	1830.657	100	-10	-46	-42
	1983.7	401.508	100	-10	-105	-31
	1983.7	1227.194	100	-10	-65	-49
MbA + M3	1983.9	1213.602	100	-10	-53	-55
	1983.9	1819.731	100	-10	-41	-34
	1983.9	385.3	100	-10	-95	-28
	1983.9	1169.82	100	-10	-51	-31
	1983.9	551.643	100	-10	-82	-23
	1459.1	1213.341	100	-10	-27	-17
	1459.1	1212.66	100	-10	-31	-25
	1459.1	1078.15	100	-10	-54	-30
	1459.1	1169.708	100	-10	-17	-21
	1459.1	1395.312	100	-10	-11	-19
	1322.3	1213.235	100	-10	-20	-21
	1322.3	1212.478	100	-10	-21	-55
	1322.3	1116.091	100	-10	-71	-34
	1322.3	94.909	100	-10	-164	-7
	1322.3	243.2	100	-10	-114	-16

1349.6	1220.096	100	-10	-17	-17
1349.6	1212.744	100	-10	-21	-47
1349.6	1017.824	100	-10	-61	-41
1349.6	1213.417	100	-10	-21	-14
1349.6	305.295	100	-10	-83	-12

Liquid chromatography

Agilent Integrated System:	Binary Pump G7120A - DEBA205316
	Binary Pump G7120A - DEBA205320
	Multisampler G7167B - DEBAS03162
	Column Comp. G7116B - DEBA407674
Column:	Zorbax eclipse plus C18 RRHD 1.8 µm 2.1 x 50 mm
Injection volume	10 µL
Solvent A:	100.0 % Water + 15 mм TEAB + 100 mм HFIP
Solvent B:	90% ACN 10% Water + 15 mм TEAB + 100 mм HFIP

Gradient:

Time (min)	A (%)	B (%)	Flow (mL/min)
1	99	1	0.7
2	99	1	0.7
5	40	60	0.7
7	5	95	0.7
8	99	1	0.7

3 Trimethyl lock - a tetrazine based click-to-release approach

3.1 Introduction

3.1.1 Linkers

Linkers are chemical structures connecting two otherwise independent molecules. They are widely used in various areas of chemistry, including solid-phase peptide synthesis,[177] target fishing,[178] and drug conjugates.[179-180] Wide varieties of linkers have been developed to suit their applications. They can be categorized into cleavable and non-cleavable linkers (Figure 40), with cleavable linkers being of particular interest in the context of chemical biology and drug development.

A major area that has contributed to developing diverse cleavable linkers is the field of drug conjugates, and especially antibody-drug conjugates. In drug conjugates, a targeting entity or carrier is connected to an effector (drug or reporter) via a linker. Targeting entities used in literature include peptides,[181] carbohydrates,[182] antibodies,[183] and siderophores.[184] Most of the time, the carrier's purpose is either to increase the specificity of the payload, i.e., the drug, by transporting it to its site of action, or to overcome natural barriers the drug would not be able to overcome by itself (e.g., the outer membrane of gram-negative bacteria). However, conjugates having carriers with high molecular weight may have poorer binding to the target due to their high steric demand, resulting in lower efficacy.[185] If the effector/drug is released from the carrier in a controlled manner, the ability to bind the target can be restored (Figure 40). Thus, the development of controllable release systems is of high interest.[185-186]
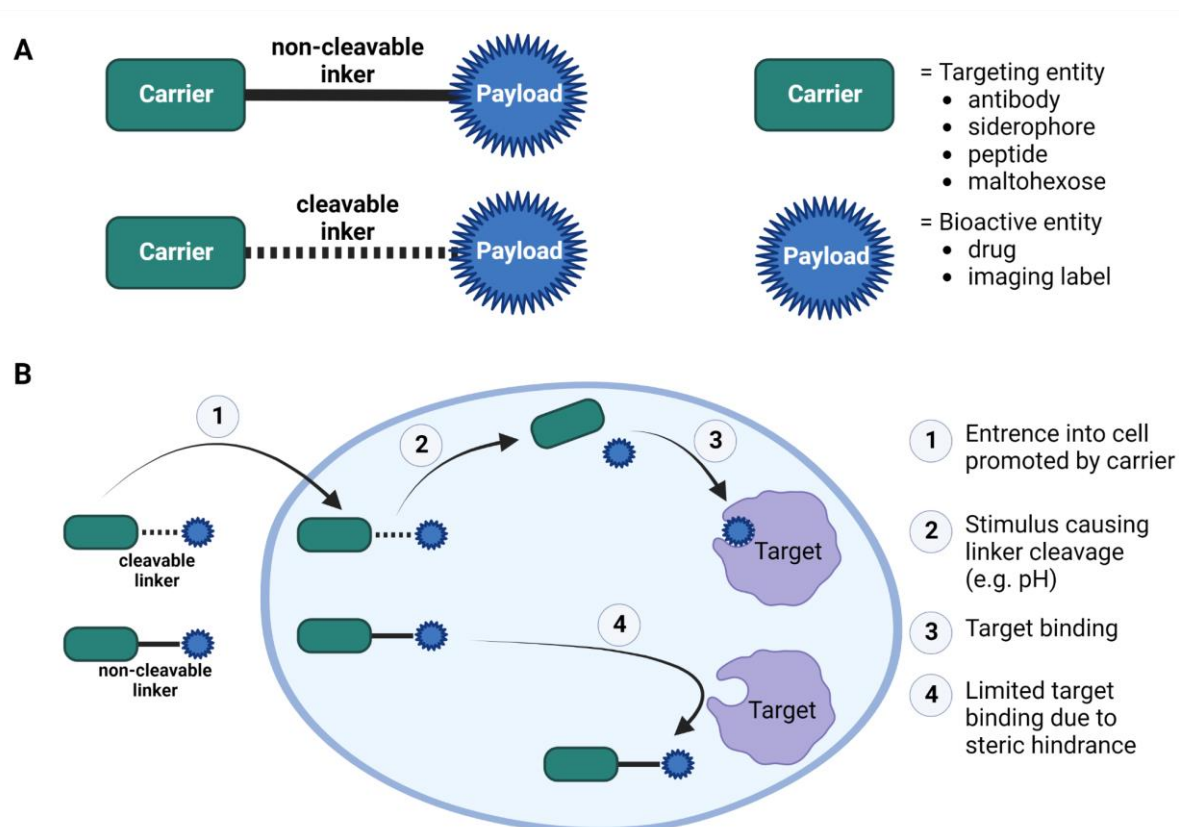
Figure 40: A) General structure of a conjugate employing a non-cleavable or cleavable linker; B) Limited target binding of the conjugate due to steric hindrance of high molecular weight carrier. Created with BioRender.

Accordingly, several cleavable linkers relying on different cleavage strategies have been developed. They can be split into two types: enzyme-cleavable linkers and chemically cleavable linkers.[179] Enzyme-sensitive systems exploit different expression levels of enzymes depending on the tissue or on the location within a cell. One group of enzymes utilized by this strategy are proteases, and the corresponding linkers consist of a peptide sequence that serves as the proteases' substrate. An example from this group are cathepsin B–sensitive linkers (Scheme 41). Attaching a payload to the peptide-based linker can increase the steric burden and thus negatively influence the proteolytic cleavability of the conjugate. This problem can be resolved using a self-immolative spacer unit like *para*-aminobenzyloxycarbonyl (PABC).[187]
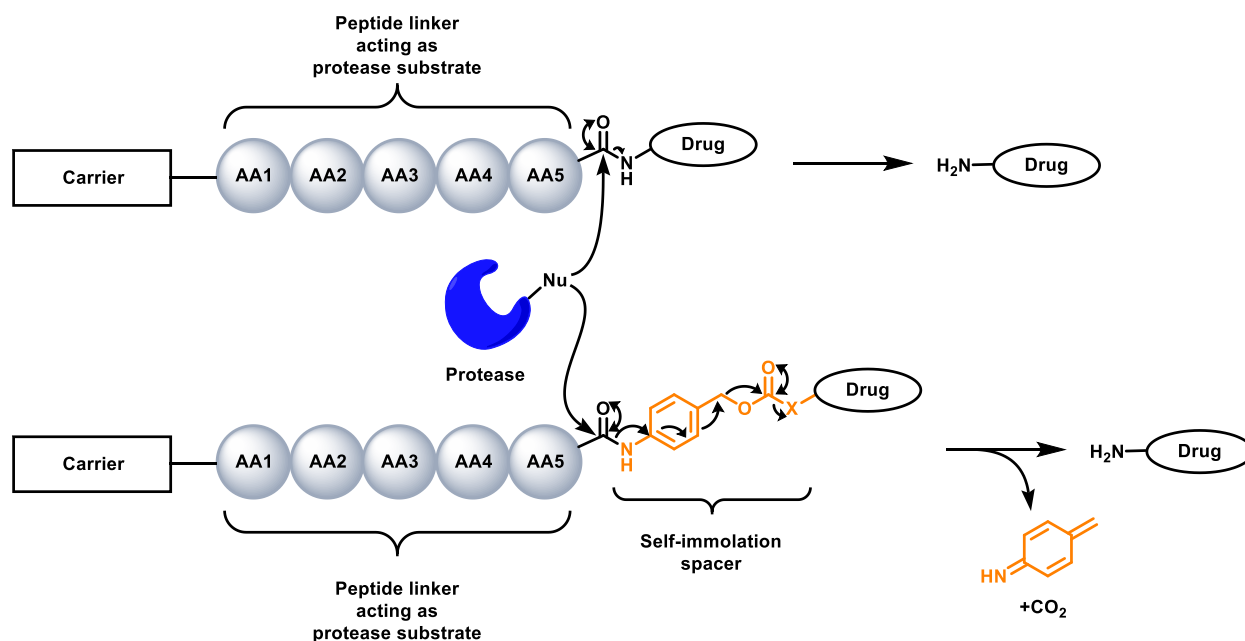
Scheme 41: Mechanism of protease-mediated linker cleavage with and without a self-immolative spacer. Created in analogy to[187]

Chemically cleavable linkers can be cleaved by a vast array of different conditions, however disulfide linkers and pH-sensitive linkers enjoy particularly widespread application. Disulfides can be converted to the corresponding thiols by reducing agents like glutathione (GSH). GSH is the most abundant intracellular thiol-containing small molecule (intracellular concentration approx. 1-10 mM).[188]

The stability of a disulfide bond can be altered through the introduction of sterically demanding substituents. The imposed steric hindrance leads to a stabilization effect (Figure 41).[189]

A

B

C Stability towards disulfide cleavage:
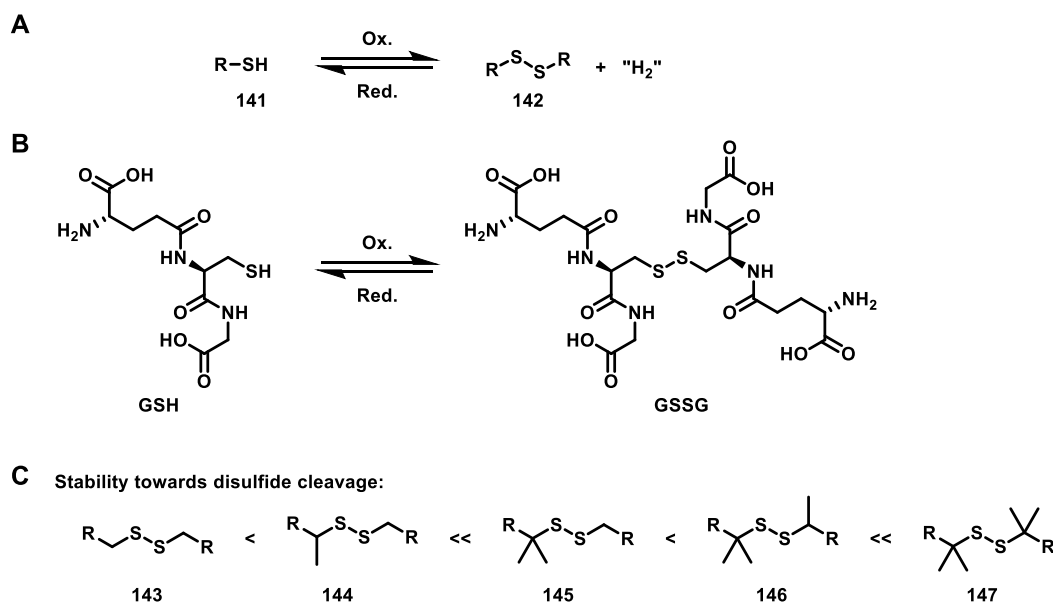
Figure 41: A) Oxidation and reduction of thiols/disulfide bonds; **B)** Oxidation and reduction of GSH;[188] **C)** Stability of disulfide bonds towards cleavage increases with more sterically hindered substituents.[189]

Differences in pH can also be utilized to cleave linkers. pH-sensitive linkers are, for example, based on oximes or hydrazones. A low pH environment, as found in the lysosome, triggers the hydrolysis of the hydrazone/oxime leading to the cleavage of the linker and thus releasing the payload (Figure 42A). An example of the utilization of a disulfide and a hydrazone linker is gemtuzumab ozogamicin, an ADC depicted in Figure 42B.[187]

A

Oxime: X = O
Hydrazone: X = NH

B

Gemtuzumab ozogamicin
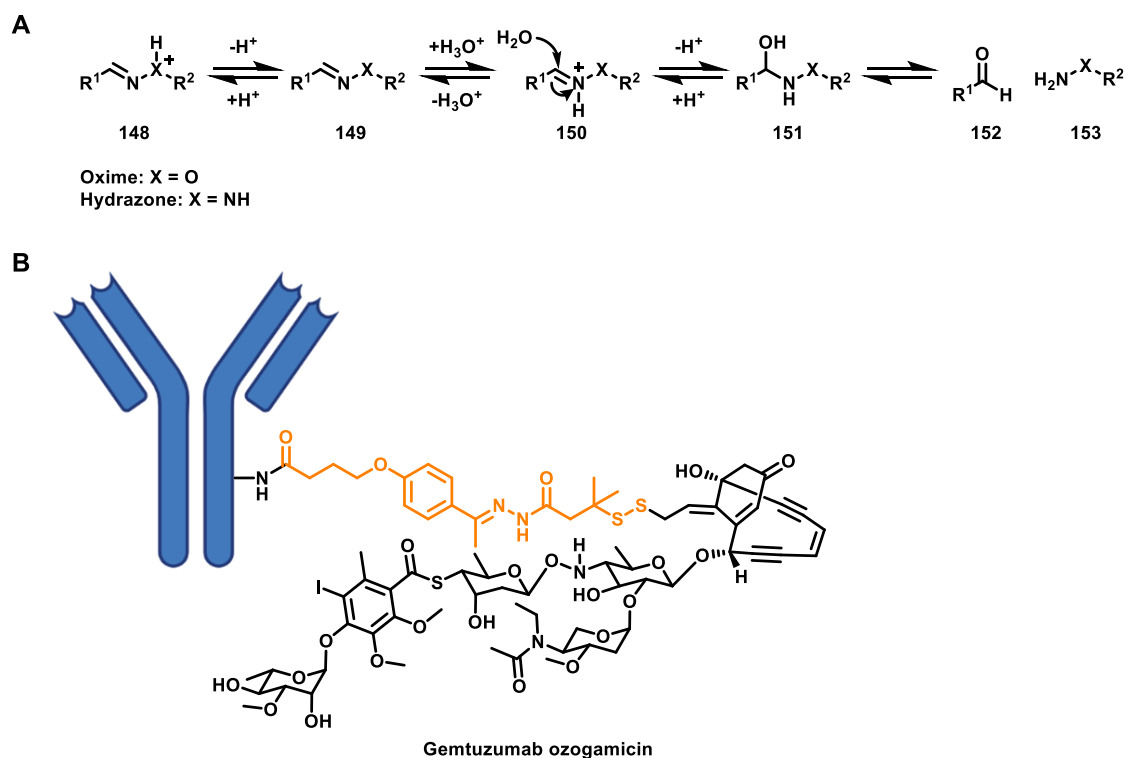
Figure 42: A) Acid-catalyzed hydrolysis and subsequent cleavage of hydrazone/oxime linkers; B) Gemtuzumab ozogamicin as an example for the usage of a disulfide and a hydrazone linker in ADCs.[187]

However, problems can arise, if a non-specific release occurs, leading to off-target toxicity. A well-known example is the case of the previously mentioned pH-sensitive gemtuzumab ozogamicin (Mylotarg®), which was developed by Pfizer. The deficient linker design resulted in a premature release of the drug calicheamicin and, thus, liver toxicity.[190] One way to overcome such problems is to avoid endogenous stimuli/triggers and to facilitate cleavage upon exogenous stimuli/triggers, thus become independent from concentration differences of the trigger between general circulation in the body and at the target. In this regard, bio-orthogonal reactions provide desirable attributes and are, therefore, of high interest. While this class of reactions is traditionally used to connect molecular substructures, they can also be deployed to cleave bonds. This concept is known as click-to-release and will be discussed in the following chapter.

3.1.2 Click-to-release concept

The click-to-release concept is a prodrug approach, which relies on the reversible derivatization of an active drug. In contrast to classical prodrug approaches that utilize endogenous stimuli, e.g., enzymes and pH, click-to-release based prodrugs utilize exogenous stimuli, by employing bioorthogonal reactions, e.g., IEDDA and Staudinger reactions (i.e. reactions that do not interfere with biological systems).

The click-to-release strategy is of particular interest regarding the controlled release of drugs to mitigate unwanted side effects or toxicity, as well as to influence factors such as half-life, metabolic stability, or membrane permeability.[11]

There are several examples of successful applications of the click-to-release concept; a selection covering major underlying reactions will be discussed in more detail in this chapter.

3.1.2.1 Release based on the Staudinger ligation and the Staudinger reduction

An example of a click-to-release approach using the Staudinger ligation was described by Florent and co-workers.[191] The anti-cancer drug doxorubicin was concealed carrying a phosphine moiety (**154**). Upon addition of the azide component, the aza-ylide intermediate **155** is formed. This intermediate then undergoes an intramolecular Staudinger ligation, which leads to the liberation of a phenolate (**156**) (Scheme 42). Afterwards, **156** undergoes a 1,6-elimination forming a quinone methide (**158**) and releasing the drug and CO_2.[191]
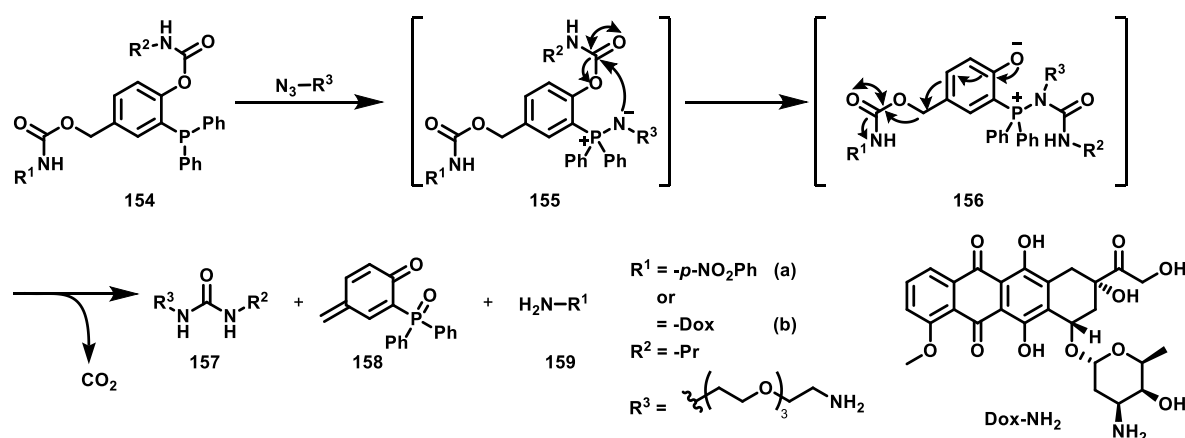
Scheme 42: Prodrug activation utilizing the Staudinger ligation. Created in analogy to[191]

Apart from the Staudinger ligation also the Staudinger reduction can be used to trigger a drug release as applied by Robillard and co-workers to convert the azide **160** into the amine

161, which subsequently undergoes a 1,6-elimination releasing the free payload, i.e. doxorubicin (Scheme 43).[192]
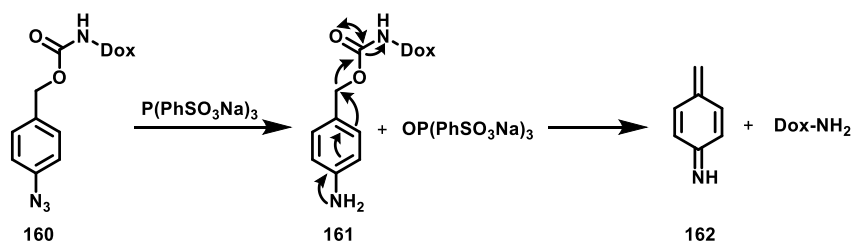
Scheme 43: Prodrug activation utilizing the Staudinger reduction. Created in analogy to[192]

However, click-to-release approaches based on the different Staudinger reactions are limited by several factors. First, the phosphine reagents are prone to oxidation, which limits their *in vivo* usage. Additionally, alkyl or aryl phosphines are often large hydrophobic molecules, which also makes them unattractive for *in vivo* usage. Besides, the rate constants of these reactions are low ($\sim 10^{-3}$ $M^{-1}s^{-1}$);[170] therefore, high concentrations are needed to release the payload on a reasonable time scale.[11]

3.1.2.2 Release based on *trans*-cyclooctene (TCO)

Cyclooctenes can have two geometric isomers, i.e., *cis* or *trans*. However, both isomers exhibit vastly differing reactivity. While the *cis*-cyclooctene is more stable, the *trans*-cyclooctene (TCO) is more reactive. In fact, TCO is the smallest trans-cycloalkene that is stable enough to be isolated. The difference in reactivity is a direct consequence of the different ring strain energies of both isomers, which are 7.4 kcal/mol for *cis*-cyclooctene and 16.7 kcal/mol for TCO.[193]

In contrast to simple alkynes TCO can, due to its high ring strain, undergo a 1,3-cycloaddition with azides without the need of a catalyst. This reaction used to be out of focus in the field of bioorthogonal chemistry, since it forms hydrolysis-susceptible adducts. Nevertheless, Gamble and co-workers turned its drawback into an advantage by developing a doxorubicin prodrug **160**, activated by a TCO (Scheme 44).[194] In the first step, the azide **160** reacts with TCO in a 1,3-cycloaddition. Subsequent rearrangement of the formed 1,2,3-triazoline **163** forms imine **164**. The imine then undergoes hydrolysis and self-immolates, releasing the free drug.[194]
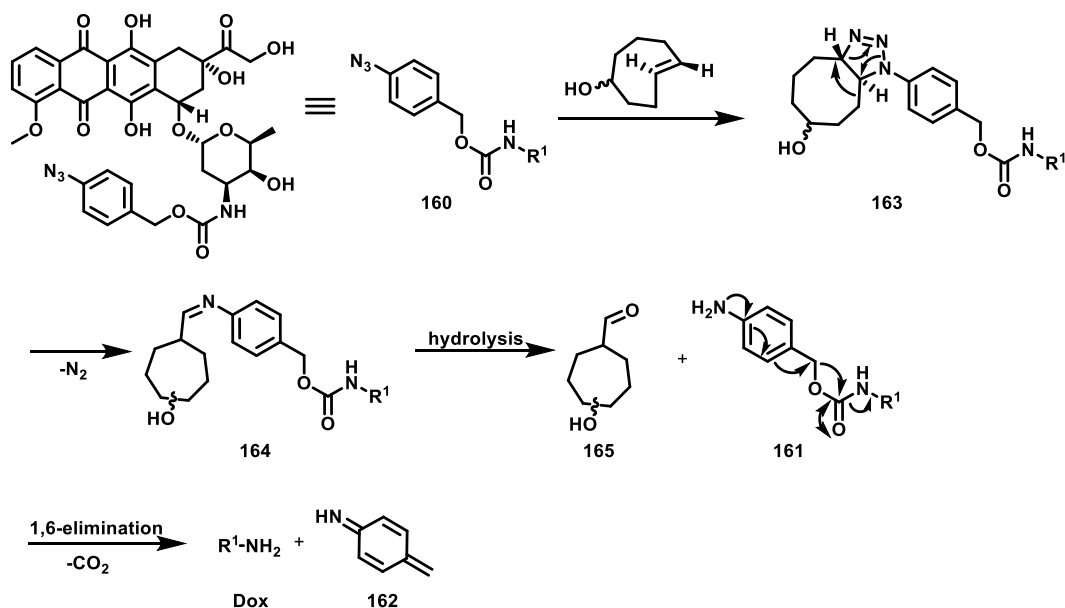
Scheme 44: TCO-triggered release of doxorubicin from an azide prodrug. Created in analogy to[194]

This concept was also used by Chen and co-workers to activate a protein in a controlled fashion.[195] The approach used a genetically modified protein having a N^ε-*p*-azidobenzyloxycarbonyl lysine residue at the protein's active site acting as a self-immolative protection group. Upon TCO addition, the lysine is released, and the activity of the protein is restored.[195]

Apart from 1,3-cycloadditions, TCO can also undergo inverse-electron-demand Diels–Alder (IEDDA) reactions with tetrazines. In turn, this reaction can also serve as the basis for a click-to-release approach by introducing a carbonate/carbamate functionality at the allylic position of TCO, opening up the way for an 1,2 as well as 1,4 elimination (Scheme 45). The IEDDA between the TCO and a tetrazine first gave a 1,4-dihydropyridazine intermediate **167**, which either directly eliminates the carbamate to release the free drug or tautomerises. One of the resulting tautomers (**168**) can undergo 1,4- elimination giving the free drug, while the other tautomer **169** is trapped since the follow-up elimination is impossible.[196]
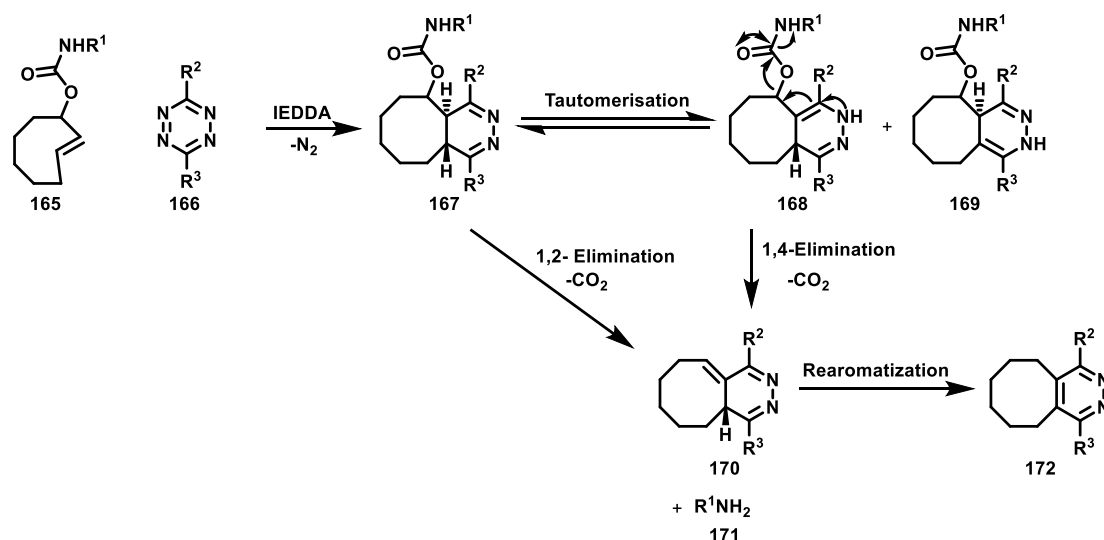
Scheme 45: Drug release based on an inverse-electron-demand Diels–Alder of a tetrazine and a TCO. Created in analogy to[196]

This method was also used to activate proteins. In this scenario, a lysine at the active site was concealed by connecting it to TCO via a carbamate. The addition of a tetrazine restored the protein activity by unlocking the active site lysine.[197-199]

Apart from the TCO, the tetrazine, being the reaction partner, plays a major role in the release. It could be shown that the usage of the simple 3,6-dimethyltetrazine can lead to a reduced release.[200] After the formation of the 1,4-dihydropyridazine intermediate **173**, the carbamate nitrogen can perform an intramolecular nucleophilic attack. The formed six-membered ring represents a dead-end product, from which the drug cannot be released (Scheme 46A).

One way to address this problem is to introduce an alkyl group at the carbamate nitrogen, thus blocking the intramolecular nucleophilic attack and leading to full release, albeit coming along with a methylation of the drug (Scheme 46B).[200]

A second approach, that has been shown to improve release yields, is equipping the tetrazine with a carboxylic acid moiety.[200] Hence, the close-by dihydropyridazine nitrogen can be protonated (Scheme 46C) resulting in an accelerated tautomerization and subsequent 1,4-elimination.
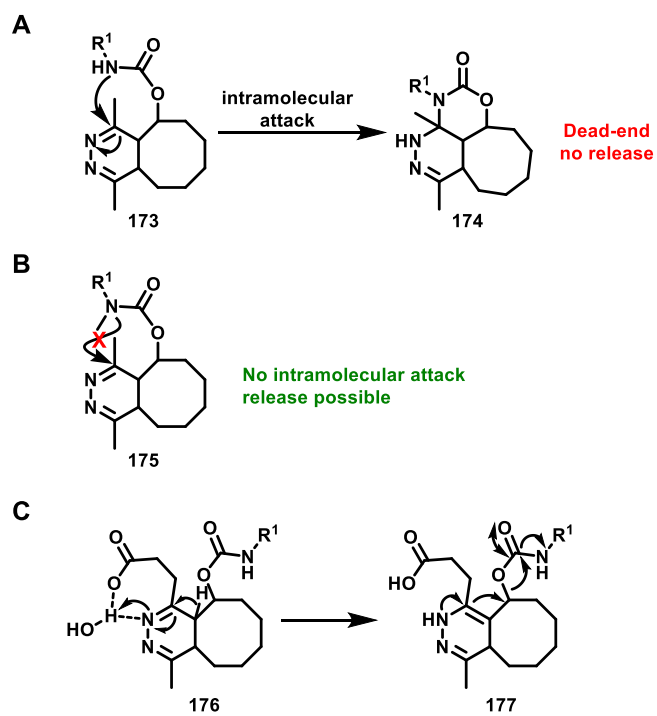
Scheme 46: A) Intramolecular aminal formation leading to a dead-end product; B) Introduction of a methyl at the carbamate nitrogen blocking the intramolecular nucleophilic attack; C) Intramolecular acid assisted elimination. Created in analogy to[200]

3.1.2.3 Release based on vinyl ethers

Bernardes and co-workers introduced the usage of vinyl ether–tetrazine pairs, enabling the release of alcohols.[201] A duocarmycin analog was equipped with a vinyl ether at the phenol (Scheme 47). To release the original drug, the vinyl ether was reacted with a tetrazine forming the intermediate **178**, which subsequently tautomerizes and releases the alcohol **181** via a 1,4-elimination. In case of the masked drug **182**, the next step, after the release of the phenol **183**, is the Winstein spirocyclisation of **183** generating the active drug. This click-to-release system was successfully tested in A549 cells, showing restoration of cytotoxicity upon a tetrazine addition, whereas the concealed prodrug alone did not show significant cytotoxicity.[201]
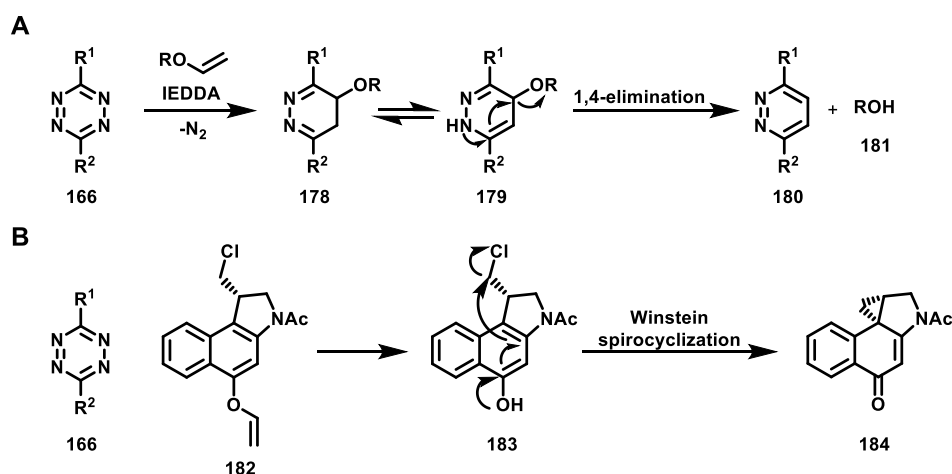
Scheme 47: A) General release mechanism of vinyl ether triggered by tetrazines; B) Release of duocarmycin from its vinyl ether prodrug. Created in analogy to[201]

This concept was further evolved by Bradley and co-workers, who combined the masking vinyl ether group with a self-immolative linker (Scheme 48), broadening the scope of drugs that can be masked with vinyl ether.[202]

As a consequence, this method can also be applied to other functional groups such as amines. The vinyl ether undergoes an IEDDA and the formed intermediate **187** subsequently frees the phenol of the linker via 1,4-elimination. This again causes the formation of *p*-quinomethane **188** and the release of the amine. This system was shown to release the fluorophore nile blue efficiently from **190** (Scheme 48). Additionally, the authors demonstrated an efficient tetrazine-mediated switch-on of cytotoxicity of doxorubicin, which was masked with the self-immolative linker and conjugated to a PEG-containing nanoparticle.[202]
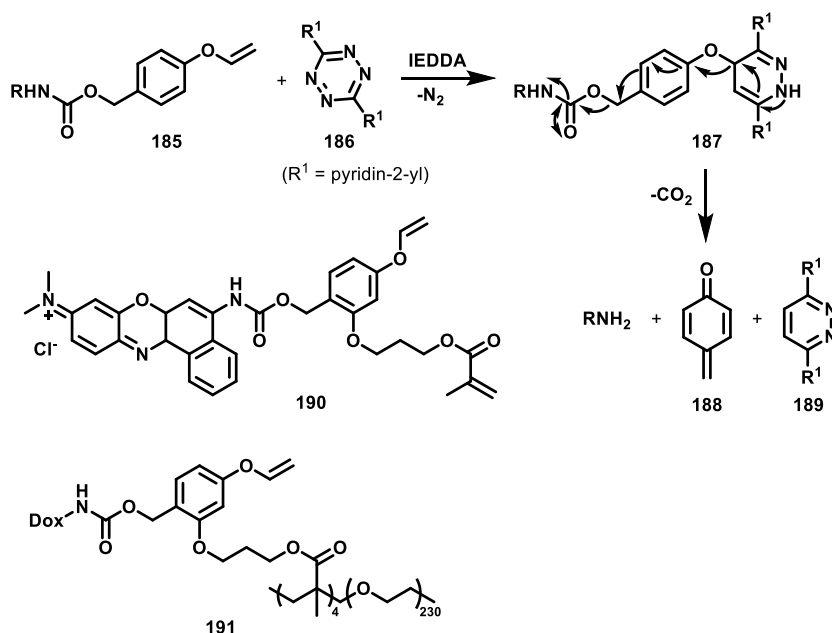
Scheme 48: Self-immolative linker triggered upon tetrazine treatment. Created in analogy to[202]

On the one hand, vinyl ether–based click-to-release systems are more stable under near physiological conditions compared to TCO-based systems and they do not encounter the problem of dead ends. Moreover, they represent only small changes to the overall scaffold, and their synthesis is straightforward. On the other hand, the vinyl ether systems suffer from lower reaction rates compared to TCO.[11]

3.1.2.4 Release based on benzonorbornadienes

Franzini and co-workers developed a click-to-release strategy based on the IEDDA reaction between benzonorbornadienes and tetrazines (Scheme 49).[203]

The first IEDDA step resulted in intermediate **194**, which then undergoes a retro-Diels–Alder cycloreversion yielding the self-immolative isobenzofuran/isoindole **196** and the pyridazine **195**. Finally, the concealed drug is released through self-immolative cleavage of the isobenzofuran/isoindole **196**.[203]
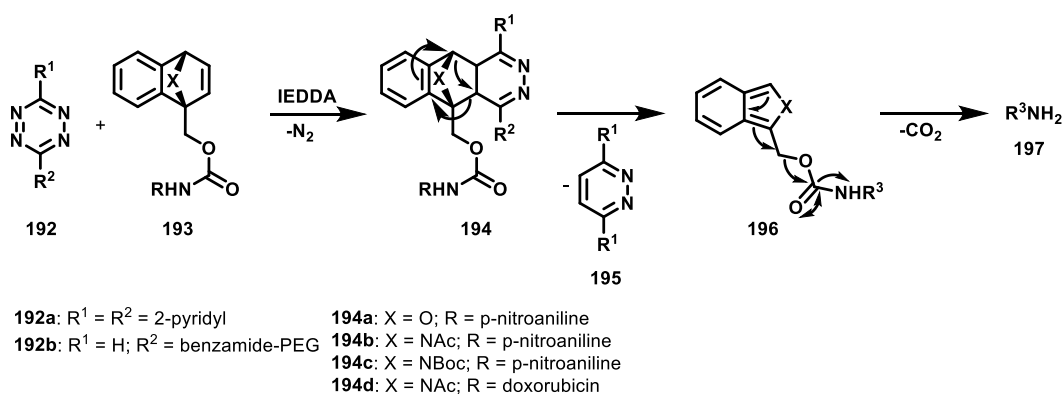
Scheme 49: Tetrazine-triggered benzonorbornadiene derivatives. Created in analogy to[203]

3.1.3 Trimethyl lock (TML)

The trimethyl lock describes a molecular release system with a vast spectrum of applications. The core structure builds on *ortho*-hydroxydihydrocinnamic acid equipped with three methyl groups, thus the name "trimethyl lock". These strategically placed methyl groups constrain the molecule such that the formation of hydrocoumarins is promoted. In fact, the rates of the lactonization of such systems are in the range of enzyme-catalyzed reactions (Figure 43).[204-205]
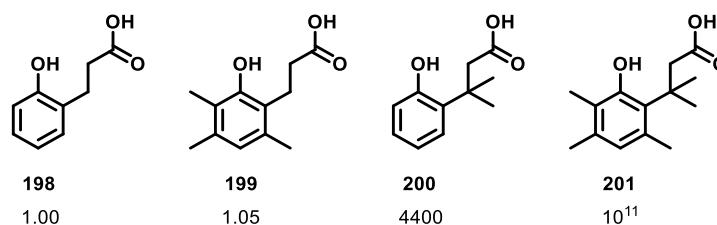
Figure 43: Relative lactonization rate constants of different 3-(2-hydroxyphenyl)propanoic acid derivatives.[205]

Mechanistic studies lead to the assumption, that the steric interactions of the three methyl groups force the molecule into a conformer which is structurally similar to the transition state, hence facilitating the conversion into the transition state. Cohen and co-workers assigned the increased reaction rate to stereopopulation control. [204-208] This phenomenon describes the limited freedom of rotation of single bonds due to a set of forces and interactions including hydrogen bonding, electrostatic attraction or repulsion, van-der-Waals interactions, lone pair repulsion, etc.. The sum of these factors narrows the distribution of conformer populations leading to an enhancement of the reaction rate.[204-208]

Another relevant effect in order to explain the observations is the Thorpe-Ingold effect, which is based on the van-der-Waals repulsion of two geminal methyl groups. The presence

of the geminal methyl groups causes a compression of the angle between the two other residues bound by a quaternary carbon and thus cause a pre-orientation enhancing reaction rates of intramolecular reactions e.g. ring closing reactions.[209] Nevertheless, other effects of enthalpic and entropic nature may play an important role in explaining the exceptionally high lactonisation rates.[209]

The rapid lactone formation described above is exploited in the TML system to release a payload. The acid moiety can be replaced by an ester or amide to introduce the payload, while the phenol is protected to avoid premature cyclization. Only when the protecting group is removed, the payload gets released by intramolecular cyclization. (Scheme 50).[210]
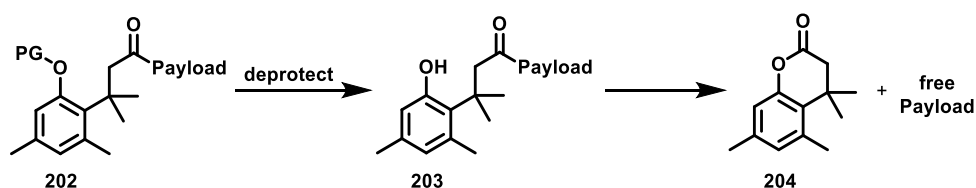
Scheme 50: General concept of TML-based linkers.

Commonly the phenol is masked by a protection/masking group. These masking groups need to be specifically labile towards defined conditions to release the payload.[211] The manner in which such masking groups are cleaved, using the so-called triggers, may be systematically divided and subdivided into the following classes:

Enzymatic cleavage

- Esterase-sensitive masking groups
- Phosphatase-sensitive masking groups
- Quinone-oxidoreductase-sensitive masking groups
- Nitroreductase-sensitive masking groups
- Cytochrome-P450-sensitive masking groups

Small molecule triggered release

- Thiol-sensitive masking groups
- Hydrogen sulfide-sensitive masking groups
- Phosphine-sensitive masking groups

Non-chemical cleavage

- Photosensitive masking groups
- Electrochemically triggered masking groups

The following sections discuss selected examples of each class and subclasses, respectively.

3.1.3.1 Enzymatic cleavage

3.1.3.1.1 Esterase-sensitive masking groups

Esterases can be exploited as a trigger by protecting the TML phenol with an ester group. Royzen and co-workers designed an esterase-sensitive TML system connecting the payload daunorubicin and a PEG chain attached to the phenol via an ester (Scheme 51).[212] In ovarian tumor cells, an esterase cleaves the ester bond, leaving the phenol **206** behind, which subsequently attacks the amide in a nucleophilic intramolecular fashion causing the release of the amine, i.e., the free daunorubicin **208**.[212]
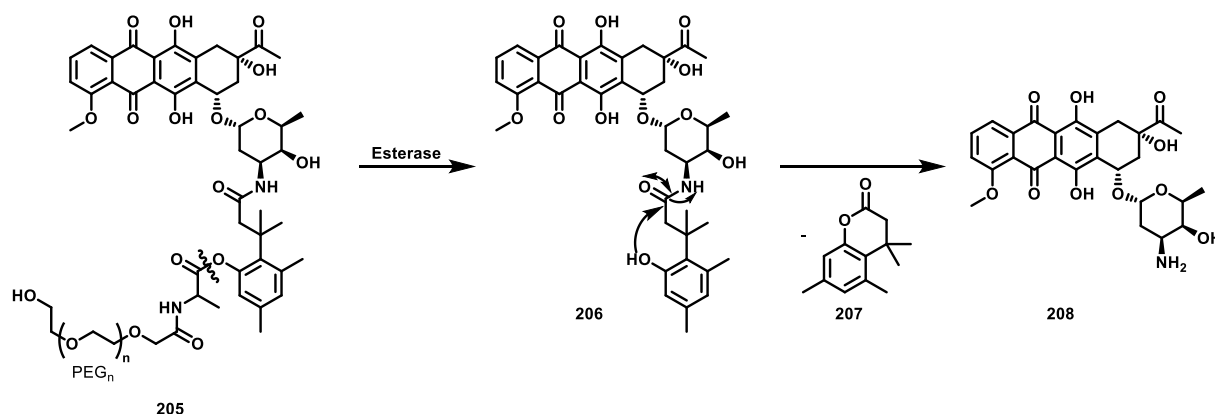
Scheme 51: Esterase-sensitive TML daunorubicin prodrug. Created in analogy to[212]

Another elegant example of esterase-cleavable TML systems was reported by Borchardt and co-workers.[213-215] They connected the *C*-terminus of a peptide via an ester bond with the phenol moiety of the TML core and the *N*-terminus of the same peptide via an amide bond with the acid moiety of the TML system, creating a cyclic derivative of the peptide (Scheme 52). This strategy was applied to a model peptide. In this example, the peptide functions as both the payload and the protecting group at the phenol. This cyclic prodrug approach was chosen to prevent drug degradation due to peptidases. Upon esterase cleavage, the linear peptide is released.[213-215]
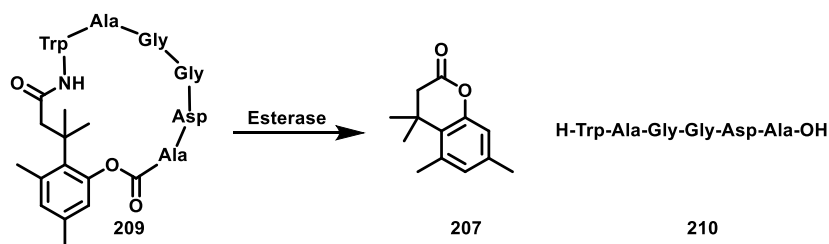
Scheme 52: TML-based esterase-triggered peptide linearization.

3.1.3.1.2 Phosphatase-sensitive masking groups

The phenol moiety can likewise be protected with a phosphate ester, which can be cleaved by an alkaline phosphatase. Being highly polar and hydrophilic, the usage of phosphate esters has the advantage of increasing the water solubility of the overall construct and can be beneficial for oral drug formulations.[216-219]

On the contrary, the alkaline phosphatase shows a narrow substrate specificity, which limits the varieties of drugs that can utilize this approach.[220-221] Nevertheless, to alleviate poor aqueous solubility of taxol, Bristol-Myers-Squibb employed this approach by synthesizing a phosphatase-sensitive TML prodrug of paclitaxel (Scheme 53).[222]
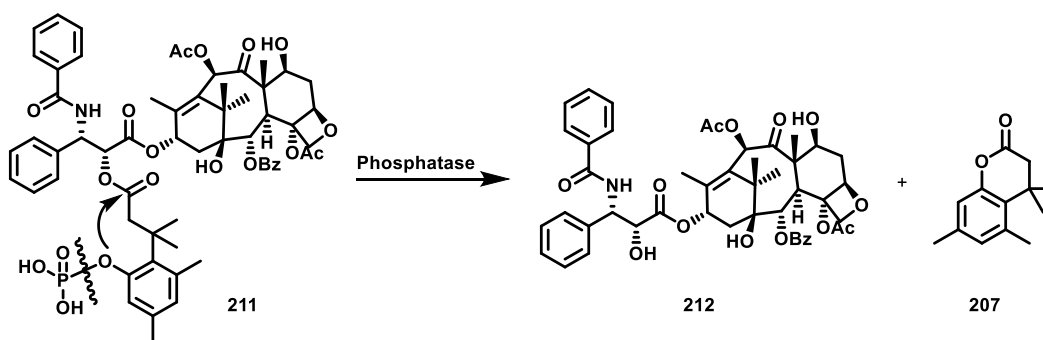
Scheme 53: Phosphatase-sensitive TML prodrug of paclitaxel. Created in analogy to[222]

3.1.3.1.3 Quinone-oxidoreductase-sensitive masking groups

Other enzymes, which can be utilized to unmask the TML phenol functionality, are quinone-oxidoreductases. Those enzymes catalyze the reduction of a vast variety of quinolones either by one-electron or direct two-electron reduction, using NADH or NADPH as cofactors.[223] To exploit these enzymes, the phenol needs to be converted into a benzoquinone. Those benzoquinone TML structures can serve as a substrate for quinone-oxidoreductases leading

to the formation of dihydroquinones, which subsequently release the payload via intramolecular nucleophilic attack on the carbonyl.[224]

Based on this concept, Wu and co-workers designed a theranostic camptothecin prodrug, exploiting a strong fluorescence exhibited by camptothecin (λ_{ex} = 369 nm, λ_{em} = 455 nm) (Scheme 54).[225-226] Using this TML system, the quenching properties of the quinone based on photoinduced electron transfer (PET)[227] could be leveraged. This made it possible to explore the release of camptothecin since cleavage from the quenching TML system led to fluorescence recovery. On the same basis, this construct can be used to monitor NQO1 levels in cells.[225-226]
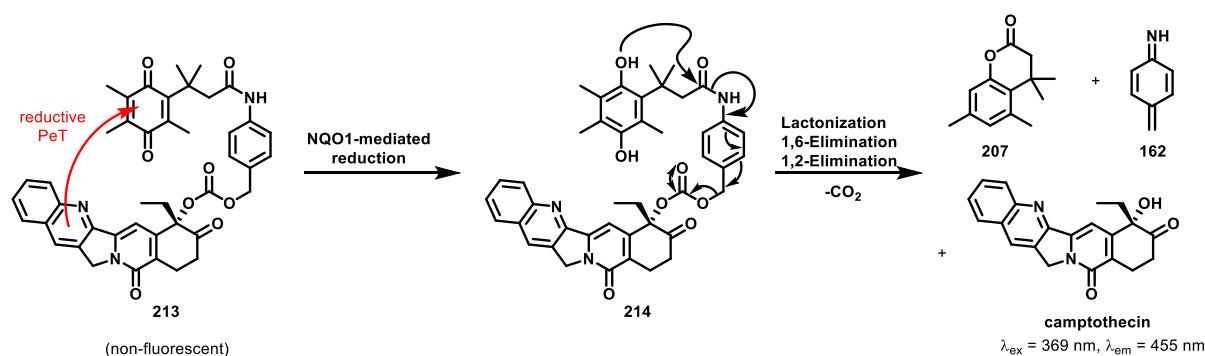
Scheme 54: NQO1-triggered camptothecin prodrug. Created in analogy to[225]

3.1.3.1.4 Nitroreductase-sensitive masking groups

Shigenaga *et al*. designed a nitroreductase-sensitive TML system employing a *p*-nitrobenzyl ether as the phenol masking group.[228]

This new TML system was implemented as an amino acid side chain, creating a distinct cleavage site if the unnatural amino acid is integrated into a peptide (Scheme 55). Nitroreductases, which generally catalyze the reduction of nitrogen-containing compounds, e.g., nitro-, nitroso- and hydroxylamine groups, convert the *p*-nitrobenzyl group into the amine. The free amine subsequently undergoes self-immolative cleavage and releases the active phenol, leading to lactonization and cleavage of the peptide.[228]
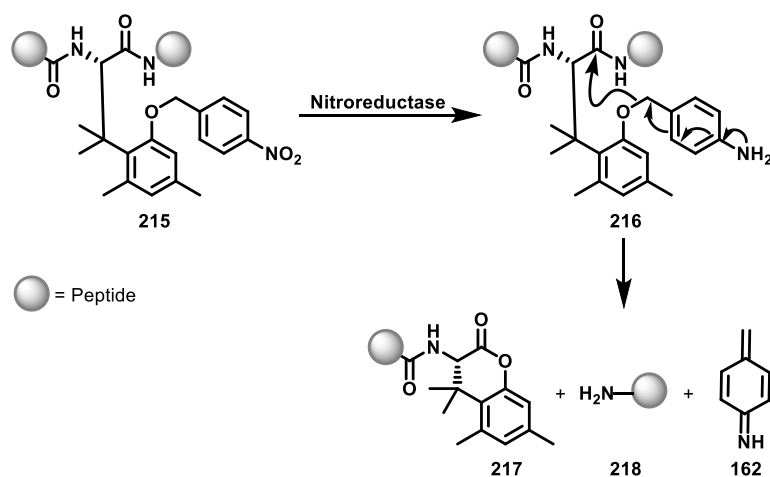
Scheme 55: Nitroreductase-sensitive TML-based amino acid, incorporated into a peptide to serve as a cleavage site. Created in analogy to[228]

3.1.3.1.5 Cytochrome-P450-sensitive masking groups

Raines and co-workers developed a cytochrome-P450-sensitive TML system (Scheme 56).[229] An ethyl ether was introduced to mask the reactive phenol functionality. Cytochrome P450 oxidizes the ether to hemiacetal **178**, which is labile in physiological conditions, triggering a reaction cascade, resulting in an eventual release of the fluorogenic payload morpholinourea rhodamine (MURh). This approach allowed real-time imaging of P450 levels *in cellulo*.[229]
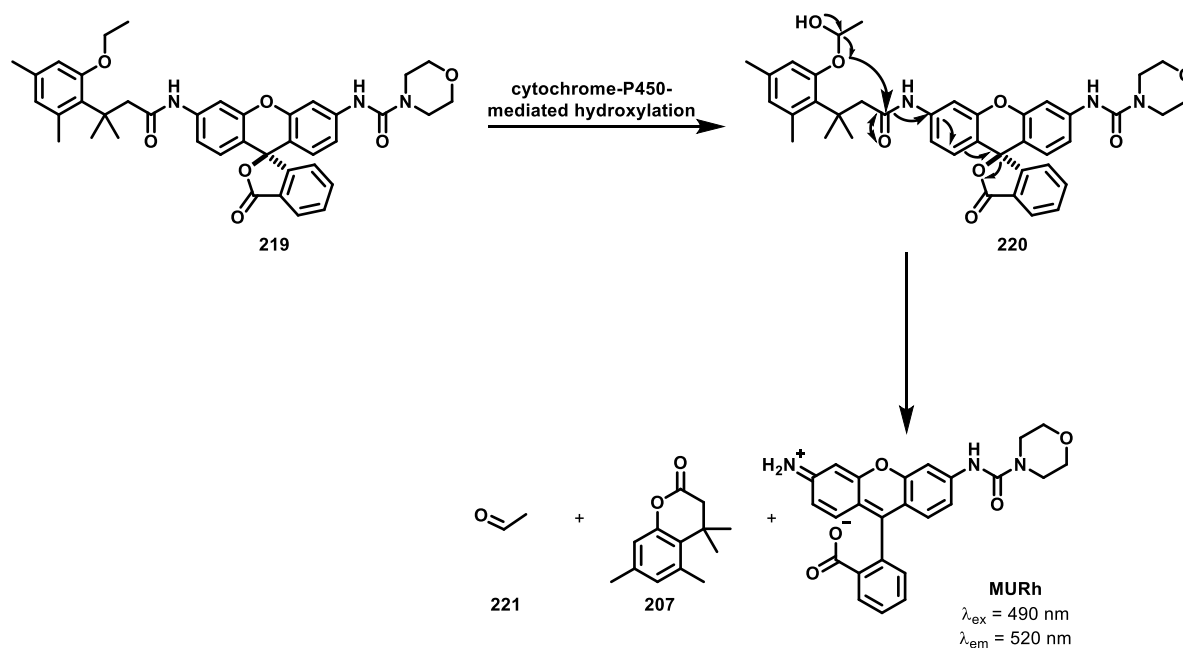
Scheme 56: Cytochrome-P450-sensitive TML releasing MURh. Created in analogy to[229]

3.1.3.2   Small-molecule-triggered release

3.1.3.2.1   Thiol-sensitive masking groups

Michael acceptor systems like acrylic acid represent effective warheads for targeting thiols due to their soft character according to the HSAB theory. Thiols add to Michael systems at the 4-position, i.e. the soft position, via a nucleophilic attack.

By introducing an acrylic acid phenyl ester as a masking group to the TML core, Zhao co-workers were able to trigger a TML system carrying a fluorogenic probe using a thiol.[230] In addition, this system shows selectivity towards glutathione (GSH) over cysteine and homocysteine (hCy), which enabled the selective detection of glutathione. The authors explained this selectivity by referring to the highly sterically demanding structure of the TML ester restraining an appropriate attack on the carbonyl in the Bürgi–Dunitz angle, which the longer flexible chain of GSH can overcome (Scheme 57).[230]
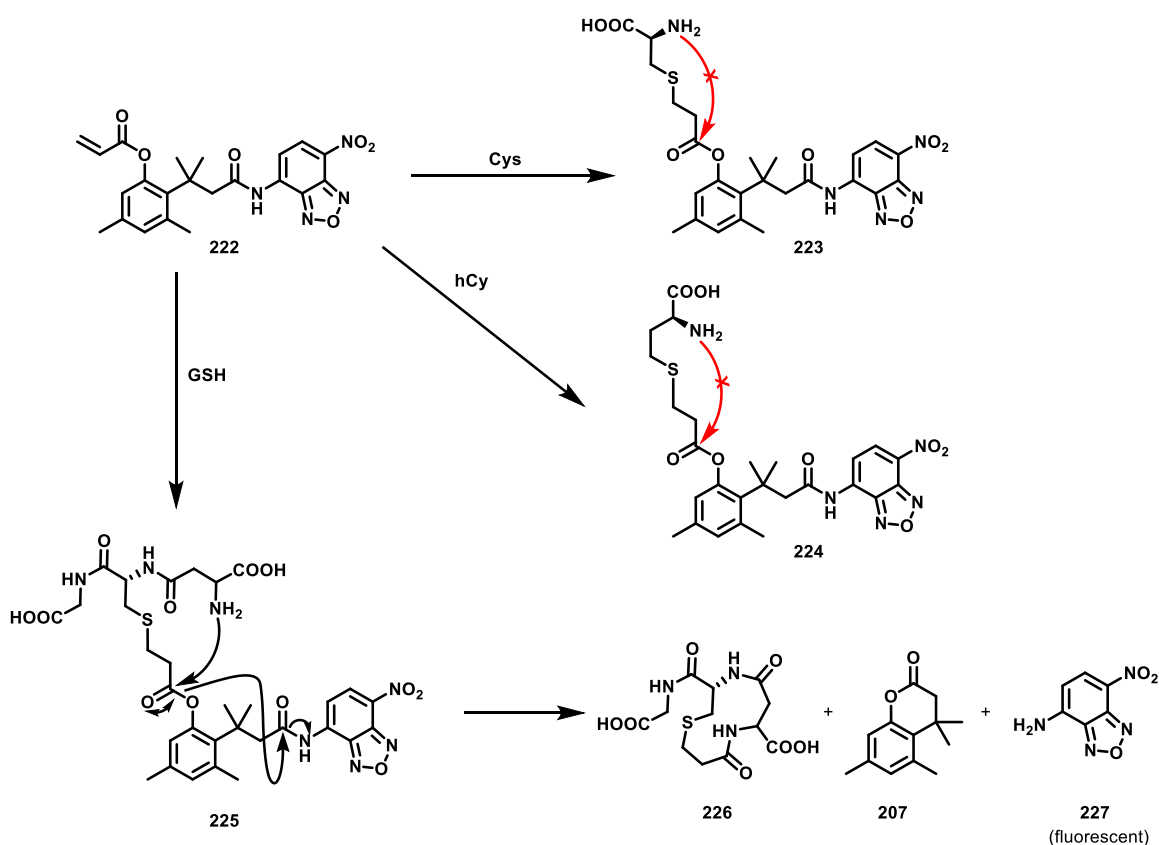
Scheme 57: TML approach with a fluorogenic probe, which is selectively activated by glutathione. Created in analogy to[230]

Using a slightly different approach, Shigenaga *et al.* introduced a thiol-sensitive TML containing a *p*-nitrobenzenesulfonate moiety, which is susceptible to a nucleophilic aromatic substitution in order to induce an amide bond cleavage in a PNA (peptide nucleic acid) macromolecule capable of pairing with DNA (Scheme 58).[231]
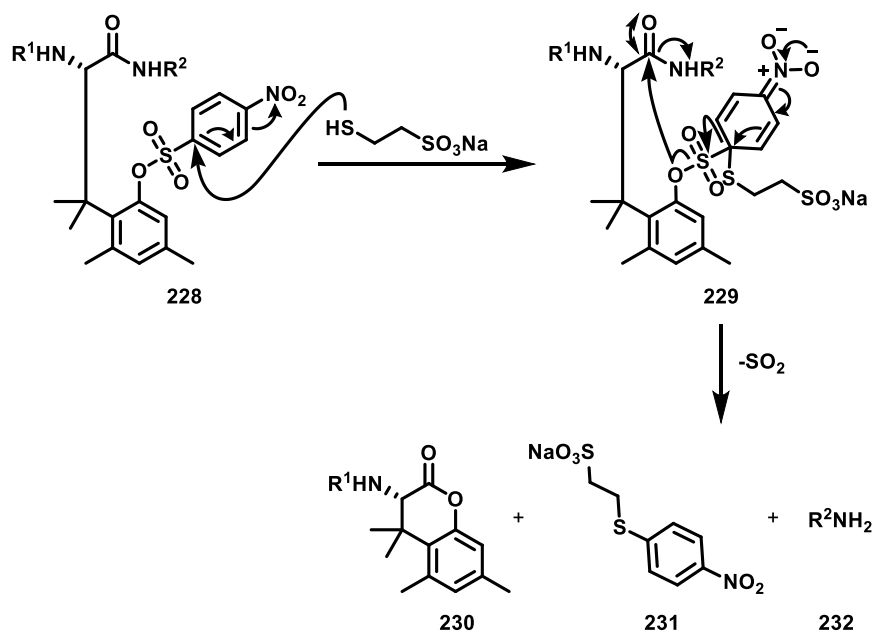
Scheme 58: *p*-nitrobenzenesulfonate masked TML leading to peptide bond cleavage upon thiol treatment. Created in analogy to[231]

3.1.3.2.2 Hydrogen sulfide–sensitive masking groups

Klahn and co-workers introduced a novel TML system substituting the classical phenol by an aniline. This amino TML system, which is based on derivatives of *ortho*-aminodihydrocinnamic acid, was masked by converting the amine into an azide.[232] This azide is reduced to the free aniline in a bio-responsive manner when encountering H_2S. Connecting the N_3-TML to the fluorescent dye MURh, enabled the monitoring of the evolution of H_2S in an *in vivo* cell culture model (Scheme 59).[232]
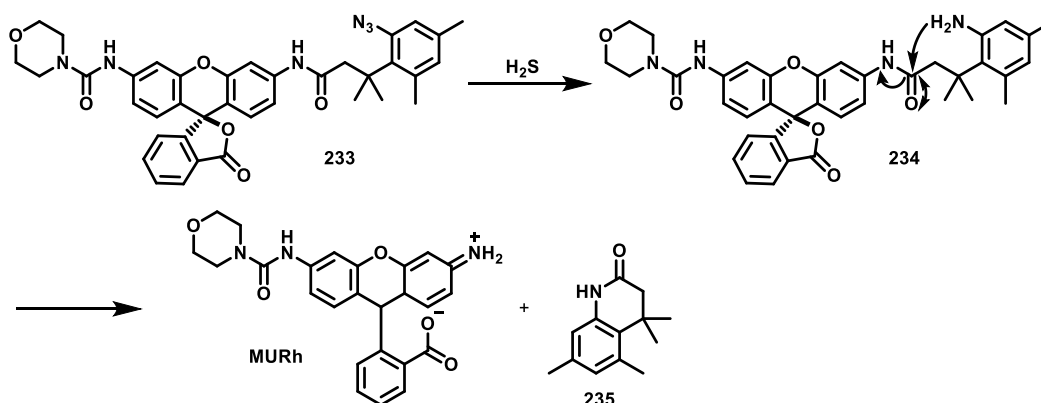
Scheme 59: Amino TML masked as an azide triggered by H_2S. Created in analogy to[232]

3.1.3.2.3 Phosphine-sensitive masking groups

The above-mentioned azide derivative of TML can be triggered not only by hydrogen sulfide but also by phosphines via a Staudinger reduction, resulting in the payload release in a similar fashion. Klahn and co-workers reported short reaction times of 2 min at 23 °C in PBS at pH 7.4 for the release of MURh and 7-amino-4-methylcoumarine (Cou) as fluorescent payloads (Scheme 60).[232]
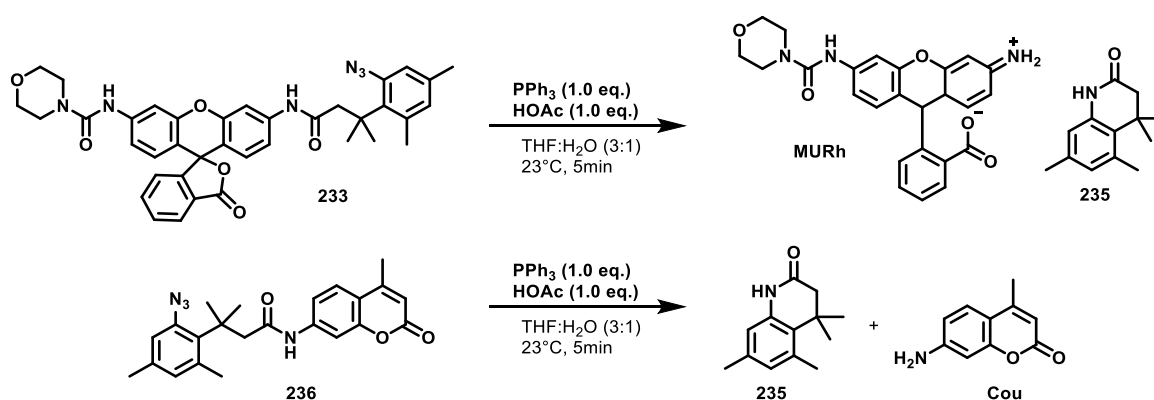
Scheme 60: Phosphine-sensitive azide derivatives of TML-masked fluorophores.[232]

3.1.3.2.4 Novel click-to-release trigger

Brönstrup and co-workers developed a new TML based on the click-to-release concept (unpublished data) introducing a vinyl ether at the TML core to mask the reactive phenol functionality. Upon treatment with a tetrazine, the IEDDA reaction is designed to cleave the vinyl, releasing the phenol and subsequently the payload. The synthesis of this novel TML starts from 3,5-xylenol (**237**), which undergoes a Friedel–Crafts alkylation with subsequent lactonization (Scheme 61). After the reduction of the lactone and TBS protection of the primary alcohol, the phenol is alkylated by a Mitsunobu reaction. The resulting alkyl ether **242** is treated with KO*t*Bu to introduce the novel vinyl moiety. The final TML moiety is obtained upon deprotection of the primary alcohol followed by a step-wise oxidation forming the acid.

Further studies on this linker are part of this thesis and will thus be discussed in the results and discussion section.
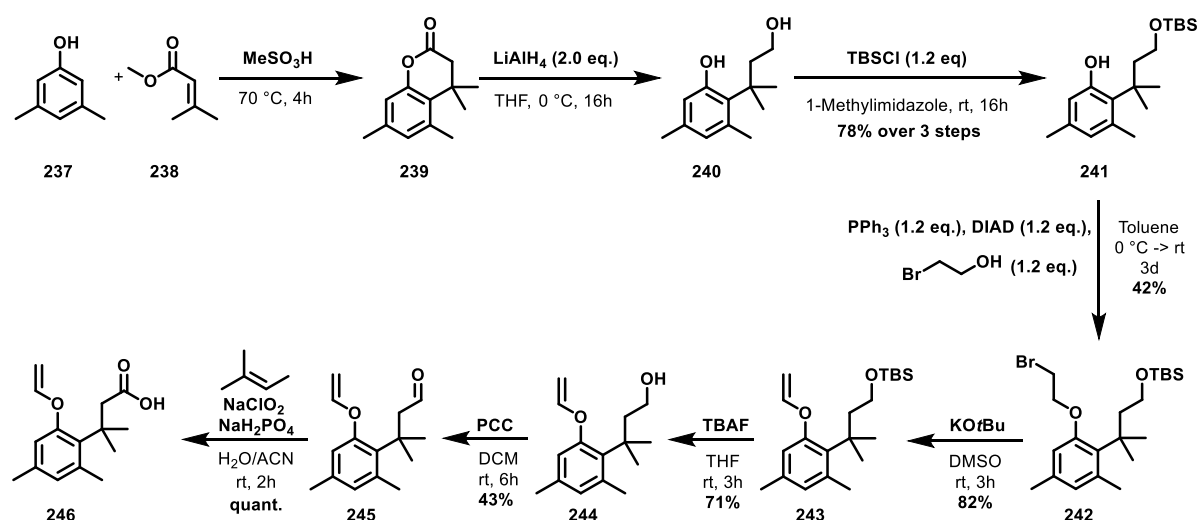
Scheme 61: Synthesis of a novel click-to-release TML moiety developed by Dr. Chunfa Xu in the Brönstrup group.

3.1.3.3 Non-chemical cleavage

3.1.3.3.1 Photosensitive masking groups

Over the years, mainly two different types of photosensitive masks have been developed. The first one is the TML protected with an *ortho*-nitrobenzyl ether. When activated by a UV radiation, the *ortho*-nitrobenzyl moiety undergoes a Norrish type II reaction followed by radical recombination and cyclization, yielding acetal **248** (Scheme 62). The ensuing spontaneous hydrolysis unmasks the phenol. This approach has been applied to induce peptide bond cleavages upon irradiation *in vivo*.[233-234]
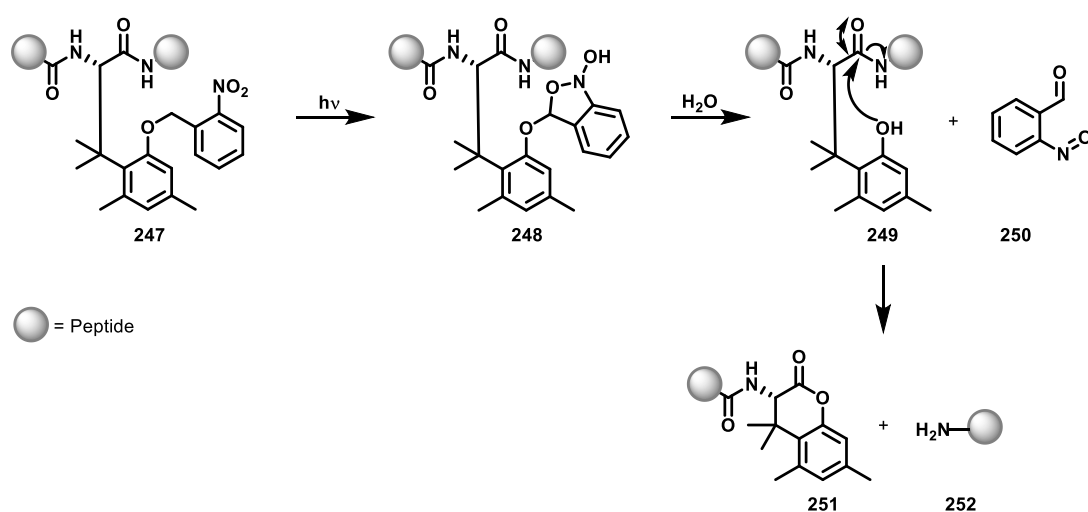
Scheme 62: TML-based system utilized in a photosensitive peptide cleavage. Created in analogy to [233]

The second type involves a quinone based TML core, which, as previously mentioned, need to be reduced to the respective dihyroquinones to be able to lactonize and thus release the payload. Apart from previously mentioned methods for the reduction of quinones, dihyroquinones can be obtained via photoinduced reduction, which is mediated by an adjacent sulfide or amine function. This strategy has been successfully employed in releasing fluorogenic payload **254** (Scheme 63).[235]
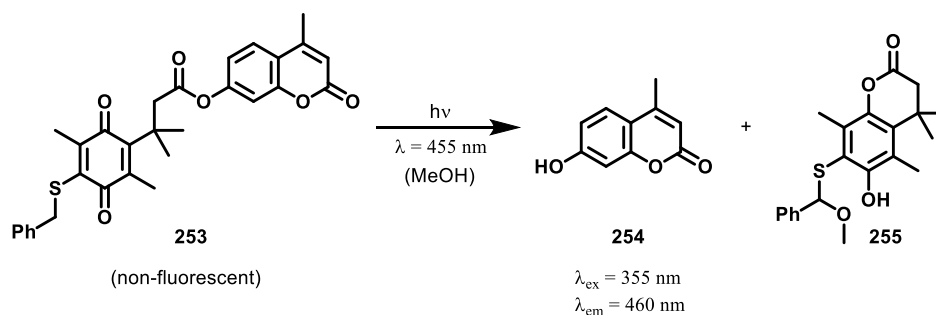
Scheme 63: Photosensitive quinone derivatives of TML-masked fluorophores. Created in analogy to[235]

3.1.3.3.2 Electrochemical cleavage

Quinones can also be electrochemically reduced to the dihyroquinones, which subsequently leads to lactonization of the TML system, similar to the enzymatic and the photoinduced reduction (see section 3.1.3.1.2 and 3.1.3.3.1). This type of trigger has so far only been used in the material sciences but not in a biological context.[236-238]

3.2 Objective

The development of novel, chemically triggered, highly selective cleavable linkers is of great interest. Such linkers offer a high degree of control over the cleavage process and, thus, the release of the respective payload. Bio-orthogonal reactions can be used to address this need. Brönstrup and co-workers undertook initial efforts to synthesize a new TML system based on the bioorthogonal inverse electron demand Diels-Alder reaction.

Building on the group's previous works, this study aimed to evolve the vinyl TML system further. Thus, the kinetic characteristics of the click-to-release TML system was to be identified and evaluated, aiming for a deeper understanding of the release process.

On this basis, conclusions were to be drawn about the molecular design, which was to be adapted in order to increase the reaction rate. Furthermore, the kinetic potential of the reaction should be evaluated. In this course, different electron-deficient tetrazines were to be synthesized and kinetically characterized.

Possibilities to enhance the applicability of the vinyl TML and, thus, the extension of the vinyl TML to a true linker were to be explored.

3.3 Results and discussion

3.3.1 Novel click-to-release triggered TML - Evaluation of the kinetic problem

In unpublished work by the group of Prof. Brönstrup, Dr. Xu developed a TML system that utilizes a vinyl ether as the trigger. For further details, see section 3.1.3.2.4. As shown in Scheme 64, the trigger was supposed to be released via an inverse electron demand Diels-Alder reaction with a tetrazine. However, it was found that the reaction kinetics are too slow for biological applications. Even after three days, no significant drug release could be detected by monitoring the reaction via NMR.
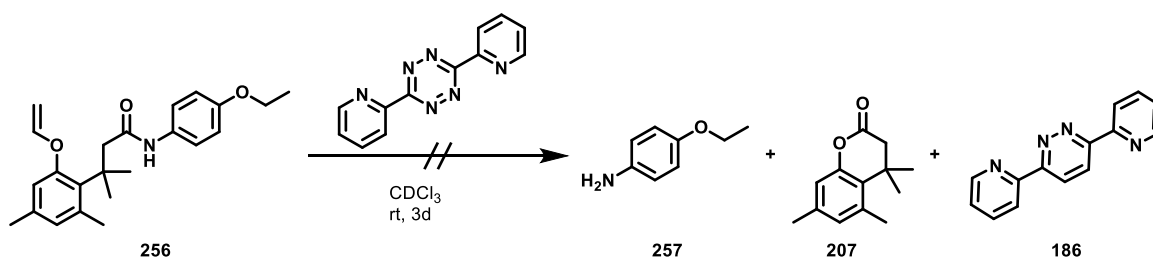
Scheme 64: Tetrazine triggered release of the model compound **257** showing slow reaction kinetics.

Understanding the underlying kinetic problem is the basis of a rational design and development of a biologically applicable TML system deploying a vinyl ether trigger. Therefore, a test system was developed in order to analyze the rate-determining step in the reaction cascade. Phenyl vinyl ether (**258**), being readily available and giving very distinct NMR signals, was used as a test system to simplify the monitoring process via NMR and allow an economic usage of the new TML derivative. Additionally, the phenyl vinyl sulfide (**266**) was explored to test how the heteroatom affects the reactivity and kinetics. 3,6-Diphenyl-1,2,4,5-tetrazine was used as the electron-deficient diene. As illustrated in Scheme 65, the overall reaction can be subdivided into three steps. The first step is the inverse electron demand Diels-Alder (IEDDA) reaction that leads to a dihydropyridazine (**260/264/267**). This intermediate undergoes an elimination in the next step giving the phenol (**262/265**) or the thiophenol (**268**), respectively, as well as the corresponding pyridazine (**261**). The third step is the intramolecular lactonization, which cannot take place in the test system, since only unsubstituted phenyl vinyl ether and its thio derivative were used. Nevertheless, the simplified test system can also deliver information about this step. If the test reactions go to completion, the intramolecular lactonization would have to be the rate-determining step, since in the original system (Scheme 65) the lactone is not formed. As a

wide variety of applications of the TML are known, and lactonization was previously not reported to be problematic, a kinetic problem in this step is considered unlikely.

Allowing to draw conclusions in each case, this simplified test system is sufficient to gain a deeper understanding of the kinetics and identify the rate-limiting step.
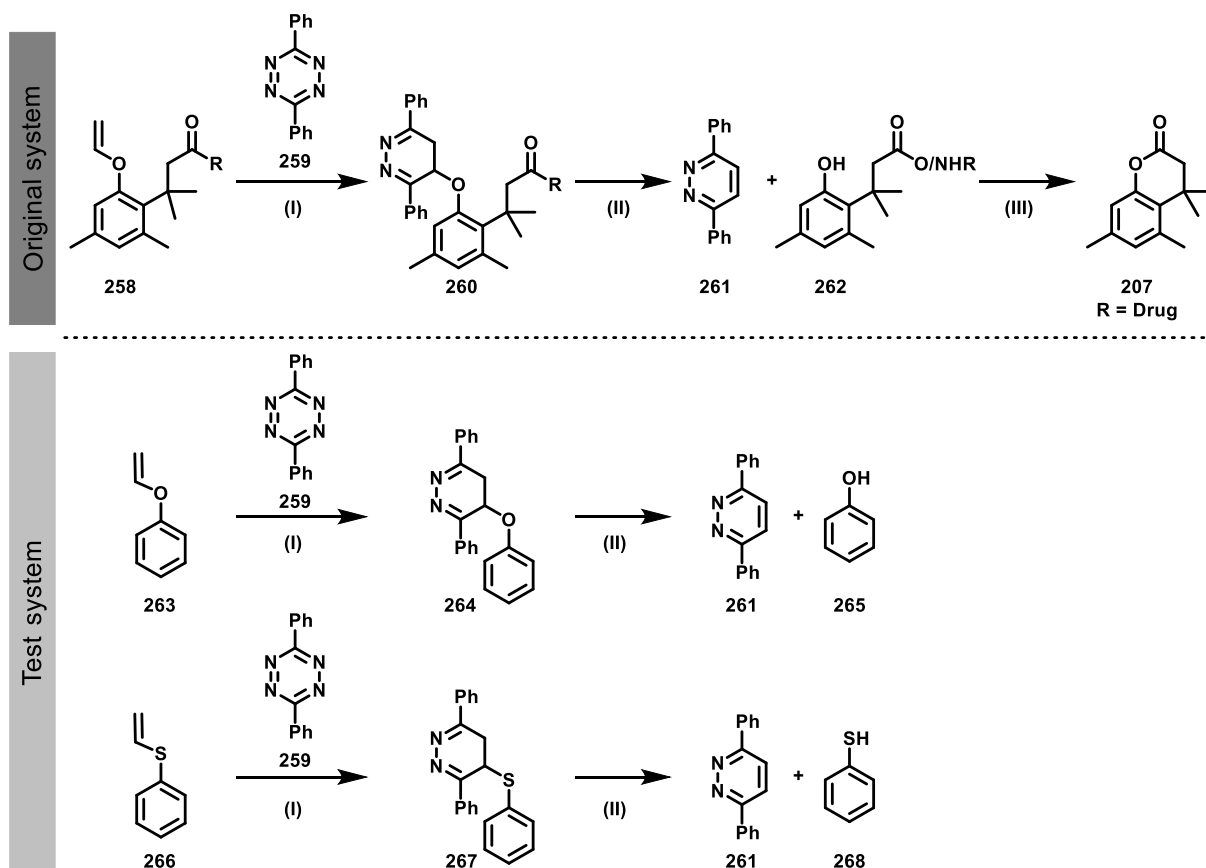
Scheme 65: Comparison of the original vinyl ether TML system and the phenyl vinyl ether based test system. The overall reaction is divided into three individual reaction steps, i.e. (I) inverse electron demand Diels-Alder (IEDDA), (II) elimination and (III) intramolecular lactonization.

The test reactions were carried out in CDCl$_3$. NMRs were measured in 18 min intervals, corresponding to the shortest possible time difference due to technical reasons when alternately measuring two samples (vinyl phenol ether and vinyl thiophenyl ether). The measurements were taken over a period of 1 h 45 min. An additional measurement was taken after 18 h 23 min. Figure 44 shows an overlay of the first measurement at t = 0 (red) and each last measurement at t = 18 h 23 min (cyan) for the phenyl vinyl ether based and the vinyl thiophenyl ether based test reaction, respectively. Both test systems do not show any conversion after 18 h 23 min, as can be clearly seen in both overlays. These findings suggest that the first step in the reaction cascade, i.e., the IEDDA, is the rate-limiting step.

183
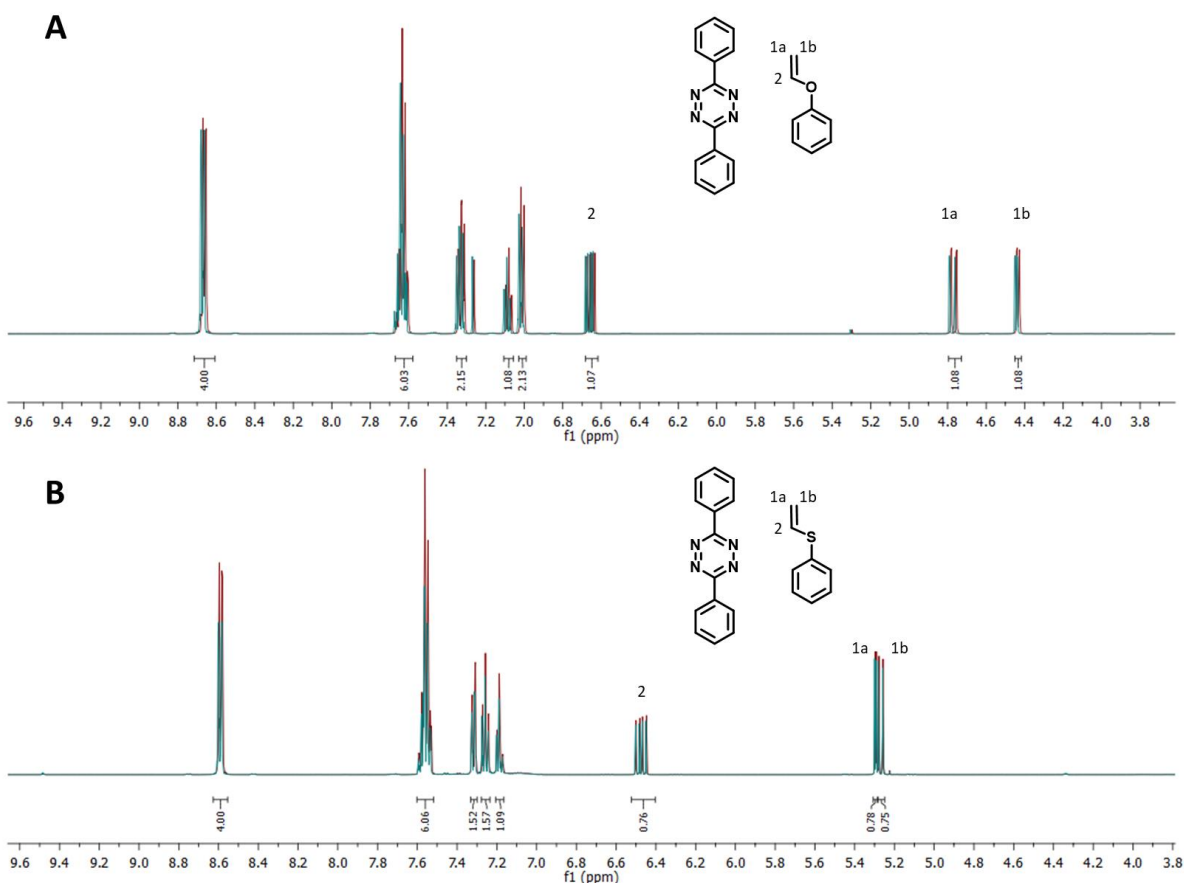
Figure 44: A) Overlay of ^{1}H NMR spectra at t = 0 (red) and t = 18 h 23 min (cyan) of the reaction between phenyl vinyl ether (**263**) and 3,6-diphenyl-1,2,4,5-tetrazine (**259**). The characteristic vinyl ether signals are additionally labeled; B) Overlay of ^{1}H NMR at t = 0 (red) and t = 18 h 23 min (cyan) of the reaction between vinyl thiophenyl ether (**266**) and 3,6-diphenyl-1,2,4,5-tetrazine (**259**). The characteristic vinyl ether signals are additionally labeled.

Taking those findings into account, there are two possible strategies to accelerate the reaction. One possibility is to enhance the electron density of the dienophile, i.e., the vinyl ether. The other possibility is to reduce the electron density of the diene. Both measures would result in an improved overlap of the diene's LUMO and the dienophile's HOMO (Figure 45). From a synthetic point of view, it is more feasible to reduce the electron density at the diene, since tetrazines are more accessible than TML derivatives.

A *Diels-Alder* energy diagram

B Inverse electron demand *Diels-Alder* energy diagram
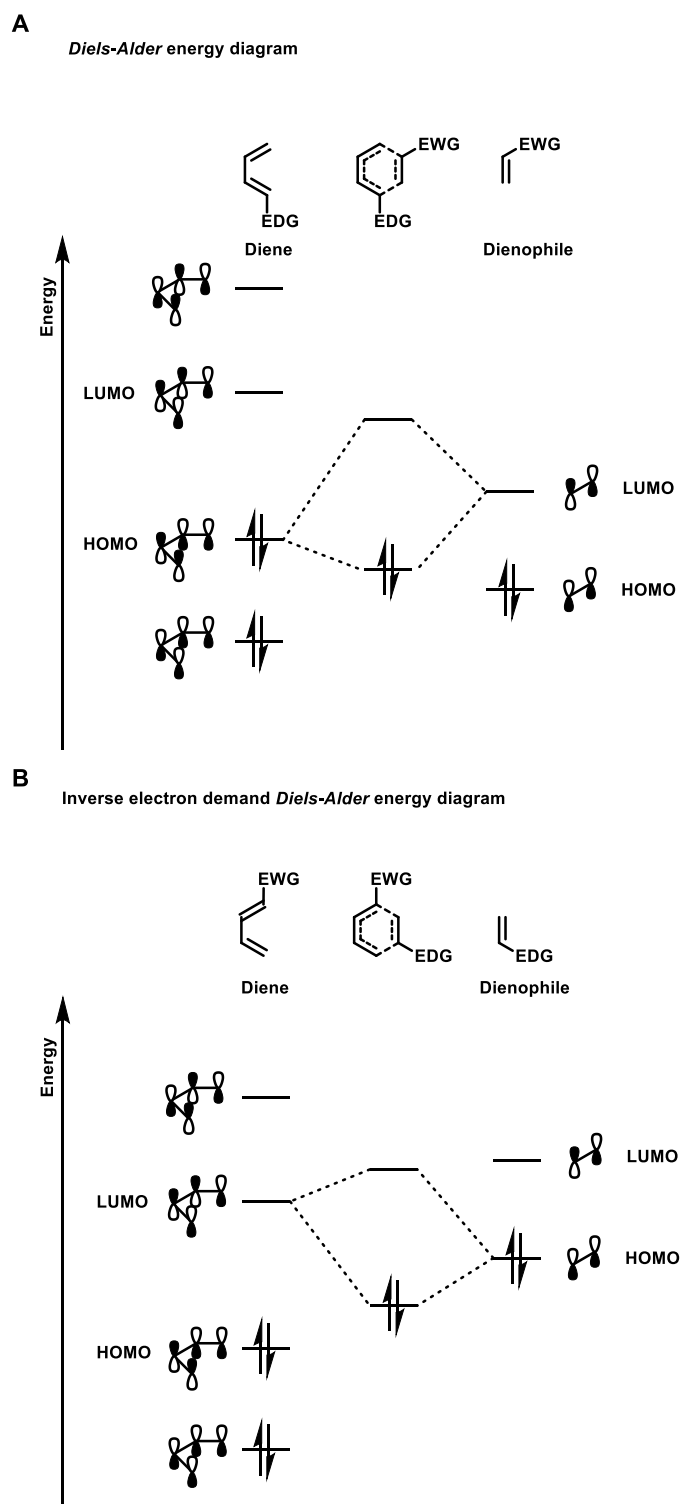
Figure 45: A) Generic molecular orbital diagram for a Diels Alder reaction, showing the overlap of the diene's HOMO and the dienophile's LUMO; B) Generic molecular orbital diagram for an inverse electron demand Diels Alder, showing the overlap of the diene's LUMO and the dienophile's HOMO.

3.3.2 Synthesis of the tetrazine derivatives

One way to enhance the reaction rate of the tetrazine-triggered TML system is via a shift of the tetrazines LUMO towards lower energies. Lowering the LUMO of the tetrazine can be achieved by introducing electron-withdrawing substituents at the tetrazine core.
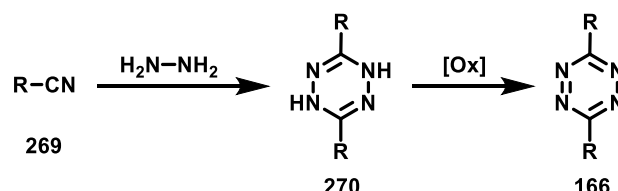
Scheme 66: Method for the tetrazine synthesis based on the Pinner synthesis.

Tetrazines can be obtained using the Pinner synthesis and its advancements (Scheme 67). Here, aromatic or alkyl nitriles condense with hydrazine forming a dihydrotetrazine intermediate, which is subsequently oxidized to the final tetrazine.[239-240]

First, the two phenyl substituents of diphenyl tetrazine were exchanged by two pyridine rings, thereby reducing the electron density in the tetrazine ring. 3,6-di(pyridin-2-yl)-1,2,4,5-tetrazine (**289**) was obtained from picolinonitrile (**271**) and hydrazine, followed by oxidation with sodium nitrite. Even though the synthesis of tetrazines is well known, it often suffers from low yields[239],[241] which was also the case here.
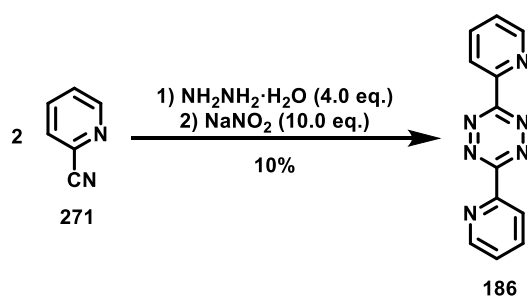
Scheme 67: Preparation of 3,6-di(pyridin-2-yl)-1,2,4,5-tetrazine (**186**).

In another approach, the electron density of the tetrazine was reduced by introducing one benzoic acid moiety. The synthesis of the resulting tetrazine **274** is illustrated in Scheme 68. In the first step, 4-cyanobenzoic acid (**272**) and formamidine acetate (**273**) were treated with hydrazine hydrate. In the second step, an oxidation to the final product **274** using sodium nitrite was performed. As expected the yields were also low in this case.
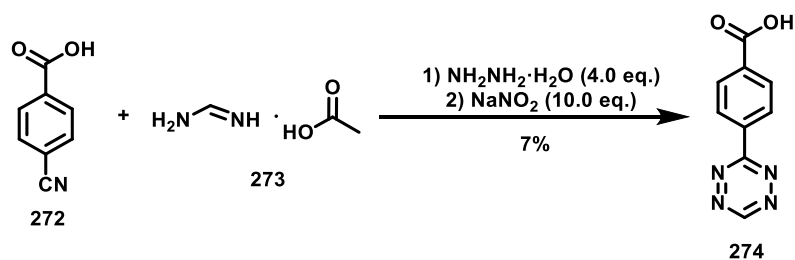
Scheme 68: Synthesis of 4-(1,2,4,5-tetrazin-3-yl)benzoic acid (**274**).

Next, a nitrogen atom was introduced in the phenyl ring, giving rise to a nicotinic acid substituted tetrazine (**276**). Herein, the same synthetic approach was used. The dihydrotetrazine intermediate was formed using 6-cyanonicotinic acid (**275**), while the intermediate was oxidized again by sodium nitrite (Scheme 69).
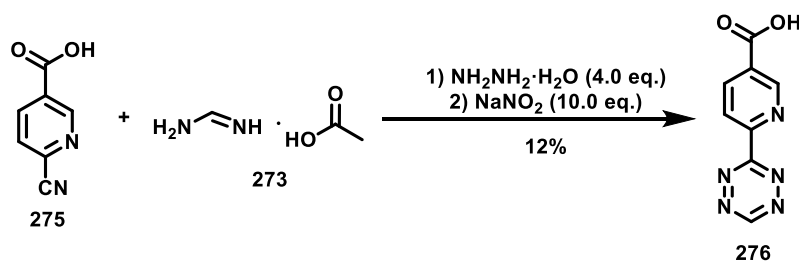
Scheme 69: Synthesis of 6-(1,2,4,5-tetrazin-3-yl)nicotinic acid (**276**).

To further lower the LUMO of the tetrazine, the nicotinic acid substituent was altered by introducing a second nitrogen atom in the ring, changing the pyridine to a pyrimidine. Thus, the corresponding nitrile **277** was reacted with formamidine acetate (**273**) and hydrazine hydrate. Subsequently, the oxidation via sodium nitrite was performed (Scheme 70). Yet, the characteristic color change to bright violet or pink did not occur, and no product could be isolated.
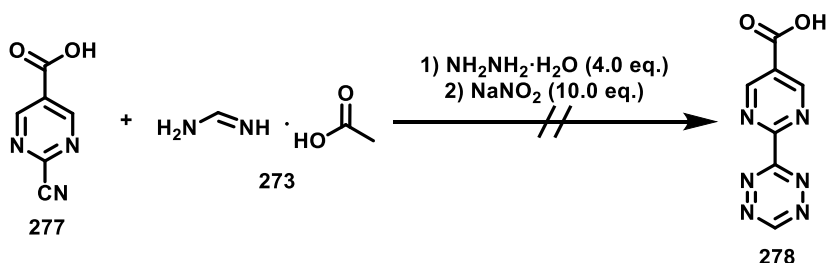
Scheme 70: Synthetic attempt towards 2-(1,2,4,5-tetrazin-3-yl)pyrimidine-5-carboxylic acid (**278**).

However, instead of adding a nitrogen to the successfully synthesized tetrazine **276**, it is also possible to reduce the electron density by introducing a second substituent on the tetrazine,

thus forming the symmetric analog of **276**. In order to synthesize the symmetric dinicotinic acid substituted tetrazine (**280**), the synthesis of **276** was adjusted by removing the formamidine acetate (**273**), leaving only the nitriles as the building blocks for the tetrazine ring (Scheme 71). Even though this strategy worked well for the dipyridinyl tetrazine **186**, it did not work in the case of 6,6'-(1,2,4,5-tetrazine-3,6-diyl)dinicotinic acid (**280**).
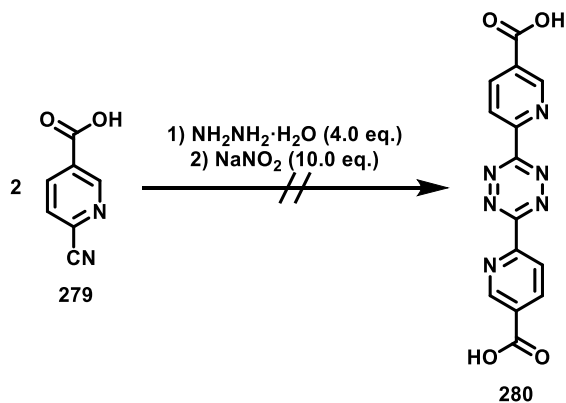
Scheme 71: Synthetic attempt towards 6,6'-(1,2,4,5-tetrazine-3,6-diyl)dinicotinic acid (**280**).

Furthermore, the relatively electron-rich tetrazine **284**, kindly provided by Dr. Charoenpattarapreeda, was also investigated regarding its kinetic properties in the further course of this thesis. An overview of the synthesis of **284** is provided in Scheme 72. Starting from 4-(aminomethyl)benzonitrile (**281**), the free amine was Boc-protected and subsequently the tetrazine ring was formed by applying the same method as described above. Still, there are some distinctions. Acetonitrile was used as a second nitrile giving rise to the asymmetrically substituted tetrazine **283**. Additionally, the Lewis acid zinc triflate was added to the reaction, which led to improved yields. After Boc deprotection, the final product **284** was obtained.
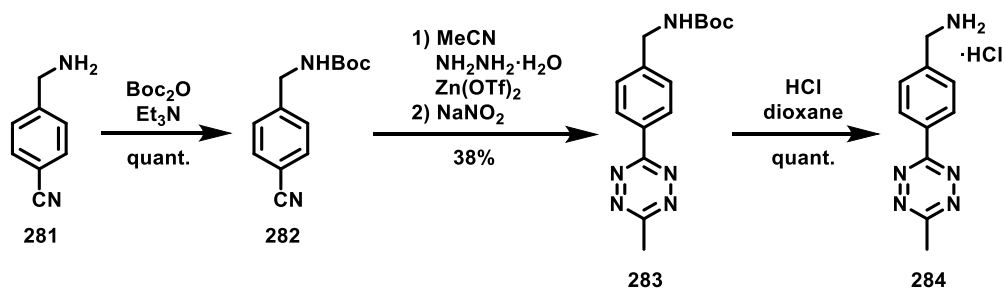
Scheme 72: Synthesis of (4-(6-methyl-1,2,4,5-tetrazin-3-yl)phenyl)methanaminium chloride (**284**) performed by Dr. Charoenpattarapreeda.

Moreover, the panel of tetrazines was expanded with three commercially available tetrazines: 3,6-diphenyl-1,2,4,5-tetrazine (**259**), 3,6-bis(methylthio)-1,2,4,5-tetrazine (**285**) and dimethyl 1,2,4,5-tetrazine-3,6-dicarboxylate (**286**) (Figure 46).
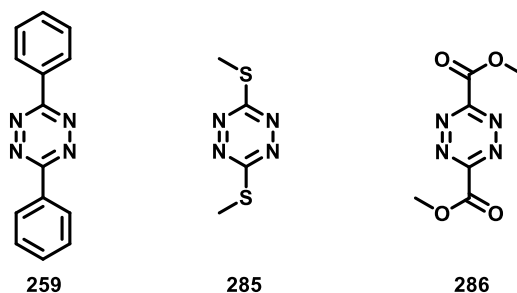
Figure 46: Commercially available tetrazines used in this thesis.

The entire panel of tetrazines sorted from electron-rich (left) to increasingly electron-poor (right), is shown in Figure 47. The two tetrazines **Tz8** and **Tz7** are depicted in gray since they could not be obtained using standard methods.
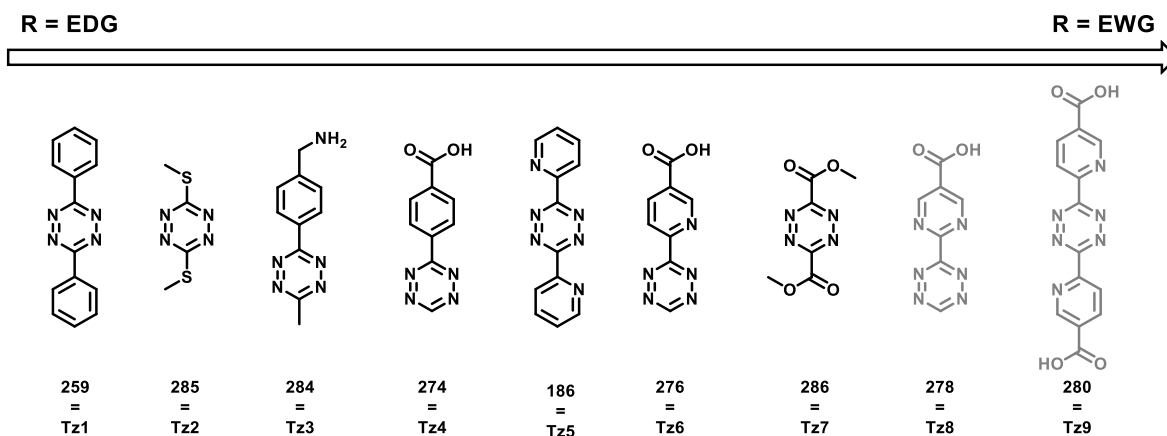
Figure 47: Panel of tetrazines sorted by the electronic properties of their substituents according to the Hammett constant σ_p (based on experimental[242] as well as predicted[243] values) from electron donating group (= EDG) (left) to increasingly electron withdrawing groups (= EWG) (right) Tetrazines depicted in gray could not be obtained using standard methods.

3.3.3   Kinetic evaluation

3.3.3.1   NMR based evaluation

The test system introduced in section 3.3.1 was used for the kinetic evaluation. Here, phenyl vinyl ether is reacted with a tetrazine and monitored by NMR.

First, the electron poorest tetrazine, tetrazine **Tz7**, was tested to get an impression of the kinetic optimization potential (Scheme 73). In Figure 48 the ^{1}H-NMR Spectrum of phenyl vinyl ether **266** before the addition of tetrazine **Tz7** (A) and the first spectrum ca. 5 min after the addition (B), as well as their overlay (C) are presented.

Due to the mixing process and technical details of the NMR, the first measurement was taken ca. 5 min after the addition of **Tz7**. This first spectrum already shows a conversion of ca. 50%, indicating enhanced reaction kinetics.

The rate of conversion was determined via two methods. On the one hand, the reduction of the integral of the vinylic hydrogen in a geminal position of the phenolic oxygen was measured. For this approach, the sum of aromatic signals corresponding to the phenyl vinyl ether and the phenolic product were set to 5. In all spectra, the integral of the vinylic hydrogen was measured in relativity to the aromatic signals. Thus, the relative decrease in the signal of the vinylic hydrogen can be determined.

On the other hand, the relative ratio between the two methyl esters, corresponding to the unreacted tetrazine **Tz7** and the respective product **287**, was calculated based on the assumption of 100% unreacted tetrazine at t = 0.

Depending on the calculation method, the conversion rate can be estimated to be 41% in the case of the vinylic hydrogen and 51% in the case of the methylesters. The difference of 10% is most likely due to integration errors, since the entire aromatic region is used as a reference, while at the same time, the signals in this region in spectrum B are quite broad. For this reason, a rate of about 50% can rather be assumed.

In any case, a vast increase of the reaction rate from no measurable reaction after 18.5 h using tetrazine **Tz1** to about 40 - 50% conversion after 5 min using tetrazine **Tz7** could be observed.

A

B

C
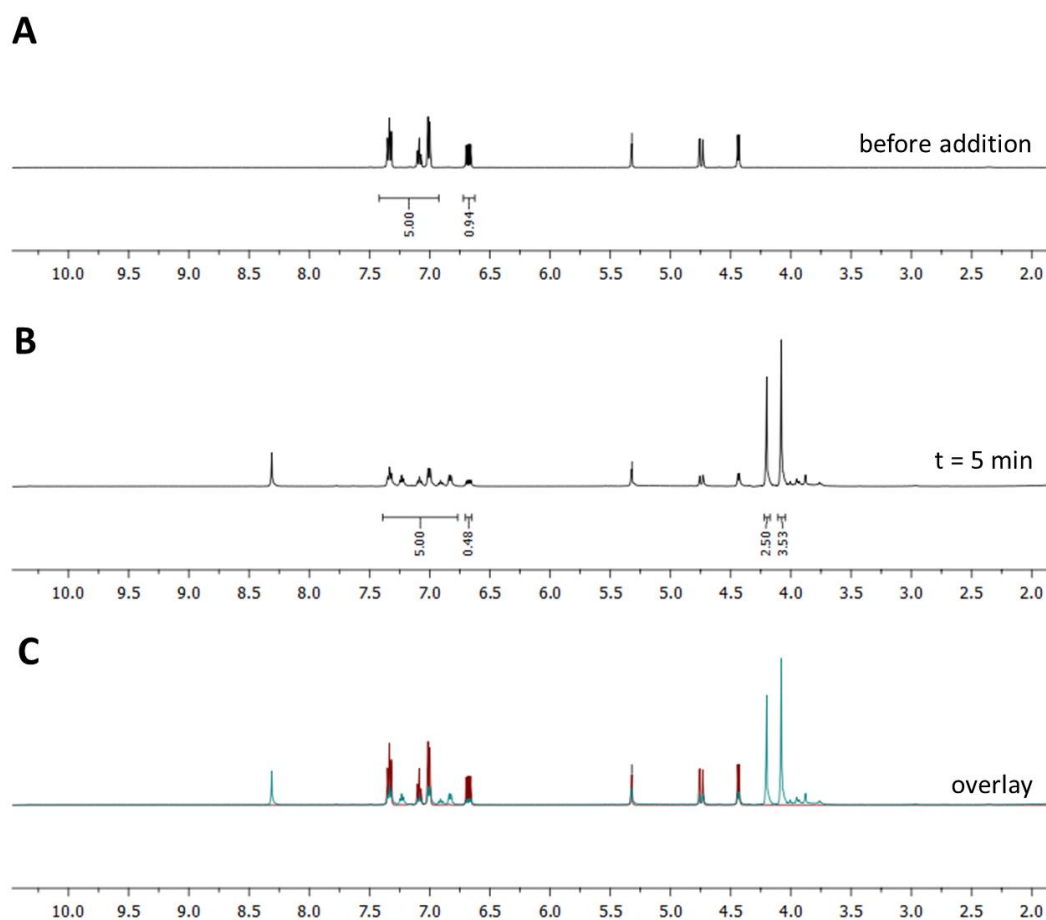
Figure 48: A) ^{1}H-NMR of phenyl vinyl ether before the addition of tetrazine **Tz7**. The aromatic protons are set to an integral of 5. For a better overview only the integrals used for the calculation of the conversion are shown; B) ^{1}H NMR of phenyl vinyl ether 5 min after the addition of tetrazine **Tz7**. The aromatic protons corresponding to phenyl vinyl ether as well as phenol (the product) are set to an integral of 5. For a better overview only the integrals used for the calculation of the conversion are shown; C) Overlay of the ^{1}H NMRs of phenyl vinyl ether before and 5 min after the addition of tetrazine **Tz7**. All spectra were recorded in DCM-d_2.
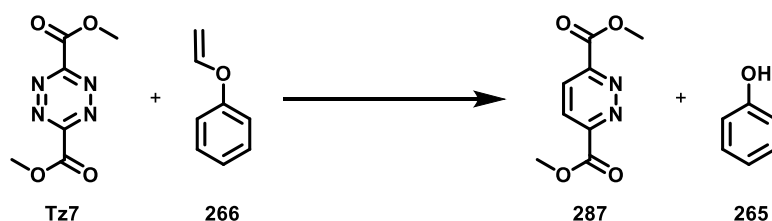
Scheme 73: Test reaction of phenyl vinyl ether (**266**) and dimethyl 1,2,4,5-tetrazine-3,6-dicarboxylate (**Tz7**) used for the evaluation of the kinetic optimization potential.

At this point, it should also be mentioned that reactivity and stability are generally inversely proportional. An increased reactivity of a tetrazine is therefore accompanied by reduced stability. This was also the case with tetrazine **Tz7**, which led to a significant acceleration of the reaction, but also decomposed directly under aqueous conditions. This is critical with

191

regard to the application in biological systems. Thus, it is important to balance the reactivity as well as the stability.

Consequently, all tetrazines in the panel had to be tested for their reactivity and stability towards water. In view of the fact that seven tetrazines should be measured in short time intervals over a period of approx. 15 h and in several different concentrations, NMR spectroscopy was found not to be feasible and thus was not used as a measurement method. Instead, a UV/Vis-based evaluation was established, which will be discussed in more detail in the next section.

3.3.3.2 UV/Vis based evaluation

Initial NMR experiments showed that the reaction is not a 0th, 1st, or 2nd order reaction. Herein the decrease or increase of the integrals of the starting materials and the products was measured over time. This data was plotted according to the time law of the 0th, 1st, and 2nd order reaction, respectively. However no linear correlation could be found. Thus, a simple determination of the rate constant was not possible. In order to determine the rate constant nonetheless, the measurement conditions were chosen in such a manner that a pseudo 1st order reaction could be assumed. The IEDDA is a bimolecular reaction of the type $A+B \rightarrow C+D$. If the concentration of reactant B is chosen to be significantly greater than that of the reactant A, it can be assumed that the concentration of B is constant during the reaction. Based on this concept, the rate constants k for the different tetrazines were determined (Figure 49).
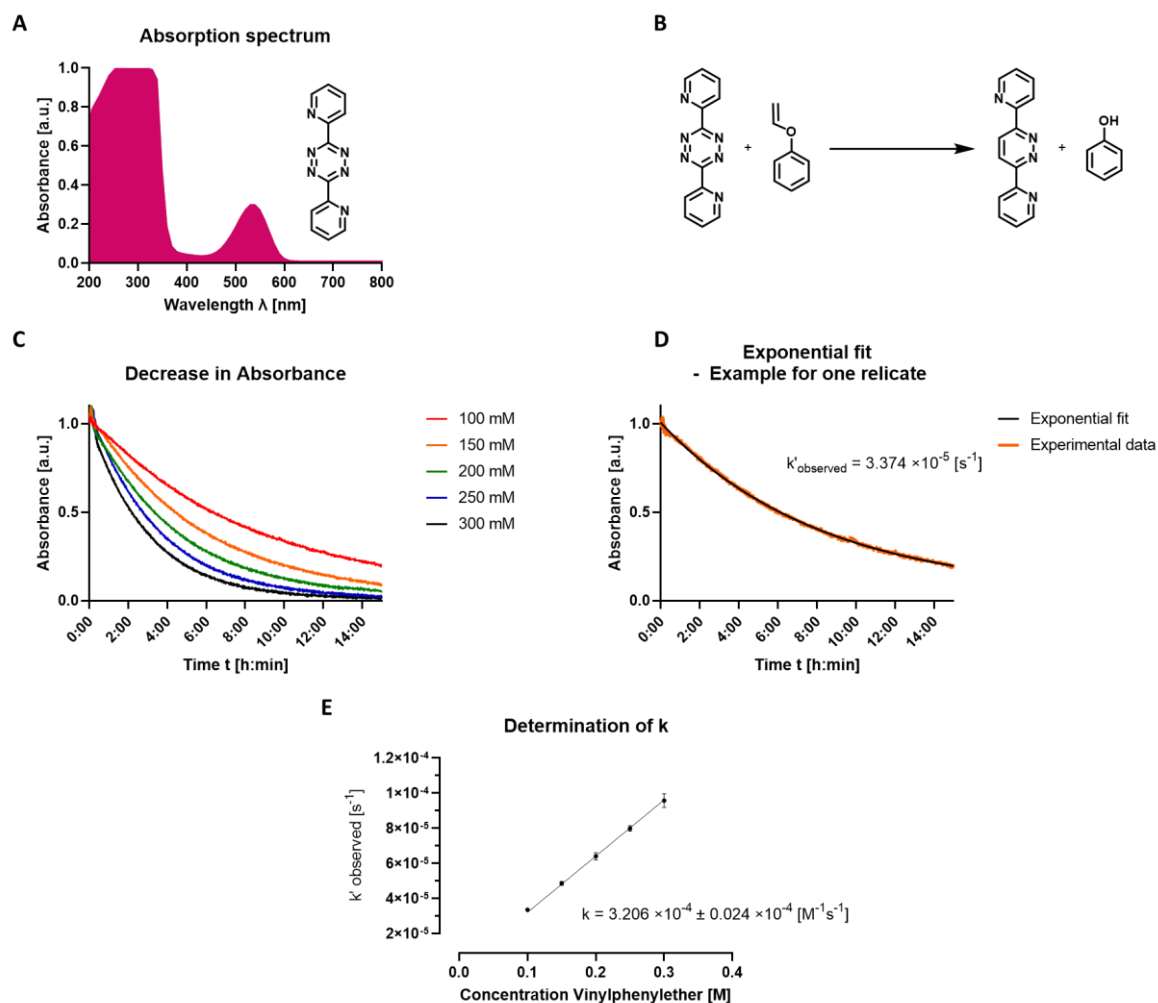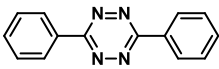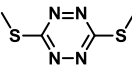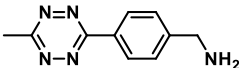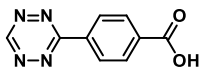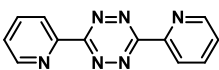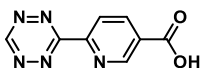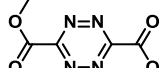
Figure 49: Overview of the process determining the rate constant *k* exemplified on the reaction between tetrazine **Tz5** and phenyl vinyl ether. A) Absorption spectrum of tetrazine **Tz5**; B) IEDDA reaction between tetrazine **Tz5** and phenyl vinyl ether. Reactions were performed in DMSO with 10% H_2O; C) Measured decrease in absorbance at $\lambda = 510$ and 540 nm (only decay at 540 nm depicted) upon reaction of tetrazine **Tz5** (final concentration 1 mM) with phenyl vinyl ether for final phenyl vinyl ether concentrations of 100 mM, 150 mM, 200 mM, 250 mM, 300 mM plotted over time; D) Determination of *k*'$_{observed}$ via an exponential fit. Data only shown for one replicate for clarity reasons; E) *k*'$_{observed}$ plotted against the concentration of phenyl vinyl ether. Final *k* determined by the slope of the resulting linear function.

First, the tetrazines were reacted with a 100- to 300-fold excess of phenyl vinyl ether. Since the tetrazines are compounds with an intense violet to pink color (Figure 49A) due to the heteroaromatic system, the course of the reaction can be monitored on the basis of the decrease in UV/Vis absorption. The fact that the pyridazine product absorbs light at other wavelengths significantly simplifies the measurement.

The decrease in absorbance was measured at five different phenyl vinyl ether concentrations (100, 150, 200, 250, and 300 nM) over a period of 15 h in time intervals of 1 min at 25 °C. All measurements were performed in triplicates. (Figure 49C) The normalized absorbances were plotted versus time, showing the expected decrease over time. Each decrease in

absorbance over time can be described by a simple exponential decay, thus a rate constant $k'_{observed}$ can be deduced from the corresponding curve function (Figure 49D). This set of observed rate constants ($k'_{observed}$) can in turn, be plotted against the phenyl vinyl ether concentrations used, resulting in a linear function. The slope of this linear function is equal to the final rate constant k (Figure 49E). All final rate constants are summarized in Table 6.

Table 6: Rate constants of the reaction between phenyl vinyl ether and tetrazines **Tz1, Tz2, Tz3, Tz5, Tz4, Tz6, Tz7**.

Tetrazine		k [M^{-1} s^{-1}]
Tz1		No reaction
Tz2		No reaction
Tz3		$4.015 \times 10^{-5} \pm 0.206 \times 10^{-5}$
Tz4		$1.998 \times 10^{-4} \pm 0.048 \times 10^{-4}$
Tz5		$3.206 \times 10^{-4} \pm 0.024 \times 10^{-4}$
Tz6		$1.725 \times 10^{-3} \pm 0.080 \times 10^{-3}$
Tz7		Not stable under measurement conditions

No rate constant could be determined for tetrazine **Tz1** since no absorbance decay could be detected. This was to be expected because **Tz1** already showed no reaction after 18.5 h in the previously discussed NMR experiments. Also, tetrazine **Tz2** did not show any decrease in absorption over time. Since the measurements were performed in DMSO and 10% H_2O, the water stability of the compound was further investigated to ensure the steady absorption level was not due to any decomposition of the tetrazine. For this purpose, an NMR probe of **Tz2** was prepared using water-contaminated DMSO-d_6 at t = 0 and after 1 day. However, no change in spectra could be observed (Figure 50A). Additionally, the reaction with phenyl vinyl ether was also monitored via NMR. Here again, no change could be observed even after 3 days of reaction time (Figure 50B), thereby confirming that **Tz2** does not undergo a reaction with phenyl vinyl ether under these conditions.
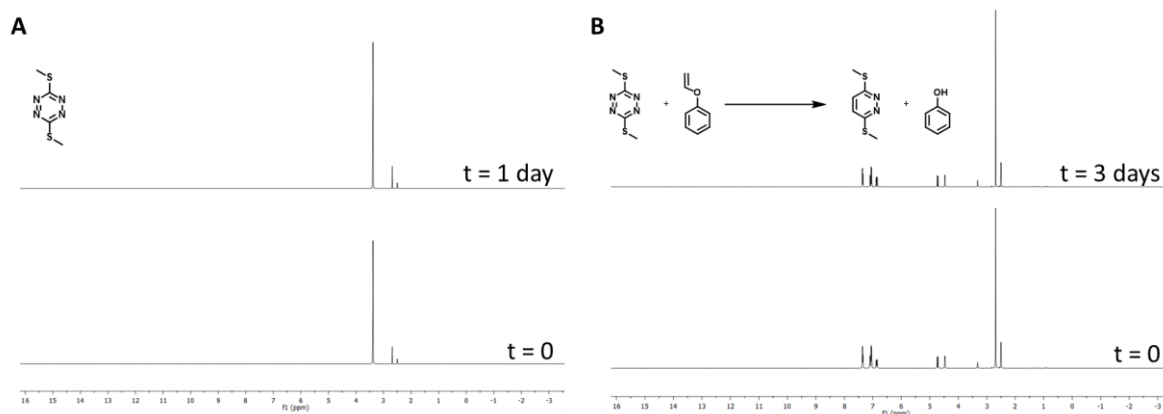
Figure 50: A) ^{1}H-NMR Spectra of tetrazine **Tz 2** in DMSO-d$_6$ and water at t = 0 and after 1 day; B) ^{1}H-NMR Spectra of a mixture of tetrazine **Tz 2** and phenyl vinyl ether.

Tz3 is the first tetrazine electron poor enough to react notably with phenyl vinyl ether, thereby allowing to determine a rate constant. However, the rate constant of $4.015 \times 10^{-5} \pm 0.206 \times 10^{-5}$ M^{-1} s^{-1} is the lowest one out of the tested compounds, with a difference of about one order of magnitude to the next tetrazine, the benzoic acid-substituted tetrazine **Tz4** with a rate constant of $1.998 \times 10^{-4} \pm 0.048 \times 10^{-4}$ M^{-1} s^{-1}. The reaction could be further accelerated by introducing two pyridine residues to the tetrazine core, yet this increase was not as dramatic as the previous change. The highest rate constant of $1.725 \times 10^{-3} \pm 0.080 \times 10^{-3}$ M^{-1} s^{-1} was observed for the nicotinic acid substituted tetrazine **Tz6**. This displays an ~43-fold improvement compared to **Tz3**. Yet, the electron poorest tetrazine used in this study is **Tz7**, which is why it is expected to give the highest reaction rate. Nevertheless, no rate constant could be determined since **Tz7** decomposed in the presence of water. For this reason, all measurements were complemented with stability controls in DMSO/10% water at room temperature (Figure 51), showing the fast decrease in signal for **Tz7**, whereas tetrazines **Tz1** to **Tz5** did not encounter significant changes over the investigated time period. **Tz6**, which showed the highest reaction rate measured, encountered slight decay in water (complete decay over 14h). While this is the case, the reaction of the vinyl with **Tz6** went to completion within approx. 2h for all concentrations tested. Thus, the slight decay in water would give enough room for applications especially compared to **Tz7**, which should complete decay within approx. 20 min.

These findings suggest that the right choice of the tetrazine can significantly accelerate the IEDDA, but the stability towards water must also always be taken into account.
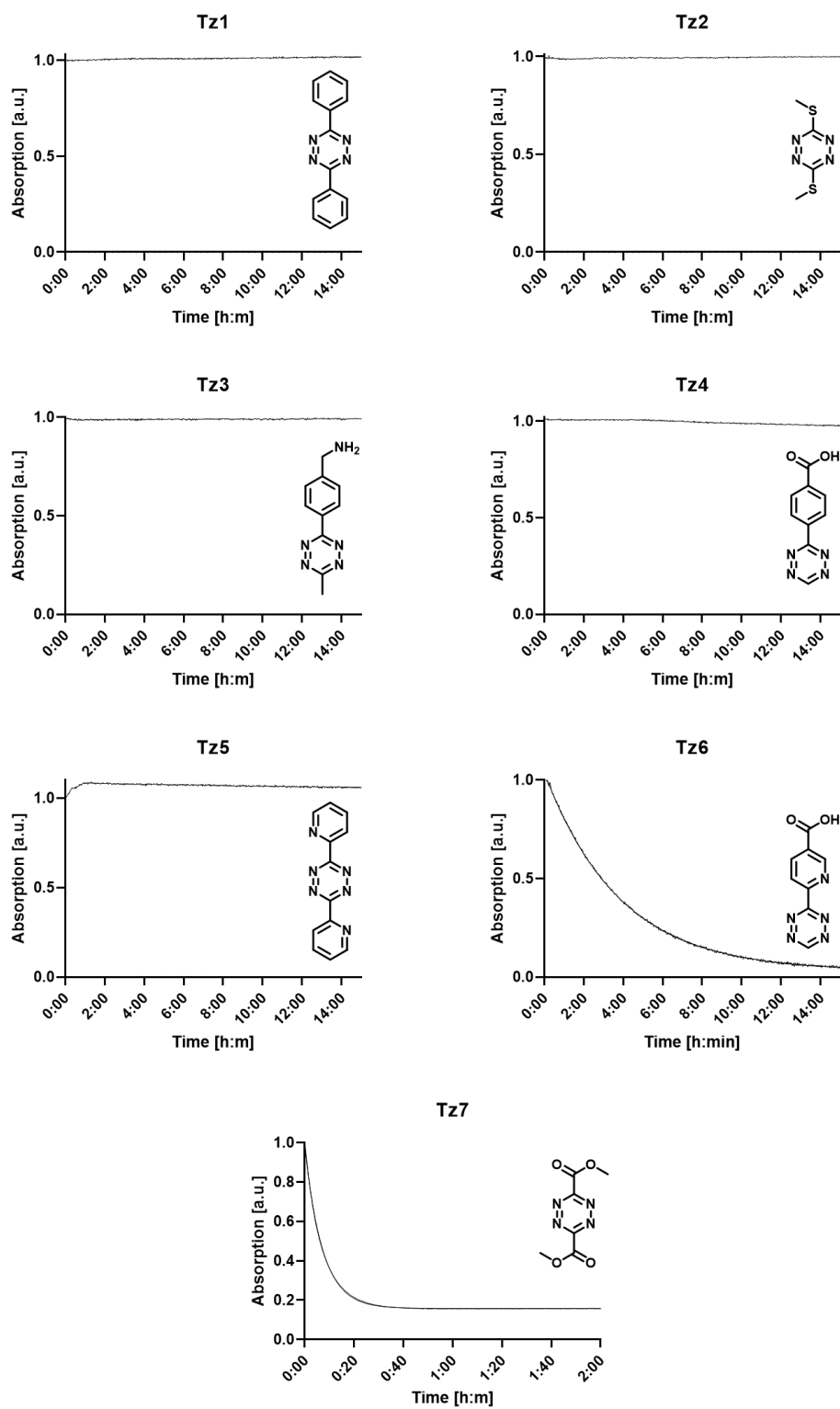
Figure 51: Stability controls for all tetrazines tested.

3.3.4   Synthesis towards a novel linker system

The new IEDDA-based TML described so far has in its previously discussed form mainly the role of a masking group. This section will focus on extending this TML system to a linker system. For this purpose, a new functional group has to be inserted into the scaffold, which allows conjugations with other molecules (Figure 52A). Depending on the application, these other molecules may be carrier systems (siderophores, antibodies, etc.) or functionalized surfaces.
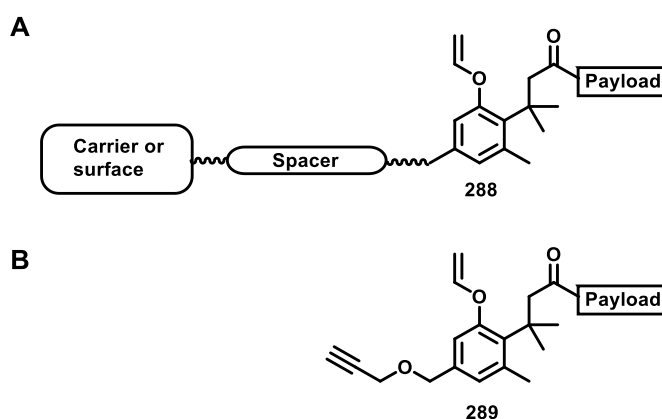
Figure 52: A) Schematic depiction of the extension of the TML to a true linker system; B) TML extended through an alkyne connected via an ether bridge.

When selecting the new functional group to be added to the framework, two criteria particularly must be taken into account. First, orthogonality to the existing functional groups must be ensured. Second, the conjugation step should be straightforward, fast, high yielding, selective, and suitable for a large substrate class. Based on these criteria, the CuAAC reaction presents a suitable choice for the conjugation step. Thus, the core structure was extended by an alkyne group.

The synthesis of the linker-extended TML should be based on the pathway to the IEDDA-triggered TML previously developed in the Brönstrup group. For the first attempt to introduce a linker, one of the two aromatic methyl groups should be brominated and subsequently substituted with propargyl alcohol (Figure 52B). In principle, the substitution should be performed immediately after the bromination, since the benzylic bromide is very reactive and not sufficiently stable to be carried through several steps. Within the original synthetic route different intermediates were identified at which the bromination could be carried out (Scheme 74).
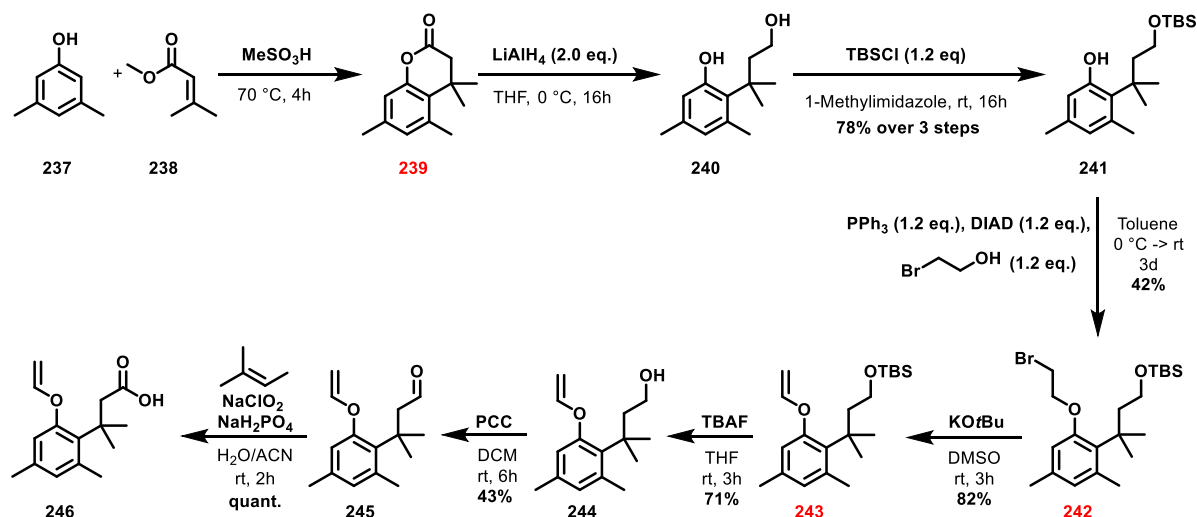
Scheme 74: Original synthetic route of the vinyl TML with potential sites for bromination highlighted in red.

One possibility is the bromination of the lactone intermediate **239**. However, the subsequent reduction conditions are very harsh. Moreover, this would be a modification already in the second step of the synthesis so that the advantages of a late-stage modification cannot be exploited. Two further possibilities are offered by the bromination of intermediates **241** and **243**. In all three cases (**239**, **242**, **243**), there is a risk of bromination at the core instead of the side chain. The electrophilic substitution rate depends on the ring's electron density and, thus, on the substituents of the ring and their mesomeric and inductive properties. **242** and **243** differ in their substituents only at the phenolic position. Based on the mesomeric structures it is clear that the alkyl ether **242** leads to a higher electron density in the ring than the vinyl ether **243**. For this reason, the problem of side reactions, i.e., bromination at the core, is expected to be more pronounced with the alkyl ether. In addition, the bromination of intermediate **243** is slightly advantageous, since it is a later functionalization within the route.

However, the vinyl ether complicates a selective bromination of intermediate **243**, since a bromination at the double bond can take place under various reaction conditions resulting in unwanted side products. After considering all options, it was therefore decided to attempt a bromination of intermediate **242**.

The synthesis of the new linker system began with the Friedel-Crafts alkylation of phenol **237**, which subsequently led to the formation of the lactone **239**. Successive reduction with LiAlH₄ yielded **240**. By TBS-protecting the primary alcohol, **241** could be obtained in 78% yield over 3 steps (Scheme 75).
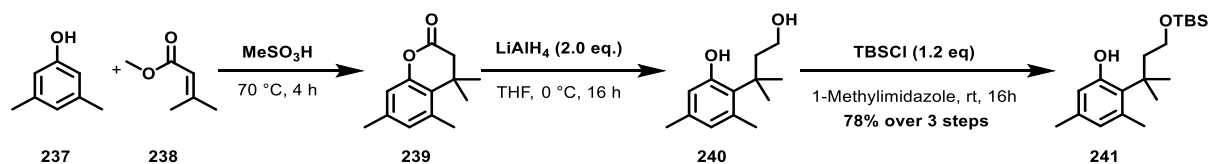
Scheme 75: Synthesis of intermediate **241** starting from phenol **237** via a Friedel-Crafts alkylation followed by reduction and TBS-protection.

Various conditions summarized in Table 7 were tested to optimize the ether formation in the next step. First, an S_N2 reaction was attempted with 1,2-dibromoethane and potassium carbonate (Table 7, entry 1) as the base. Since no conversion was observed under these conditions, the phenol was treated with a stronger base, i.e., *n*-BuLi, to form the phenolate followed by addition of 1,2-dibromoethane. Yet, again no product could be obtained (Table 7, entry 2). Even with a significant excess of *n*-BuLi (Table 7, entry 3), no product formation was observed.

Since an excess of *n*-BuLi ruled out incomplete deprotonation, the Mitsunobu reaction was investigated next, although in a previous work it could already be shown that the desired product only gets formed with poor yields (approx. 20%) (Table 7, entry 4). In addition to the reaction conditions, the workup was optimized. In particular, the use of MnO_2 during the workup led to an improvement in yield since interfering residual triphenylphosphine was oxidized to easily separable triphenylphosphine oxide. With the newly developed procedure (Table 7, entry 5), the yield could be increased to 42%, which eliminated the need to recover the starting material and react it again. Nevertheless, it is still possible to reisolate the unreacted starting material.

Table 7: Conditions tested for the phenolic ether formation.

	Conditions	Yield
1	K_2CO_3 (200 eq.), $(CH_2)_2Br_2$ (10 eq.) DMF, 50 °C, 24 h	No product obtained
2	*n*-BuLi (0.95 eq.), $(CH_2)_2Br_2$ (10 eq.) THF, -78 °C → rt, 24 h	No product obtained
3	*n*-BuLi (10 eq.), $(CH_2)_2Br_2$ (10 eq.) THF, -78 °C → rt, 24 h	No product obtained
4	I. PPh_3 (1.5 eq.), DIAD (1.5 eq.), 0 °C, toluene, 30 min II. starting material, $Br(CH_2)_2OH$ (1.5 eq.), toluene, 24 h	Low conversion (TLC), not isolated
5	PPh_3 (1.2 eq.), DIAD (1.2 eq.), $Br(CH_2)_2OH$ (1.2 eq.) Toluene, rt, 3 d	42%

In the next step, a Wohl-Ziegler bromination was performed. Although this implies that radical conditions were chosen, a noteworthy fraction of the aromatic bromide was formed. For this reason, conditions were screened to suppress the competitive electrophilic addition to the aromatic ring. For the optimization, 3,5-dimethylanisole (**290**) was used as the model compound (Scheme 76).
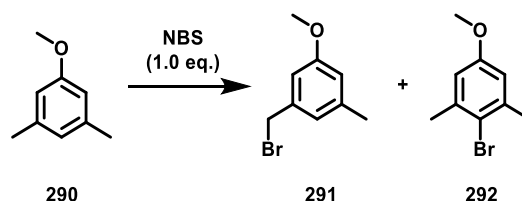
Scheme 76: Model bromination reaction deploying 3,5-dimethylanisol (**290**) as the starting material. The desired product **291** and the undesired side product **292** are shown.

Since the radical character of the reaction had to be increased to obtain higher yields of the aliphatic bromide **291**, various equivalents of different radical initiators, temperatures, and solvents were tested. A compilation of tested reaction conditions can be found in Table 8.

Table 8: Conditions tested to enhance the desired Wohl-Ziegler product using 3,5-dimethylanisol as a test compound and NBS (1.0 eq.).

	Conditions	Product	Side product	Starting material
1	Dibenzoylperoxide (0.1 eq.), ACN, 88 °C, 16 h	0%	73%	27%
2	Dibenzoylperoxide (0.1 eq.), CCl₄, 92 °C, 2 h	25%	6%	69%
3	Dibenzoylperoxide (0.2 eq.), CCl₄, 92 °C, 4 h	28%	4%	68%
4	Dibenzoylperoxide (0.5 eq.), CCl₄, 92 °C, 4 h	13%	11%	76%
5	AIBN (0.01 eq.), CCl₄, 92 °C, 1 h	70%	14%	15%
6	AIBN (0.1 eq.), CCl₄, 92 °C, 1 h	61%	34%	5%
7	AIBN (0.2 eq.), CCl₄, 92 °C, 1 h	73%	20%	7%
8	AIBN (0.5 eq.), CCl₄, 92 °C, 1 h	58%	37%	5%

All reactions were carried out with one equivalent of 3,5-dimethylanisole and one equivalent of NBS. Yields were determined by ^{1}H NMR spectroscopy of the crude mixture. In particular, changing the solvent to CCl₄ and replacing the radical initiator dibenzoylperoxide (DBO) with AIBN led to a significant improvement in yield. The greatly differing yields

with the two radical initiators can be justified by the different thermal decomposition rate constants. The thermal decomposition rate constant k_d indicates how fast the molecule dissociates into two radicals at a defined temperature. The higher the decomposition rate constant, the faster the formation of the radicals and the more dissociated product is expected. As shown in Table 9, AIBN has higher decomposition rates compared to DBO, thus having a higher rate of starter radicals present in the mixture, which led to the favored formation of the desired benzylic bromide.

Table 9: Decomposition rate constants k_d for AIBN and DBO.[244]

Initiator	Temperature	k_d (s^{-1})
AIBN	50	2.2×10^{-6}
	70	3.2×10^{-5}
	100	1.5×10^{-3}
DBO	60	2.0×10^{-6}
	78	2.3×10^{-5}
	100	5.0×10^{-4}

The decomposition rate constants are temperature dependent and favor dissociation at high temperatures (Table 9). Consequently, high reaction temperatures were chosen. The optimized reaction conditions obtained using the model system (Table 8, entry 7) were applied to the bromination of **242** (Scheme 77). A mixture of both possible regioisomers was obtained. This resulted in a 50% decrease in the yield of the preferred product. Yet, it is debatable which of the two products is the desired one, since it is irrelevant for the function of the linker on which side the alkyne arm is located. Depending on the application, there may be a preference for one isomer over the other. However, such a preference was not known at this stage, so both isomers were considered to be equally desirable. Furthermore, by preparing both isomers, any effects on the lactonization process based on the steric differences could be investigated.
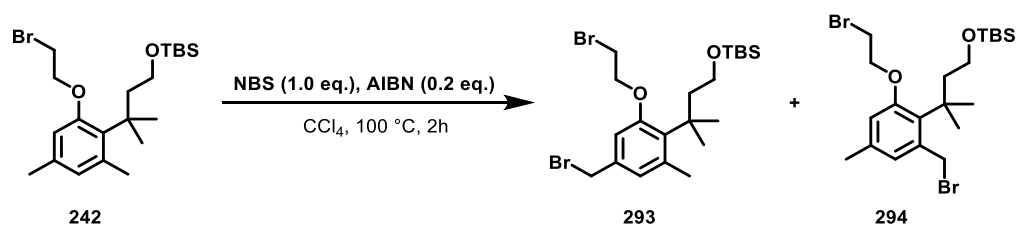
Scheme 77: Wohl-Ziegler bromination of **242** resulting in the two regioisomers **293** and **294**.

The separation of the two regioisomers was not possible at this stage, so that the subsequent Williamson ether synthesis was carried out with the mixture (Scheme 78). In this step the two regioisomers were separable and could be isolated in 6% yield over two steps, respectively, without further optimization of the reaction conditions. An identification of the regioisomers was possible by means of characteristic couplings in the NOESY spectra between the geminal methyl groups and the methyl or methylene group in *ortho*-position. The respective segment of the NOESY spectra is shown in Figure 53.
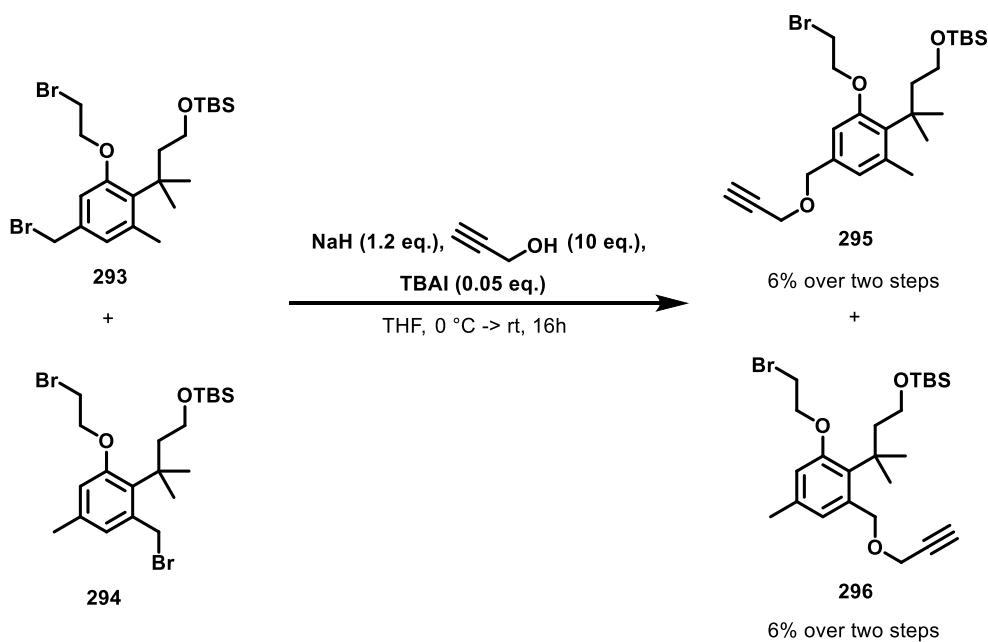
Scheme 78: Introduction of the alkyne tag using Williamson ether synthesis.
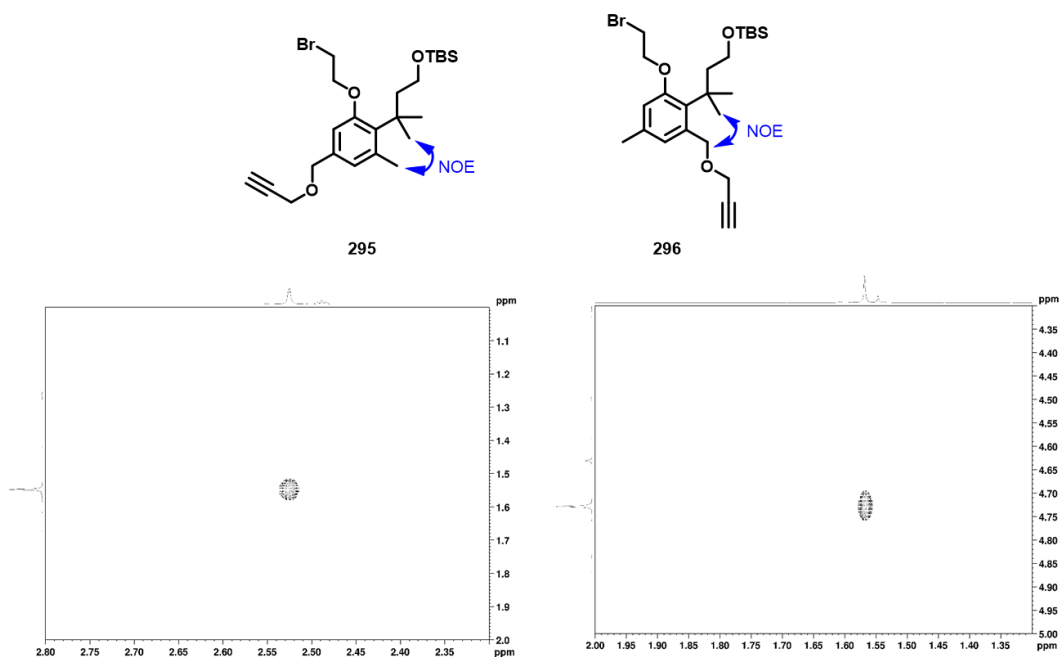
Figure 53: Observed nuclear Overhauser effects (NOE) and corresponding NOESY spectra of **295** (left) and **296** (right).

In the next step, KO^{t}Bu was used to eliminate hydrogen bromide and thus obtain the vinyl group or trigger. In addition to the elimination, a simultaneous isomerization of the triple bond to the allene was observed (Scheme 80), which can be seen in the ^{13}C-NMR spectrum from the characteristic shift of the H$_2$CC*C*H-carbon at 194 ppm. In addition, analysis by HMBC shows the correlations between the protons of the allene with the carbon at 194 ppm. Analysis by COSY and coupling constants also pointed towards allene formation. The desired alkyne could not be identified in the crude reaction mixture.
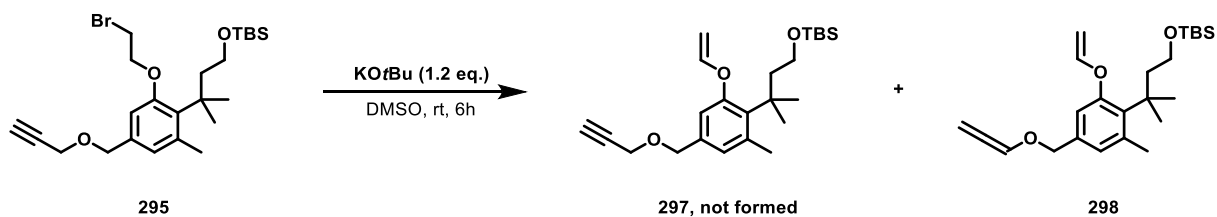
Scheme 79: Introduction of the vinyl group via an elimination using KO^{t}Bu yielding the undesired allene **298** instead of the desired alkyne **297**.

There are several ways to address this issue. One way to overcome isomerization is the optimization of the elimination conditions, e.g. by using a weaker base. Thus, several bases, equivalents, solvents, and reaction temperatures could be screened. Another approach is a change in the molecular structure to prevent isomerization by design. This could be realized by substituting the ether oxygen atom with a methylene unit, which should increase the pK_A

value of the adjacent methylene group and therefore prohibit the isomerization under basic conditions.

3.4 Summary and outlook

The Trimethyl lock represents a molecular release system with a vast spectrum of applications. Brönstrup and co-workers developed a TML system that utilizes a vinyl ether as the masking group of the phenol. Initial experiments showed that this TML system is not triggered on a reasonable time scale.

In this work, the underlying kinetic problem was identified and evaluated using a test system. The TML was mimicked by phenyl vinyl ether and treated with diphenyltetrazine. Monitoring this reaction via NMR provided information about the rate-limiting step, which could be identified as the inverse electron demand Diels-Alder.

On this basis, the molecular design was reassessed in order to accelerate the reverse electron demand Diels-Alder reaction. Two potential strategies were identified, namely enhancing the electron density at the dienophile, i.e., the vinyl, or reducing the electron density at the diene, i.e., the tetrazine. Since the synthetic expenditure of preparing several TML derivatives differs greatly from preparing a set of different tetrazines, the focus was set on the synthesis of electron-poor tetrazines.

Accordingly, the molecular design of the tetrazines was adapted. A variety of tetrazines was synthesized. Attention was paid to decreasing the electron density stepwise since an increase in reactivity comes with a decrease in stability.

A first evaluation of the kinetic potential was performed using NMR analysis, monitoring the IEDDA between dimethyl tetrazine dicarboxylate as well as diphenyltetrazine and phenyl vinyl ether. The usage of diphenyltetrazine, possessing a relatively high electron density, lead to no reaction after 18.5 h. However, if this tetrazine is exchanged by the electron-poor dimethyl tetrazine dicarboxylate, a conversion of about 40 to 50% after 5 min can be observed. This difference shows the vast potential in tuning the speed of a reaction by the appropriate choice of the tetrazine substituents.

Further kinetic studies were conducted evaluating the influence of different tetrazines substituted with electron-withdrawing groups (Figure 54). Initial experiments showed that the IEDDA between a tetrazine and a vinyl group does not follow 0th, 1st, or 2nd order. Therefore, the kinetic studies were carried out under pseudo-first-order conditions with varying excess of phenyl vinyl ether. Considering the resulting measuring time if studied by NMR, the reaction monitoring was changed to a more time-efficient UV/Vis-based evaluation. The rate constants of the different tetrazines were determined, and the stability

was assessed. This gave rise to a toolbox of tetrazines with different rate constants, allowing selection of the appropriate tetrazine depending on the application-specific requirements.
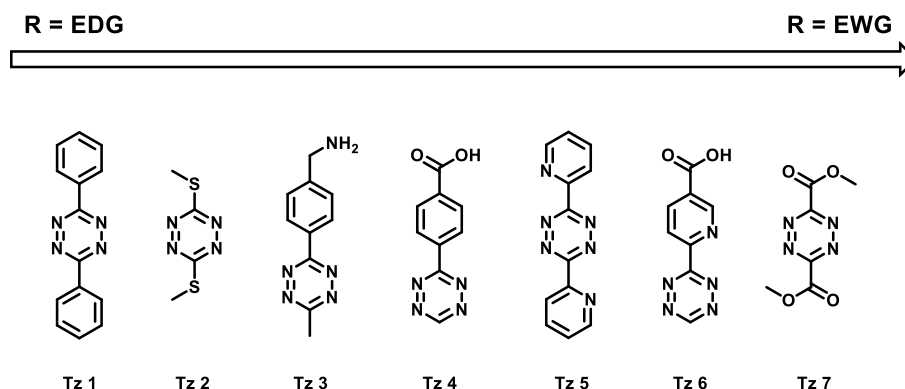
Figure 54: Kinetically evaluated tetrazines in this study.

In order to extend the deployability of the previously developed vinyl-substituted TML to a true linker, a new synthetic route was developed. The key task was to introduce a new moiety that allows further conjugation and thus displays another handle of the TML core. In this work, the possibility of extending the TML system by the introduction of an alkyne moiety, which allows for further conjugation via a CuAAC, was studied.

First, the formation of the phenol ether was optimized. Williamson ether synthesis conditions/S_N2 and Mitsunobu conditions were tested, varying the pK_A of the used base, the equivalents of the base, the electrophile for the S_N2 conditions as well as the equivalents of the reagents, the temperature and the stirring time for the Mitsunobu reaction. The best results were achieved using the Mitsunobu reaction, which was optimized from 0% to 42%. The alkyne was introduced by the bromination of the methyl side chain, followed by subsequent substitution of the resulting benzyl bromide with propargyl alcohol. The simplified model reagent 3,5-dimethylphenylmethylether was utilized to optimize the Wohl-Ziegler bromination by improving the ratio between the remaining starting material, the core bromination, and the desired side chain bromination. The parameters varied included the temperature, the order of addition, the radical initiator, and the amount of radical initiator. The most significant improvement was obtained through the exchange of the radical initiator. The desired alkyne moiety was introduced next via a simple substitution reaction using propargyl alcohol as the nucleophile. Thus, the third functionality, i.e., the conjugation handle, was successfully introduced in this intermediate while the precursor for the trigger and the precursor for drug conjugation moiety remained in place.

In the subsequent step, the vinyl ether was successfully obtained by an elimination. Nevertheless, the basic conditions also lead to isomerization of the alkyne giving the undesired allene, thereby losing the essential alkyne functionality.

To circumvent the isomerization problem, several solutions can be explored. Such solutions include screening the elimination conditions, using different alkyne derivatives, as well as designing a different synthetic route.

Since the isomerization appears to be favored, the back-isomerization may be challenging. Hence, the formation of the undesired product must be suppressed in the first place. The calculated pK_A value of the terminal alkyne is 21, and the lowest pK_A of the resulting anion at the elimination site is 28.[245] Thus, selective deprotonation cannot be assumed. However, if a stronger base is deployed, the most acidic position, i.e., the alkyne, will be predominantly deprotonated. Hence, the isomerization to the allene may be prevented, as the deprotonation results in a negative charge at the alkyne, increasing the pK_A of the adjacent position. A second deprotonation might therefore occur at the phenolic ether, yielding the desired vinyl ether.

However, the step following the elimination is a deprotection of the primary alcohol using TBAF, which may be problematic since TBAF also has basic properties. This may lead to an unwanted isomerization in this step.

Apart from screening for the appropriate base, one can also overcome the isomerization by altering the alkyne functionality. On the one hand, introducing the alkyne using 3-butinol, which possesses an additional methylene group between the alkyne and the ether, would disrupt the conjugation of the alkyne and a potential deprotonation site at the methylene next to the ether (Scheme 80).
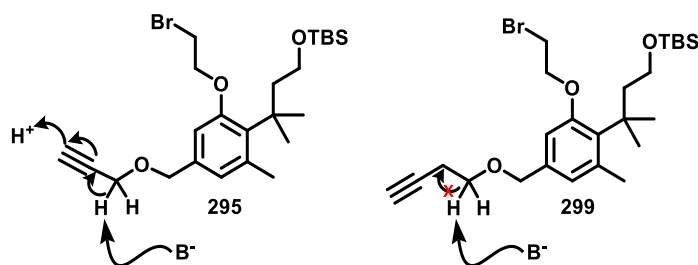
Scheme 80: Influence of a prolongation of the alkyne linker by a methylene group on the isomerization of the alkyne to the allene.

On the other hand, the electron-withdrawing effect from the oxygen atom responsible for the decreased pK_A of the adjacent methylene could be abolished by replacing the oxygen atom with a methylene group. The resulting increase in pK_A is likely to prevent any isomerization.

Finally, the synthesis could be performed via a different synthetic route. Such a route would be especially interesting if it is designed to circumvent the isomerization and, in addition, provides only one regioisomer. To achieve this, the alkyne moiety would need to be introduced in a different manner.

An alternative route could utilize an amide bond to introduce the alkyne. The underlying amine could be obtained by a nitration of the aromatic ring followed by a reduction (Scheme 81). This strategy would have the advantage of yielding only one regioisomer. Additionally, the key steps, i.e., the nitration and the reduction, do not need to be carried out sequentially since the nitro group is relatively inert and may be carried on throughout several steps. An early introduction of the nitro group may even have positive effects on the yield of the Misunobu reaction due to the increased acidity of the phenol. Introducing the alkyne via an amide coupling may also be interesting to avoid the low yielding Williamson ether synthesis of the previous route. However, the steric influence of the adjacent methyl groups on the yield of the amide coupling may not be underestimated.
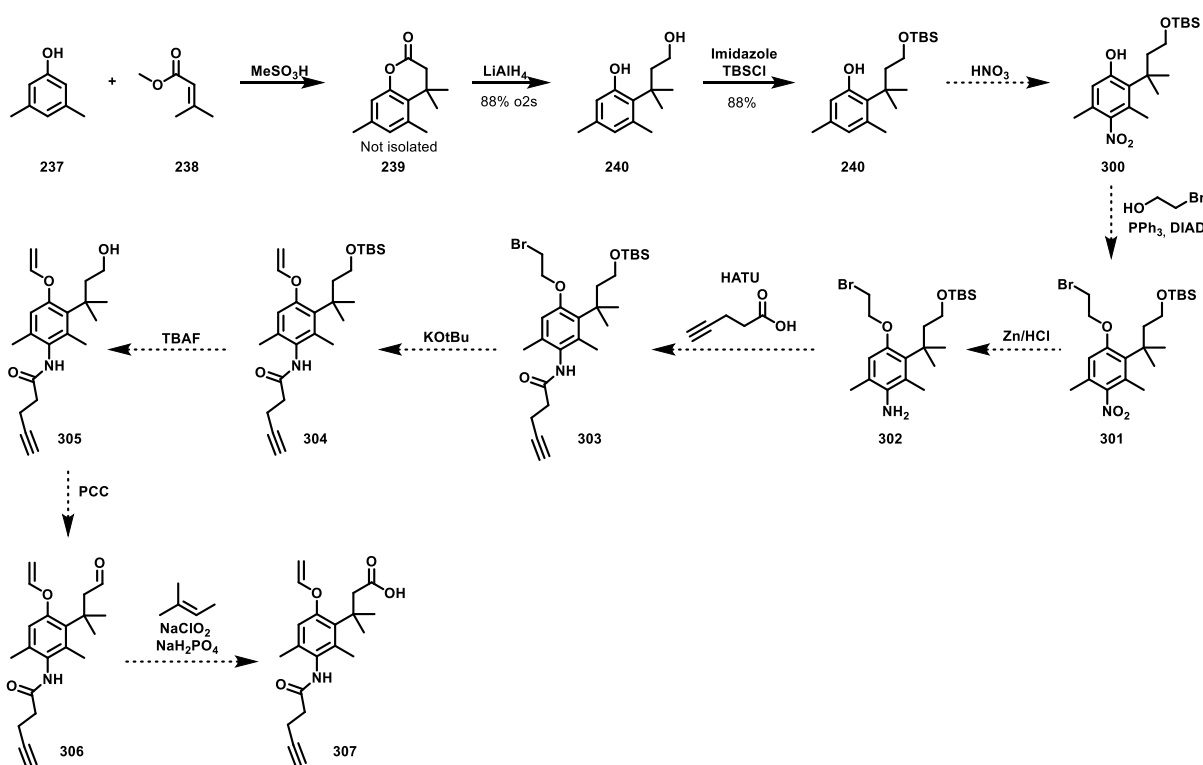
Scheme 81: Alternative synthetic route to an extended TML linker using an amide to introduce the alkyne linker.

Another approach utilizes a Sonogashira cross-coupling as the key step (Scheme 82). Hence, one could start from 3-bromo-5-methylphenol (**308**), performing the well-established Friedel–Crafts alkylation followed by lactonization, subsequent reduction, and TBS

protection. The alkyne would then be introduced using the Sonogashira reaction. From here, the desired linker could be obtained in five steps. If a longer side chain is desired, the Sonogashira reaction could also be replaced by a different cross-coupling (e.g. Negishi or Kumada) utilizing an organometallic nucleophile for the alkylation. Both synthetic approaches would overcome the isomerization issue and lead to only one regioisomer.
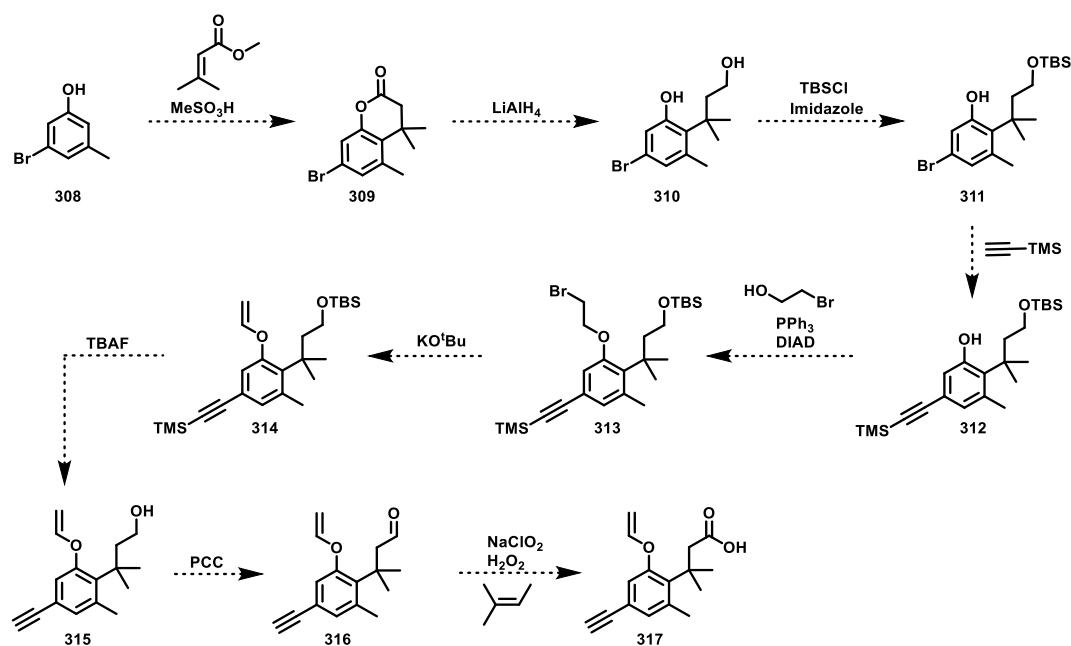
Scheme 82: Alternative synthetic route to an extended TML linker starting from 3-bromo-5-methylphenol and introducing the alkyne either via a Sonogashira or a Lewis acid catalyzed Grignard reaction.

3.5 Materials and methods

3.5.1 Chemical synthesis

3.5.1.1 General remarks

Unless stated otherwise, all reagents were purchased from commercial suppliers and used without further purification. All solvents used for workup and purification were of HPLC grade. Anhydrous solvents were used for all reactions in which water was not also used as a solvent and in which the total amount of organic solvent did not exceed 100 mL. All anhydrous solvents were purchased from commercial suppliers. Moisture-sensitive reactions were performed under argon atmosphere in dried glassware. Reactions were monitored by TLC, LC-MS or NMR. The removal of organic solvents took place using rotary evaporators at 30 °C, the removal of water at 40 °C. For lyophilization of substances, the solutions in question were frozen with liquid nitrogen and freeze-dried on an Alpha 2-4 LSCbasic (CHRIST) instrument. Centrifugations were performed using a Universal 32 R centrifuge (HETTICH). If yields are given for unpurified intermediates, this is only done for the purpose of calculating the amount of reagents needed for the next synthesis step.

3.5.1.2 Purification methods

3.5.1.2.1 Column chromatography

Column chromatographic purifications were carried out on silica gel (Si 60, 40 - 63 µm particle size) from the producer MERCK under elevated pressure (flash chromatography). The eluents used are listed after the indicated retention factors.

3.5.1.2.2 Automated column chromatography

Automatic preparative column chromatography was carried out on a Grace Reveleris® X2 instrument (BÜCHI).

Automatic preparative column chromatography with C18 Silica was performed on a Pure C-850 instrument (BÜCHI).

3.5.1.2.3 HPLC

Purifications by HPLC were performed on a Dionex Ultimate instrument (THERMO FISHER SCIENTIFIC). Unless stated otherwise, the following C18 separation columns (PHENOMENEX) were used:

- Luna 5 μm, 100 Å, 00G-4252-PO-AX.
- Gemini 10 μm, 110 Å, 00G-4436-PO.
- Gemini 10 μm, 110 Å, 00G-4436-NO.

Product containing fractions were combined, diluted with milliQ H_2O (min. 1:1/solvent:H_2O), frozen and lyophilized.

3.5.1.2.4 Preparative thin layer chromatography

Preparative thin layer chromatography was performed on pre-coated glass plates (Merck TLC Silicagel 60 F254, 1.05715.0001, 20×20 cm, max. 10-15 mg/plate and Analtech Uniplate Silica gel GF Z51305-9, 20×20 cm × 2 mm, max 100-150 mg/plate). Eluent or eluent-mixtures used are reported in parentheses. Compounds were visualized by observation under UV light ($\lambda = 254$ or 366 nm). Compound containing silica gel fractions were scratched from the plate with a scalpel, crushed to small pieces and compounds were dissolved by appropriate solvent mixtures.

3.5.1.3   Analytical methods

3.5.1.3.1   Thin layer chromatography

For thin layer chromatography TLC plates (silica gel 60 F_{254}, on aluminum) from the manufacturer MERCK were used. TLC plates were visualized by UV light ($\lambda = 254$ nm/ $\lambda = 365$ nm), or using staining reagents. A potassium permanganate solution (2 g $KMnO_4$, 6.5 g K_2CO_3, 200 mL water) or Iodine served as staining reagents.

3.5.1.3.2   NMR

Nuclear Magnetic Resonance (NMR) spectra were recorded on a BRUKER Avance III 500 with the probe head PABBO BB/^{19}F-^{1}H/D Z-GRD (500 MHz für ^{1}H, 125 MHz für ^{13}C) or a BRUKER Avance III HD 700 with the probe head CPTCI ^{1}H-^{13}C/^{15}N/D Z-GRD (700 MHz for ^{1}H, 176 MHz for ^{13}C) at room temperature. Samples were measured as solutions in deuterated solvents. Chemical shifts are reported in ppm relative to solvent signal. Multiplicity is indicated as follows: s (singlet); bs (broad singlet); d (doublet); t (triplet); q (quartet); quin (quintet), m (multiplet); as well as combination of those e.g. dd (doublet of doublets), etc.

3.5.1.3.3   Mass spectrometry

Low resolution mass spectrometry (LRMS) data were recorded using an AGILENT 1100 HPLC system equipped with DAD detector and an API 150 EX quadrupole mass detector with electrospray ionization (ESI) (ACN-H_2O + 0.05 % TFA)

High resolution mass spectrometry (HRMS) data were recorded using a DIONEX Dionex Ultimate 3000 HPLC system equipped with a DAD detector and a BRUKER maXis HD QTOF mass detector with electrospray ionization (ESI). Samples were directly injected via an Ultimate 3000RS autosampler (THERMO FISHER SCIENTIFIC). The mass-to-charge ratio *m/z* is being reported.

3.5.1.3.4 UV/Vis

UV/Vis data were recorded using a PowerWave™ microplate spectrophotometer (BioTek® Instruments, Inc.) with Gen5™ version 2.09.2 software. Samples were measured in 96 well plates (Greiner Bio-One GmbH, MICROPLATE, 96 WELL, PS, F-BOTTOM (CHIMNEY WELL) µCLEAR®, BLACK, MED. BINDING).

3.5.1.4 Kinetic measurements

Rate constants k for different tetrazines were measured under pseudo first order conditions (Figure 55) with a 100- to 300-fold excess of phenylvinylether in DMSO with 10% water by following the exponential decay in UV absorbance of the tetrazine at 510 and 540 nm over 15 h in 1 min intervals. Measurements were carried out at 25 °C shacking for 5 s before each measurement. Stock solutions of each tetrazine (2 mM) and of phenylvinylether (200, 300, 400, 500, 600 mM) in DMSO with 10% water were prepared. Equal volumes of the respective stock solutions were mixed leading to a final concentration of 1 mM of the respective tetrazine and final concentrations of 100, 150, 200, 250, 300 mM of phenylvinylether, corresponding to 100 to 300 equivalents.

Data were fit to a single-exponential equation. Each measurement was carried out in triplicates. The mean of the observed rates k' was plotted against the concentration of phenylvinylether and fit to a linear equation. The rate constant was obtained from the slope of the plot. All data processing was performed using GraphPad Prism 9 version 9.1.2.

$$A + B \rightarrow C \qquad \text{Assumption: } [B] \gg [A] \rightarrow [B] \approx const.$$

$$\frac{-d[A]}{dt} = k\,[B][A] \quad \text{with} \quad k[B] = k' \quad \Leftrightarrow \quad k = \frac{k'}{[B]}$$

$$\frac{-d[A]}{dt} = k'\,[A]$$

$$[A] = [A]_0 e^{-k't}$$

Figure 55: Mathematical description of pseudo first order reaction kinetics.

3.5.1.5 Synthesis procedures

3,6-di(pyridin-2-yl)-1,2,4,5-tetrazine (186)
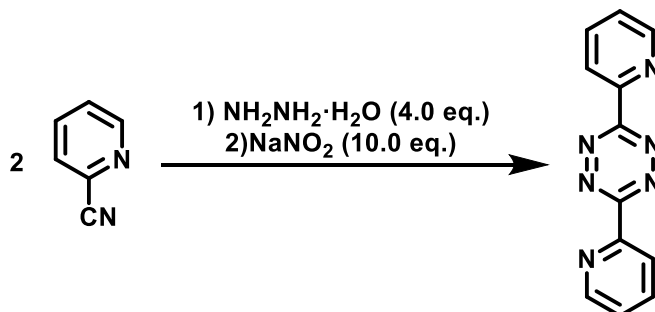
Hydrazine hydrate (3.40 mL) was added dropwise to picolinonitrile (354 mg, 3.40 mmol, 1.0 eq.). The reaction was heated to 80 °C and stirred for 35 min. After cooling down to room temperature sodium nitrate (2.89 g, 34.0 mmol, 10.0 eq.) in water (5 mL) was added to the reaction. Afterwards the product was precipitated by adding HCl (2 M) until the pH was ca. 3. The pink solid was separated by filtration. The filtrate was washed with HCl (0.5 M) and H_2O. The crude was purified by column chromatography giving 3,6-di(pyridin-2-yl)-1,2,4,5-tetrazine (0.08 g, 0.34 mmol, 10%) as a pink solid.

TLC: R_f = 0.48 (MeOH/DCM 10%) [UV]

^{1}H NMR (500 MHz, DMSO): δ [ppm] = 8.95 (ddd, J = 4.7, 1.6, 0.8 Hz, 1H), 8.62 (d, J = 7.9 Hz, 1H), 8.17 (td, J = 7.8, 1.8 Hz, 1H), 7.74 (ddd, J = 7.6, 4.7, 1.1 Hz, 1H).

^{13}C NMR (126 MHz, DMSO): δ [ppm] = 163.3, 150.7, 150.1, 137.9, 126.7, 124.4.

HRMS (ESI) *m/z*: ($C_{12}H_9N_6^+$ [M+H]$^+$)   calc.: 237.0883

                                                              found: 237.0884

4-(1,2,4,5-tetrazin-3-yl)benzoic acid (274)
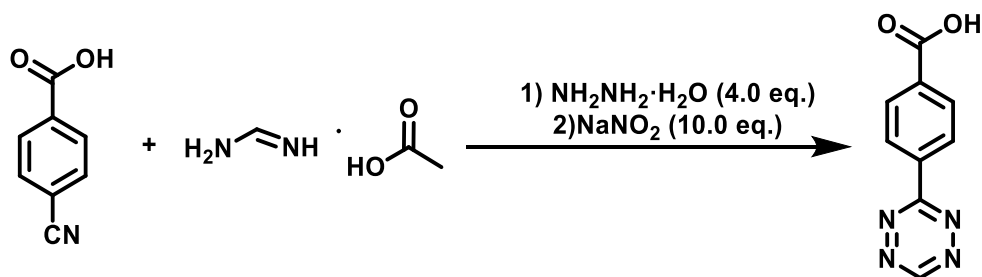
Hydrazine hydrate (34.0 mL) was added dropwise under Ar to Cyanobenzoic acid (5.00 g, 34.0 mmol, 1.0 eq.) and formamidine acetate (17.7 g, 170 mmol, 5.0 eq.). The reaction was heated to 80 °C and stirred for 35 min. After cooling down to RT sodium nitrate (11.7 g, 170 mmol, 5.0 eq.) in water (34 mL) was added to the reaction. Afterwards the product was precipitated by adding HCl (2 M) until the pH was ca. 3. The pink solid was separated by filtration. The filtrate was washed with HCl (0.5 M) and H_2O. The crude was purified by column chromatography and further purified by recrystallization (CHCl$_3$/^{i}PrOH). 4-(1,2,4,5-tetrazin-3-yl)benzoic acid (460 mg, 2.28 mmol, 7%) was obtained as a bright pink solid.

TLC: R_f = 0.38 (10% MeOH/DCM) [UV]

^{1}H NMR (500 MHz, DMSO): δ [ppm] = 13.34 (br s, 1H), 10.66 (s, 1H), 8.62 (d, J = 8.6 Hz, 2H), 8.24 – 8.20 (d, J = 8.6 Hz, 2H).

^{13}C NMR (126 MHz, DMSO): δ [ppm] = 166.8, 165.1, 158.3, 135.8, 134.4, 130.3, 128.0.

HRMS (ESI) *m/z*: (C$_9$H$_7$N$_4$O$_2^+$ [M+H]$^+$)   calc.: 203.0564

found: 203.0564

6-(1,2,4,5-tetrazin-3-yl)nicotinic acid (276)
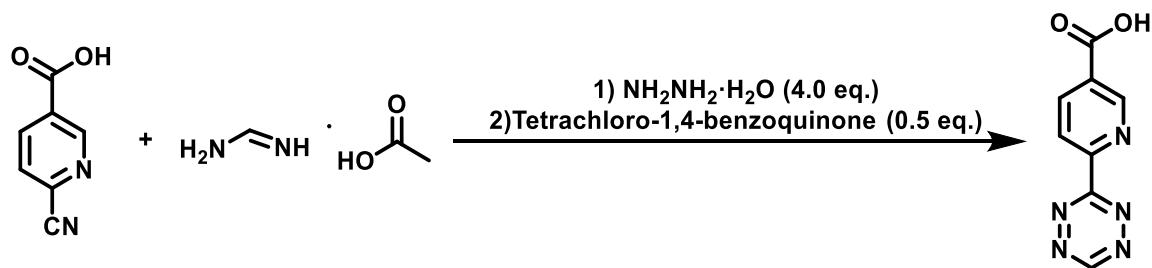
Hydrazine hydrate (1.68 mL) was added to a mixture of 6-cyanopyridine-3-carboxylic acid (250 mg, 1.68 mmol, 1.0 eq.) and formamidine acetate (875 mg, 8.40 mmol, 5.0 eq.). The resulting clear and yellow solution was stirred at 80 °C for 30 min. After cooling to RT, the solution was acidified to pH = 3 by addition of 1 M HCl and 2 M HCl while cooling with an ice bath. The orange precipitate was filtered and washed with water (3 × 10 mL), and dried to give 185 mg of solid.

The solid was suspended in MeOH (25 mL) via sonification. To this suspension was added solid tetrachloro-1.4-benzoquinone (206 mg, 0.84 mmol, 0.5 eq.) and the suspension was stirred for 15 min. The solution was filtered and washed with MeOH (2 × 5 mL) to give 6-(1,2,4,5-tetrazin-3-yl)nicotinic acid (40.0 mg, 197 µmol, 12%) as a pink solid.

TLC: R_f = 0.11 (MeOH/DCM 10%) [UV]

^{1}H NMR (500 MHz, DMSO): δ [ppm] = 13.83 (br s, 1H), 10.76 (s, 1H), 9.36 (dd, J = 2.1, 0.8 Hz, 1H), 8.68 (dd, J = 8.2, 0.8 Hz, 1H), 8.59 (dd, J = 8.2, 2.1 Hz, 1H).

^{13}C NMR (126 MHz, DMSO): δ [ppm] = 165.8, 165.0, 158.6, 153.4, 151.0, 138.8, 128.7, 124.1.

HRMS (ESI) *m/z*: ($C_8H_6N_5O_2^+$ [M+H]$^+$)   calc.:   204.0516

found: 204.0516

4,4,5,7-tetramethylchroman-2-one (239)
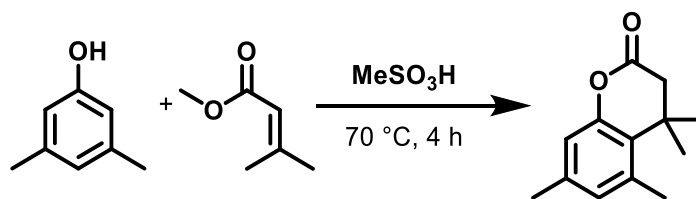
3,5-Dimethylphenol (22.3 g, 182 mmol, 1.0 eq.) was dissolved in methanesulfonic acid (38 mL). Methyl-3-methylbut-2-enoate (28.6 mL, 24.9 g, 218 mmol, 1.2 eq.) was added and the resulting amber mixture was stirred at 70 °C for 4 h. The reaction mixture was allowed to cool to room temperature, poured into iced water and was extracted with EtOAc (3×100 mL). The combined organic layers were washed with water (3×50 mL) and dried over Na_2SO_4, filtered and evaporated *in vacuo* to give the crude product as colorless crystals, which were used in the next step without further purification.

TLC: R_f = 0.90 (1% MeOH in DCM) [UV/KMnO$_4$]

2-(4-hydroxy-2-methylbutan-2-yl)-3,5-dimethylphenol (240)
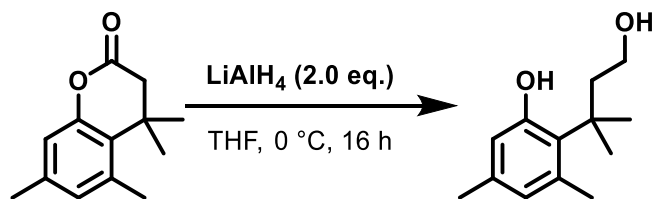
LiAlH$_4$ (13.8 g, 364 mmol, 2.0 eq.) was added carefully to a solution of crude 4,4,5,7-tetramethylchroman-2-one (37.2 g, 182 mmol, 1.0 eq.) in THF (265 mL) at 0 °C. The mixture was stirred at room temperature over night. After the TLC showed full consumption of the starting material, a sat. NH$_4$Cl (100 mL) was slowly added to the solution and the mixture was filtered over sand. The cake was washed with PE (400 mL), dissolved in EtOAc (400 mL) and neutralized with HCl (2 N). The aqueous layer was extracted with EtOAc (4 × 25 mL). The combined organic layers were dried over Na$_2$SO$_4$ and concentrated *in vacuo* to give the crude product as off-white crystals.

Additional product could be recovered from the filtrate. The filtrate was neutralized with HCl (2 N) and extracted with EtOAc (3 × 25 mL). The combined organic layers were dried over Na$_2$SO$_4$ and concentrated *in vacuo* to give the crude product as off-white crystals. The crude product was used in the next step without further purification.

TLC: R_f = 0.18 (PE:EtOAc 3:1) [UV/KMnO$_4$]

^{1}H NMR (500 MHz, CDCl$_3$): δ [ppm] = 6.48 (s, J = 9.0 Hz, 1H), 6.33 (s, 1H), 3.63 (t, J = 7.2 Hz, 2H), 2.47 (s, 3H), 2.27 − 2.23 (t, J = 7.2 Hz, 2H), 2.16 (s, 3H), 1.55 (s, 6H).

^{13}C NMR (126 MHz, CDCl$_3$): δ [ppm] = 155.4, 137.8, 136.1, 128.5, 126.9, 116.2, 61.4, 44.9, 39.5, 31.9, 25.5, 20.2.

2-(4-((tert-butyldimethylsilyl)oxy)-2-methylbutan-2-yl)-3,5-dimethylphenol (241)
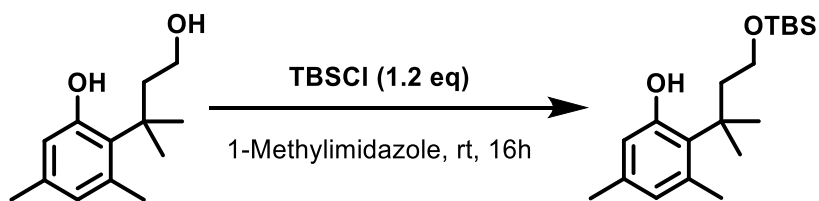
A 50% w/w solution of TBSCl in toluene (16.7 mL, 47.6 mmol, 1.2 eq.) was added slowly to a solution of 2-(4-hydroxy-2-methylbutan-2-yl)-3,5-dimethylphenol (8.26 g, 39.7 mmol, 1.0 eq.) in 1-methyl-imidazole (40 mL) at 0 °C. The mixture was allowed to warm to room temperature and was stirred over night.

The mixture was diluted with EtOAc (10 mL) and water (10 mL) and the pH was neutralized with HCl (2 N). The aqueous phase was extracted with EtOAc (3 × 10 mL). The combined organic layers were washed with water (10 mL) and brine (10 mL), dried over Na_2SO_4 and concentrated *in vacuo*. The mixture was purified via flash column chromatography (silica, 1% → 5 % Et_2O in PE) to give 2-(4-((tert-butyldimethylsilyl)oxy)-2-methylbutan-2-yl)-3,5-dimethylphenol as colorless crystals (11.2 g, 34.8 mmol, 78% over three steps).

TLC: R_f = 0.87 (PE:EtOAc 3:1) [UV/KMnO4]

^{1}H NMR (500 MHz, CDCl3): δ [ppm] = 6.49 (s, 1H), 6.42 (s, 1H), 3.60 (t, *J* = 7.0 Hz, 2H), 2.46 (s, 3H), 2.19 (s, 3H), 2.12 (t, *J* = 7.0 Hz, 2H), 1.55 (s, 6H), 0.88 (s, 9H), 0.03 (s, 6H).

^{13}C NMR (126 MHz, CDCl3): δ [ppm] = 155.6, 137.8, 136.1, 129.3, 127.0, 116.9, 61.9, 45.0, 39.4, 32.2, 26.1, 25.6, 20.4, 18.4, -5.2.

(3-(2-(2-bromoethoxy)-4,6-dimethylphenyl)-3-methylbutoxy)(*tert*-butyl)dimethyl-silane (242)
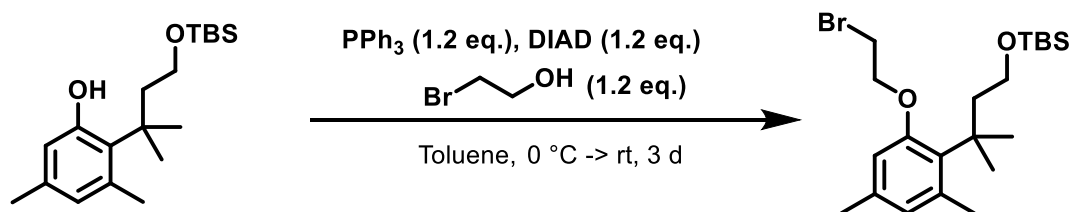
Diisopropyl azodicarboxylate (7.30 mL, 7.51 mg, 37.2 mmol, 1.2 eq.) and 2-bromoethanol (2.64 mL, 4.65 mg, 37.2 mmol, 1.2 eq.) were added directly to a solution of 2-(4-((*tert*-butyldimethylsilyl)oxy)-2-methylbutan-2-yl)-3,5-dimethylphenol (10.0 g, 31.0 mmol, 1.0 eq.) and triphenylphosphine (9.76 g, 37.2 mmol, 1.2 eq.) in toluene (56 mL) at 0 °C. The solution was allowed to warm to room temperature and was stirred over the weekend. The cloudy, yellow mixture was filtered to give a clear, yellow solution which quickly turned cloudy again. MnO_2 (4.00 g, 46.5 mmol, 1.5 eq.) was added and the suspension stirred for 1 h. The mixture was filtrated, washed with water (2 × 20 mL) and brine (1 × 20 mL), dried over Na_2SO_4 and concentrated *in vacuo*. The yellow brown liquid was purified via column chromatography (silica, PE:Et$_2$O 1:0 → 1:1) to give (3-(2-(2-bromoethoxy)-4,6-dimethylphenyl)-3-methylbutoxy)(tert-butyl)dimethyl-silane as a pale-yellow oil (5.67 g, 13.0 mmol, 42%).

TLC: R_f = 0.34 (PE:Et$_2$O 40:1) [UV/KMnO$_4$]

^{1}H NMR (500 MHz, CDCl$_3$): δ [ppm] = 6.56 (s, 1H), 6.51 (s, 1H), 4.27 (t, J = 6.3 Hz, 2H), 3.70 (t, J = 6.3 Hz, 2H), 3.48 (t, J = 7.7 Hz, 2H), 2.49 (s, 3H), 2.25 (s, 3H), 2.16 (t, J = 7.7 Hz, 2H), 1.54 (s, 6H), 0.85 (s, 9H), -0.03 (s, 6H).

^{13}C NMR (126 MHz, CDCl$_3$): δ [ppm] = 157.8, 138.0, 135.9, 131.2, 127.8, 111.7, 68.4, 61.2, 45.9, 40.0, 32.5, 29.4, 26.1, 26.0, 20.9, 18.4, -5.2.

(3-(2-(2-bromoethoxy)-6-(bromomethyl)-4-methylphenyl)-3-methylbutoxy)(tert-butyl)dimethylsilane (293)

and

(3-(2-(2-bromoethoxy)-4-(bromomethyl)-6-methylphenyl)-3-methylbutoxy)(tert-butyl)dimethylsilane (294)
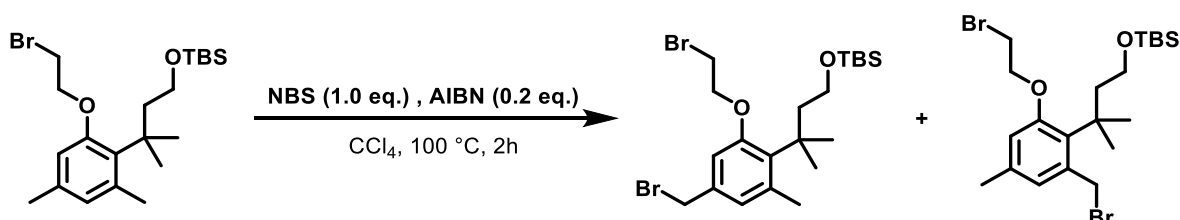
N-Bromosuccinimide (NBS) (1.98 g, 11.1 mmol, 1.0 eq.) and AIBN (365 mg, 2.22 mmol, 0.2 eq.) were added to a refluxing solution (100 °C) of **73** (4.77 g, 11.1 mmol, 1.0 eq.) in CCl$_4$ (15 mL). After stirring under reflux for 2 h the reaction mixture was diluted with DCM (5 mL) and the organic layer was washed with HCl (2 N) (5 mL), sat. NaHCO$_3$ (5 mL), H$_2$O (5 mL) and brine (5 mL), dried over Na$_2$SO$_4$ and concentrated *in vacuo* to give the crude products (3-(2-(2-bromoethoxy)-6-(bromomethyl)-4-methylphenyl)-3-methylbutoxy)(tert-butyl)dimethylsilane and (3-(2-(2-bromoethoxy)-4-(bromomethyl)-6-methylphenyl)-3-methylbutoxy)(tert-butyl)dimethylsilane. Flash column chromatography (silica, PE:Et$_2$O 70:1) was performed. The crude mixture of the two isomeric products was used without further purification.

TLC: R_f = 0.24 (PE:EtOAc 40:1) [UV/KMnO$_4$]

(3-(2-(2-bromoethoxy)-6-methyl-4-((prop-2-yn-1-yloxy)methyl)phenyl)-3-methylbutoxy)(*tert*-butyl)dimethylsilane (295, Product A)

and

(3-(2-(2-bromoethoxy)-4-methyl-6-((prop-2-yn-1-yloxy)methyl)phenyl)-3-methylbutoxy)(*tert*-butyl)dimethylsilane (296, Product B)
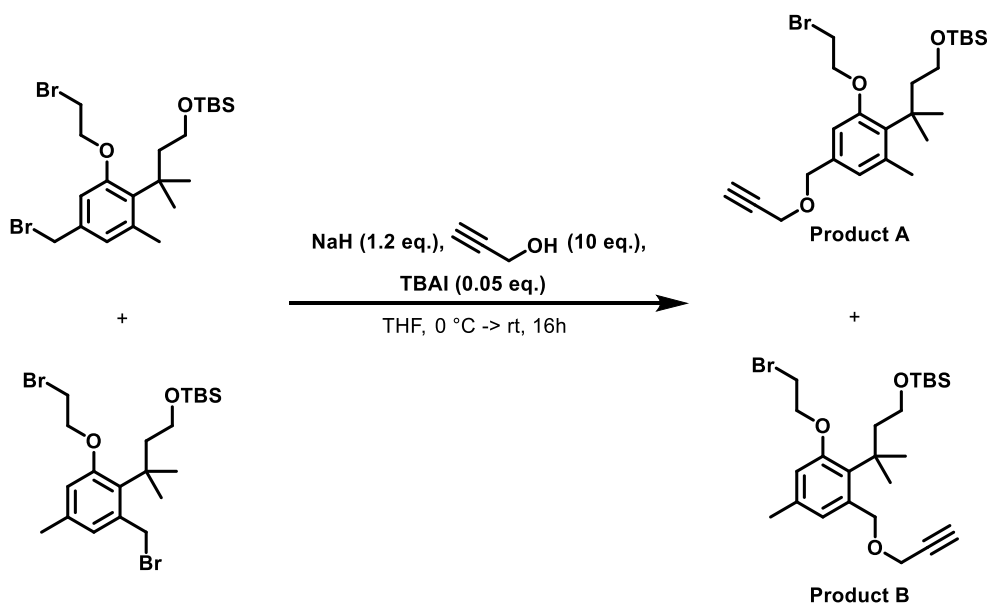
Propargyl alcohol (98.0 µL, 9.31 mg, 166 µmol, 10 eq.) was added dropwise at 0 °C to a suspension of 60% sodium hydride in mineral oil (8.8 mg, 9.8 µL 216 µmol, 1.3 eq.) in dry THF (0.8 mL) and the reaction mixture was allowed to warm to room temperature over 1 h. Tetrabutylammonium iodide (3.07 mg, 8.00 µmol, 0.05 eq.) and the crude mixture of **72** and **95** (84.3 mg, 166 µmol, 1.0 eq.) were added to the mixture successively. After stirring over night and full consumption of the starting material (observed via TLC), the mixture was diluted with DCM (5 mL) and water (5 mL). The aqueous layer was extracted with DCM (3 × 5 mL). The collected organic layers were washed with water (5 mL) and brine (5 mL), dried over Na$_2$SO$_4$ and concentrated *in vacuo* to give a colorless oil. The mixture was purified via flash column chromatography (silica, PE:Et$_2$O 15:1) to obtain (3-(2-(2-bromoethoxy)-6-methyl-4-((prop-2-yn-1-yloxy)methyl)phenyl)-3-methylbutoxy)(tert-butyl)dimethylsilane (Product A) (28.3 mg 54.6 µmol, 6% over two steps) and (3-(2-(2-bromoethoxy)-4-methyl-6-((prop-2-yn-1-yloxy)methyl)phenyl)-3-methylbutoxy)(tert-butyl)dimethylsilane (Product B) (26.5 mg, 58.4 µmol, 6% over two steps) as colorless oils.

(3-(2-(2-bromoethoxy)-6-methyl-4-((prop-2-yn-1-yloxy)methyl)phenyl)-3-methylbutoxy)(*tert*-butyl)dimethylsilane (295, Product A):

TLC: R_f = 0.19 (PE:Et$_2$O 20:1) [UV/I$_2$]

^{1}H NMR (500 MHz, DMSO): δ [ppm] = 6.81 (d, J = 1.2 Hz, 1H), 6.63 (d, J = 1.5 Hz, 1H), 4.74 (s, 2H), 4.28 (t, J =6.2 Hz, 2H), 4.13 (d, J = 2.4 Hz, 2H), 3.71 (t, J = 6.3 Hz, 2H), 3.44 (t, J = 7.8 Hz, 2H), 2.46 (t, J = 2.4 Hz, 1H) 2.29 (s, 3H), 2.18 (t, J = 7.8 Hz, 2H), 1.58 (s, 6H), 0.84 (s, 9H), -0.04 (s, 6H).

^{13}C NMR (126 MHz, DMSO): δ [ppm] = 158.1, 138.4, 135.1, 134.0, 126.7, 110.2, 79.8, 74.8, 71.2, 68.4, 61.5, 57.3, 45.8, 40.2, 32.4, 29.3, 26.1, 18.4, -5.1.

(3-(2-(2-bromoethoxy)-4-methyl-6-((prop-2-yn-1-yloxy)methyl)phenyl)-3-methylbutoxy)(*tert*-butyl)dimethylsilane (296, Product B):

TLC: R_f = 0.31 (PE:Et$_2$O 20:1) [UV/I$_2$]

^{1}H NMR (500 MHz, DMSO): δ [ppm] = 6.70 (s, 2H), 4.51 (s, 2H), 4.30 (t, J = 6.2 Hz, 2H), 4.18 (d, J = 2.4 Hz, 2H), 3.71 (t, J = 6.3 Hz, 2H), 3.46 (t, J = 7.6 Hz, 2H), 2.52 (s, 3H), 2.46 (t, J = 2.4 Hz, 1H), 2.18 (t, J = 7.8 Hz, 2H), 1.55 (s, 6H), 0.84 (s, 9H), -0.04 (s, 6H).

^{13}C NMR (126 MHz, DMSO): δ [ppm] = 158.0, 136.7, 136.3, 132.4, 127.2, 113.9, 79.9, 74.7, 72.5, 68.5, 61.5, 56.9, 45.7, 39.9, 31.5, 29.2, 26.1, 20.9, 18.4, -5.1.

4 Outlook

The field of click chemistry and bioorthogonal reactions and their applications, especially in the areas of chemical biology and drug development, has grown rapidly in recent years.[246-249] Based on bioorthogonal reactions new techniques have been developed (e.g., activity based protein profiling[250],[251]). They also provide the basis for the creative solution of major problems in the field of drug discovery, for example, by designing prodrugs on the basis of concepts such as the *click-to-release*.[11]

This thesis contributes to the advancement of the field in two ways. On the one hand, new applications of bond-forming bioorthogonal reactions as *in situ*-activated drugs by the example of tomaymycin derivatives were explored. On the other hand, a new *click-to-release* system was developed. This lays the foundation for a novel, cleavable linker system.

In the case of the studies carried out on the novel tomaymycin derivatives as *in situ* activated drugs, challenges in the *in situ* dimerization could be identified. However, a heterodimer utilizing the CuAAC as the dimerization step was synthesized and biologically evaluated, showing well-defined target binding, i.e., DNA-binding, and thus providing grounds for further studies, including the activity of the heterodimer in cancer cell lines, currently carried out in cooperation with Prof. Rahman and Prof. Thurston.

The second part of this thesis built on utilizing the bioorthorgonal IEDDA reaction of a tetrazine and a vinyl moiety as a chemical trigger for the Trimehtyl lock. Tetrazines with different electron withdrawing groups have been synthesized and kinetically evaluated. This gave rise to a toolbox of tetrazines with different rate constants, allowing the selection of the appropriate tetrazine depending on the application-specific requirements. Extending the deployability of the previously developed vinyl-substituted TML to a linker, first synthetic strategies have been explored. These findings build the foundation for further studies on utilizing the TML as a click-to-release linker system, providing researchers with another tool to chemically cleave conjugates of any kind in a highly selective and controlled manner.

Overall, the field of bioorthogonal reactions offers a seemingly endless diversity in its applications, which is expected to continue to grow in the coming years, e.g., through the development of new click-to-release mechanisms. Such efforts form the basis for drug activation approaches and thus enable the future development of improved as well as novel drugs.

5 Literature

[1]   NobelPrize.org, **2022**.

[2]   C. W. Tornøe, C. Christensen, M. Meldal, *The Journal of Organic Chemistry* **2002**, *67*, 3057-3064.

[3]   V. V. Rostovtsev, L. G. Green, V. V. Fokin, K. B. Sharpless, *Angewandte Chemie International Edition* **2002**, *41*, 2596-2599.

[4]   R. Huisgen, A. Padwa, *Wiley, New York* **1984**, *1*, 55-92.

[5]   J.-F. Lutz, *Angewandte Chemie International Edition* **2007**, *46*, 1018-1025.

[6]   H. C. Kolb, K. B. Sharpless, *Drug Discovery Today* **2003**, *8*, 1128-1137.

[7]   R. Manetsch, A. Krasiński, Z. Radić, J. Raushel, P. Taylor, K. B. Sharpless, H. C. Kolb, *Journal of the American Chemical Society* **2004**, *126*, 12809-12818.

[8]   V. P. Mocharla, B. Colasson, L. V. Lee, S. Röper, K. B. Sharpless, C.-H. Wong, H. C. Kolb, *Angewandte Chemie International Edition* **2005**, *44*, 116-120.

[9]   J. A. Prescher, D. H. Dube, C. R. Bertozzi, *Nature* **2004**, *430*, 873-877.

[10]   R. E. Bird, S. A. Lemmel, X. Yu, Q. A. Zhou, *Bioconjugate Chemistry* **2021**, *32*, 2457-2479.

[11]   X. Ji, Z. Pan, B. Yu, L. K. De La Cruz, Y. Zheng, B. Ke, B. Wang, *Chemical Society Reviews* **2019**, *48*, 1077-1094.

[12]   A. G. Cheetham, R. W. Chakroun, W. Ma, H. Cui, *Chemical Society Reviews* **2017**, *46*, 6638-6663.

[13]   S. Neidle, *Journal of Biological Chemistry* **2021**, *296*, 100553.

[14]   P. B. Dervan, *Bioorganic & Medicinal Chemistry* **2001**, *9*, 2215-2235.

[15]   T. Siggers, R. Gordân, *Nucleic Acids Research* **2013**, *42*, 2099-2111.

[16]   N. P. Pavletich, C. O. Pabo, *Science* **1991**, *252*, 809-817.

[17]   T. E. Ellenberger, C. J. Brandl, K. Struhl, S. C. Harrison, *Cell* **1992**, *71*, 1223-1237.

[18]   Y. Kim, J. H. Geiger, S. Hahn, P. B. Sigler, *Nature* **1993**, *365*, 512-520.

[19]   J. J. Love, X. Li, D. A. Case, K. Giese, R. Grosschedl, P. E. Wright, *Nature* **1995**, *376*, 791-795.

[20]   J. H. Geiger, S. Hahn, S. Lee, P. B. Sigler, *Science* **1996**, *272*, 830-836.

[21]   J. J. Love, X. Li, J. Chung, H. J. Dyson, P. E. Wright, *Biochemistry* **2004**, *43*, 8725-8734.

[22]   A. Ali, S. Bhattacharya, *Bioorganic & Medicinal Chemistry* **2014**, *22*, 4506-4521.

[23]   L. Xu, W. Wang, J. Wu, J. H. Shin, P. Wang, I. C. Unarta, J. Chong, Y. Wang, D. Wang, *Proceedings of the National Academy of Sciences* **2017**, *114*, E7082-E7091.

[24]   P. Borst, *IUBMB Life* **2005**, *57*, 745-747.

[25]   C. Carvalho, X. R. Santos, S. Cardoso, S. Correia, J. P. Oliveira, S. M. Santos, I. P. Moreira, *Current Medicinal Chemistry* **2009**, *16*, 3267-3285.

[26]   G. Finocchiaro, *Neuro-Oncology* **2020**, *22*, 1235-1236.

[27]   L. S. Lerman, *Journal of Molecular Biology* **1961**, *3*, 18-IN14.

[28]   L. S. Lerman, *Proceedings of the National Academy of Sciences* **1963**, *49*, 94-102.

[29]   A. A. Almaqwashi, J. Andersson, P. Lincoln, I. Rouzina, F. Westerlund, M. C. Williams, *Scientific Reports* **2016**, *6*, 37993.

[30]   C. Avendaño, J. C. Menéndez, in *Medicinal Chemistry of Anticancer Drugs* (Eds.: C. Avendaño, J. C. Menéndez), Elsevier, Amsterdam, **2008**, pp. 199-228.

[31]   V. Sharma, M. Gupta, P. Kumar, A. Sharma, *Current Pharmaceutical Design* **2021**, *27*, 15-42.

[32]   J. Ren, J. B. Chaires, *Biochemistry* **1999**, *38*, 16067-16075.

[33]   B. S. P. Reddy, S. M. Sondhi, J. W. Lown, *Pharmacology & Therapeutics* **1999**, *84*, 1-111.

[34]   R. C. Young, R. F. Ozols, C. E. Myers, *New England Journal of Medicine* **1981**, *305*, 139-153.

[35]   W. E. Ross, D. Glaubiger, K. W. Kohn, *Biochimica et Biophysica Acta (BBA) - Nucleic Acids and Protein Synthesis* **1979**, *562*, 41-50.

[36]   D. Fu, J. A. Calvo, L. D. Samson, *Nature Reviews Cancer* **2012**, *12*, 104-120.

[37]   N. Shrivastav, D. Li, J. M. Essigmann, *Carcinogenesis* **2009**, *31*, 59-70.

[38]   F. Drabløs, E. Feyzi, P. A. Aas, C. B. Vaagbø, B. Kavli, M. S. Bratlie, J. Peña-Diaz, M. Otterlei, G. Slupphaug, H. E. Krokan, *DNA Repair* **2004**, *3*, 1389-1407.

[39]   R. Saffhill, G. P. Margison, P. J. O'Connor, *Biochimica et Biophysica Acta (BBA) - Reviews on Cancer* **1985**, *823*, 111-145.

[40]   K. W. Kohn, J. A. Hartley, W. B. Mattes, *Nucleic Acids Research* **1987**, *15*, 10531-10549.

[41]   W. A. Denny, *Current Medicinal Chemistry* **2001**, *8*, 533-544.

[42]   D. Basak, S. Arrighi, Y. Darwiche, S. Deb, *Life* **2022**, *12*, 48.

[43]   A. Emadi, R. J. Jones, R. A. Brodsky, *Nature Reviews Clinical Oncology* **2009**, *6*, 638-647.

[44]   J. A. Hickman, *Cancer and Metastasis Reviews* **1992**, *11*, 121-139.

[45]   C. Avendaño, J. C. Menéndez, in *Medicinal Chemistry of Anticancer Drugs* (Eds.: C. Avendaño, J. C. Menéndez), Elsevier, Amsterdam, **2008**, pp. 139-176.

[46]   S. Puyo, D. Montaudon, P. Pourquier, *Critical Reviews in Oncology/Hematology* **2014**, *89*, 43-61.

[47]   S. Park, N. Tretyakova, *Chemical Research in Toxicology* **2004**, *17*, 129-136.

[48]   A. Eastman, *Pharmacology & Therapeutics* **1987**, *34*, 155-166.

[49]   A. Basu, S. Krishnamurthy, *Journal of Nucleic Acids* **2010**, *2010*, 201367.

[50]   R. J. Browning, P. J. T. Reardon, M. Parhizkar, R. B. Pedley, M. Edirisinghe, J. C. Knowles, E. Stride, *ACS Nano* **2017**, *11*, 8560-8578.

[51]   E. Wong, C. M. Giandomenico, *Chemical Reviews* **1999**, *99*, 2451-2466.

[52]   K. Wielenberg, M. Wang, M. Yang, A. Ozer, J. T. Lis, H. Lin, *RSC Advances* **2020**, *10*, 39870-39874.

[53]   J. Dekker, A. S. Belmont, M. Guttman, V. O. Leshyk, J. T. Lis, S. Lomvardas, L. A. Mirny, C. C. O'Shea, P. J. Park, B. Ren, J. C. R. Politz, J. Shendure, S. Zhong, D. N. N. the, *Nature* **2017**, *549*, 219-226.

[54]   T. Sakamoto, Y. Tanaka, K. Fujimoto, *Organic Letters* **2015**, *17*, 936-939.

[55]   C.-X. Song, C. He, *Accounts of Chemical Research* **2011**, *44*, 709-717.

[56]   W. P. Zhen, O. Buchardt, H. Nielsen, P. E. Nielsen, *Biochemistry* **1986**, *25*, 6598-6603.

[57]   S. Couvé-Privat, G. Macé, F. Rosselli, M. K. Saparbaev, *Nucleic Acids Research* **2007**, *35*, 5672-5682.

[58]   J. Mantaj, P. J. M. Jackson, K. M. Rahman, D. E. Thurston, *Angewandte Chemie International Edition* **2017**, *56*, 462-488.

[59]   W. Leimgruber, V. Stefanović, F. Schenker, A. Karr, J. Berger, *Journal of the American Chemical Society* **1965**, *87*, 5791-5793.

[60]   D. Antonow, D. E. Thurston, *Chemical Reviews* **2011**, *111*, 2815-2864.

[61]   B. Gerratana, *Medicinal Research Reviews* **2012**, *32*, 254-293.

[62]   J. A. Hartley, *Expert Opinion on Investigational Drugs* **2011**, *20*, 733-744.

[63]   R. P. Hertzberg, S. M. Hecht, V. L. Reynolds, I. J. Molineux, L. H. Hurley, *Biochemistry* **1986**, *25*, 1249-1258.

[64]   M. S. Puvvada, S. A. Forrow, J. A. Hartley, P. Stephenson, I. Gibson, T. C. Jenkins, D. E. Thurston, *Biochemistry* **1997**, *36*, 2478-2484.

[65]   K. M. Rahman, C. H. James, D. E. Thurston, *Organic & Biomolecular Chemistry* **2011**, *9*, 1632-1641.

[66]   W. Li, A. Khullar, S. Chou, A. Sacramo, B. Gerratana, *Applied and Environmental Microbiology* **2009**, *75*, 2869-2878.

[67]   K. M. Rahman, A. S. Thompson, C. H. James, M. Narayanaswamy, D. E. Thurston, *Journal of the American Chemical Society* **2009**, *131*, 13756-13766.

[68]   D. Glaubiger, K. W. Kohn, E. Charney, *Biochimica et Biophysica Acta (BBA) - Nucleic Acids and Protein Synthesis* **1974**, *361*, 303-311.

[69]   G. B. Jones, C. L. Davey, T. C. Jenkins, A. Kamal, G. G. Kneale, S. Neidle, G. D. Webster, D. E. Thurston, *Anticancer Drug Des* **1990**, *5*, 249-264.

[70]   M. Narayanaswamy, W. J. Griffiths, P. W. Howard, D. E. Thurston, *Analytical Biochemistry* **2008**, *374*, 173-181.

[71]   D. E. Graves, C. Pattaroni, B. S. Krishnan, J. M. Ostrander, L. H. Hurley, T. R. Krugh, *Journal of Biological Chemistry* **1984**, *259*, 8202-8209.

[72]   L. H. Hurley, T. Reck, D. E. Thurston, D. R. Langley, K. G. Holden, R. P. Hertzberg, J. R. Hoover, G. Gallagher, L. F. Faucette, S. M. Mong, *Chemical Research in Toxicology* **1988**, *1*, 258-268.

[73]   L. H. Hurley, C. S. Allen, J. M. Feola, W. C. Lubawy, *Cancer Res* **1979**, *39*, 3134-3140.

[74]   Y. Nishioka, T. Beppu, M. Kohsaka, K. Arima, *The Journal of Antibiotics*, *25*, 660-667.

[75]   L. H. HURLEY, *The Journal of Antibiotics* **1977**, *30*, 349-370.

[76]   L. H. Hurley, C. Gairola, M. Zmijewski, *Biochimica et Biophysica Acta (BBA) - Nucleic Acids and Protein Synthesis* **1977**, *475*, 521-535.

[77]   M. D. Barkley, S. Cheatham, D. E. Thurston, L. H. Hurley, *Biochemistry* **1986**, *25*, 3021-3031.

[78]   G. Wells, C. R. H. Martin, P. W. Howard, Z. A. Sands, C. A. Laughton, A. Tiberghien, C. K. Woo, L. A. Masterson, M. J. Stephenson, J. A. Hartley, T. C. Jenkins, S. D. Shnyder, P. M. Loadman, M. J. Waring, D. E. Thurston, *Journal of Medicinal Chemistry* **2006**, *49*, 5442-5461.

[79]   M. Kotecha, J. Kluza, G. Wells, C. C. O'Hare, C. Forni, R. Mantovani, P. W. Howard, P. Morris, D. E. Thurston, J. A. Hartley, D. Hochhauser, *Molecular Cancer Therapeutics* **2008**, *7*, 1319-1328.

[80]   W. Leimgruber, A. D. Batcho, R. C. Czajkowski, *Journal of the American Chemical Society* **1968**, *90*, 5641-5643.

[81]   A. Guiotto, P. W. Howard, P. G. Baraldi, D. E. Thurston, *Bioorganic & Medicinal Chemistry Letters* **1998**, *8*, 3017-3018.

[82]   D. E. Thurston, D. S. Bose, P. W. Howard, T. C. Jenkins, A. Leoni, P. G. Baraldi, A. Guiotto, B. Cacciari, L. R. Kelland, M.-P. Foloppe, S. Rault, *Journal of Medicinal Chemistry* **1999**, *42*, 1951-1964.

[83]   A. Kamal, P. Ramulu, O. Srinivas, G. Ramesh, P. P. Kumar, *Bioorganic & Medicinal Chemistry Letters* **2004**, *14*, 4791-4794.

[84]   F. Brucoli, J. D. Guzman, M. A. Basher, D. Evangelopoulos, E. McMahon, T. Munshi, T. D. McHugh, K. R. Fox, S. Bhakta, *The Journal of Antibiotics* **2016**, *69*, 843-849.

[85]   A. Kamal, G. Ramesh, P. Ramulu, O. Srinivas, T. Rehana, G. Sheelu, *Bioorganic & Medicinal Chemistry Letters* **2003**, *13*, 3451-3454.

[86]   A. Kamal, O. Srinivas, P. Ramulu, G. Ramesh, P. P. Kumar, *Bioorganic & Medicinal Chemistry Letters* **2004**, *14*, 4107-4111.

[87]   S. J. Gregson, P. W. Howard, J. A. Hartley, N. A. Brooks, L. J. Adams, T. C. Jenkins, L. R. Kelland, D. E. Thurston, *Journal of Medicinal Chemistry* **2001**, *44*, 737-748.

[88]   A. Kamal, N. Shankaraiah, L. K. Reddy, V. Devaiah, A. Juvekar, S. Sen, *Letters in Drug Design & Discovery* **2007**, *4*, 596-604.

[89]   A. Kamal, V. Devaiah, K. L. Reddy, M. S. Kumar, *Bioorganic & Medicinal Chemistry* **2005**, *13*, 2021-2029.

[90]   A. Kamal, B. S. N. Reddy, G. S. K. Reddy, G. Ramesh, *Bioorganic & Medicinal Chemistry Letters* **2002**, *12*, 1933-1935.

[91]   A. Iacobino, F. Giannoni, L. Fattorini, F. Brucoli, *The Journal of Antibiotics* **2018**, *71*, 831-834.

[92]   M. A. Basher, K. M. Rahman, P. J. M. Jackson, D. E. Thurston, K. R. Fox, *Biophysical Chemistry* **2017**, *230*, 53-61.

[93]   F. Brucoli, R. M. Hawkins, C. H. James, P. J. M. Jackson, G. Wells, T. C. Jenkins, T. Ellis, M. Kotecha, D. Hochhauser, J. A. Hartley, P. W. Howard, D. E. Thurston, *Journal of Medicinal Chemistry* **2013**, *56*, 6339-6351.

[94]   S. J. Gregson, P. W. Howard, D. R. Gullick, A. Hamaguchi, K. E. Corcoran, N. A. Brooks, J. A. Hartley, T. C. Jenkins, S. Patel, M. J. Guille, D. E. Thurston, *Journal of Medicinal Chemistry* **2004**, *47*, 1161-1174.

[95]   D. S. Bose, A. S. Thompson, M. Smellie, M. D. Berardini, J. A. Hartley, T. C. Jenkins, S. Neidle, D. E. Thurston, *Journal of the Chemical Society, Chemical Communications* **1992**, 1518-1520.

[96]   M. Smellie, L. R. Kelland, D. E. Thurston, R. L. Souhami, J. A. Hartley, *British Journal of Cancer* **1994**, *70*, 48-53.

[97]   M. L. Kopka, D. S. Goodsell, I. Baikalov, K. Grzeskowiak, D. Cascio, R. E. Dickerson, *Biochemistry* **1994**, *33*, 13593-13610.

[98]   F. L. Boyd, D. Stewart, W. A. Remers, M. D. Barkley, L. H. Hurley, *Biochemistry* **1990**, *29*, 2387-2403.

[99]   D. Antonow, T. C. Jenkins, P. W. Howard, D. E. Thurston, *Bioorganic & Medicinal Chemistry* **2007**, *15*, 3041-3053.

[100] B. S. P. Reddy, S. K. Sharma, J. W. Lown, *Current Medicinal Chemistry* **2000**, *8*, 475-508.

[101] A. Kamal, G. Ramesh, N. Laxman, P. Ramulu, O. Srinivas, K. Neelima, A. K. Kondapi, V. B. Sreenu, H. A. Nagarajaram, *Journal of Medicinal Chemistry* **2002**, *45*, 4679-4688.

[102] A. Kamal, G. Ramesh, O. Srinivas, P. Ramulu, N. Laxman, T. Rehana, M. Deepak, M. S. Achary, H. A. Nagarajaram, *Bioorganic & Medicinal Chemistry* **2004**, *12*, 5427-5436.

[103] M. P. Foloppe, S. Rault, D. E. Thurston, T. C. Jenkins, M. Robba, *European Journal of Medicinal Chemistry* **1996**, *31*, 407-410.

[104] S. J. Gregson, P. W. Howard, D. E. Thurston, T. C. Jenkins, L. R. Kelland, *Chemical Communications* **1999**, 797-798.

[105] J. A. Hartley, N. Brooks, P. J. Mchugh, P. H. Clingen, S. J. Gregson, P. W. Howard, D. E. Thurston, *Proceedings of the American Association for Cancer Research Annual Meeting* **2000**, *41*, 425-425.

[106] S. J. Gregson, P. W. Howard, K. E. Corcoran, T. C. Jenkins, L. R. Kelland, D. E. Thurston, *Bioorganic & Medicinal Chemistry Letters* **2001**, *11*, 2859-2862.

[107] J. A. Hartley, V. J. Spanswick, N. Brooks, P. H. Clingen, P. J. McHugh, D. Hochhauser, R. B. Pedley, L. R. Kelland, M. C. Alley, R. Schultz, M. G. Hollingshead, K. M. Schweikart, J. E. Tomaszewski, E. A. Sausville, S. J. Gregson, P. W. Howard, D. E. Thurston, *Cancer Research* **2004**, *64*, 6693-6699.

[108] S. J. Morris, D. E. Thurston, T. G. Nevell, *The Journal of Antibiotics* **1990**, *43*, 1286-1292.

[109] T. Hadjivassileva, D. E. Thurston, P. W. Taylor, *Journal of Antimicrobial Chemotherapy* **2005**, *56*, 513-518.

[110] K. Arima, M. Kohsaka, G. Tamura, H. Manaka, H. Sakai, *The Journal of Antibiotics* **1972**, *25*, 437-444.

[111] Y. Hu, V. Phelan, I. Ntai, C. M. Farnet, E. Zazopoulos, B. O. Bachmann, *Chemistry & Biology* **2007**, *14*, 691-701.

[112] W. Li, S. Chou, A. Khullar, B. Gerratana, *Applied and Environmental Microbiology* **2009**, *75*, 2958-2963.

[113] A. von Tesmar, M. Hoffmann, J. Pippel, A. A. Fayad, S. Dausend-Werner, A. Bauer, W. Blankenfeldt, R. Müller, *Cell Chemical Biology* **2017**, *24*, 1216-1227.e1218.

[114] J. D. Farmer, S. M. Rudnicki, J. W. Suggs, *Tetrahedron Letters* **1988**, *29*, 5105-5108.

[115] J. D. Farmer, Jr, G. R. Gustafson, A. Conti, M. B. Zimmt, J. W. Suggs, *Nucleic Acids Research* **1991**, *19*, 899-903.

[116] D. S. Bose, A. S. Thompson, J. Ching, J. A. Hartley, M. D. Berardini, T. C. Jenkins, S. Neidle, L. H. Hurley, D. E. Thurston, *Journal of the American Chemical Society* **1992**, *114*, 4939-4941.

[117] S. J. Morris, University of Portsmouth **1992**.

[118] G. P. Wilkinson, J. P. Taylor, S. Shnyder, P. Cooper, P. W. Howard, D. E. Thurston, T. C. Jenkins, P. M. Loadman, *Investigational New Drugs* **2004**, *22*, 231-240.

[119] G. Lenglet, M.-H. David-Cordonnier, *Journal of Nucleic Acids* **2010**, *2010*, 290935.

[120] C. Martin, T. Ellis, C. J. McGurk, T. C. Jenkins, J. A. Hartley, M. J. Waring, D. E. Thurston, *Biochemistry* **2005**, *44*, 4135-4147.

[121] J. A. Hartley, *Expert Opinion on Biological Therapy* **2021**, *21*, 931-943.

[122] S. Baah, M. Laws, K. M. Rahman, *Molecules* **2021**, *26*, 2943.

[123] H. Kaplon, A. Chenoweth, S. Crescioli, J. M. Reichert, *mAbs* **2022**, *14*, 2014296.

[124] A. Lee, *Drugs* **2021**, *81*, 1229-1233.

[125] J. T. W. Tong, P. W. R. Harris, M. A. Brimble, I. Kavianinia, *Molecules* **2021**, *26*, 5847.

[126] J. A. Hartley, M. J. Flynn, J. P. Bingham, S. Corbett, H. Reinert, A. Tiberghien, L. A. Masterson, D. Antonow, L. Adams, S. Chowdhury, D. G. Williams, S. Mao, J. Harper, C. E. G. Havenith, F. Zammarchi, S. Chivers, P. H. van Berkel, P. W. Howard, *Scientific Reports* **2018**, *8*, 10479.

[127] P. B. Farmer, R. Singh, *Mutation Research/Reviews in Mutation Research* **2008**, *659*, 68-76.

[128] J. J. Klaene, V. K. Sharma, J. Glick, P. Vouros, *Cancer Letters* **2013**, *334*, 10-19.

[129] B. E. Erickson, *Analytical Chemistry* **2000**, *72*, 711 A-716 A.

[130] F. Blum, *British Journal of Hospital Medicine* **2014**, *75*, C18-C21.

[131] M. Gilar, E. S. P. Bouvier, *Journal of Chromatography A* **2000**, *890*, 167-177.

[132] C. G. Huber, H. Oberacher, *Mass Spectrometry Reviews* **2001**, *20,* 310-343.

[133] M. Gilar, *Analytical Biochemistry* **2001**, *298*, 196-206.

[134] K. Bleicher, E. Bayer, *Biological Mass Spectrometry* **1994**, *23*, 320-322.

[135] A. Apffel, J. A. Chakel, S. Fischer, K. Lichtenwalter, W. S. Hancock, *Journal of Chromatography A* **1997**, *777*, 3-21.

[136] C. G. Huber, A. Krajete, *Analytical Chemistry* **1999**, *71*, 3730-3739.

[137] B. Aslam, M. Basit, M. A. Nisar, M. Khurshid, M. H. Rasool, *J Chromatogr Sci* **2017**, *55*, 182-196.

[138] B. Zhou, J. F. Xiao, L. Tuli, H. W. Ressom, *Mol Biosyst* **2012**, *8*, 470-481.

[139] V. Rodríguez Robledo, W. F. Smyth, *Electrophoresis* **2009**, *30*, 1647-1660.

[140] M. J. Pavlovich, B. Musselman, A. B. Hall, *Mass Spectrom Rev* **2018**, *37*, 171-187.

[141] J. Hendy, *Science Advances* **2021**, *7*, eabb9314.

[142] J. H. Hoffman, R. C. Chaney, H. Hammack, *Journal of the American Society for Mass Spectrometry* **2008**, *19*, 1377-1383.

[143] K.-Y. Wu, S.-Y. Chiang, W.-C. Shih, C.-C. J. Huang, M.-F. Chen, J. A. Swenberg, *Mass Spectrometry Reviews* **2011**, *30*, 733-756.

[144] N. Tretyakova, P. W. Villalta, S. Kotapati, *Chemical Reviews* **2013**, *113*, 2395-2436.

[145] M. Dizdaroglu, P. Jaruga, M. Birincioglu, H. Rodriguez, *Free Radical Biology and Medicine* **2002**, *32*, 1102-1115.

[146] Y. Tang, J.-L. Zhang, *Journal of Separation Science* **2020**, *43*, 31-55.

[147] S. Balbo, R. J. Turesky, P. W. Villalta, *Chemical Research in Toxicology* **2014**, *27*, 356-366.

[148] S. Pourshahian, *Mass Spectrometry Reviews* **2021**, *40*, 75-109.

[149] P. Wang, M. G. Bartlett, L. B. Martin, *Rapid Communications in Mass Spectrometry* **1997**, *11*, 846-856.

[150] A. Kulyyassov, M. Fresnais, R. Longuespée, *Proteomics* **2021**, *21*, 2100153.

[151] A. A. Fazli, B. K. Panigrahy, V. Kumar, S. N. Raza, B. A. Zarger, T. U. Wani, S. Ahmad, A. Khuroo, N. A. Khan, *Scientific Reports* **2022**, *12*, 9322.

[152] C. J. Silva, *Journal of Agricultural and Food Chemistry* **2018**, *66*, 8435-8450.

[153] F. Hannauer, R. Black, A. D. Ray, E. Stulz, G. J. Langley, S. W. Holman, *Analytical Science Advances* **2022**, *3*, 90-102.

[154] R. A. Yost, C. G. Enke, *Analytical Chemistry* **1979**, *51*, 1251-1264.

[155] T. Calogeropoulou, D. C. Rideout, **1991**.

[156] D. Rideout, *Science* **1986**, *233*, 561-563.

[157] D. Rideout, *Cancer Investigation* **1994**, *12*, 189-202.

[158] D. Rideout, J. Jaworski, R. Dagnino, *Biochemical Pharmacology* **1988**, *37*, 4505-4512.

[159] D. Rideout, T. Calogeropoulou, J. Jaworski, M. McCarthy, *Biopolymers* **1990**, *29*, 247-262.

[160] S. A. Rotenberg, T. Calogeropoulou, J. S. Jaworski, I. B. Weinstein, D. Rideout, *Proceedings of the National Academy of Sciences* **1991**, *88*, 2490-2494.

[161] J. Clavadetscher, E. Indrigo, S. V. Chankeshwara, A. Lilienkampf, M. Bradley, *Angewandte Chemie International Edition* **2017**, *56*, 6864-6868.

[162] A. Logan, Victoria R. Pell, Karl J. Shaffer, C. Evans, Nathan J. Stanley, Ellen L. Robb, Tracy A. Prime, Edward T. Chouchani, Helena M. Cochemé, Ian M. Fearnley, S. Vidoni, Andrew M. James, Carolyn M. Porteous, L. Partridge, T. Krieg, Robin A. J. Smith, Michael P. Murphy, *Cell Metabolism* **2016**, *23*, 379-385.

[163] D. Zhang, T. H. Pillow, Y. Ma, J. d. Cruz-Chuh, K. R. Kozak, J. D. Sadowsky, G. D. Lewis Phillips, J. Guo, M. Darwish, P. Fan, J. Chen, C. He, T. Wang, H. Yao, Z. Xu, J. Chen, J. Wai, Z. Pei, C. E. C. A. Hop, S. C. Khojasteh, P. S. Dragovich, *ACS Medicinal Chemistry Letters* **2016**, *7*, 988-993.

[164] I. Glassford, C. N. Teijaro, S. S. Daher, A. Weil, M. C. Small, S. K. Redhu, D. J. Colussi, M. A. Jacobson, W. E. Childers, B. Buttaro, A. W. Nicholson, A. D. MacKerell, Jr., B. S. Cooperman, R. B. Andrade, *Journal of the American Chemical Society* **2016**, *138*, 3136-3144.

[165] S. K. Mamidyala, M. G. Finn, *Chemical Society Reviews* **2010**, *39*, 1252-1261.

[166] https://www.marketwatch.com/press-release/hydroxyproline-market-2022-global-growth-insight-top-countries-data-share-size-future-demand-research-top-leading-player-emerging-trends-region-by-forecast-to-2028-2022-09-19.

[167] R. Y. Zhao, Q. Yang, Y. Huang, S. Gai, L. Zhao, H. Ye, H. Guo, q. Tong, M. Cao, J. Jia, C. Yang, Not classified ed. (Eds.: L. SUZHOU M-CONJ BIOTECH CO., L. HANGZHOU DAC BIOTECH CO), **2016**.

[168] J. Pícha, M. Buděšínský, K. Macháčková, M. Collinsová, J. Jiráček, *Journal of Peptide Science* **2017**, *23*, 202-214.

[169] S. Wiejak, E. Masiukiewicz, B. Rzeszotarska, *Chemical and Pharmaceutical Bulletin* **2001**, *49*, 1189-1191.

[170] K. Lang, J. W. Chin, *ACS Chemical Biology* **2014**, *9*, 16-20.

[171] J. Dommerholt, F. P. J. T. Rutjes, F. L. van Delft, *Topics in Current Chemistry* **2016**, *374*, 16.

[172] T. Shintou, T. Mukaiyama, *Journal of the American Chemical Society* **2004**, *126*, 7359-7367.

[173] S. W. Millward, H. D. Agnew, B. Lai, S. S. Lee, J. Lim, A. Nag, S. Pitram, R. Rohde, J. R. Heath, *Integrative Biology* **2012**, *5*, 87-95.

[174] K. Kiakos, J. M. Hartley, J. A. Hartley, in *Drug-DNA Interaction Protocols* (Ed.: K. R. Fox), Humana Press, Totowa, NJ, **2010**, pp. 283-302.

[175] M. Lavesa, K. R. Fox, *Analytical Biochemistry* **2001**, *293*, 246-250.

[176] K. M. Rahman, H. Rosado, J. B. Moreira, E.-A. Feuerbaum, K. R. Fox, E. Stecher, P. W. Howard, S. J. Gregson, C. H. James, M. de la Fuente, D. E. Waldron, D. E. Thurston, P. W. Taylor, *Journal of Antimicrobial Chemotherapy* **2012**, *67*, 1683-1696.

[177] D. M. M. Jaradat, *Amino Acids* **2018**, *50*, 39-68.

[178] A. B. Berger, P. M. Vitorino, M. Bogyo, *American Journal of Pharmacogenomics* **2004**, *4*, 371-381.

[179] J. D. Bargh, A. Isidro-Llobet, J. S. Parker, D. R. Spring, *Chemical Society Reviews* **2019**, *48*, 4361-4374.

[180] Y. Wang, A. G. Cheetham, G. Angacian, H. Su, L. Xie, H. Cui, *Advanced Drug Delivery Reviews* **2017**, *110-111*, 112-126.

[181] W. Tegge, G. Guerra, A. Höltke, L. Schiller, U. Beutling, K. Harmrolfs, L. Gröbe, H. Wullenkord, C. Xu, H. Weich, M. Brönstrup, *Angewandte Chemie International Edition* **2021**, *60*, 17989-17997.

[182] X. Ning, S. Lee, Z. Wang, D. Kim, B. Stubblefield, E. Gilbert, N. Murthy, *Nature Materials* **2011**, *10*, 602-607.

[183] S. M. Lehar, T. Pillow, M. Xu, L. Staben, K. K. Kajihara, R. Vandlen, L. DePalatis, H. Raab, W. L. Hazenbos, J. Hiroshi Morisaki, J. Kim, S. Park, M. Darwish, B.-C. Lee, H. Hernandez, K. M. Loyet, P. Lupardus, R. Fong, D. Yan, C. Chalouni, E. Luis, Y. Khalfin, E. Plise, J. Cheong, J. P. Lyssikatos, M. Strandh, K. Koefoed, P. S. Andersen, J. A. Flygare, M. Wah Tan, E. J. Brown, S. Mariathasan, *Nature* **2015**, *527*, 323-328.

[184] C. Peukert, S. Popat Gholap, O. Green, L. Pinkert, J. van den Heuvel, M. van Ham, D. Shabat, M. Brönstrup, *Angewandte Chemie International Edition* **2022**, *61*, e202201423.

[185] P. T. Wong, S. K. Choi, *Chemical Reviews* **2015**, *115*, 3388-3432.

[186] A. Alouane, R. Labruère, T. Le Saux, F. Schmidt, L. Jullien, *Angewandte Chemie International Edition* **2015**, *54*, 7492-7509.

[187] X. Yang, Z. Pan, M. R. Choudhury, Z. Yuan, A. Anifowose, B. Yu, W. Wang, B. Wang, *Medicinal Research Reviews* **2020**, *40*, 2682-2713.

[188] M. H. Lee, Z. Yang, C. W. Lim, Y. H. Lee, S. Dongbang, C. Kang, J. S. Kim, *Chemical Reviews* **2013**, *113*, 5071-5109.

[189] D. Toader, in *Cancer II* (Ed.: M. J. Waring), Springer International Publishing, Cham, **2018**, pp. 289-289.

[190] Z. Su, D. Xiao, F. Xie, L. Liu, Y. Wang, S. Fan, X. Zhou, S. Li, *Acta Pharmaceutica Sinica B* **2021**, *11*, 3889-3907.

[191] M. Azoulay, G. Tuffin, W. Sallem, J.-C. Florent, *Bioorganic & Medicinal Chemistry Letters* **2006**, *16*, 3147-3149.

[192] R. v. Brakel, R. C. M. Vulders, R. J. Bokdam, H. Grüll, M. S. Robillard, *Bioconjugate Chemistry* **2008**, *19*, 714-718.

[193] P. v. R. Schleyer, J. E. Williams, K. R. Blanchard, *Journal of the American Chemical Society* **1970**, *92*, 2377-2386.

[194] S. S. Matikonda, D. L. Orsi, V. Staudacher, I. A. Jenkins, F. Fiedler, J. Chen, A. B. Gamble, *Chemical Science* **2015**, *6*, 1212-1218.

[195] Y. Ge, X. Fan, P. R. Chen, *Chemical Science* **2016**, *7*, 7055-7060.

[196] R. M. Versteegen, R. Rossin, W. ten Hoeve, H. M. Janssen, M. S. Robillard, *Angewandte Chemie International Edition* **2013**, *52*, 14112-14116.

[197] J. Li, S. Jia, P. R. Chen, *Nature Chemical Biology* **2014**, *10*, 1003-1005.

[198] G. Zhang, J. Li, R. Xie, X. Fan, Y. Liu, S. Zheng, Y. Ge, P. R. Chen, *ACS Central Science* **2016**, *2*, 325-331.

[199] L. Liu, Y. Liu, G. Zhang, Y. Ge, X. Fan, F. Lin, J. Wang, H. Zheng, X. Xie, X. Zeng, P. R. Chen, *Biochemistry* **2018**, *57*, 446-450.

[200] J. C. T. Carlson, H. Mikula, R. Weissleder, *Journal of the American Chemical Society* **2018**, *140*, 3603-3612.

[201] E. Jiménez-Moreno, Z. Guo, B. L. Oliveira, I. S. Albuquerque, A. Kitowski, A. Guerreiro, O. Boutureira, T. Rodrigues, G. Jiménez-Osés, G. J. L. Bernardes, *Angewandte Chemie International Edition* **2017**, *56*, 243-247.

[202] K. Neumann, S. Jain, A. Gambardella, S. E. Walker, E. Valero, A. Lilienkampf, M. Bradley, *ChemBioChem* **2017**, *18*, 91-95.

[203] M. Xu, J. Tu, R. M. Franzini, *Chemical Communications* **2017**, *53*, 6271-6274.

[204] S. Milstien, L. A. Cohen, *Journal of the American Chemical Society* **1972**, *94*, 9158-9165.

[205] S. Milstien, L. A. Cohen, *Proceedings of the National Academy of Sciences* **1970**, *67*, 1143-1147.

[206] R. T. Borchardt, L. A. Cohen, *Journal of the American Chemical Society* **1972**, *94*, 9166-9174.

[207] R. T. Borchardt, L. A. Cohen, *Journal of the American Chemical Society* **1972**, *94*, 9175-9182.

[208] M. M. King, L. A. Cohen, *Journal of the American Chemical Society* **1983**, *105*, 2752-2760.

[209] M. E. Jung, G. Piizzi, *Chemical Reviews* **2005**, *105*, 1735-1766.

[210] M. N. Levine, R. T. Raines, *Chemical Science* **2012**, *3*, 2412-2420.

[211] O. A. Okoh, P. Klahn, *ChemBioChem* **2018**, *19*, 1668-1694.

[212] R. B. Greenwald, Y. H. Choe, C. D. Conover, K. Shum, D. Wu, M. Royzen, *Journal of Medicinal Chemistry* **2000**, *43*, 475-487.

[213] S. Gangwar, G. M. Pauletti, T. J. Siahaan, V. J. Stella, R. T. Borchardt, *The Journal of Organic Chemistry* **1997**, *62*, 1356-1362.

[214] J. Z. Yang, W. Chen, R. T. Borchardt, *Journal of Pharmacology and Experimental Therapeutics* **2002**, *303*, 840.

[215] B. Wang, S. Gangwar, G. M. Pauletti, T. J. Siahaan, R. T. Borchardt, *The Journal of Organic Chemistry* **1997**, *62*, 1363-1367.

[216] R. Walther, J. Rautio, A. N. Zelikin, *Advanced Drug Delivery Reviews* **2017**, *118*, 65-77.

[217] X. Zhang, X. Li, Q. You, X. Zhang, *European Journal of Medicinal Chemistry* **2017**, *139*, 542-563.

[218] J. M. Ferriz, J. Vinsova, *Current Pharmaceutical Design* **2010**, *16*, 2033-2052.

[219] V. J. Stella, K. W. Nti-Addae, *Advanced Drug Delivery Reviews* **2007**, *59*, 677-694.

[220] J. B. Zawilska, J. Wojcieszak, A. B. Olejniczak, *Pharmacological Reports* **2013**, *65*, 1-14.

[221] S. Jana, S. Mandlekar, P. Marathe, *Current Medicinal Chemistry* **2010**, *17*, 3874-3908.

[222] Y. Ueda, A. B. Mikkilineni, J. O. Knipe, W. C. Rose, A. M. Casazza, D. M. Vyas, *Bioorganic & Medicinal Chemistry Letters* **1993**, *3*, 1761-1766.

[223] A. M. P. Melo, T. M. Bandeiras, M. Teixeira, *Microbiology and Molecular Biology Reviews* **2004**, *68*, 603-616.

[224] M. F. Mendoza, N. M. Hollabaugh, S. U. Hettiarachchi, R. L. McCarley, *Biochemistry* **2012**, *51*, 8014-8026.

[225] P. Liu, J. Xu, D. Yan, P. Zhang, F. Zeng, B. Li, S. Wu, *Chemical Communications* **2015**, *51*, 9567-9570.

[226] B. Li, P. Liu, D. Yan, F. Zeng, S. Wu, *Journal of Materials Chemistry B* **2017**, *5*, 2635-2643.

[227] G. G. Dias, A. King, F. de Moliner, M. Vendrell, E. N. da Silva Júnior, *Chemical Society Reviews* **2018**, *47*, 12-27.

[228] A. Shigenaga, K. Ogura, H. Hirakawa, J. Yamamoto, K. Ebisuno, L. Miyamoto, K. Ishizawa, K. Tsuchiya, A. Otaka, *ChemBioChem* **2012**, *13*, 968-971.

[229] M. M. Yatzeck, L. D. Lavis, T.-Y. Chao, S. S. Chandran, R. T. Raines, *Bioorganic & Medicinal Chemistry Letters* **2008**, *18*, 5864-5866.

[230] J. Zhou, J. Zhang, H. Ren, X. Dong, X. Zheng, W. Zhao, *Journal of Photochemistry and Photobiology A: Chemistry* **2018**, *355*, 94-100.

[231] A. Shigenaga, J. Yamamoto, H. Hirakawa, K. Ogura, N. Maeda, K. Morishita, A. Otaka, *Tetrahedron Letters* **2010**, *51*, 2525-2528.

[232] C. C. Jimidar, J. Grunenberg, B. Karge, H. L. S. Fuchs, M. Brönstrup, P. Klahn, *Chemistry – A European Journal* **2022**, *28*, e202103525.

[233] A. Shigenaga, D. Tsuji, N. Nishioka, S. Tsuda, K. Itoh, A. Otaka, *ChemBioChem* **2007**, *8*, 1929-1931.

[234] C. G. Bochet, *Journal of the Chemical Society, Perkin Transactions 1* **2002**, 125-142.

[235] D. P. Walton, D. A. Dougherty, *Journal of the American Chemical Society* **2017**, *139*, 4655-4658.

[236] D. A. Unruh, C. Mauldin, S. J. Pastine, M. Rolandi, J. M. J. Fréchet, *Journal of the American Chemical Society* **2010**, *132*, 6890-6891.

[237] S. Ciampi, M. James, M. H. Choudhury, N. A. Darwish, J. J. Gooding, *Physical Chemistry Chemical Physics* **2013**, *15*, 9879-9890.

[238] S. Ciampi, M. James, G. Le Saux, K. Gaus, J. Justin Gooding, *Journal of the American Chemical Society* **2012**, *134*, 844-847.

[239] G. Clavier, P. Audebert, *Chemical Reviews* **2010**, *110*, 3299-3314.

[240] B. L. Oliveira, Z. Guo, G. J. L. Bernardes, *Chemical Society Reviews* **2017**, *46*, 4895-4950.

[241] H. Wu, N. K. Devaraj, *Accounts of Chemical Research* **2018**, *51*, 1249-1259.

[242] C. Hansch, A. Leo, R. W. Taft, *Chemical Reviews* **1991**, *91*, 165-195.

[243] https://bitly.com/getsigmas

[244] J. Brandrup, E. H. Immergut, E. A. Grulke, *Polymer Handbook*, 4th Edition ed., John Wiley, New York, **1999**.

[245] https://chemaxon.com/.

[246] X. Jiang, X. Hao, L. Jing, G. Wu, D. Kang, X. Liu, P. Zhan, *Expert Opinion on Drug Discovery* **2019**, *14*, 779-789.

[247] C. G. Parker, M. R. Pratt, *Cell* **2020**, *180*, 605-632.

[248] X. Zhang, S. Zhang, S. Zhao, X. Wang, B. Liu, H. Xu, *Frontiers in Chemistry* **2021**, *9*.

[249] Y. Takayama, K. Kusamori, M. Nishikawa, *Molecules* **2019**, *24*, 172.

[250] Y. Liu, M. P. Patricelli, B. F. Cravatt, *Proceedings of the National Academy of Sciences* **1999**, *96*, 14694-14699.

[251] D. Greenbaum, K. F. Medzihradszky, A. Burlingame, M. Bogyo, *Chemistry & Biology* **2000**, *7*, 569-581.

6   Appendix

6.1 NMR Spectra

(*S*)-2-(methoxycarbonyl)-4-methylenepyrrolidiniumchloride (88)
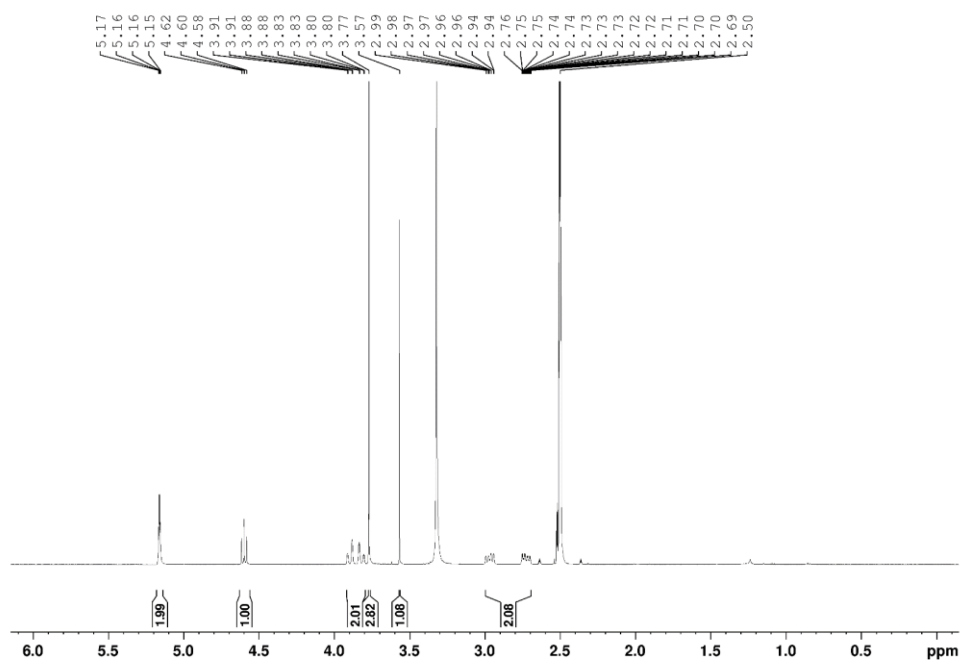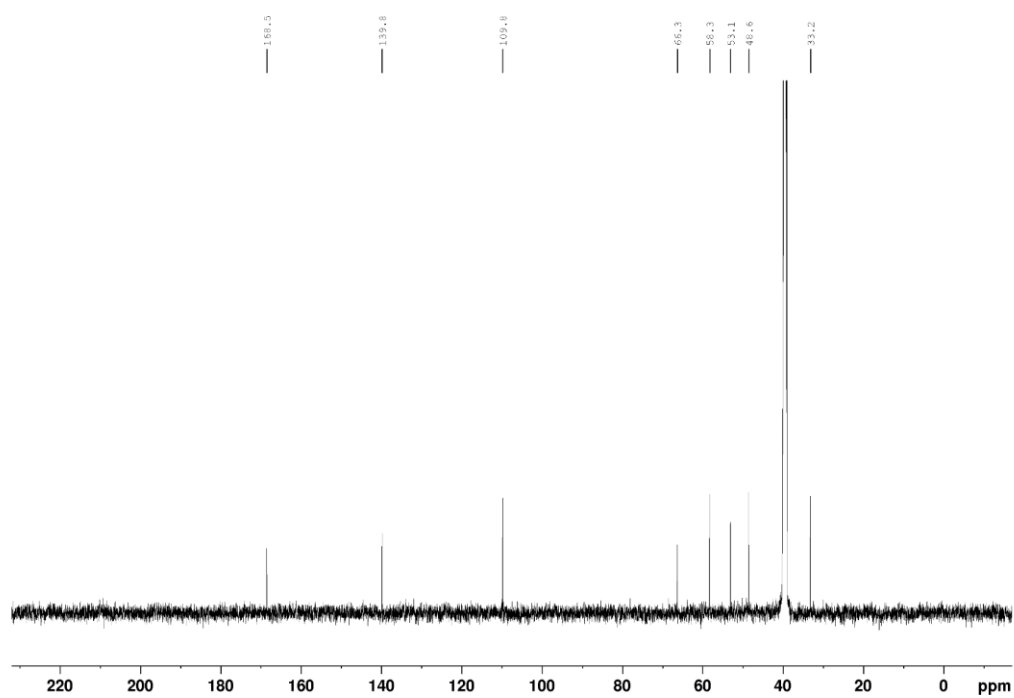
4-(benzyloxy)-3-methoxybenzoic acid (91)
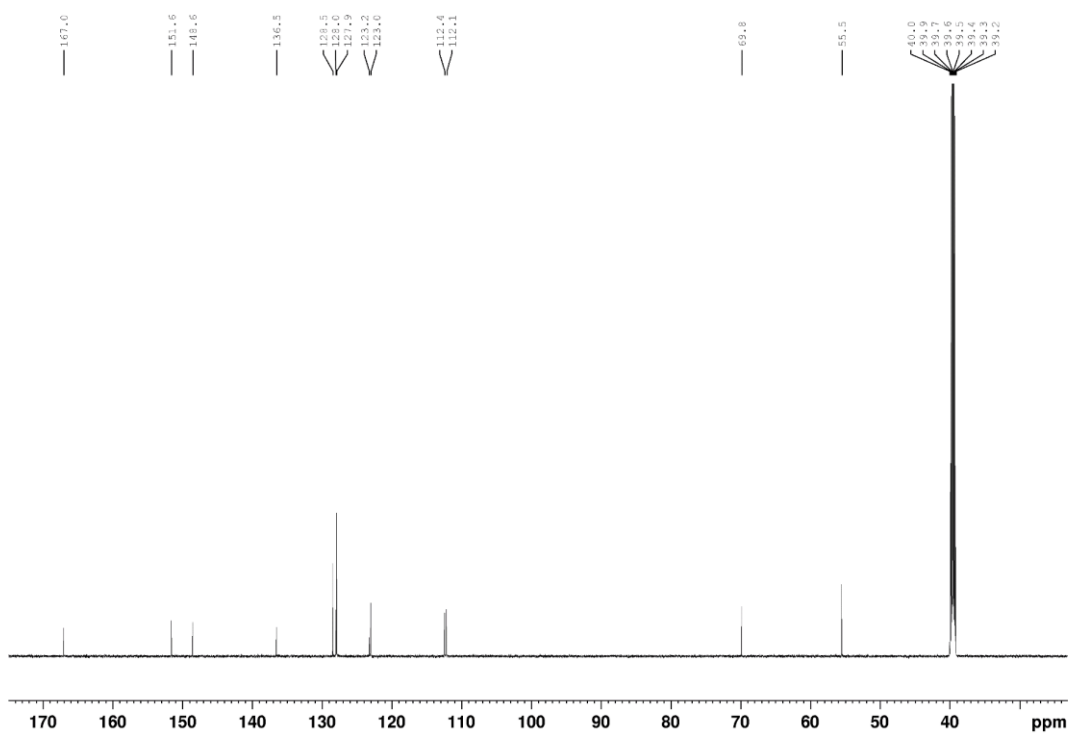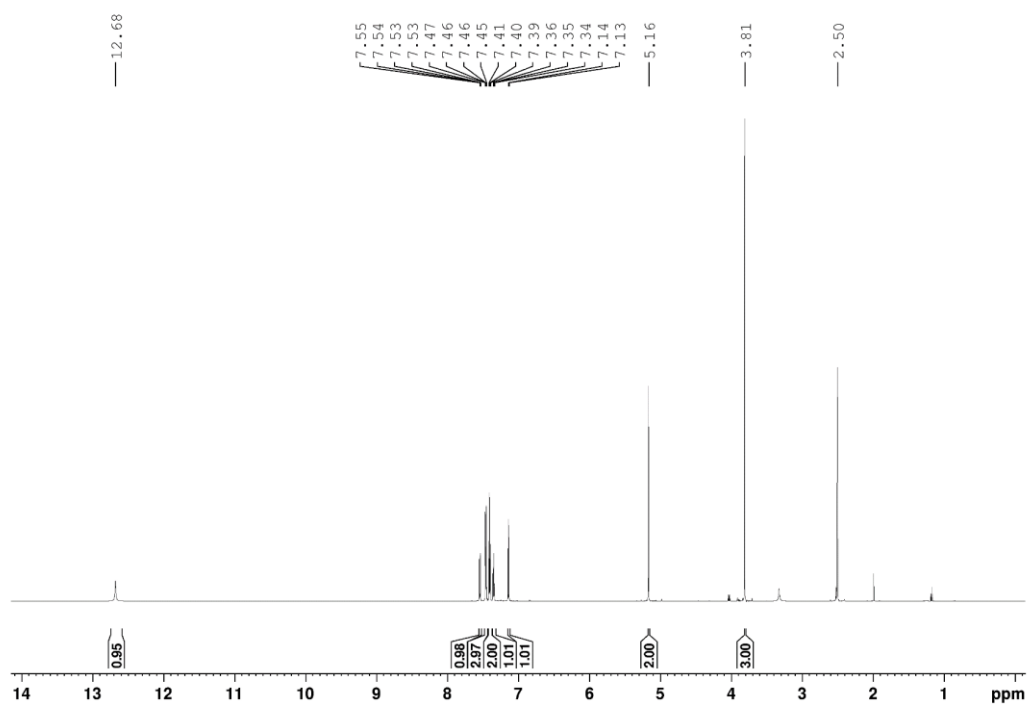
4-(benzyloxy)-5-methoxy-2-nitrobenzoic acid (92)
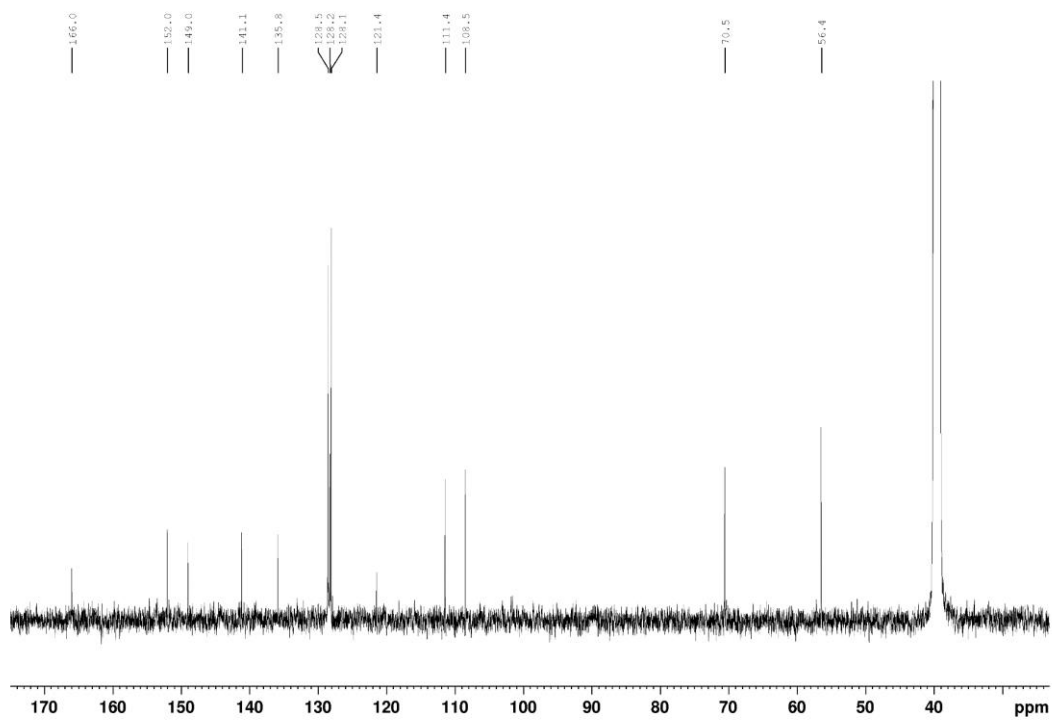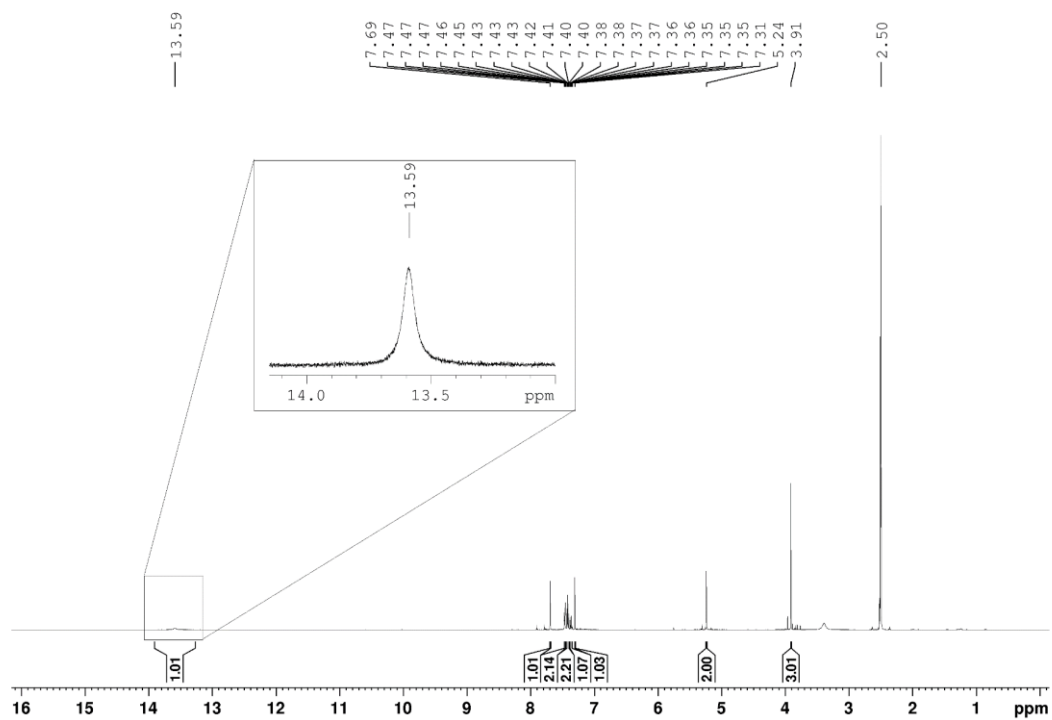
2-amino-4-(benzyloxy)-5-methoxybenzoic acid (99)
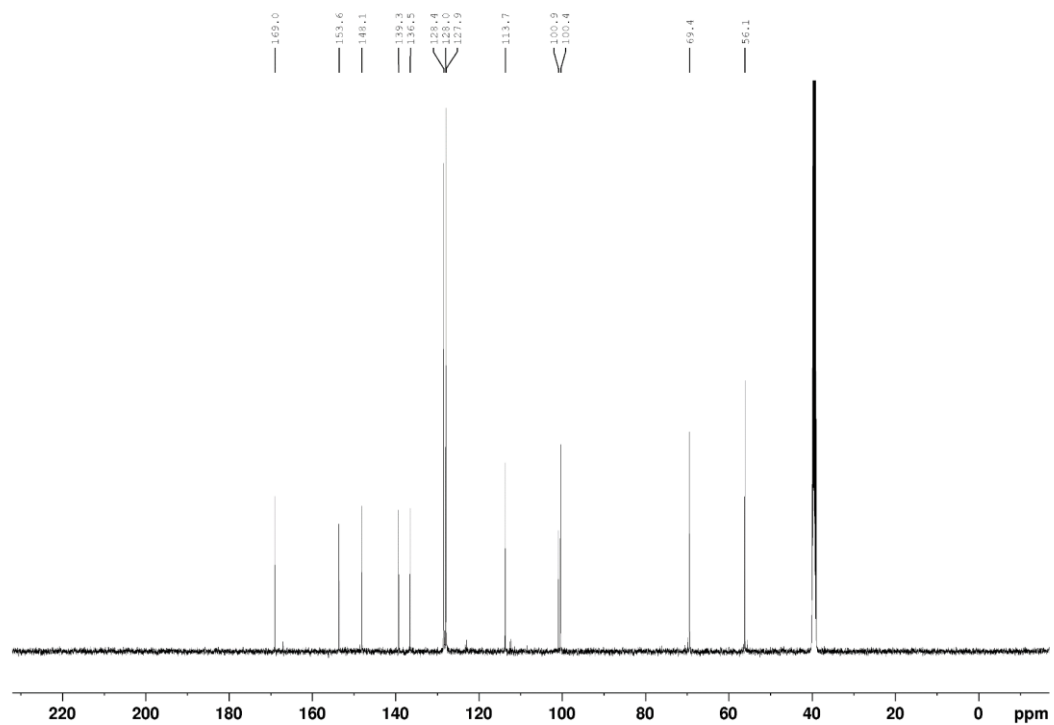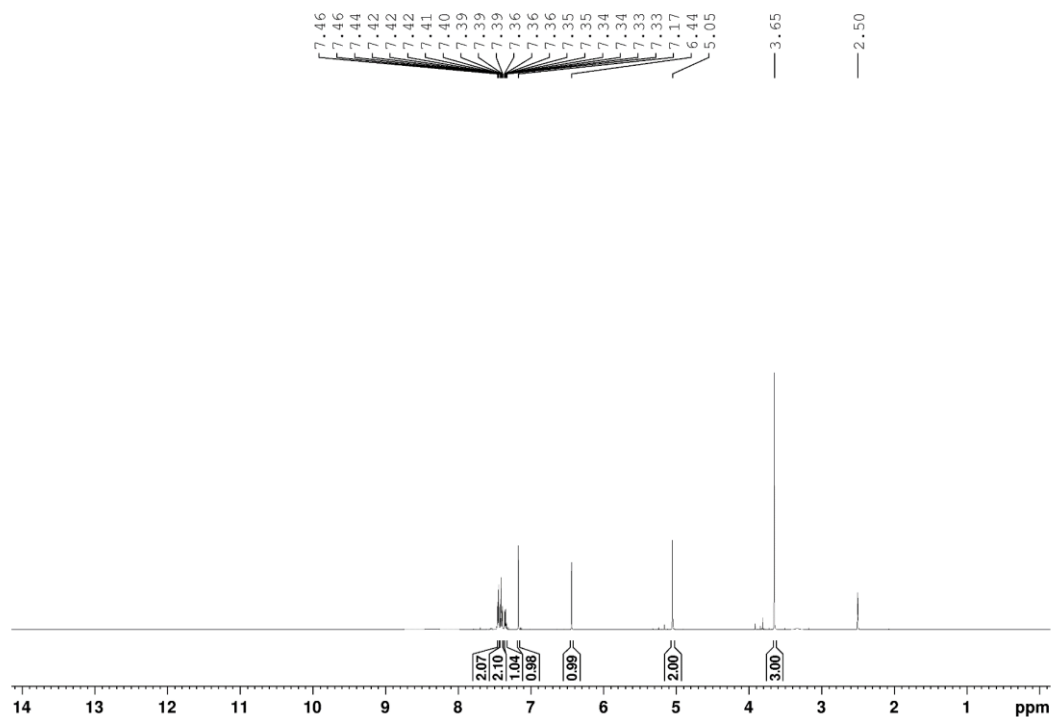
4-(benzyloxy)-2-((*tert*-butoxycarbonyl)amino)-5-methoxybenzoic acid (100)
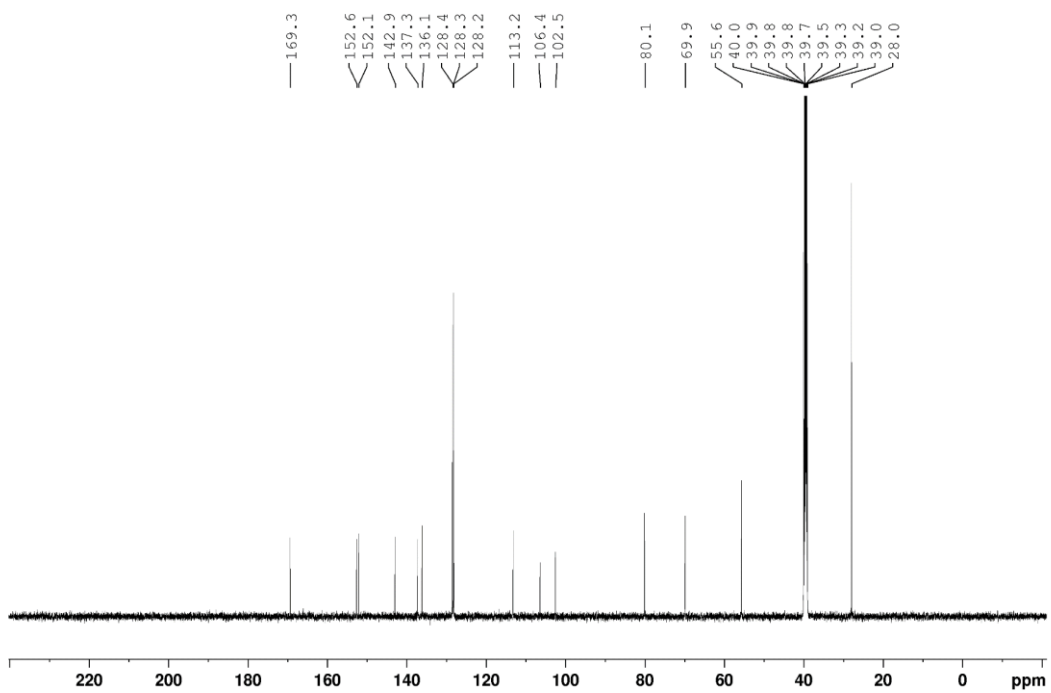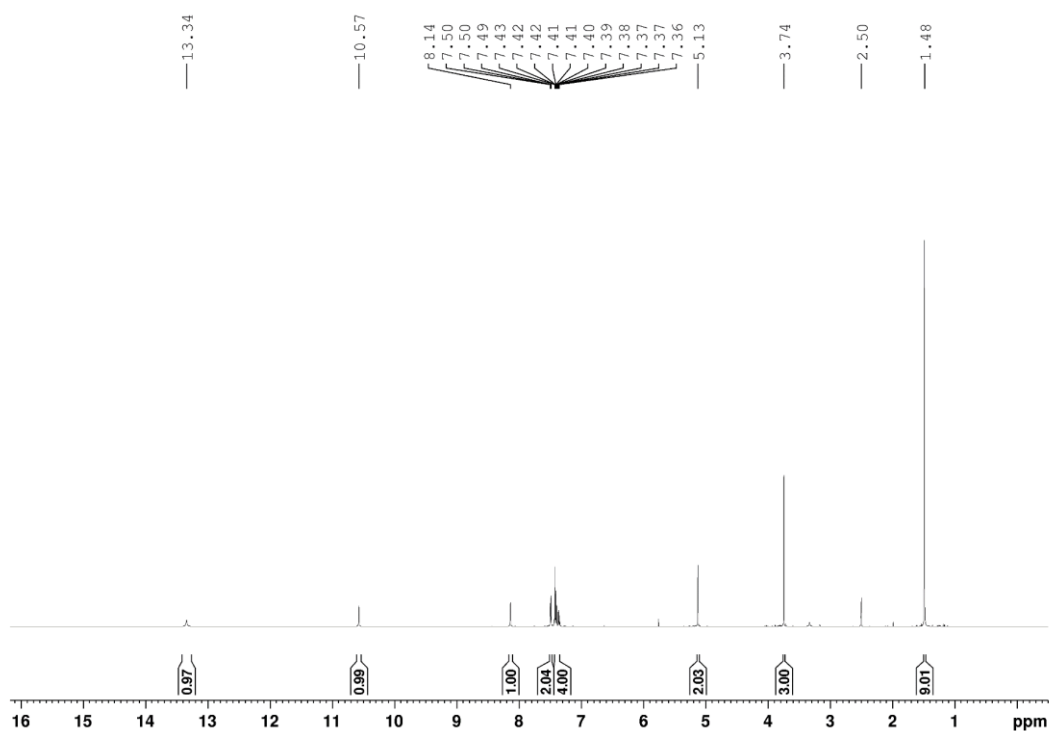
methyl(*S*)-1-(4-(benzyloxy)-2-((*tert*-butoxycarbonyl)amino)-5-methoxybenzoyl)-4-methylenepyrrolidine-2-carboxylate (101)
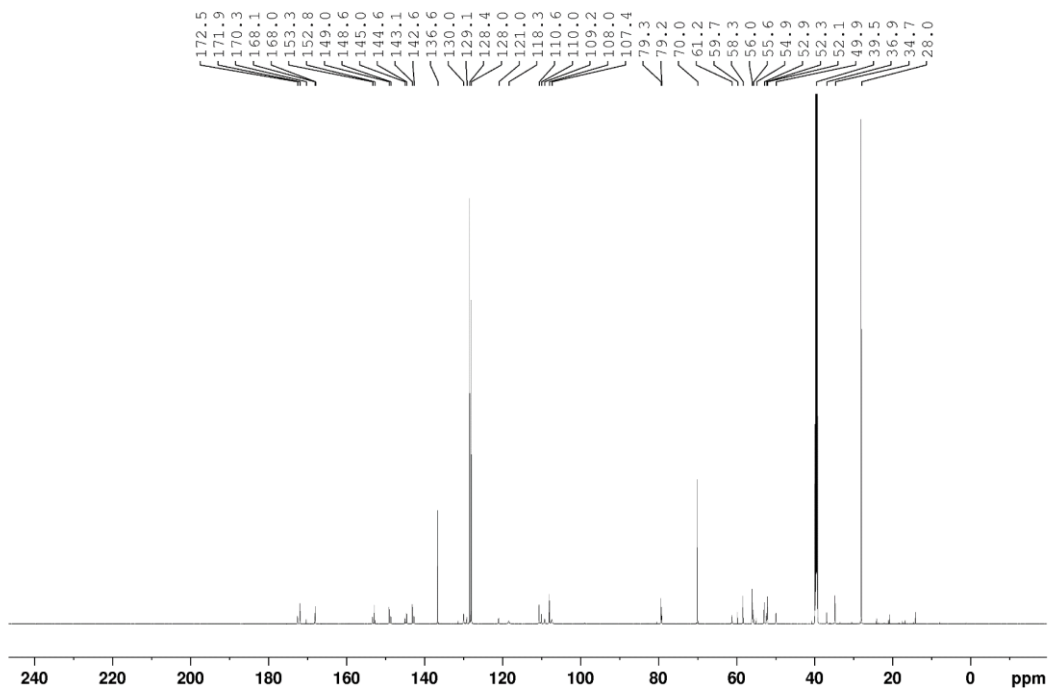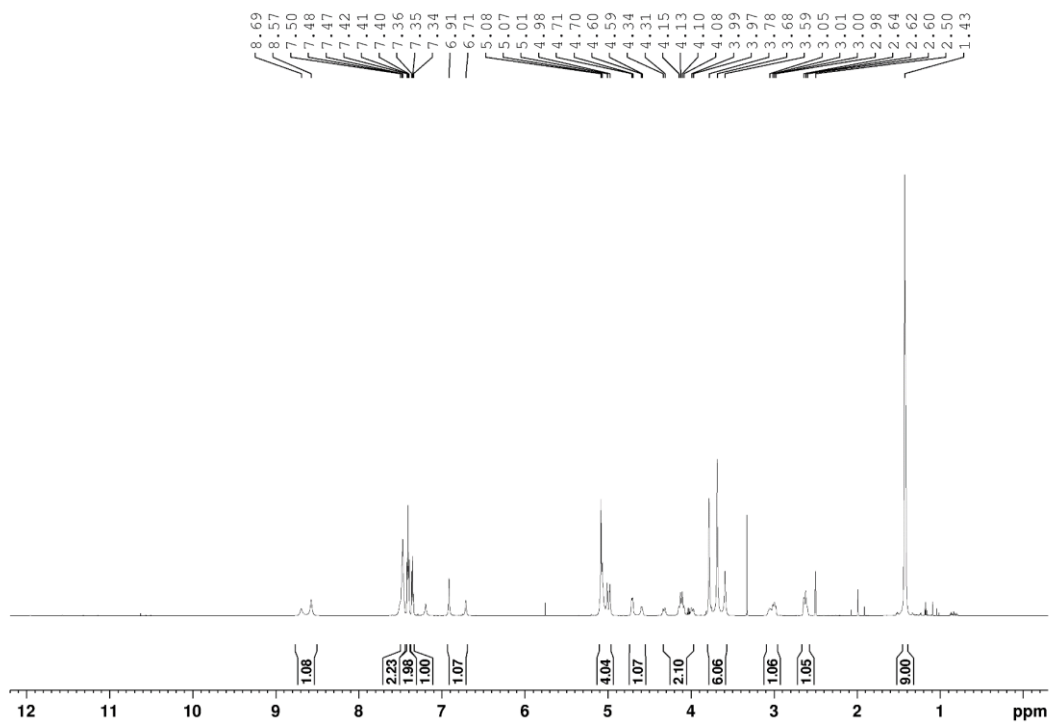
***tert*-butyl(*S*)-(5-(benzyloxy)-2-(2-formyl-4-methylenepyrrolidine-1-carbonyl)-4-methoxyphenyl)carbamate (102)**
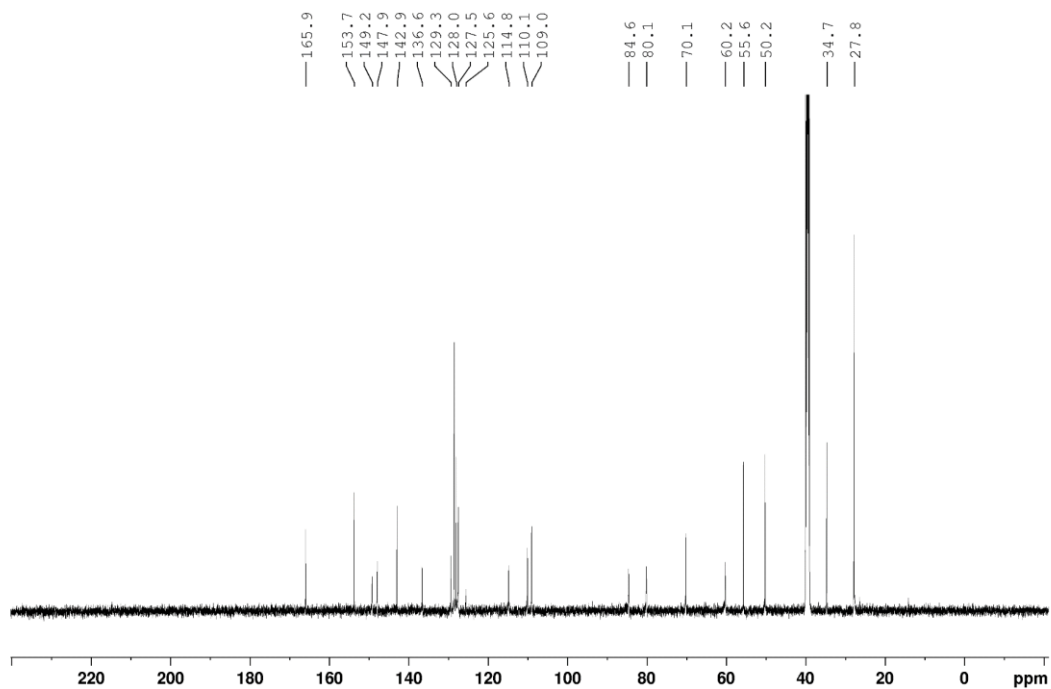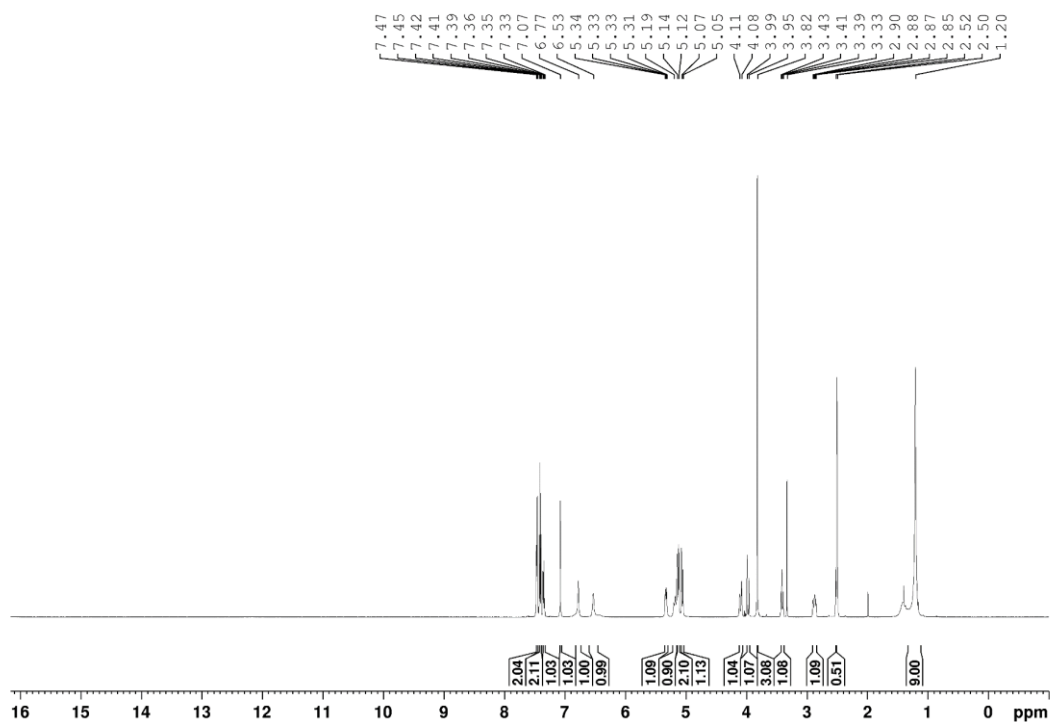
(*S*)-8-hydroxy-7-methoxy-2-methylene-1,2,3,11a-tetrahydro-5H-benzo[e]pyrrolo[1,2-a][1,4]diazepin-5-one (85)
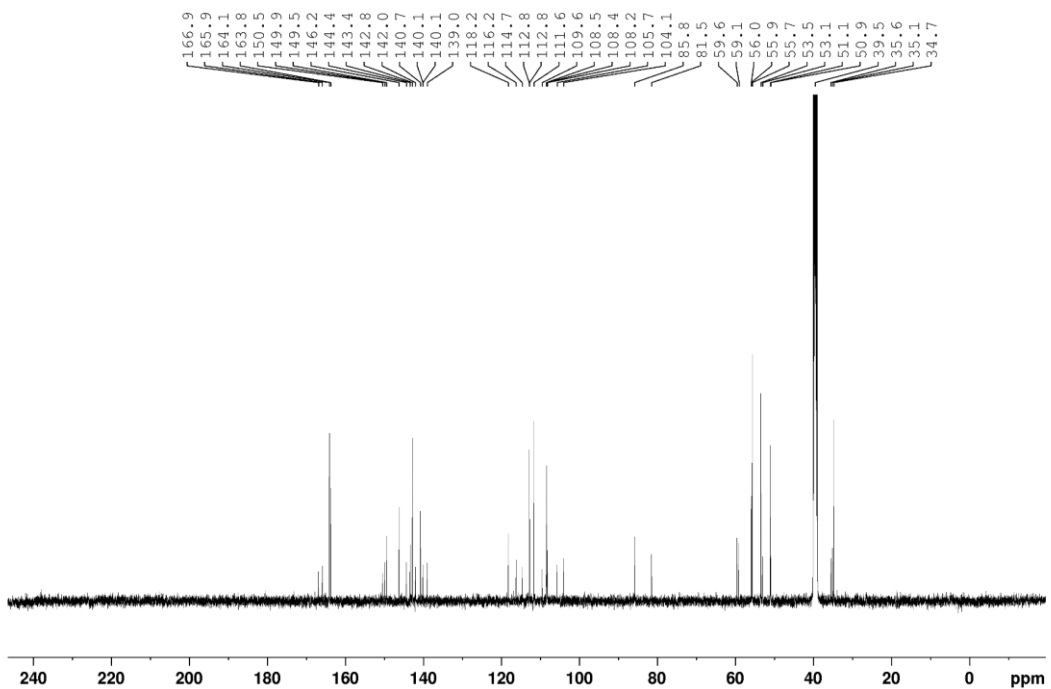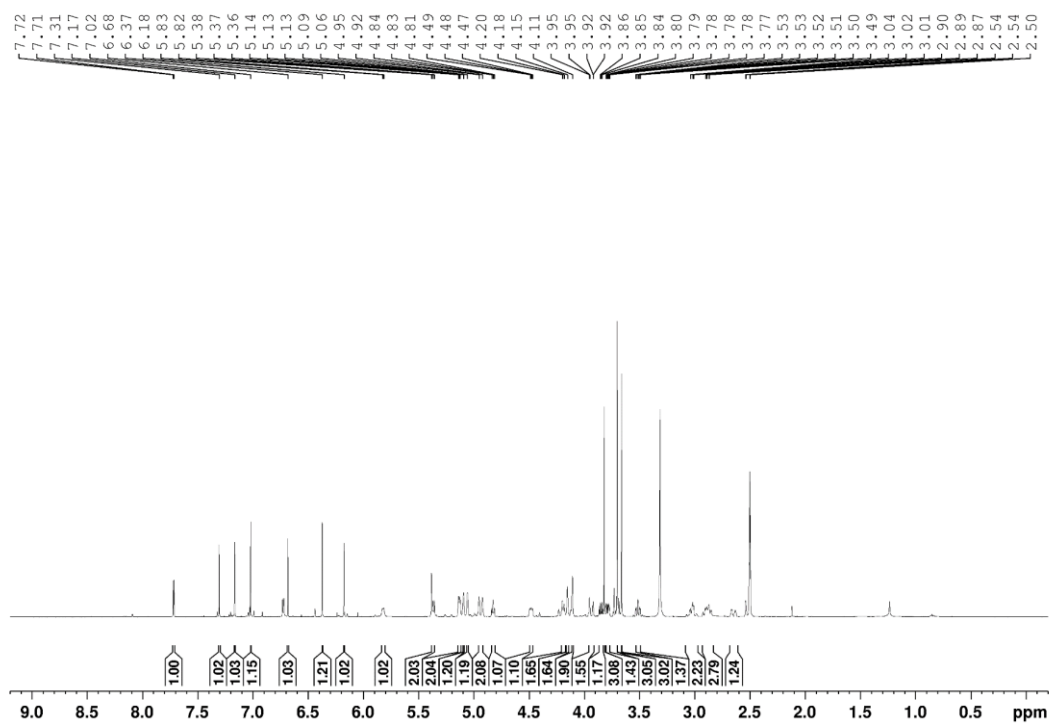
(*S*)-8-(2-bromoethoxy)-7-methoxy-2-methylene-1,2,3,11a-tetrahydro-5H-benzo[e]pyrrolo[1,2-a][1,4]diazepin-5-one (104)

(*S*)-8-(2-azidoethoxy)-7-methoxy-2-methylene-1,2,3,11a-tetrahydro-5H-
benzo[e]pyrrolo[1,2-a][1,4]diazepin-5-one (MbA)

166.6
165.7
164.5
163.5
151.1
150.4
149.9
147.1
144.2
143.2
142.9
142.7
140.8
140.5
139.9
138.9
119.8
117.2
114.8
112.9
111.4
110.5
108.5
108.4
106.3
105.9
102.2
85.8
81.4
67.5
67.3
67.0
59.5
59.1
56.0
56.0
55.8
53.5
53.2
51.2
51.0
49.6
39.5
35.6
35.1
34.7

(*S*)-7-methoxy-2-methylene-8-(prop-2-yn-1-yloxy)-1,2,3,11a-tetrahydro-5H-benzo[e]pyrrolo[1,2-a][1,4]diazepin-5-one (M1)

166.5
165.6
164.6
163.5
149.9
149.5
148.8
147.1
144.2
143.2
142.9
142.7
140.8
140.3
139.6
138.6
120.1
117.4
114.5
112.6
111.3
110.9
110.6
108.5
108.3
106.6
105.9
102.6
85.7
81.1
79.0
78.9
78.8
78.8
78.6
78.5
59.4
59.1
56.1
56.0
55.8
55.7
55.7
53.5
53.2
51.2
51.0
39.5
35.7
35.1
34.7

240 220 200 180 160 140 120 100 80 60 40 20 0 ppm
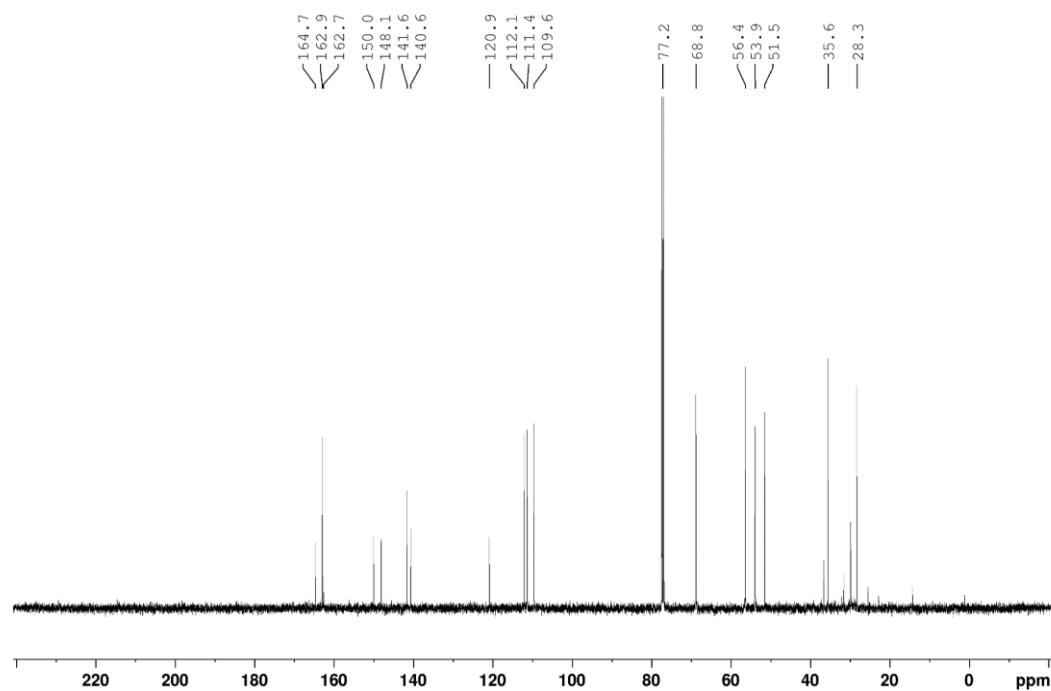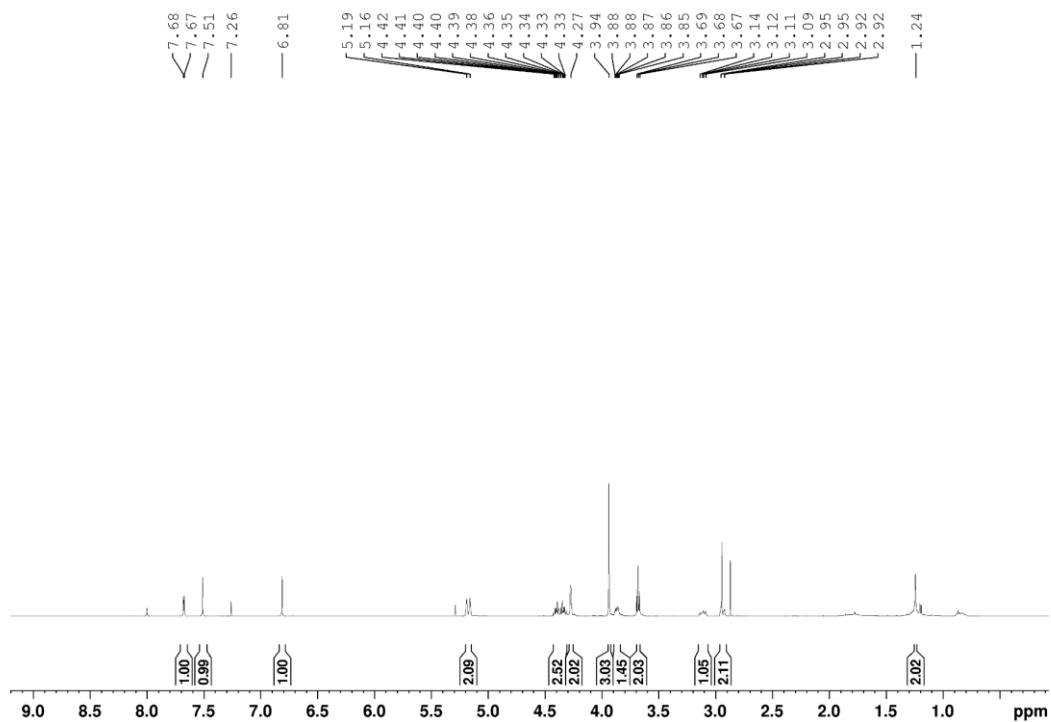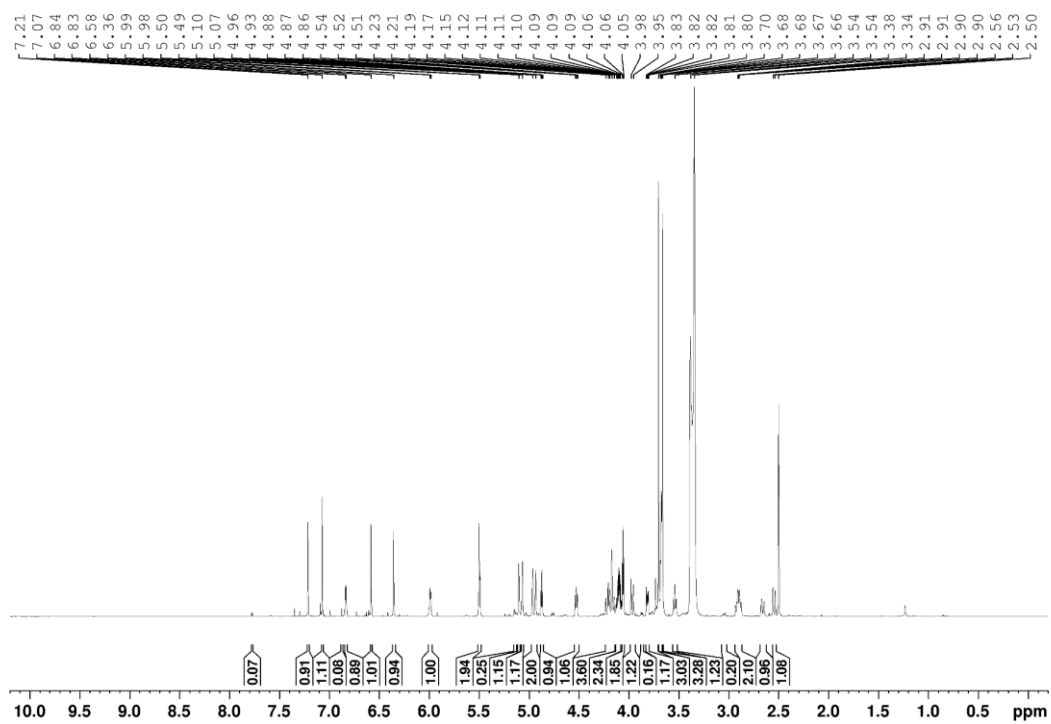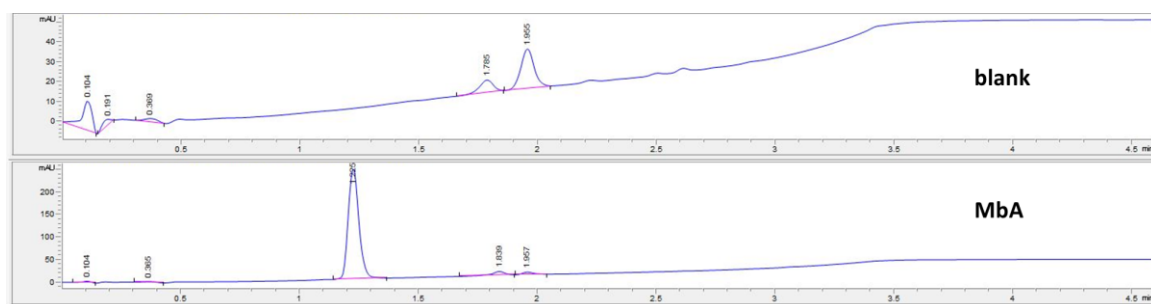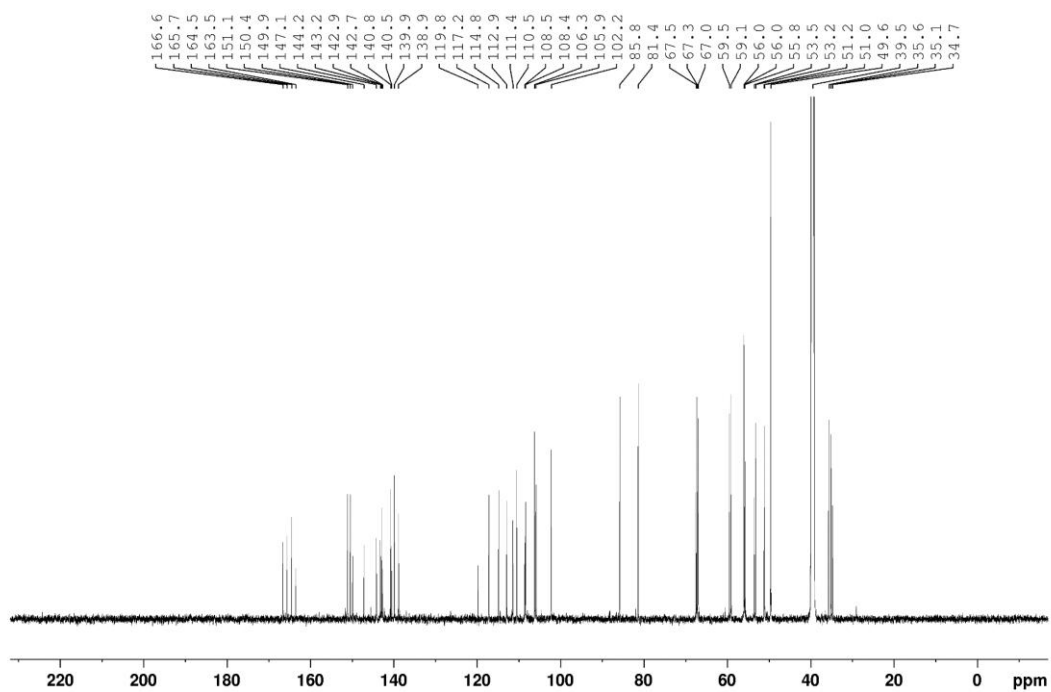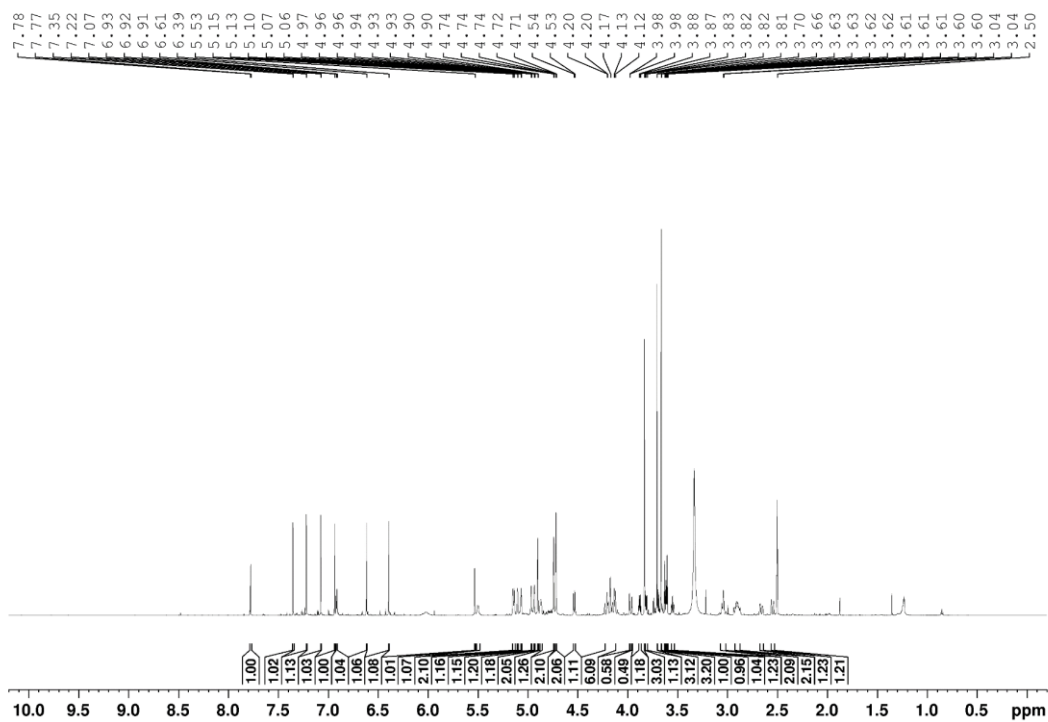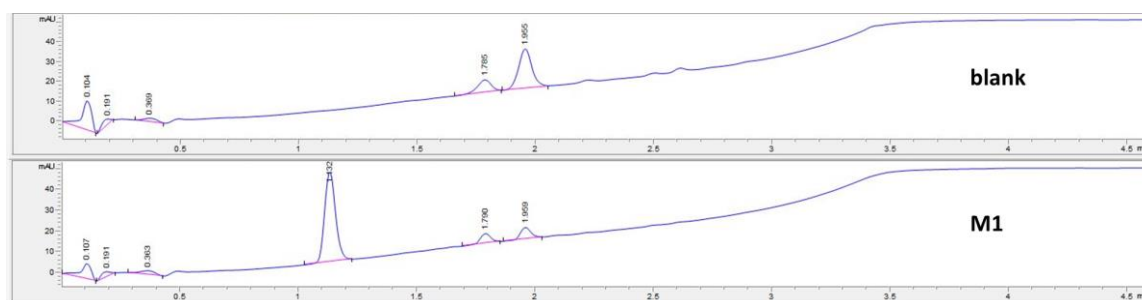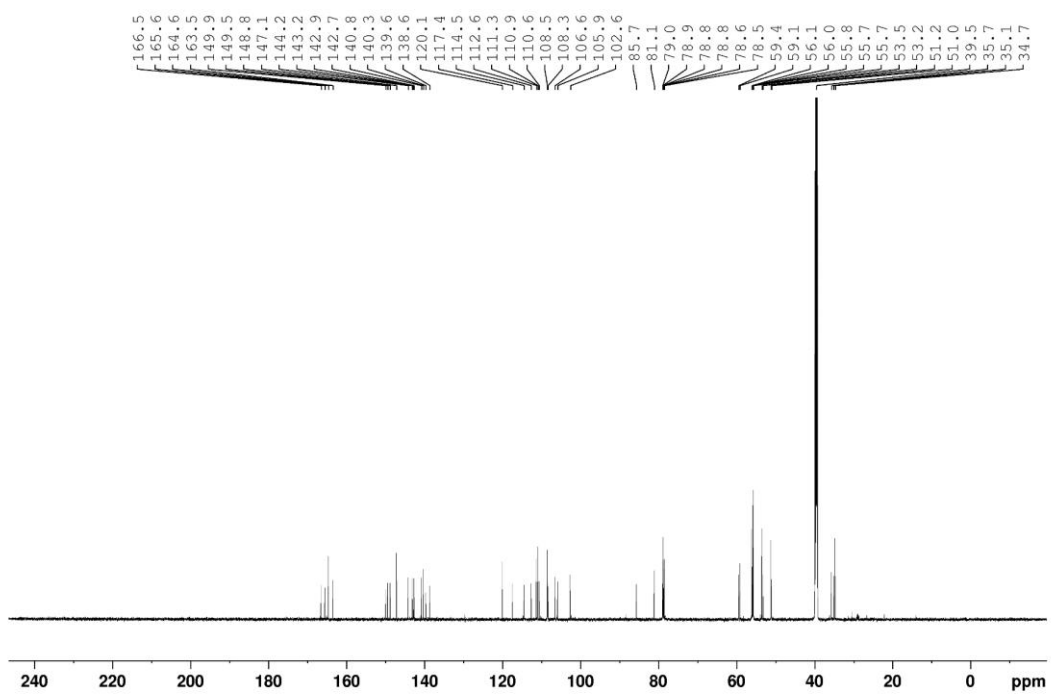
(*S*)-8-(but-3-yn-1-yloxy)-7-methoxy-2-methylene-1,2,3,11a-tetrahydro-5H-
benzo[e]pyrrolo[1,2-a][1,4]diazepin-5-one (M2)
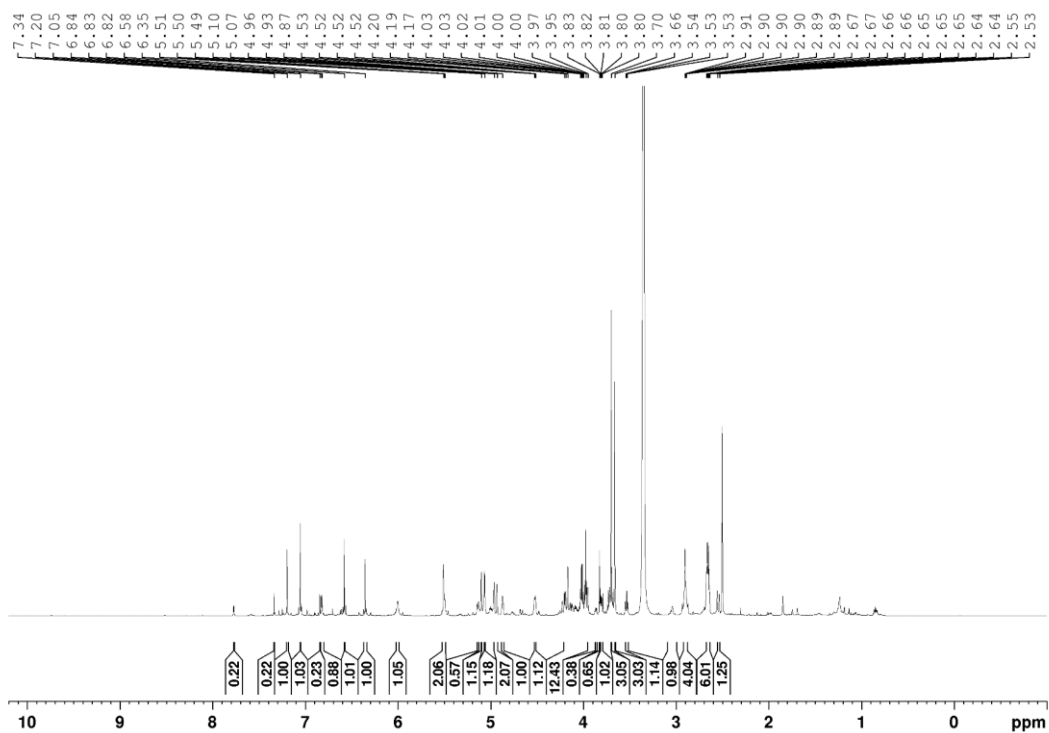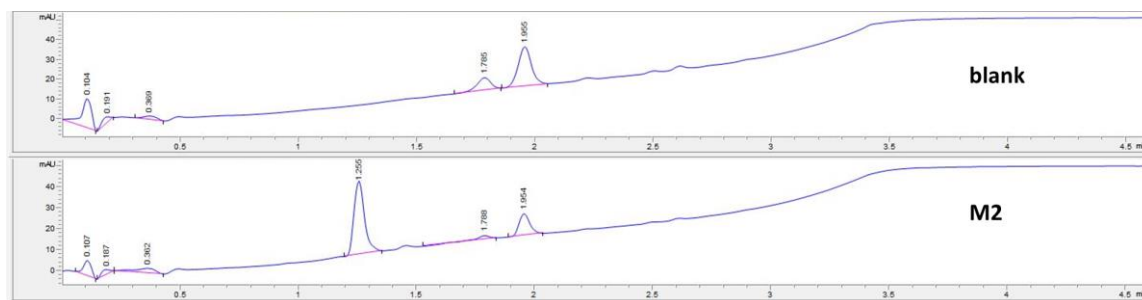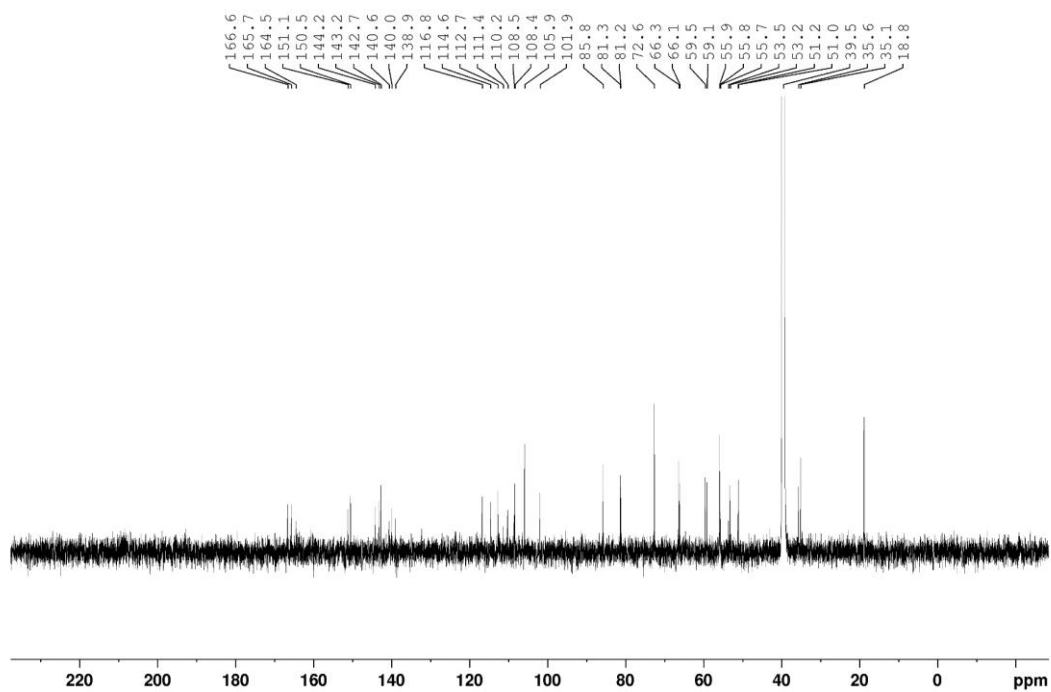
8,8-dibromobicyclo[5.1.0]octane (106)
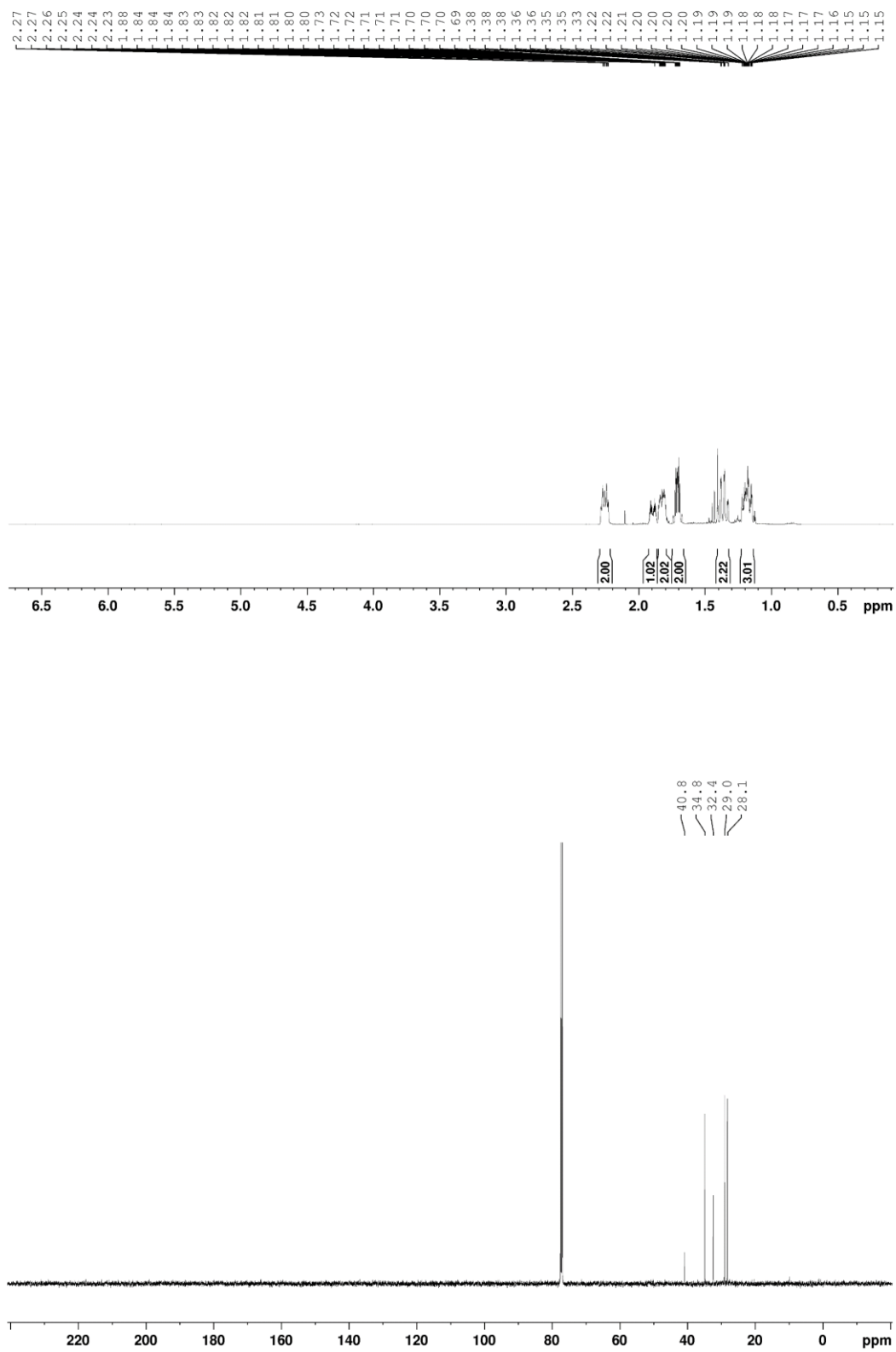
2-(cyclooct-2-yn-1-yloxy)ethan-1-ol (108)
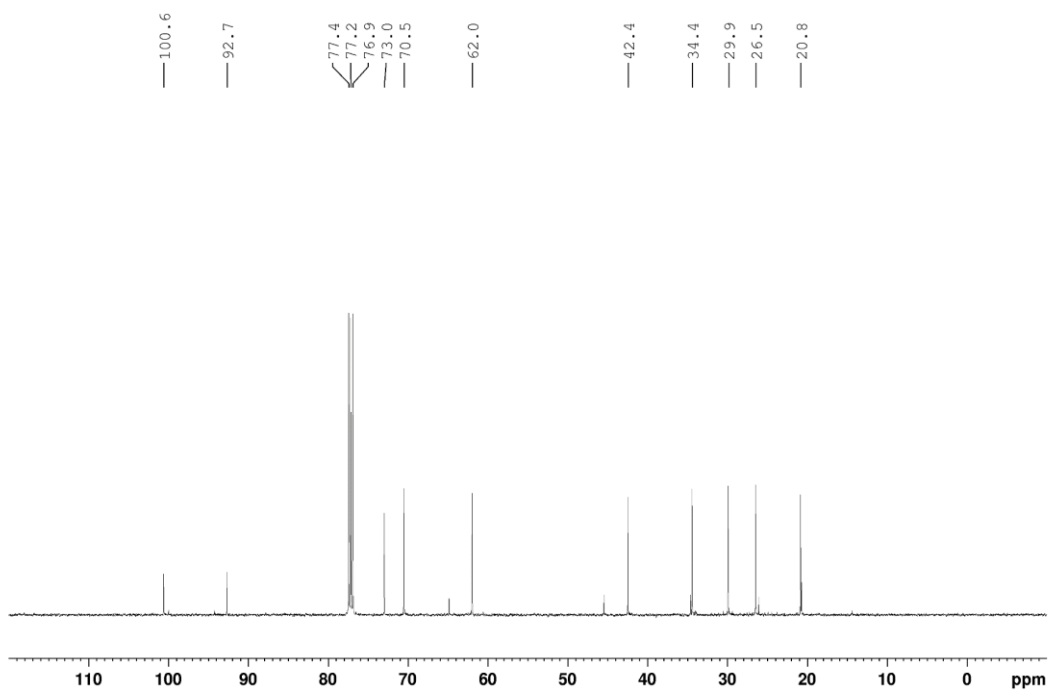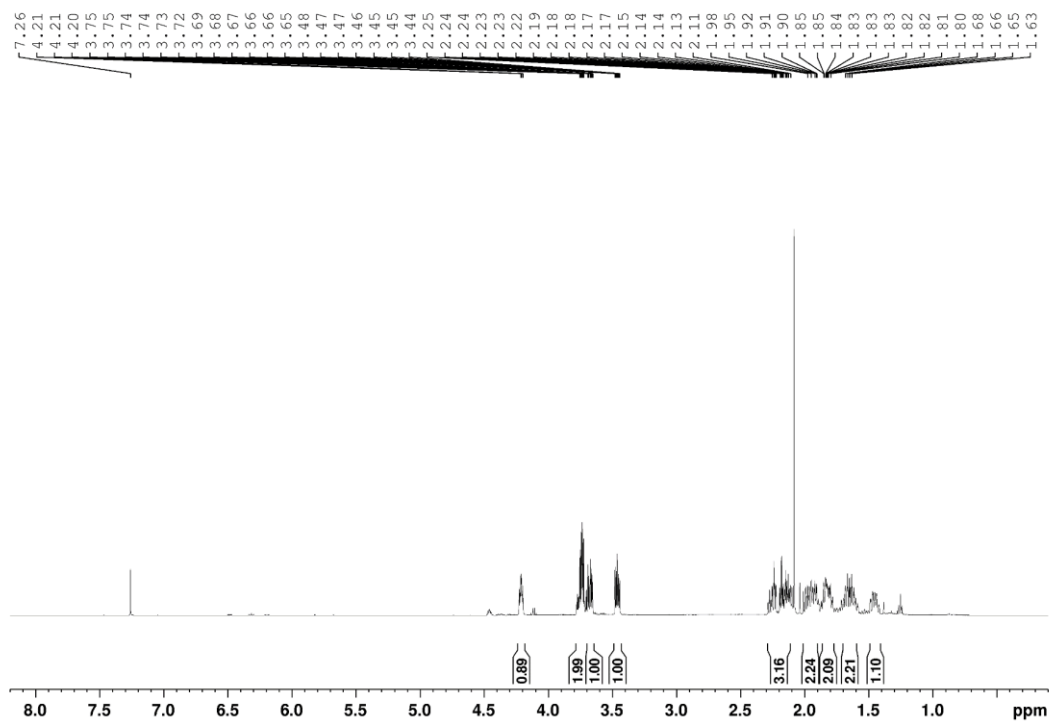
2-(cyclooct-2-yn-1-yloxy)ethyl 4-methylbenzenesulfonate (109)
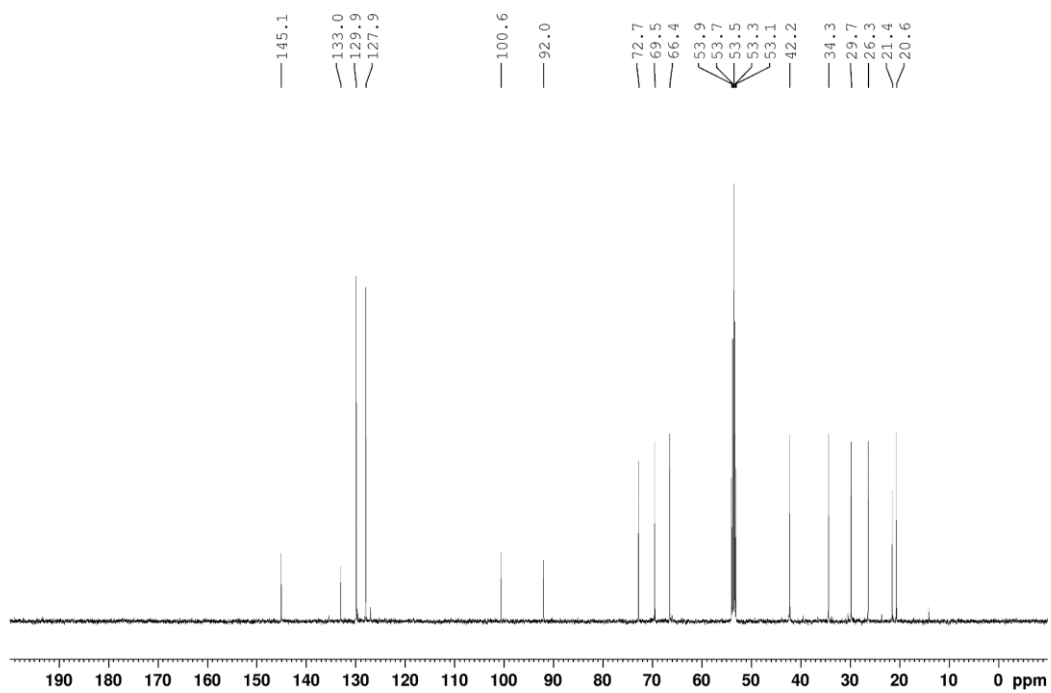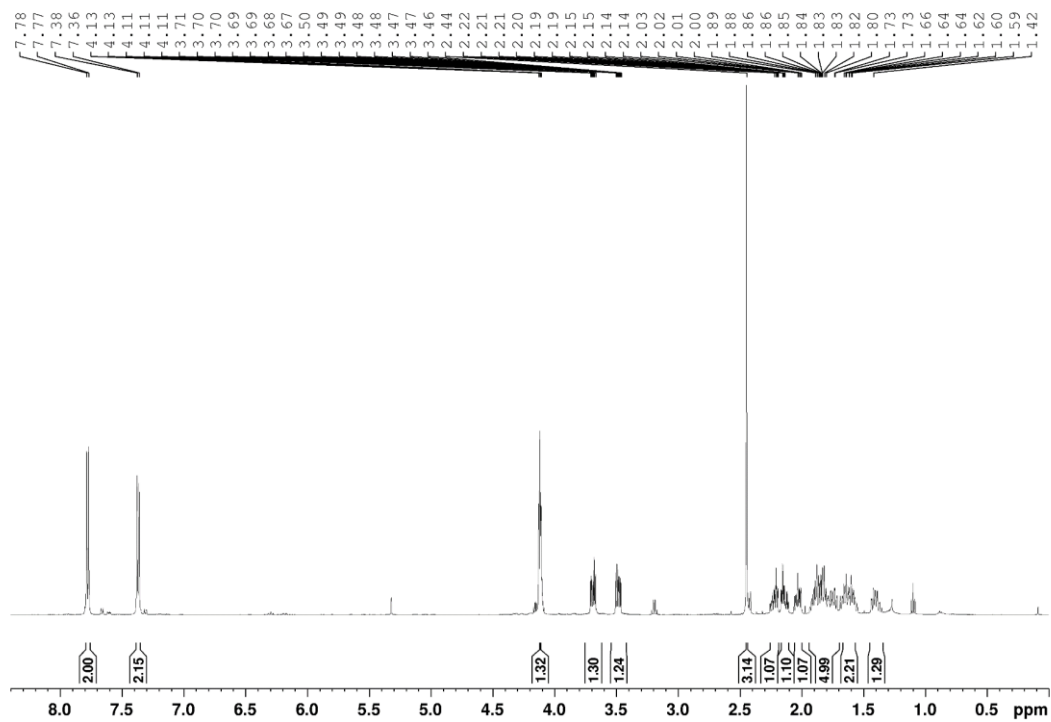
(11a*S*)-8-(2-(cyclooct-2-yn-1-yloxy)ethoxy)-7-methoxy-2-methylene-1,2,3,11a-tetrahydro-5H-benzo[e]pyrrolo[1,2-a][1,4]diazepin-5-one (M3)

166.63
165.67
165.33
164.34
163.56
151.41
150.83
150.25
147.01
144.22
143.26
142.69
140.65
140.57
139.94
139.04
131.57
119.38
116.57
114.55
112.69
111.25
110.30
110.02
108.49
108.29
105.82
101.86
100.00
92.96
85.76
81.27
75.26
71.93
69.78
67.90
67.87
67.55
67.32
66.90
59.51
59.08
55.83
55.63
53.51
53.16
51.12
51.02
41.86
35.63
35.11
34.72
33.87
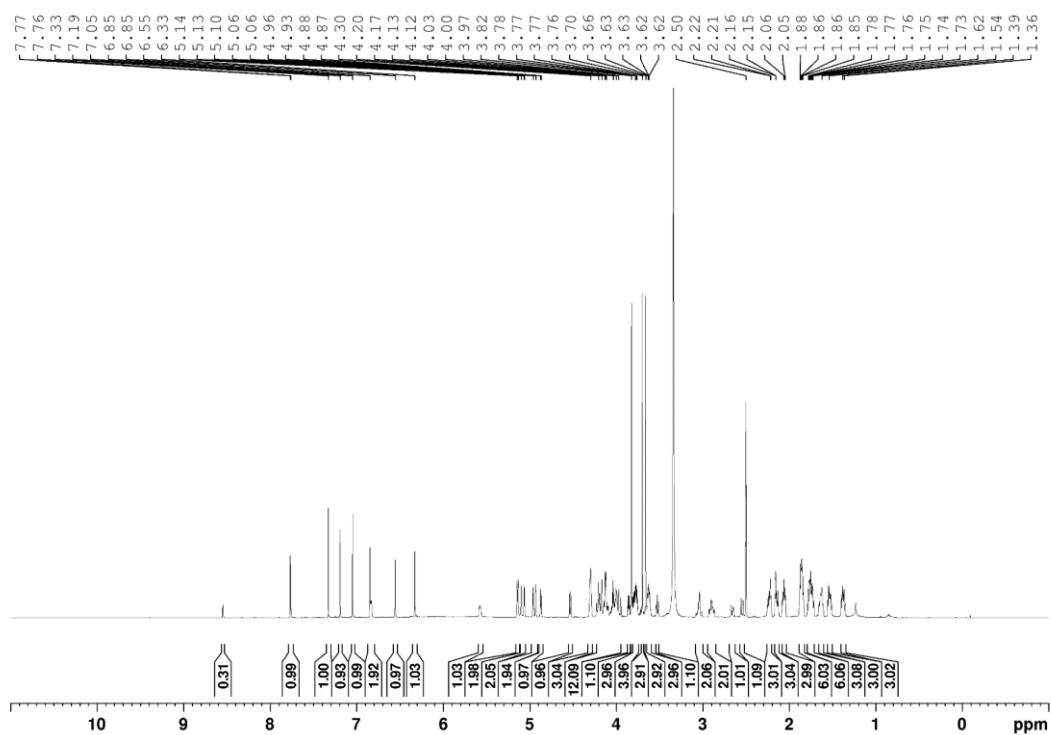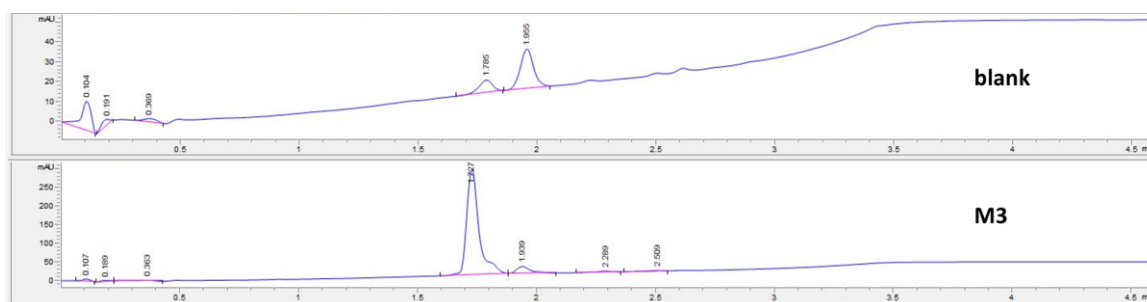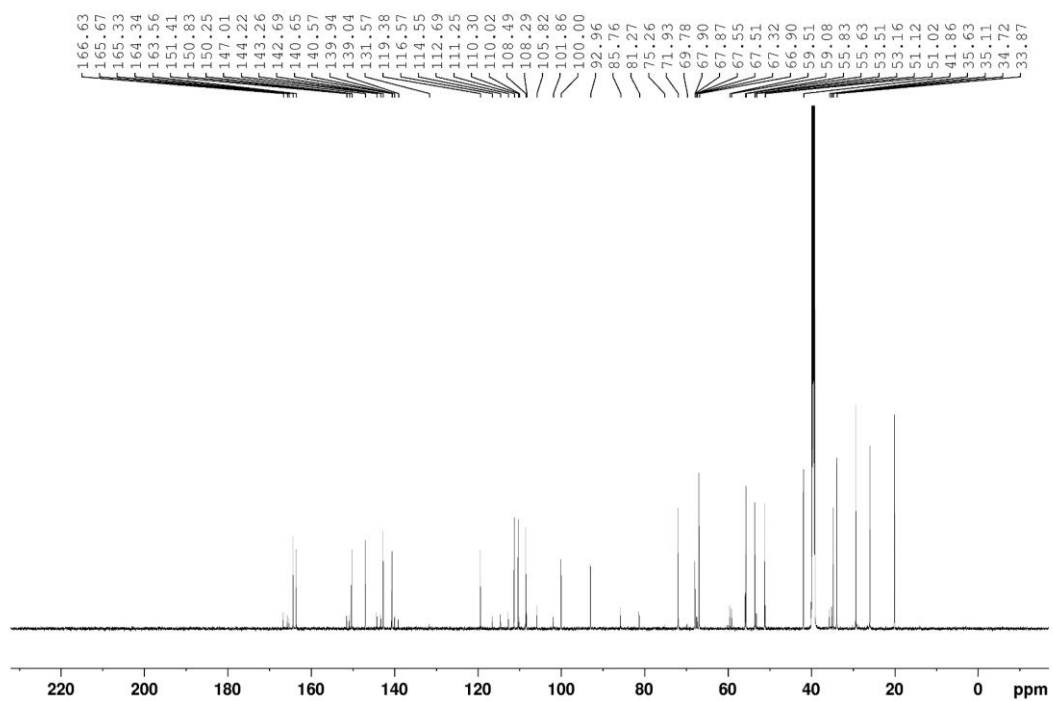
bicyclo[6.1.0]non-4-yn-9-ylmethyl (4-nitrophenyl) carbonate (115)

bicyclo[6.1.0]non-4-yn-9-ylmethyl((*S*)-7-methoxy-2-methylene-5-oxo-2,3,5,11a-tetrahydro-1H-benzo[e]pyrrolo[1,2-a][1,4]diazepin-8-yl) carbonate (M4)

165.7
163.0
152.1
148.9
142.5
141.6
139.7
125.7
120.8
112.6
108.7
98.9
67.3
56.2
54.9
53.5
51.2
49.8
39.5
34.7
28.5
20.8
19.9
17.1

210 200 190 180 170 160 150 140 130 120 110 100 90 80 70 60 50 40 30 20 10 0 ppm

(*S*)-8-(furan-2-ylmethoxy)-7-methoxy-2-methylene-1,2,3,11a-tetrahydro-5H-benzo[e]pyrrolo[1,2-a][1,4]diazepin-5-one (M5)

165.0
164.4
163.5
149.6
147.1
143.8
143.7
142.7
140.4
119.7
111.2
111.1
110.7
110.6
108.5
62.1
55.7
55.6
53.5
51.1
40.1
40.0
39.9
39.8
39.7
39.5
39.3
39.2
39.0
34.7

240   220   200   180   160   140   120   100   80   60   40   20   0   ppm
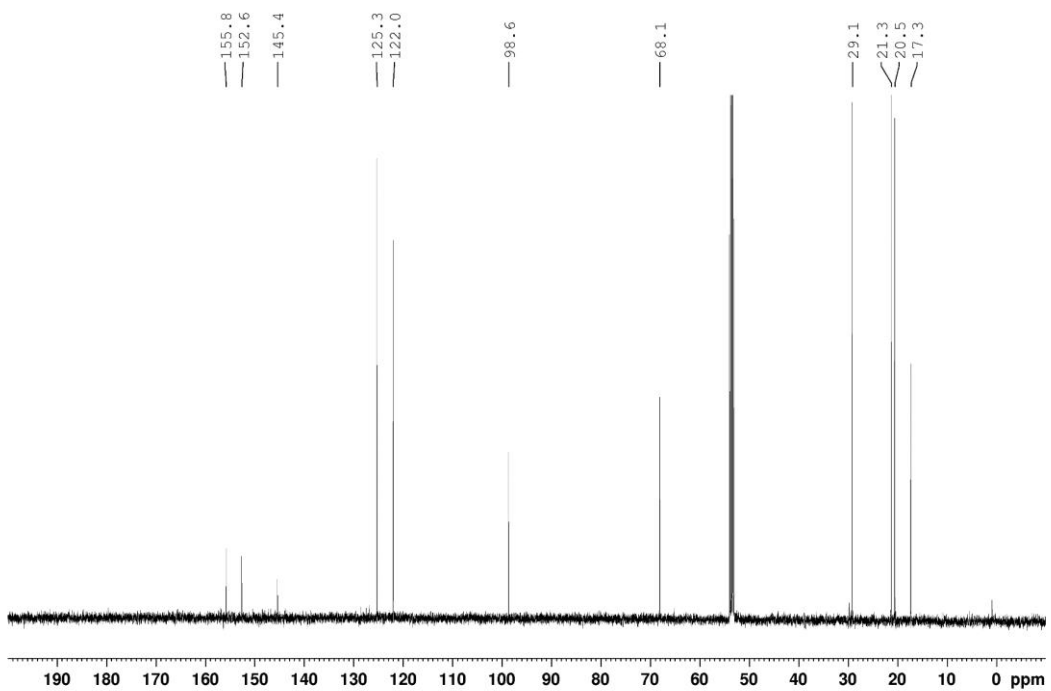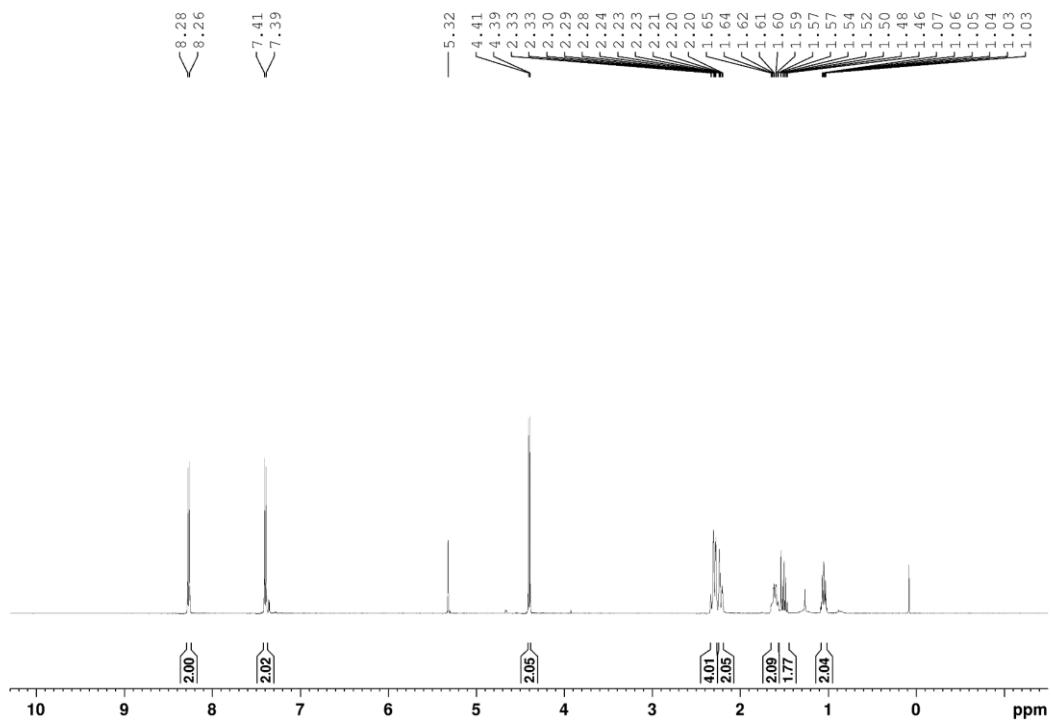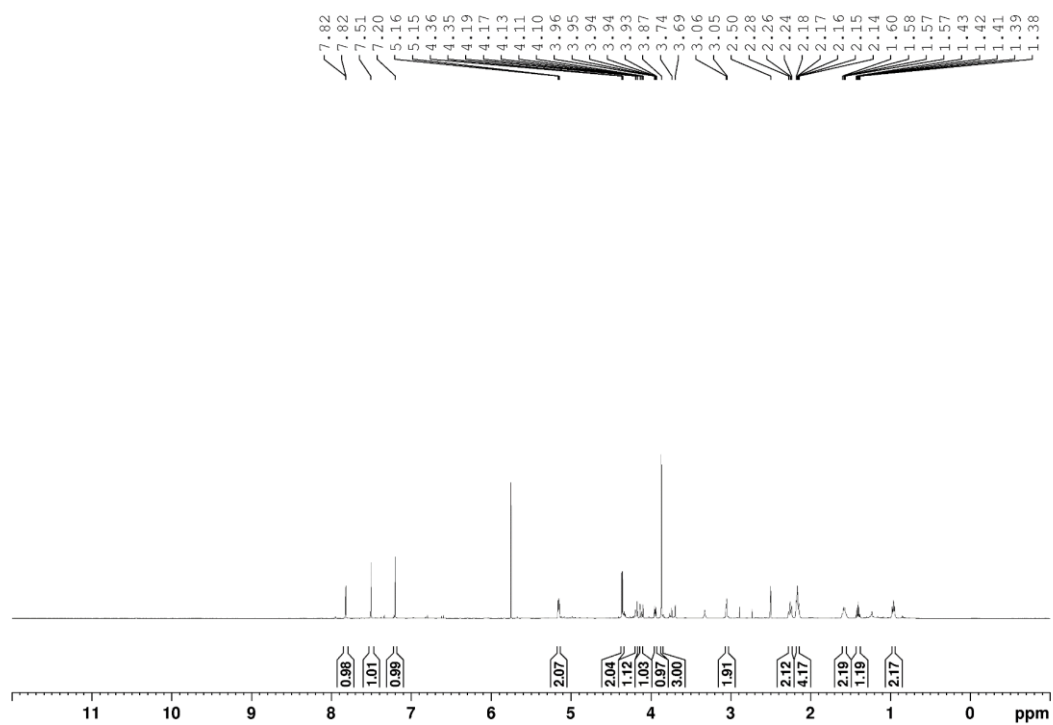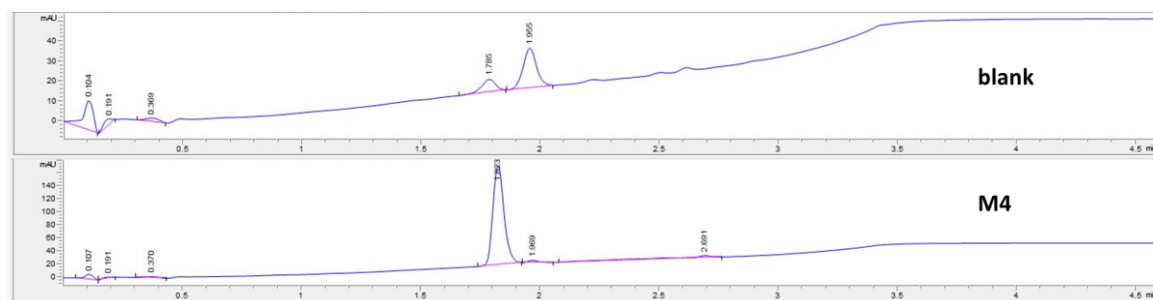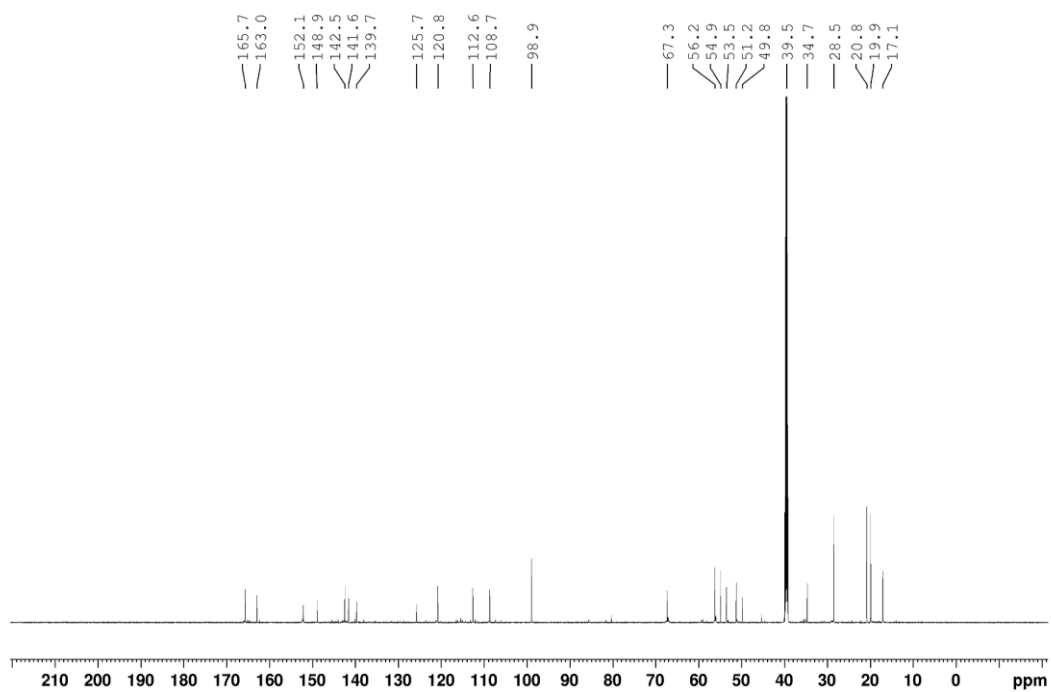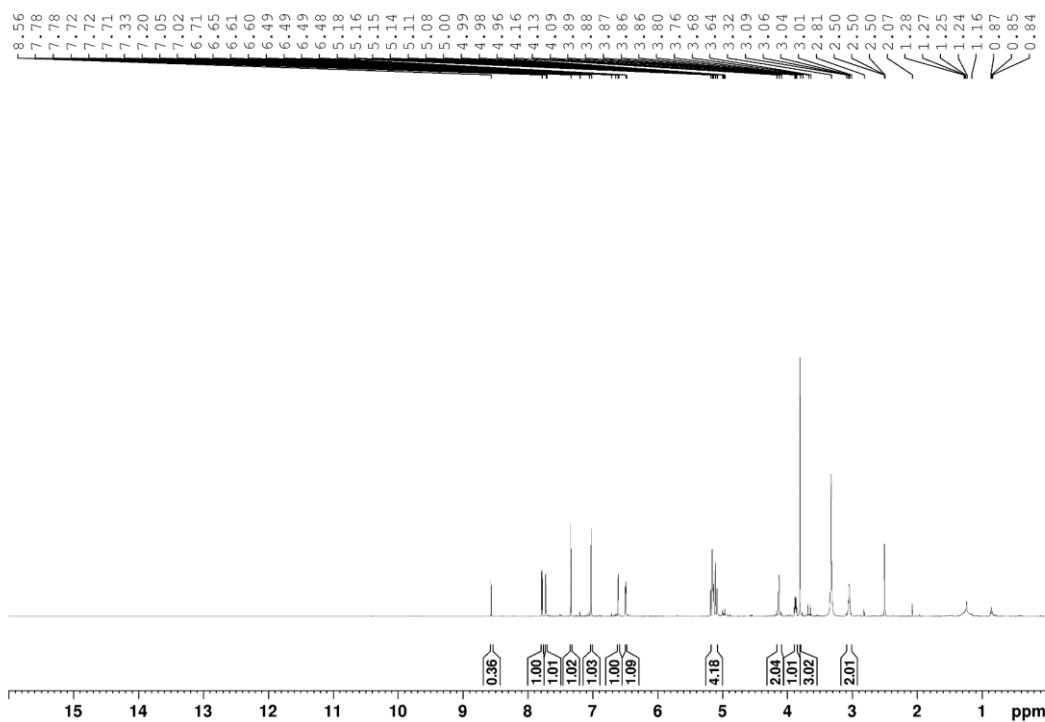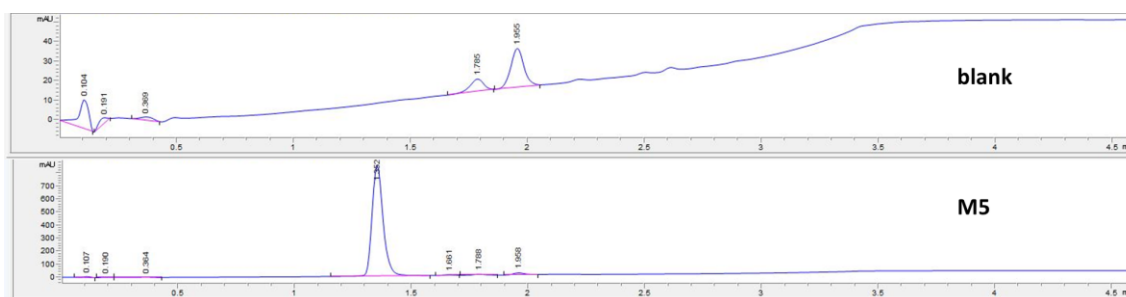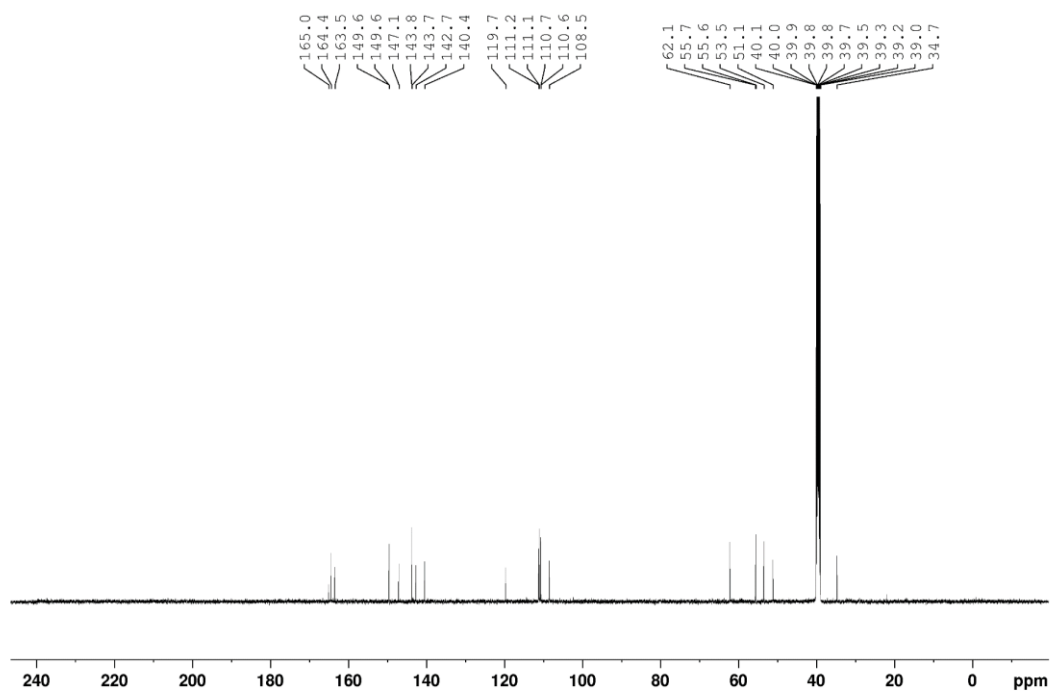
triethyl(prop-2-yn-1-yloxy)silane (126)
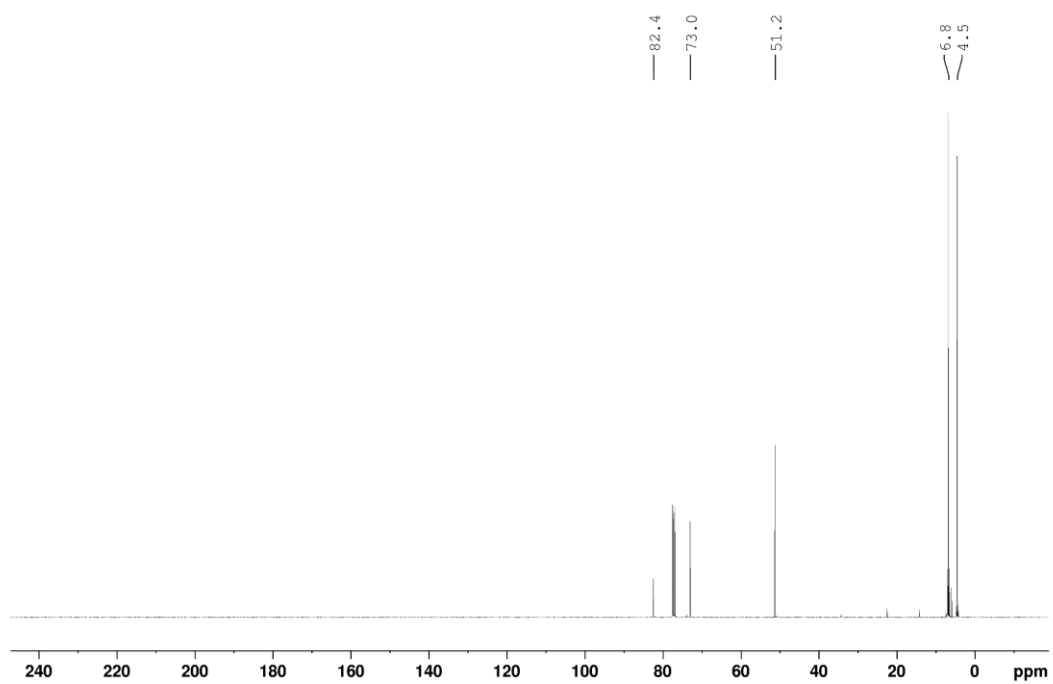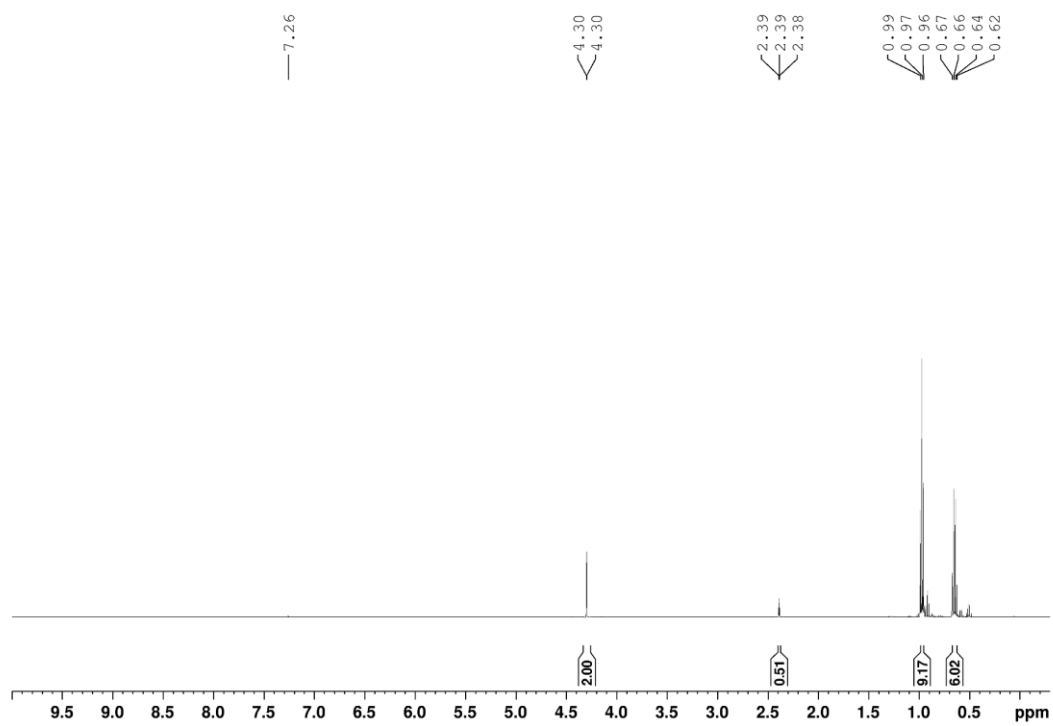
triisopropyl(prop-2-yn-1-yloxy)silane (129)
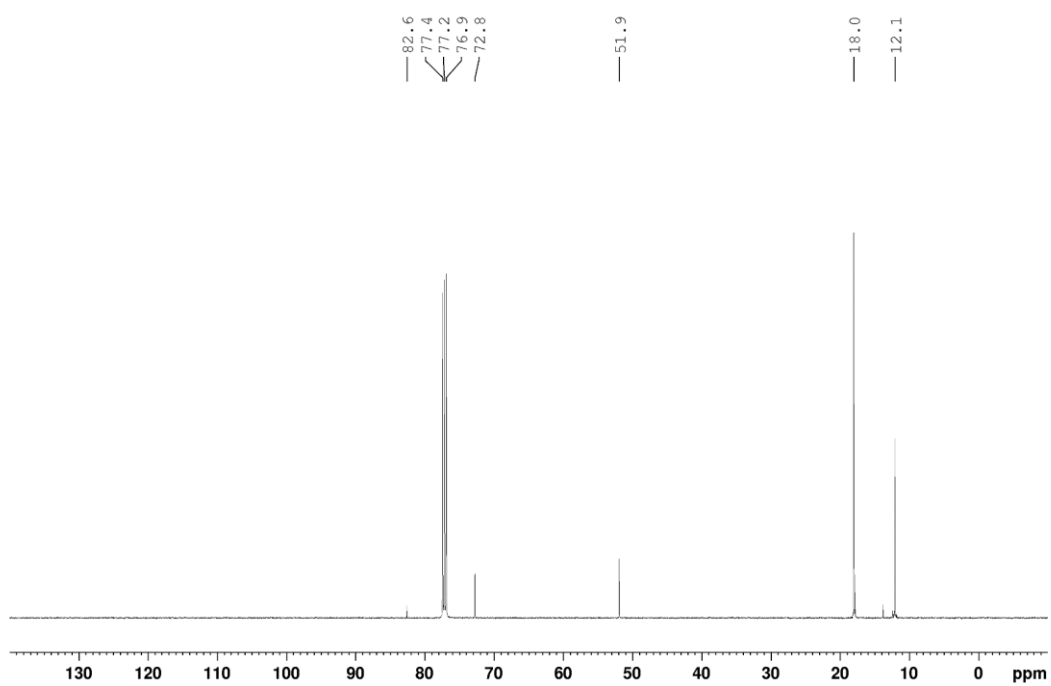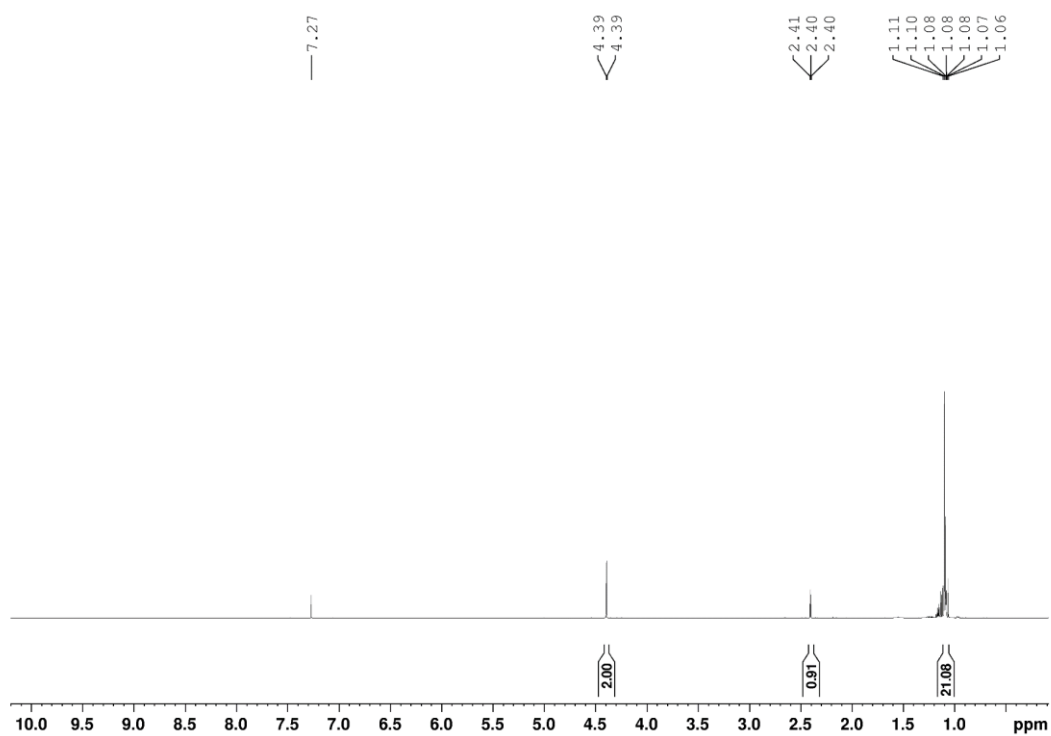
methyl 4-((triisopropylsilyl)oxy)but-2-ynoate (130)
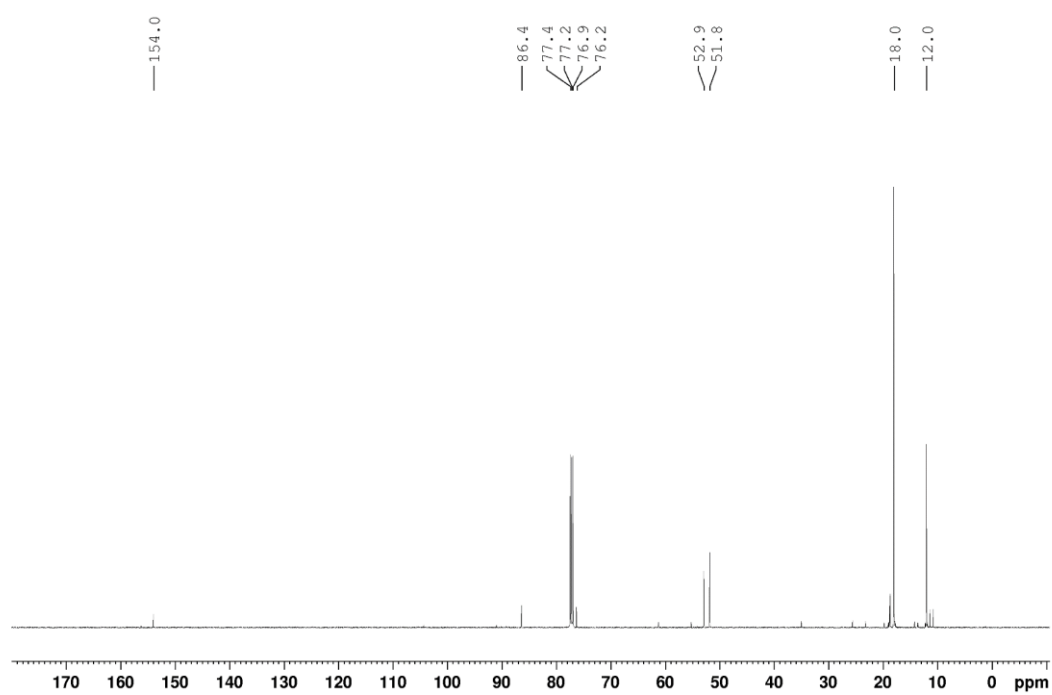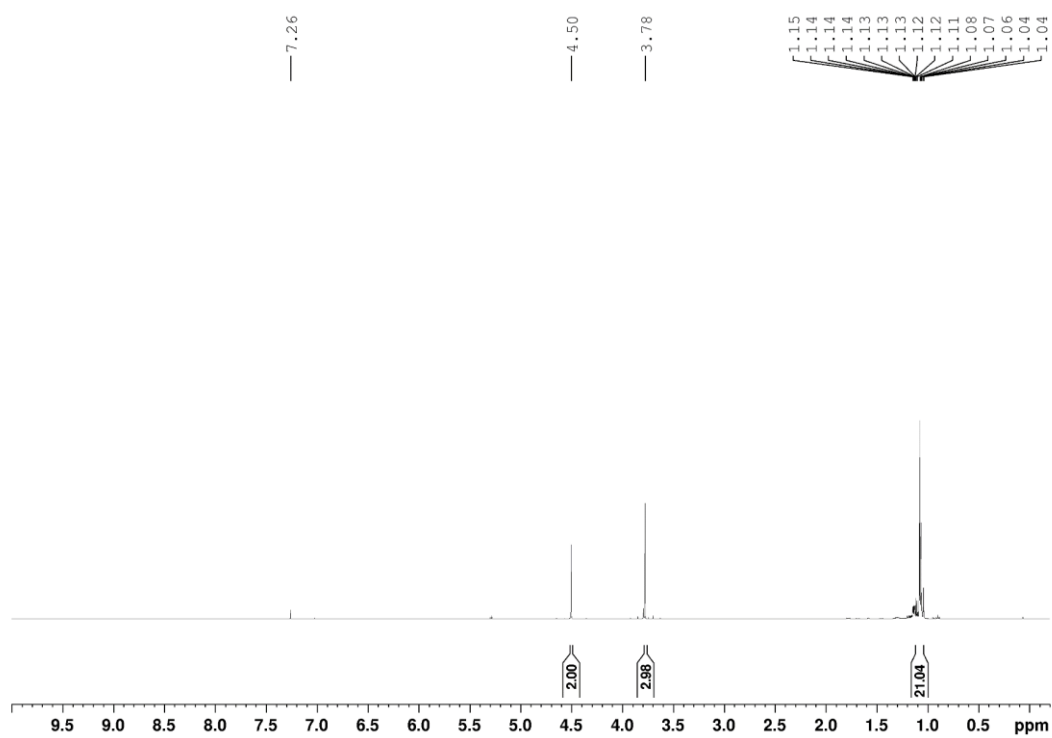
1-bromopropyn-3-ol (135)
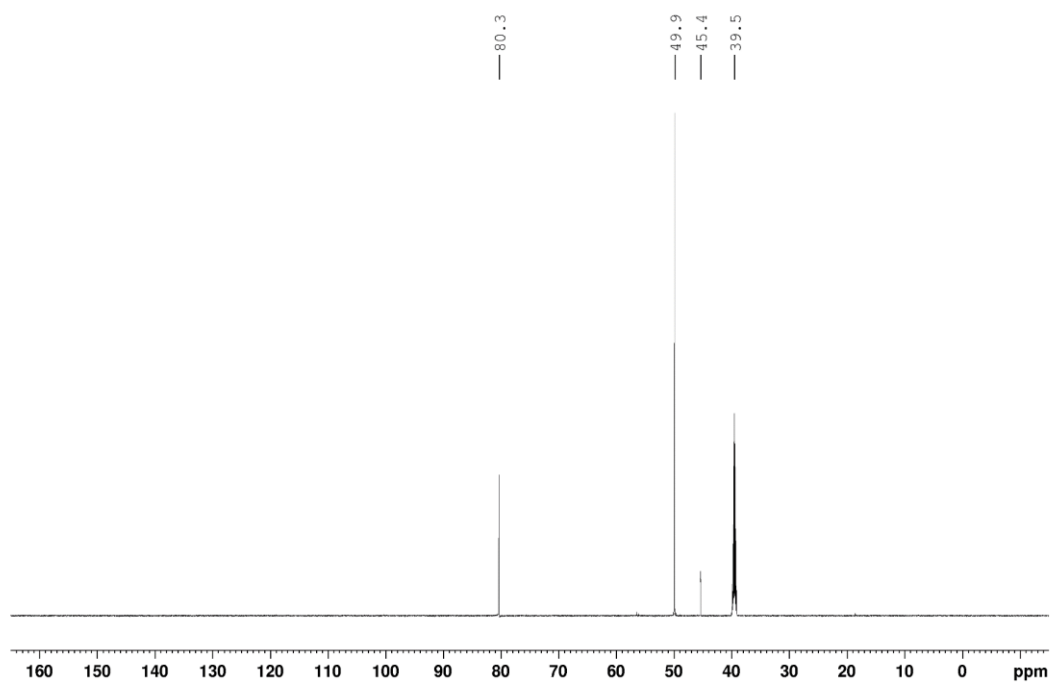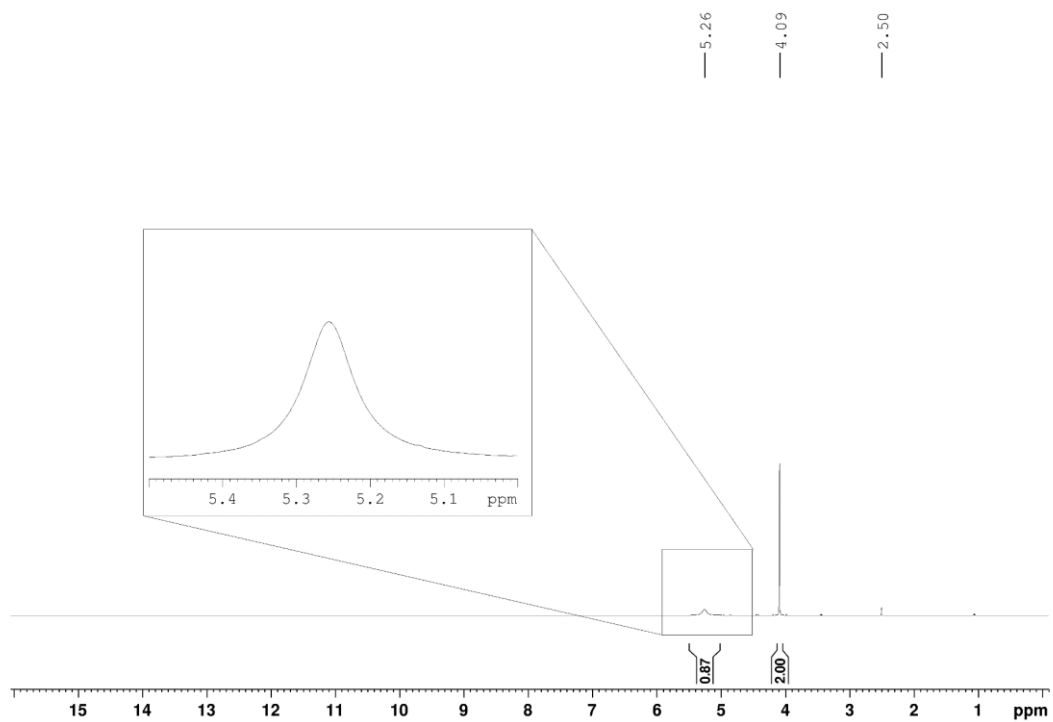
4-hydroxybut-2-ynenitrile (136)
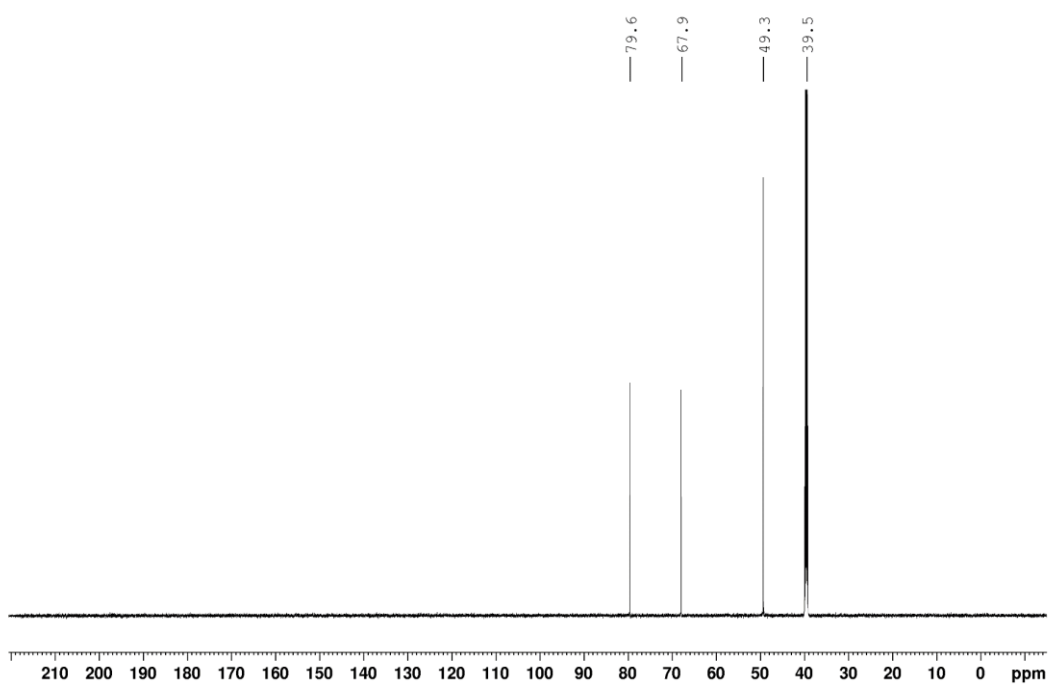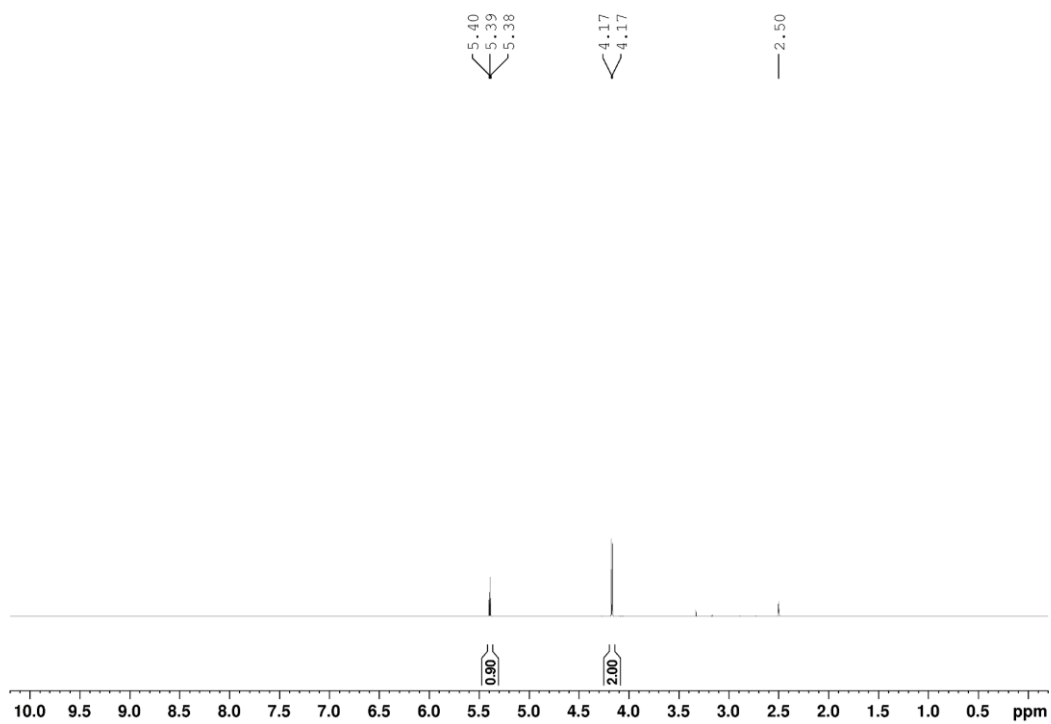
4-bromobut-2-ynenitrile (137)

(*S*)-7-methoxy-8-((1-(2-(((*S*)-7-methoxy-2-methylene-5-oxo-2,3,5,11a-tetrahydro-1H-benzo[e]pyrrolo[1,2-a][1,4]diazepin-8-yl)oxy)ethyl)-1H-1,2,3-triazol-4-yl)methoxy)-2-methylene-1,2,3,11a-tetrahydro-5H-benzo[e]pyrrolo[1,2-a][1,4]diazepin-5-one (D1)

166.8
166.7
165.1
151.0
150.1
143.8
143.7
143.2
143.1
140.8
139.2
138.1
129.6
129.6
125.3
125.3
120.3
119.8
112.9
112.2
110.2
108.5
108.4
107.8
106.0
94.5
88.4
88.3
67.0
61.6
58.3
58.2
58.2
56.1
56.0
55.8
55.7
55.6
55.6
54.9
54.2
54.1
53.9
53.5
53.4
51.1
50.8
49.0
49.0
36.2
35.3
35.3
28.7
28.6
22.1
13.9

(11a*S*,11a'*S*)-8,8'-(((1H-1,2,3-triazole-1,4-diyl)bis(ethane-2,1-diyl))bis(oxy))bis(7-methoxy-2-methylene-1,2,3,11a-tetrahydro-5H-benzo[e]pyrrolo[1,2-a][1,4]diazepin-5-one) (D2)

164.5
164.4
163.5
162.3
151.5
150.2
147.0
143.8
143.3
142.7
142.6
140.7
140.6
140.5
139.3
123.3
120.0
119.4
111.6
111.3
110.4
110.1
108.5
106.0
102.2
101.7
88.4
88.3
67.4
67.1
66.9
59.1
58.3
56.1
55.9
55.7
55.6
54.9
54.2
53.9
53.5
53.4
53.1
51.1
48.8
40.0
39.9
39.7
39.6
39.5
39.4
39.3
39.1
36.2
35.8
34.7
30.7
25.4
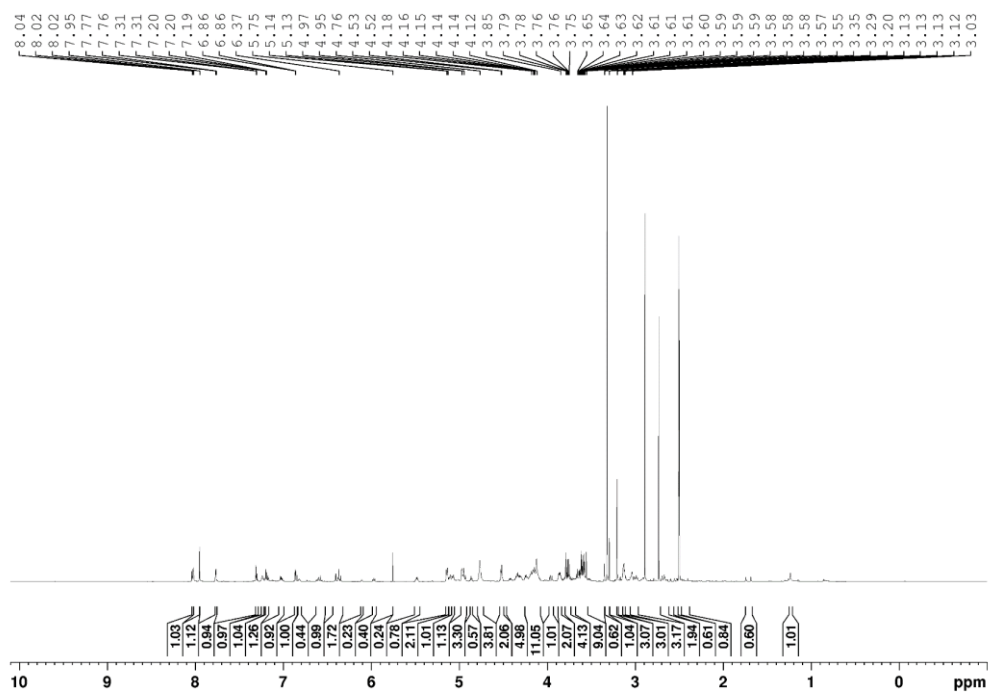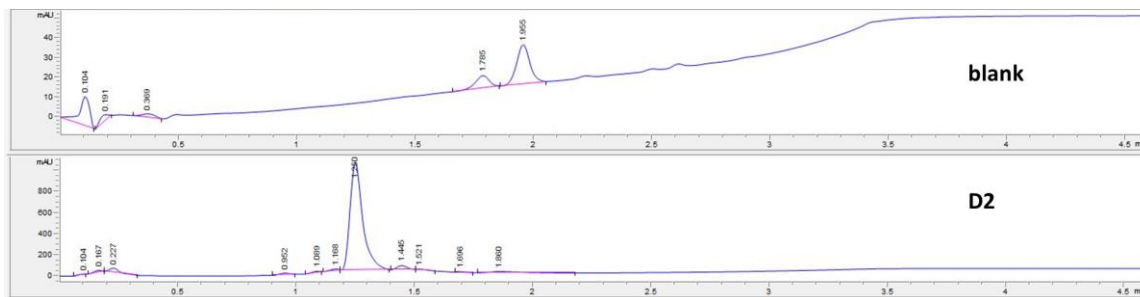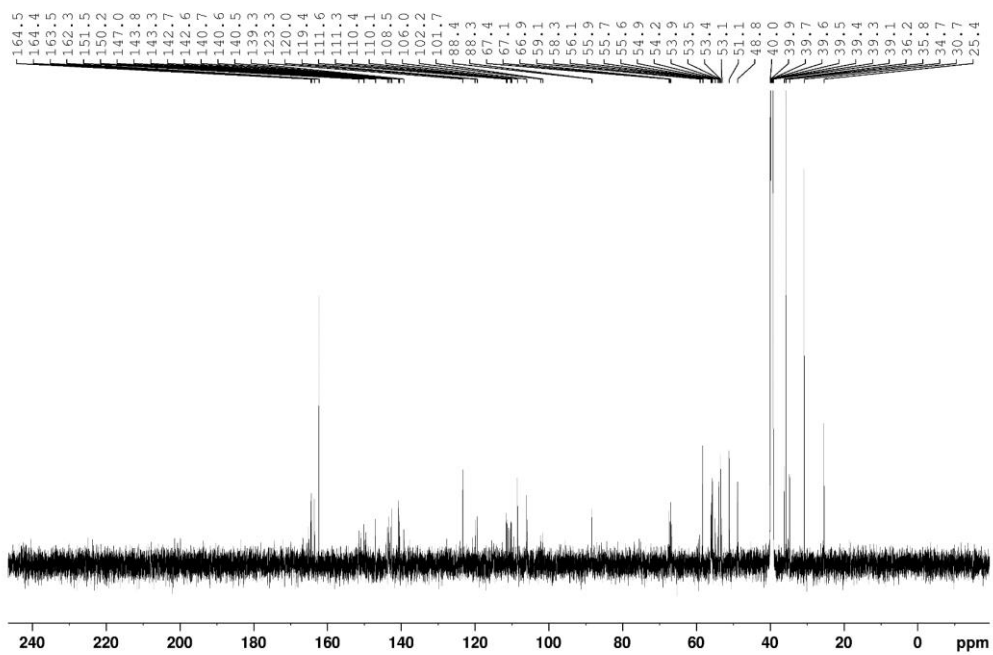
(11a*S*)-7-methoxy-8-(2-(4-(2-(((*S*)-7-methoxy-2-methylene-5-oxo-2,3,5,11a-tetrahydro-1H-benzo[e]pyrrolo[1,2-a][1,4]diazepin-8-yl)oxy)ethoxy)-4,5,6,7,8,9-hexahydro-1H-cycloocta[d][1,2,3]triazol-1-yl)ethoxy)-2-methylene-1,2,3,11a-tetrahydro-5H-benzo[e]pyrrolo[1,2-a][1,4]diazepin-5-one (D3)

(*S*)-7-methoxy-2-methylene-5-oxo-2,3,5,11a-tetrahydro-1H-benzo[e]pyrrolo[1,2-a]
[1,4]diazepin-8-yl   (((5aS,6R,6aR)-1-(2-(((*S*)-7-methoxy-2-methylene-5-oxo-2,3,5,11a-
tetrahydro-1H-benzo[e]pyrrolo[1,2-a][1,4]diazepin-8-yl)oxy)ethyl)-1,4,5,5a,6,6a,7,8-
octahydrocyclopropa[5,6]cycloocta[1,2-d][1,2,3]triazol-6-yl)methyl) carbonate (D4)
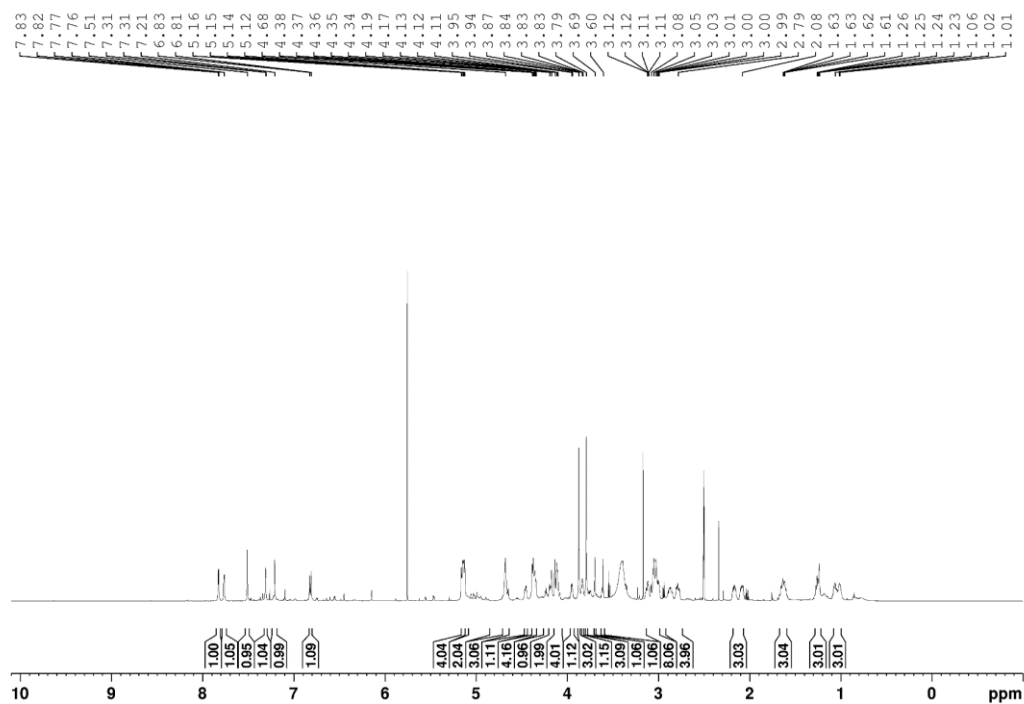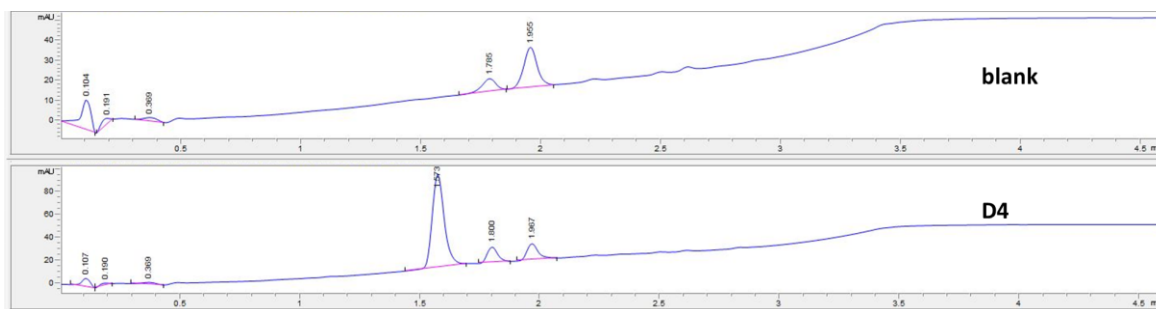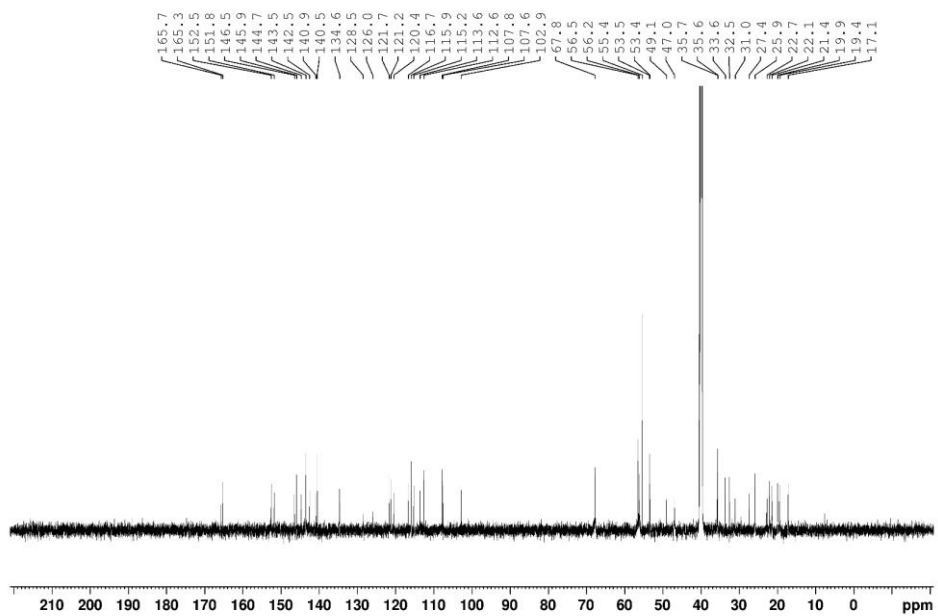
3,6-di(pyridin-2-yl)-1,2,4,5-tetrazine (186)
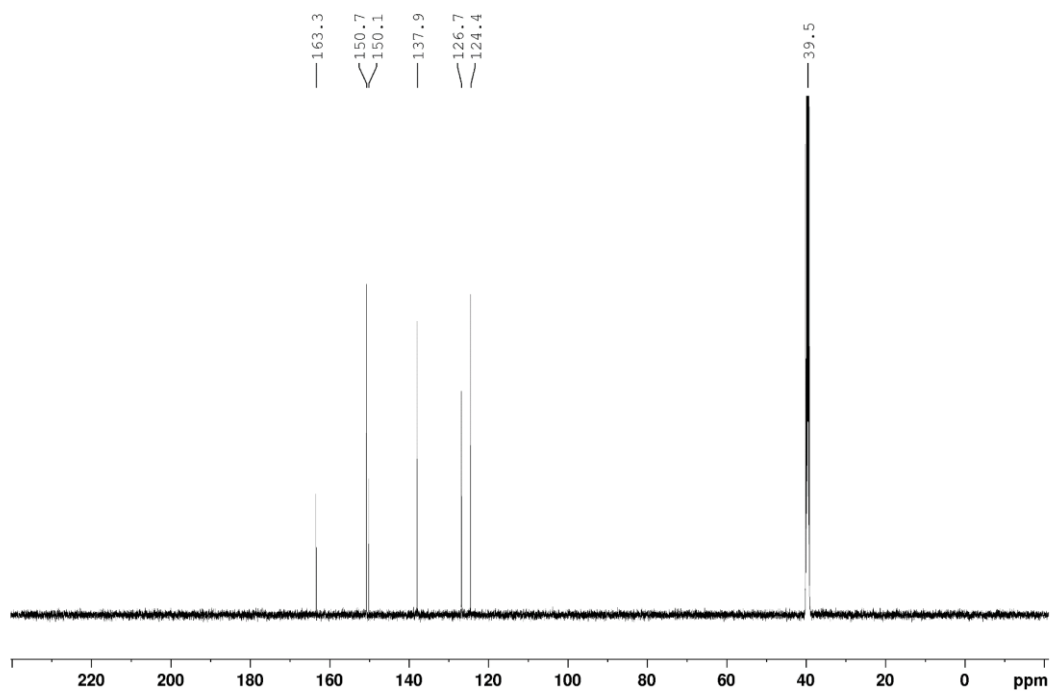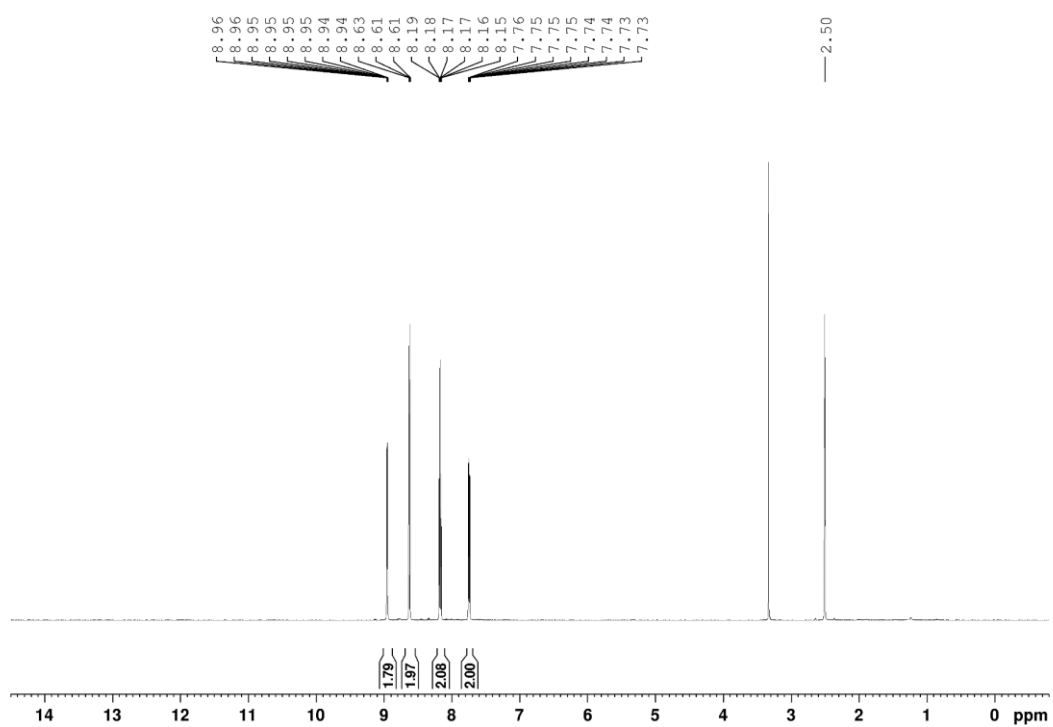
4-(1,2,4,5-tetrazin-3-yl)benzoic acid (274)
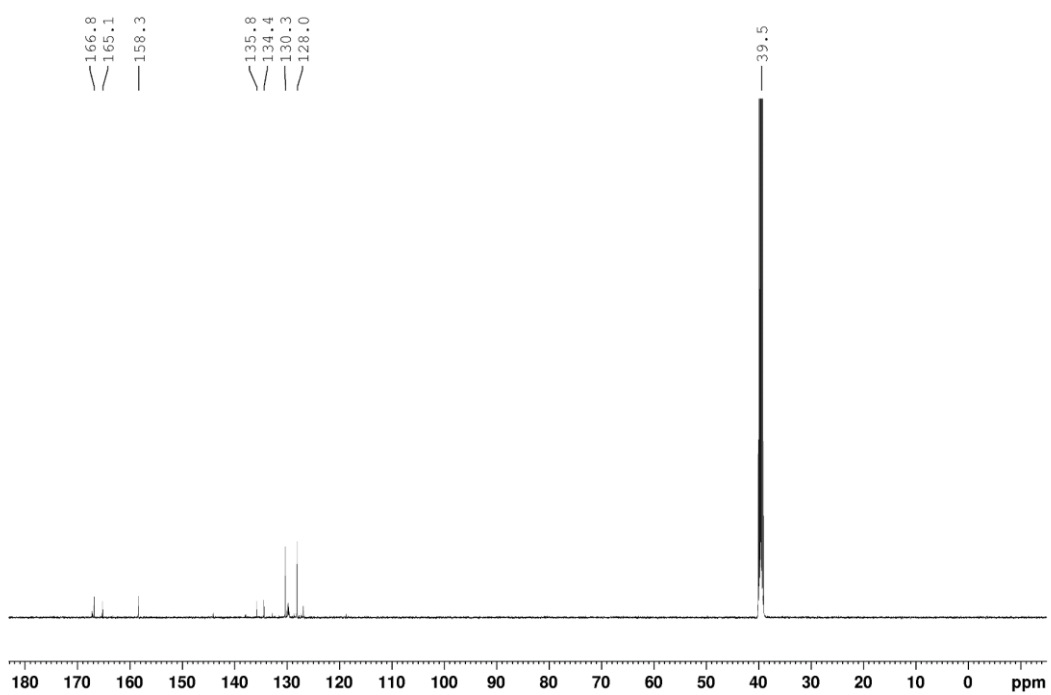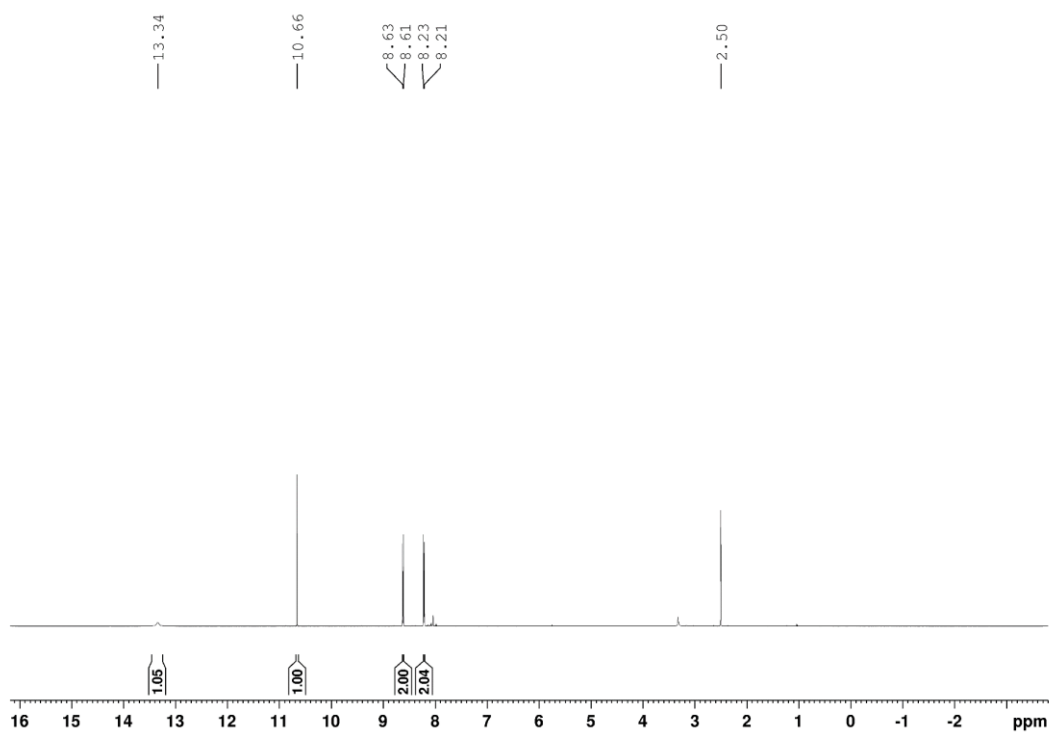
6-(1,2,4,5-tetrazin-3-yl)nicotinic acid (276)
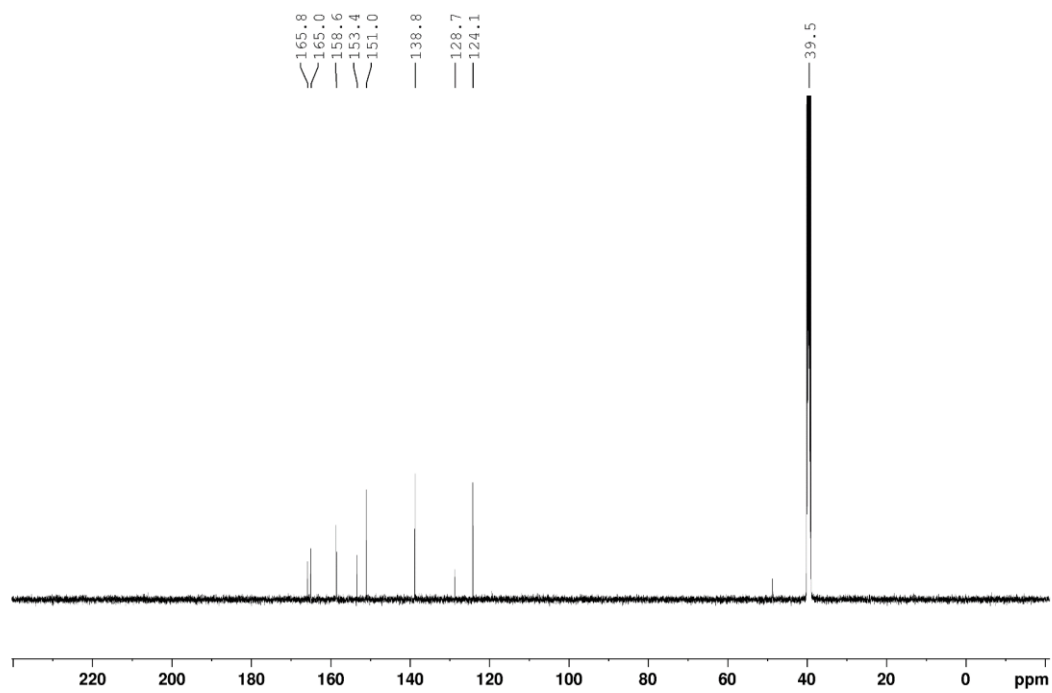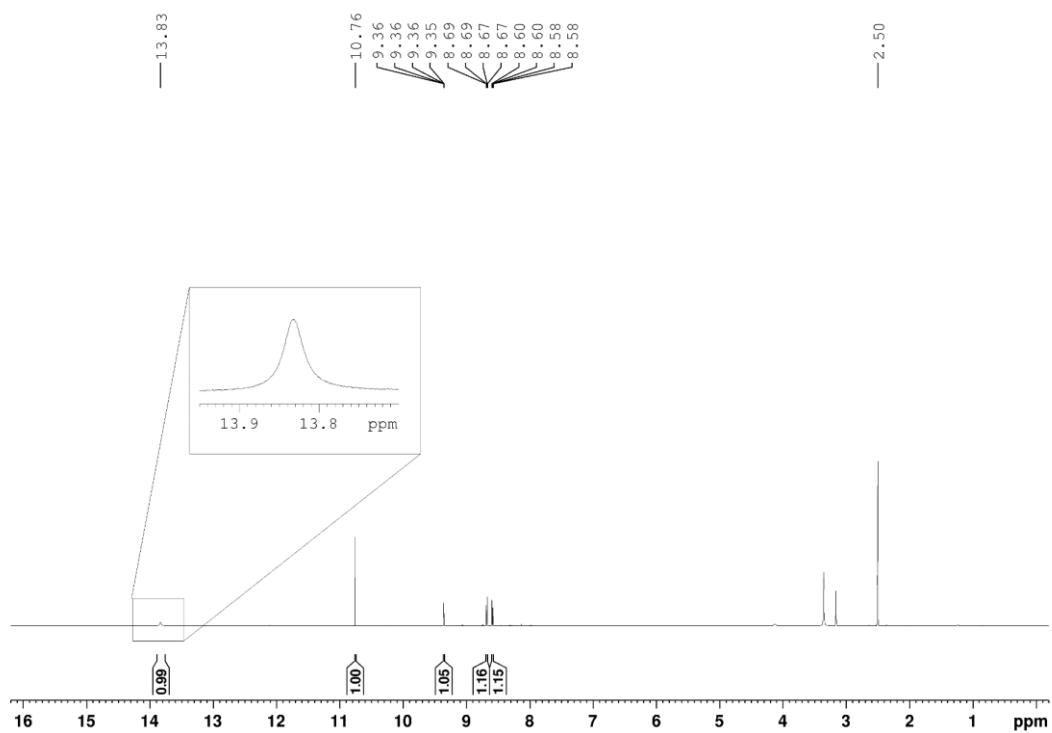
2-(4-hydroxy-2-methylbutan-2-yl)-3,5-dimethylphenol (240)
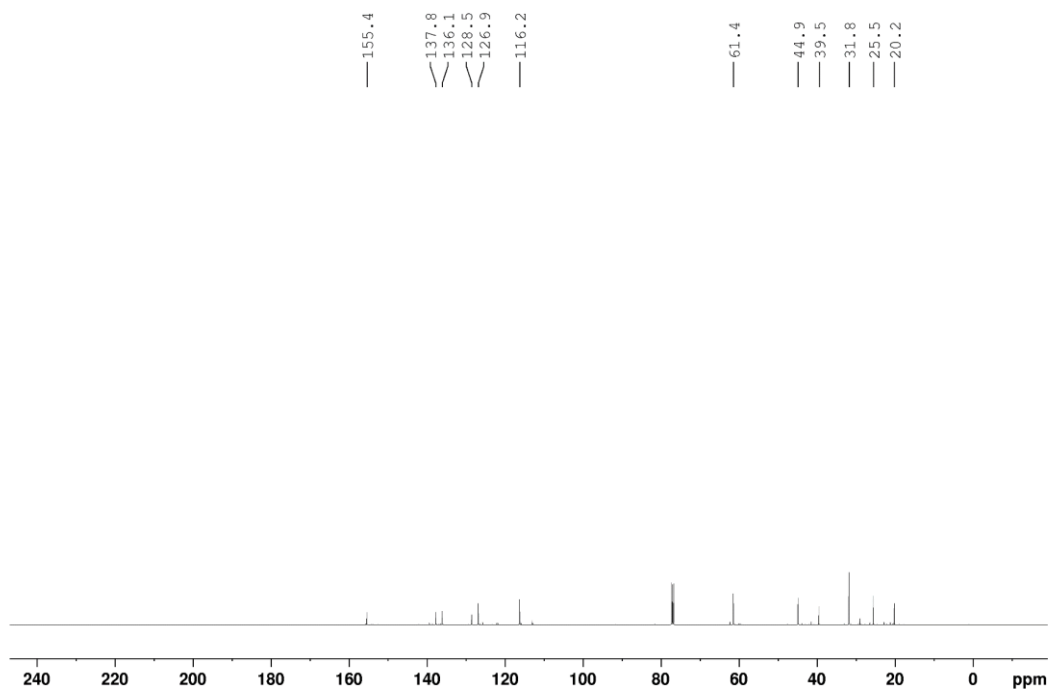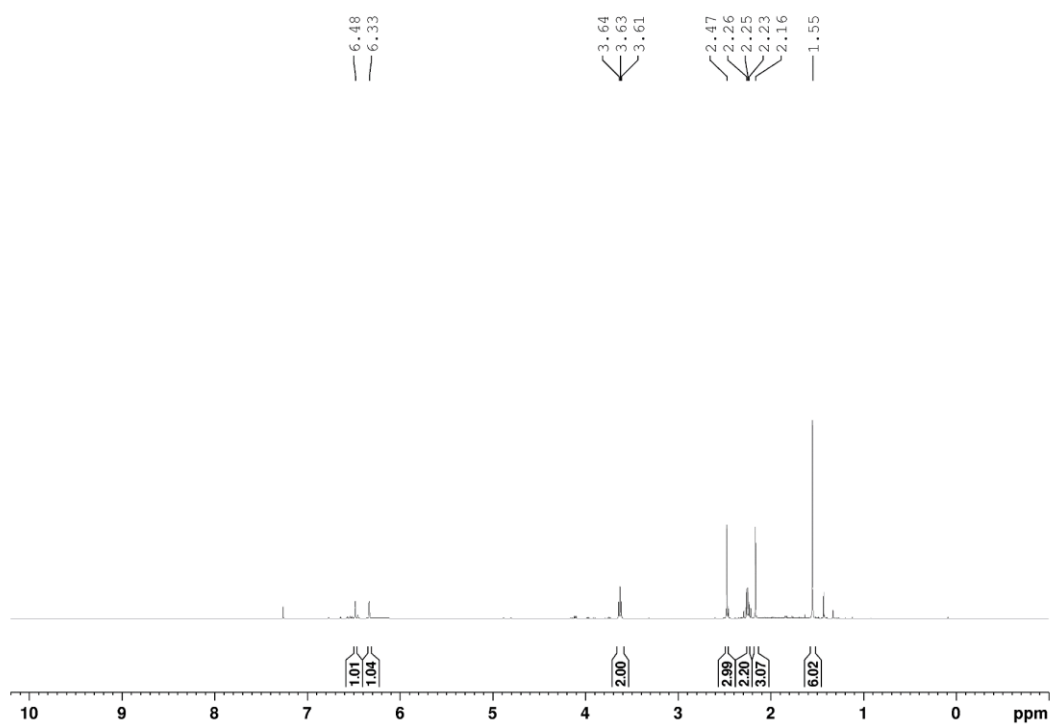
2-(4-((*tert*-butyldimethylsilyl)oxy)-2-methylbutan-2-yl)-3,5-dimethylphenol (241)
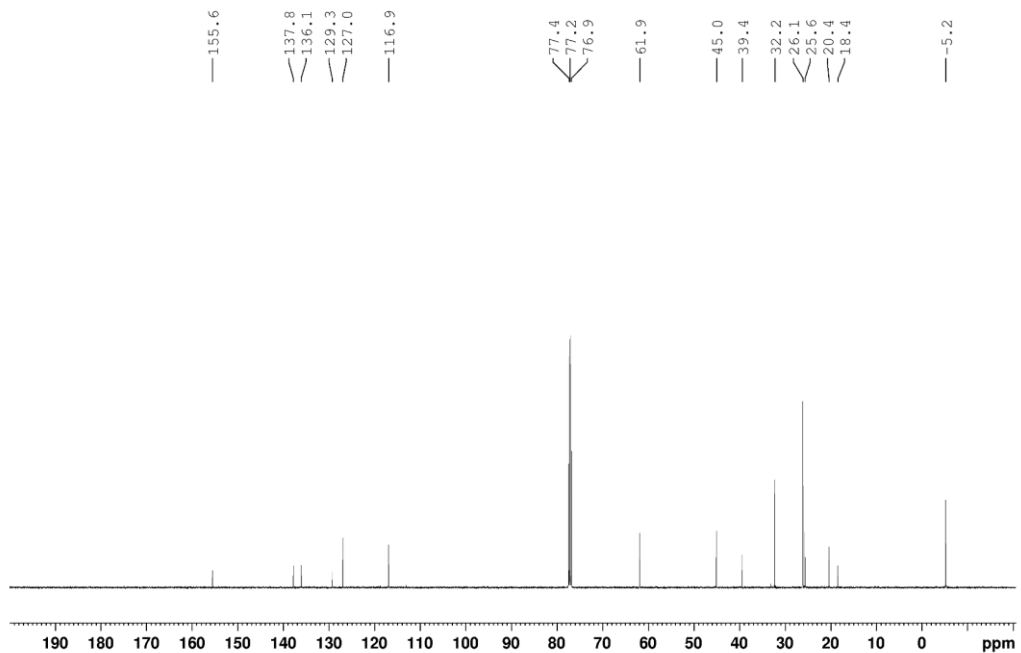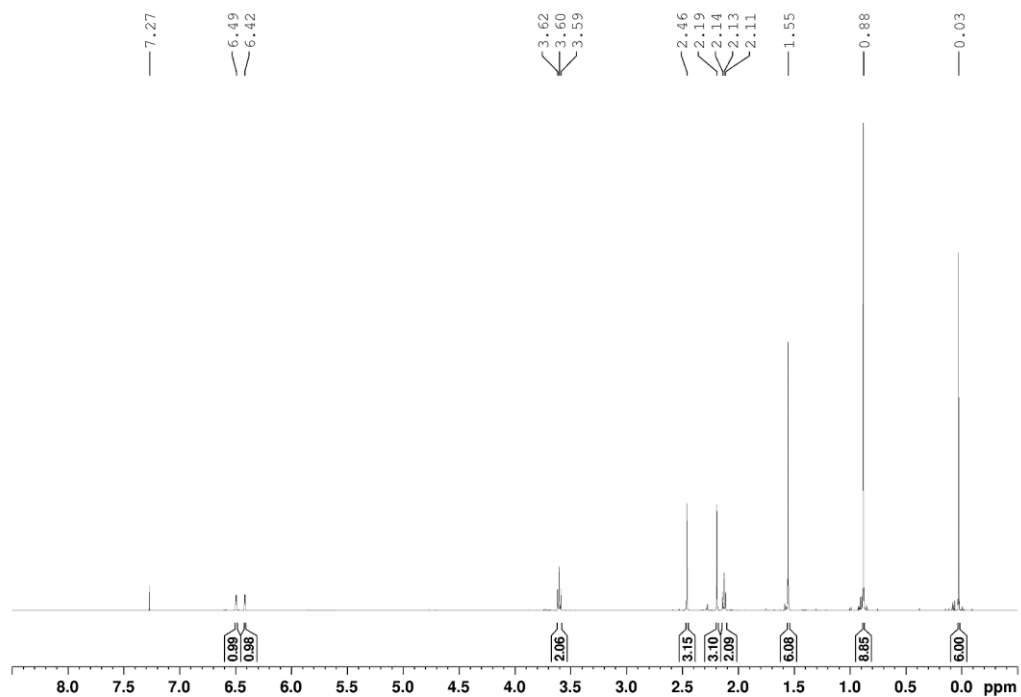
(3-(2-(2-bromoethoxy)-4,6-dimethylphenyl)-3-methylbutoxy)(*tert*-butyl)dimethyl-silane (242)
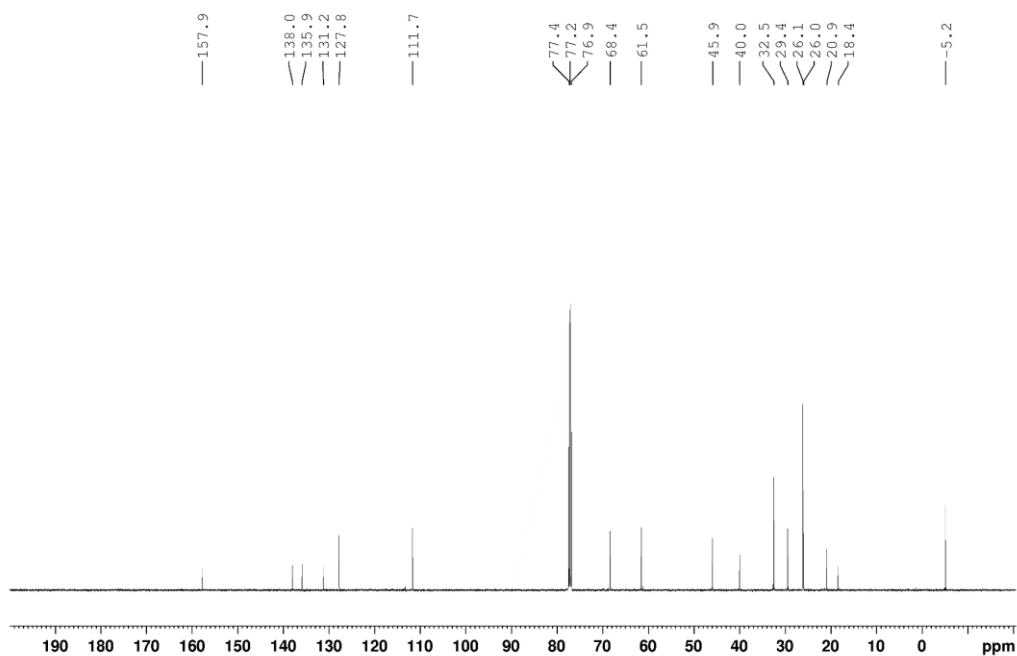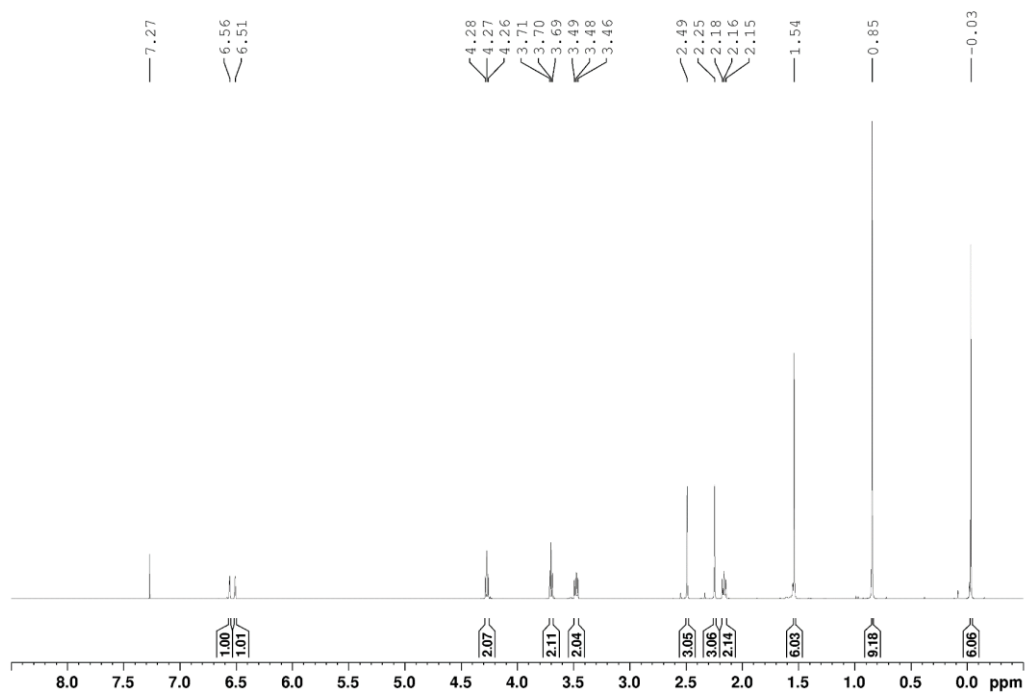
(3-(2-(2-bromoethoxy)-6-methyl-4-((prop-2-yn-1-yloxy)methyl)phenyl)-3-methylbutoxy)(*tert*-butyl)dimethylsilane (295)
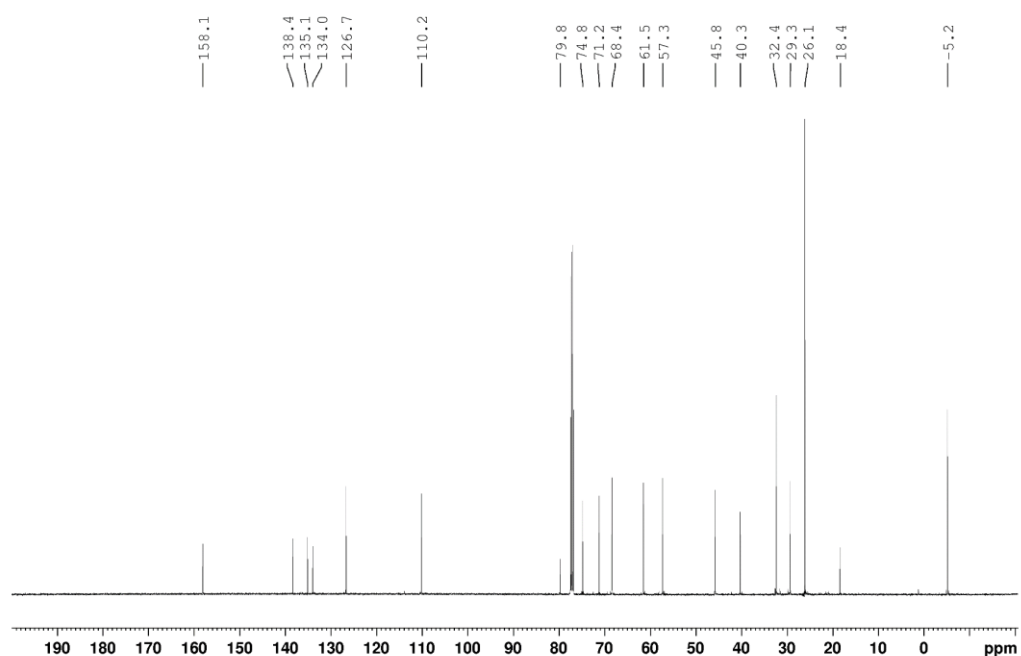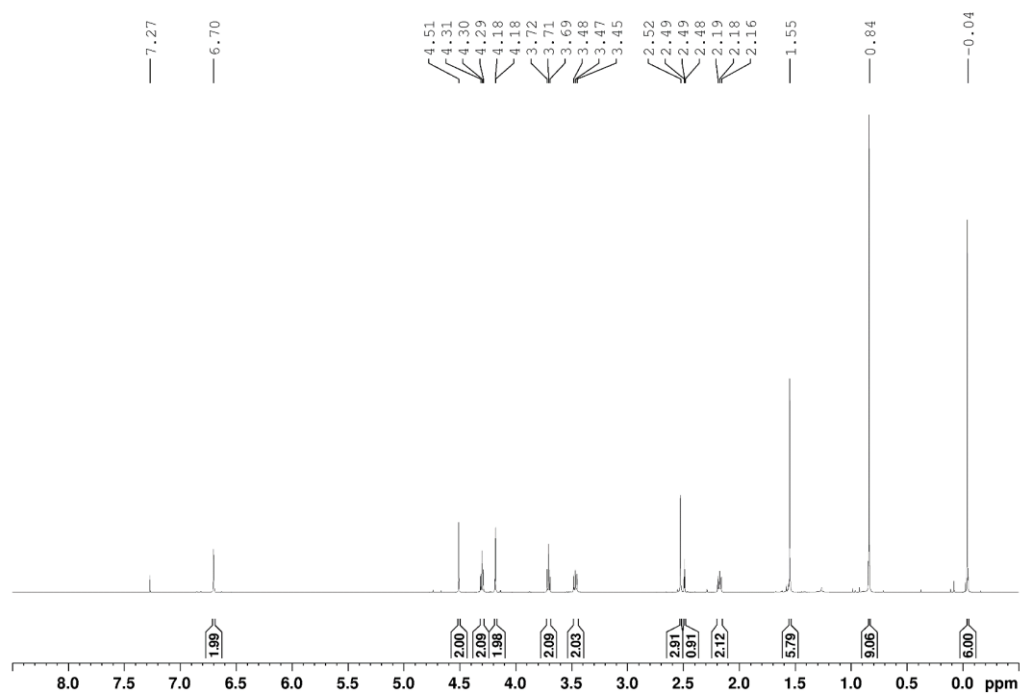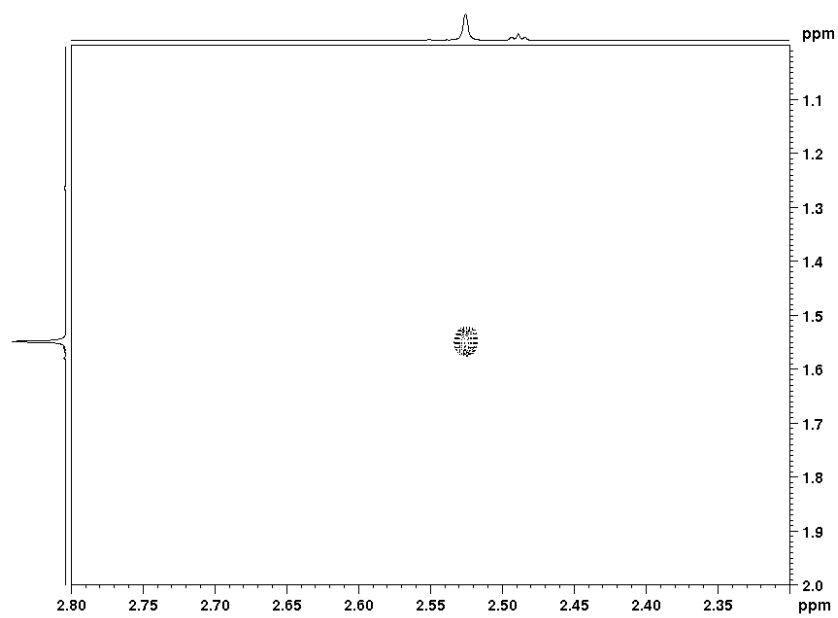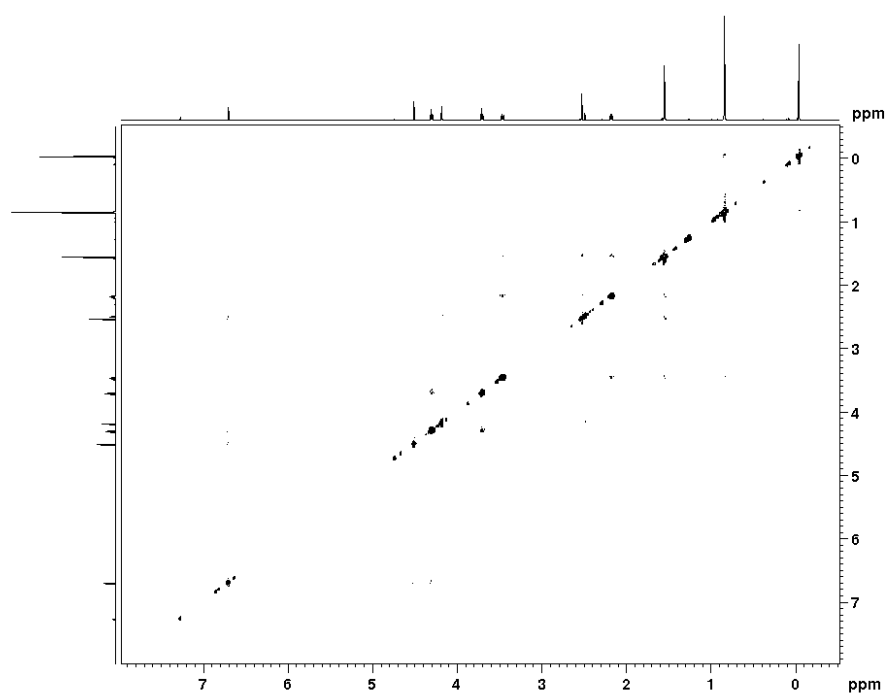
(3-(2-(2-bromoethoxy)-4-methyl-6-((prop-2-yn-1-yloxy)methyl)phenyl)-3-methylbutoxy)(*tert*-butyl)dimethylsilane (296)
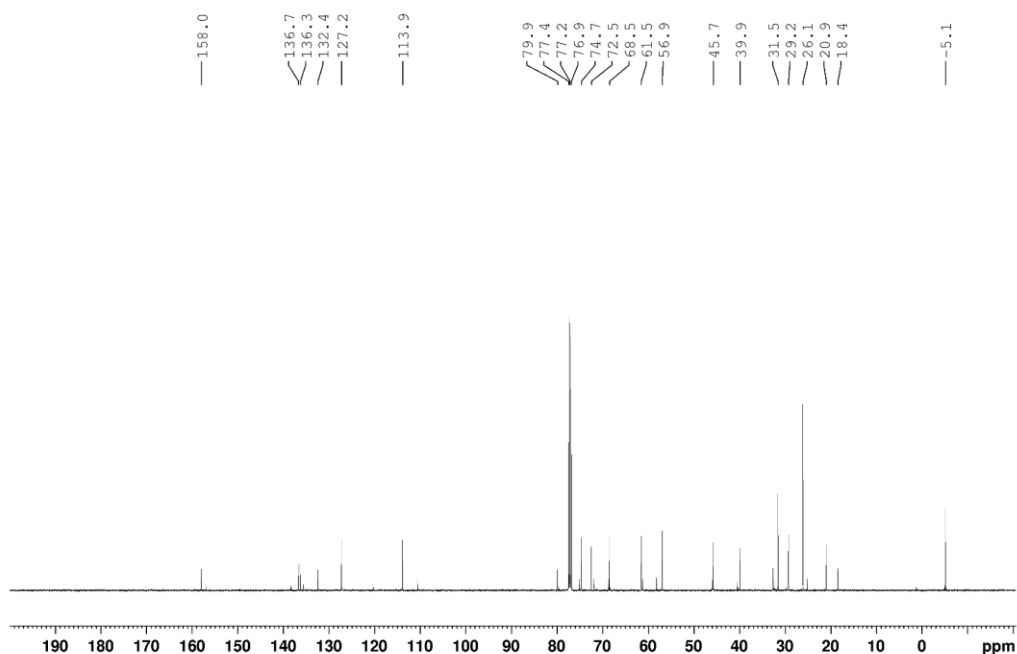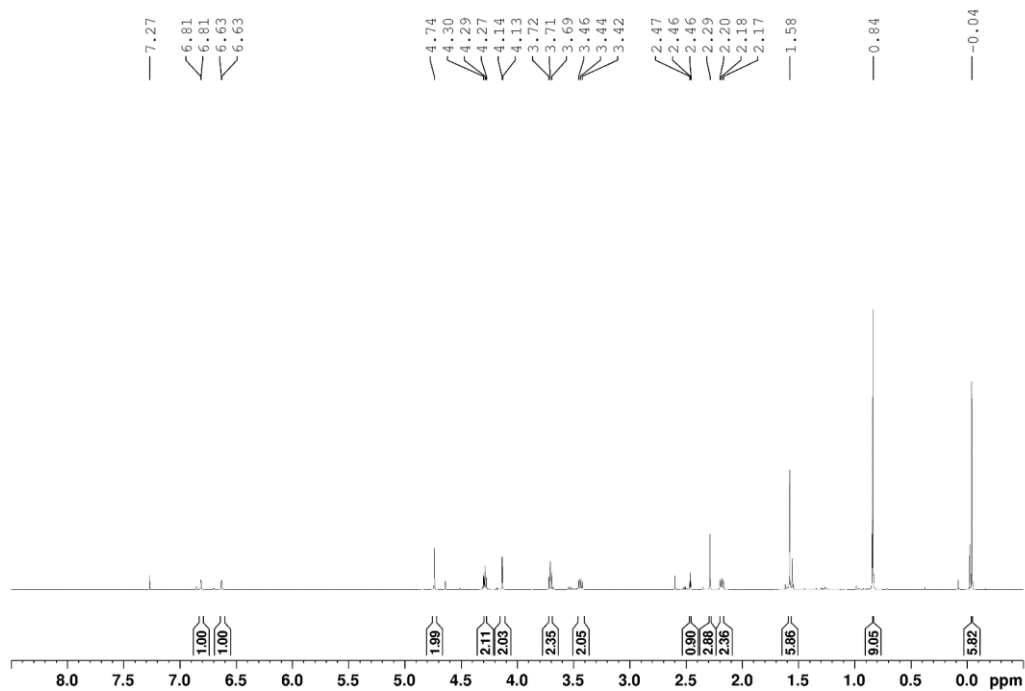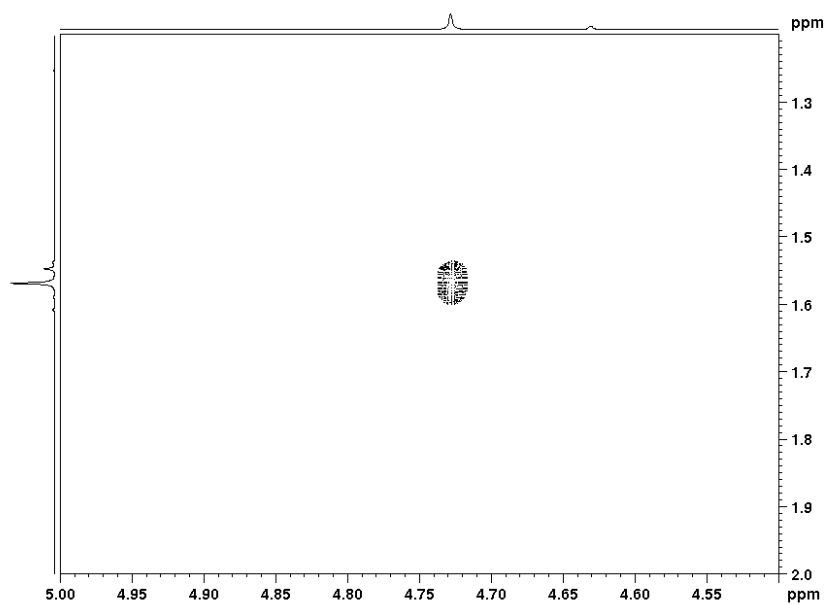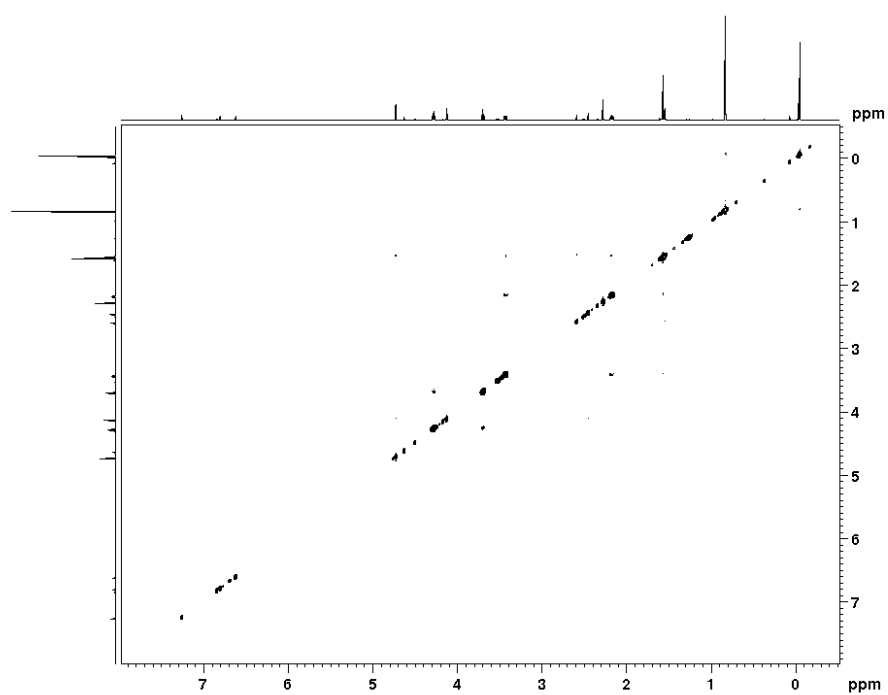
Exemplary crude NMR of a mixture of :

1-(bromomethyl)-3-methoxy-5-methylbenzene,

1-methoxy-3,5-dimethylbenzene,

and 2-bromo-5-methoxy-1,3-dimethylbenzene

The integration for each respective compound is shown:

7.27
6.61
6.55
3.78
2.30

0.93
1.93
3.00
6.02

8.0 7.5 7.0 6.5 6.0 5.5 5.0 4.5 4.0 3.5 3.0 2.5 2.0 1.5 1.0 0.5 0.0 ppm

7.27
6.66
3.77
2.39

2.08
2.93
6.00

8.0 7.5 7.0 6.5 6.0 5.5 5.0 4.5 4.0 3.5 3.0 2.5 2.0 1.5 1.0 0.5 0.0 ppm

7 Danksagung

Meinen Praktikantinnen und Bachelorandinnen Mareike Gora, Eva Brechner und Anne Prowald danke ich für ihre Unterstützung bei den Synthesen und biologischen Experimenten.

Christel Kakoschke und Kirsten Harmrolfs möchte ich für die Aufnahme unzähliger NMRs danken. Ebenso danke ich Heike Overwin und Raimo Franke für die HRMS-Messungen meiner Verbindungen.

Ich möchte mich bei der ganzen CBIO-Arbeitsgruppe bedanken, die die letzten vier Jahre zu vier unvergesslichen Jahren gemacht haben. Bettina Mehner für ihre herzliche Art von der der Arbeitskreis tagtäglich profitiert. Werner Tegge für seine stoische Gelassenheit in Anbetracht der Hürden in der Kommunikation mit dem TB. Für die interessanten Unterhaltungen, amüsanten Mittagspausen, die gute Labor und Büro Atmosphäre, sowie der guten Stimmung außerhalb des Labors danke ich Daniel Kohnhäuser, Thomas Siemon, Simon Hilker, Anna Vetter, Moritz Stappert, Sven-Kevin Hotop, Carsten Peukert, Lukas Pinkert, Aditya Shekhar, Giulia Guerra und Travis Coyle.

Ein besonderer Dank geht außerdem an Eugenio Loi und Karoline Jerye, die ich zu meinen engsten Freunden zählen darf und die immer ein offenes Ohr für mich haben und mich durch alle Hochs und Tiefs einer Doktorarbeit begleitet haben. Ich habe selten Personen getroffen, die so für ihre Ideale einstehen, der Diskussion nicht müde werden und einen solch positiven Einfluss auf ihre Umgebung haben.

Obwohl ich die Liste an Personen ins Endlose weiterführen könnte, so sind doch meine Eltern die wohl wichtigsten Unterstützer auf diesem Weg gewesen. Ohne sie würde ich sicherlich nicht hier sitzen und diese Zeilen unter meine Dissertation schreiben.

Ohne über den Ist-Zustand zu richten, sondern immer den Fokus auf den nächsten Schritt, egal wie klein er auch sein mag, zu lenken, standen und stehen sie immer verlässlich hinter mir. Sie haben mir beigebracht, dass die Stärke darin liegt Versuche zu wagen und sich nicht von der Angst des potentiellen Scheiterns oder in manchen Fällen auch den enttäuschenden Gefühlen des tatsächlichen Scheiterns gängeln zu lassen.

Danke.

8 CV

Persönliche Angaben

Name:	Julia Alisa Friederich
Geburtsdatum:	08.09.1995
Geburtsort:	Heppenheim (Bergstraße)

Studium und Ausbildung:

04/2019 – 04/2023   **Promotion**
Helmholtz-Zentrum für Infektionsforschung
Abteilung Chemische Biologie
Betreuer: Prof. Dr. Mark Brönstrup
Titel der Arbeit: *"Two sides of click chemistry: Synthesis of linkable Tomaymycin derivatives as in situ activated drugs and a trimethyl lock/tetrazine-based click-to-release system"*

10/2016 – 09/2018   **Master of Science**
Technische Universität München
Fach: Chemie
Betreuer: Prof. Dr. Stephan A. Sieber
Titel der Arbeit: *"Synthese und Validierung von kovalenten Pyridoxalkinase Inhibitoren in Staphylococcus aureus"*
Abschlussnote: 1,1 (sehr gut)

09/2017 – 02/2018   **Auslandssemester**
University of California, San Diego (UCSD)
GPA: 3,9 (sehr gut)

10/2013 – 09/2016   **Bachelor of Science**
Ruprecht-Karls-Universität Heidelberg
Fach: Chemie
Betreuer: Prof. Dr. Uwe Bunz
Titel der Arbeit: *"Syn and anti annelierte Tetraazapentaarene"*
Abschlussnote: 2,1 (gut)

06/2013   **Abitur**
Starkenburg Gymnasium Heppenheim
Abschlussnote: 1,5 (sehr gut)

9 Publications

Hübner I., Dienemann J.-N., <u>Friederich J.</u>, Schneider S., and Sieber S. A. (2020) **Tailored Cofactor Traps for the in Situ Detection of Hemithioacetal-Forming Pyridoxal Kinases**. ACS Chem. Biol. 2020, 15, 12, 3227–3234. DOI: 10.1021/acschembio.0c00787